UNIVERSITÄT DUISBURG ESSEN

Open-Minded

Morphology and Ultrastructure of Teeth: From the Middle Ages to Today

Dissertation

zur Erlangung des akademischen Grades eines

Doktor der Naturwissenschaften

Dr. rer. nat.

vorgelegt von

Jana Storsberg

Fakultät für Chemie

Universität Duisburg-Essen

2023

DOI: 10.17185/duepublico/81302
URN: urn:nbn:de:hbz:465-20231130-143106-8

Die vorliegende Arbeit wurde im Zeitraum von Dezember 2020 bis August 2023 am Institut für Anorganische Chemie der Universität Duisburg-Essen unter Anleitung von Prof. Dr. Matthias Epple angefertigt.

Tag der Disputation:	21.11.2023
Prüfungsvorsitz:	Prof. Dr. Bettina Siebers
Gutachter:	Prof. Dr. Matthias Epple
	Prof. Dr. Ottmar Kullmer

Teeth!

You find them everywhere!

On mountaintops!

And in the air!

And if you care to poke around

you'll find them even underground.

Theo LeSieg (Theodor Seuss Geisel—aka Dr Seuss), The Tooth Book

Content

1 Introduction 1

2 Theoretical Background 3

2.1 Tooth structure 3

2.2 Terminology 4

2.3 Tooth wear 5

2.4 Tooth enamel development 8

2.5 Tooth enamel structures 11

2.6 Chemical composition of teeth 15

2.7 Fluoride in dental care 15

3 Materials and Methods 18

3.1 Materials 18

3.1.1 Recent human tooth sample for comparison 18

3.1.2 Medieval human tooth samples from Gevensleben 18

3.1.3 Recent Human tooth samples for fluoride immersion 20

3.1.4 Chemicals 21

3.2 Methods 22

3.2.1 Scanning electron microscopy (SEM) 22

3.2.2 Energy-dispersive X-ray spectroscopy (EDX) 23

3.2.3 X-ray powder diffraction (PXRD) 24

3.2.4 Optical microscopy 26

4 Experimental 28

4.1 Recent Tooth 28

4.2 Gevensleben 28

4.2.1 Preparation for SEM analyses and histological thin sectioning 28

4.2.2 SEM and EDX 29

4.2.3 Histological thin sectioning 30

4.2.4 Digital analyses 31

4.2.5 PXRD 33

4.3 Fluoride immersion of recent teeth 34

5 Results and Discussion 35

5.1 Recent Human Tooth 35

5.1.1 SEM 35
5.1.2 EDX 37
5.1.3 PXRD 38
5.1.4 Microstructural analysis 40
5.2 Gevensleben 42
5.2.1 Individual 41b – SEM and EDX 42
5.2.2 Individual 63a – PXRD 45
5.2.3 Individual 12 46
5.2.4 Individual 22 52
5.2.5 Individual 30 57
5.2.6 Individual 33 64
5.2.7 Individual 38a 71
5.2.8 Individual 39 78
5.2.9 Individual 43 86
5.2.10 Individual 45 93
5.2.11 Individual 53 100
5.2.12 Individual 63a 106
5.2.13 Combined Results 113
5.3 Fluoride Immersion 125
5.3.1 250 ppm fluoride solution 127
5.3.2 250 ppm fluoride solution (pH 4.6) 131
5.3.3 18,998 ppm fluoride solution 135
5.3.4 18,998 fluoride solution (pH 4.7) 139
5.3.5 Solution without fluoride (pH 4.6) 143
5.3.6 Water 147
5.3.7 Statistical analyses and combined results 150
6 Summary 154
6.1 Zusammenfassung 156
7 References 158
8 Appendix 171
8.1 Abbreviations 171
8.2 Gevensleben 172

8.3 Fluoride content in human teeth measured by EDX 176
8.4 Descriptive statistics and statistical test for the Gevensleben sample 179
8.5 Curriculum vitae 180
8.7 Acknowledgments 186
8.8 Statutory declaration 188

1 Introduction

Teeth play a vital role in the energy intake of vertebrates as they serve as a crucial functional unit. They are involved in various essential functions, including capturing prey, defending against predators, and, most importantly, the mastication of food. During chewing, teeth shred the food while mixing it with saliva, increasing the food particles' surface area. This increased surface area provides an advantage by allowing digestive enzymes to have more contact with the food, enhancing the efficiency of decomposition and nutrient extraction (Maier, 1978, Ungar, 2014).

Since teeth are often the only remains found of humans in excavations, investigating teeth morphology and ultrastructure has been a subject of constant scientific interest. Scientists span centuries and encompass various disciplines, including palaeontology, dentistry, anthropology, and archaeology (Forshaw, 2015, Lumsden and Osborn, 1977, Scott, 2014).

From the medieval era to the contemporary period, teeth have served as invaluable repositories of information, offering profound insight into the evolutionary history, dietary habits, and health conditions of various vertebrate species (Hillson, 2005, Ungar, 2010).

Furthermore, the historical significance of dental findings, particularly in the archaeological context, will be explored. The examination of teeth from human remains has not only provided valuable evidence of past diets and health, but it has also shed light on ancient migration patterns, cultural practices, and social structures (Brickley and Morgan, 2023, Fiorenza and Kullmer, 2013, Joannes-Boyau et al., 2019, Schweissing and Grupe, 2003, Ungar, 2011).

Teeth serve as remarkable biological archives, preserving information about an individual's life history and experiences. Due to their remarkable stability and resistance to change, the internal structures of teeth remain well-preserved and unaltered over time (Kendall et al., 2018, Parker et al., 1974). This exceptional preservation makes dental tissues an invaluable resource for researchers, enabling them to delve into the past with unparalleled accuracy and illuminate the stories hidden within our teeth.

In the current era, teeth still occupy a crucial place in our daily lives and are essential to our nutritional intake. As the human diet has undergone significant transformations over time, the maintenance and preservation of teeth demand specialised attention. Sugar in modern diets has become a prominent factor contributing to tooth decay, necessitating effective preventive measures (Sheiham and James, 2015).

Integrating fluoride-containing dental care products has emerged as a pivotal strategy in combatting tooth decay and promoting oral health. By harnessing the protective properties of fluoride, these products fortify the enamel, preserving it against the corrosive effects of sugar and acidic substances (Epple et al., 2022). With regular use of such dental care products, tooth decay can be substantially mitigated (Cieplik et al., 2018, Marsh, 2012, Needleman et al., 2015, Terezhalmy et al., 2008, van Loveren, 2013), thereby safeguarding the long-term integrity of our teeth.

The primary objective of this research is twofold. Firstly, it seeks to conduct a comprehensive histological examination of medieval teeth from a burial site in Gevensleben (700-1000 AD), aiming to establish a basis for comparison with prior archaeological and anthropological investigations. The ultimate aspiration is to substantiate and reinforce the findings through the invaluable insights these biological archives provide.

Moreover, this study endeavours to extend its impact beyond historical investigation: While unearthing the mysteries of past lifestyles and cultures remains pivotal, a secondary focus lies in its potential contribution to modern dental care. By exploring the role of fluoride in daily dental care products, this research aims to shed light on optimal methods for safeguarding our teeth against the persistent challenges they face while sustaining us with nourishment and energy each day.

In combining historical inquiry and contemporary oral health, this work aspires to forge meaningful connections between our past and present, enriching our understanding of human history while providing tangible benefits for modern-day dental care practices.

2 Theoretical Background

2.1 Tooth structure

Teeth comprise two primary components: a crown and one or more roots (**Figure 1**). Typically, only the crown protrudes into the mouth, though there are exceptions. The roots are securely held in the bony sockets of the jaw (alveoli) by a complex network of fibres known as the periodontal ligament. The crown is encased in a layer of hard crystalline tissue called enamel, while the root is covered by a bone-like substance known as cementum. Beneath these surface layers lies the tough and resilient dentine, which forms the primary structure of the tooth. Within the tooth, there is a central pulp chamber. Extending from this chamber is a canal that runs down the centre of the root and exits at its tip. While the arrangement may vary depending on the tooth type, these elements are found in all teeth. The uniformity in design allows us to use consistent terms across various tooth types. For instance, the highest point of the crown is referred to as the coronal end, and the furthest extremity of the root is known as the apex. The point where the crown meets the root is called the cervical region, cervix, or neck of the tooth—these standardised terms aid in describing and understanding dental anatomy accurately (Bath-Balogh and Fehrenbach, 2011, Hillson, 2005, Nanci, 2018, Schwarzbach et al., 2010).

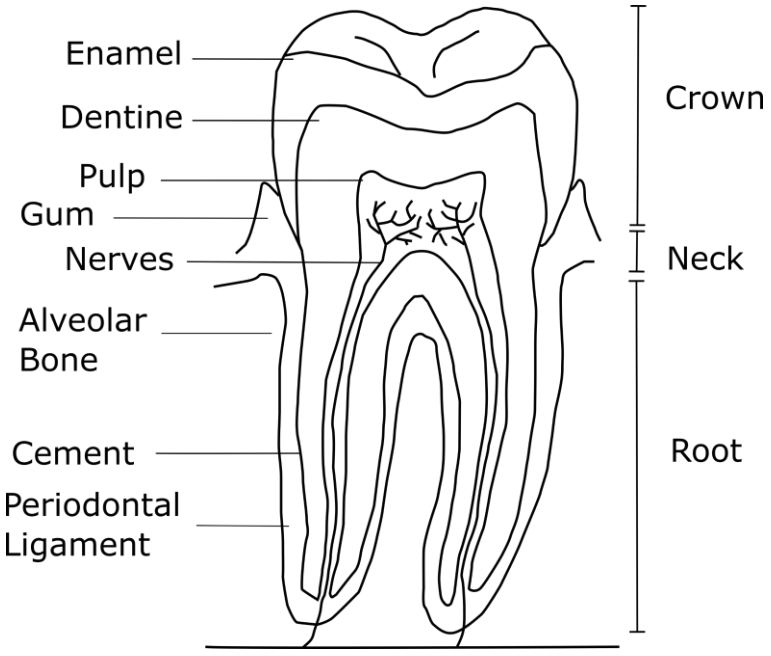

Figure 1 Schematic diagram of a human tooth.

2.2 Terminology

The oral cavity is a complex structure comprising the upper and lower jawbones, the maxilla and the mandible. The arrangement of teeth in the oral cavity can be categorised into two groups: Anterior teeth (incisors and canines), located towards the front, and posterior teeth (premolars and molars), situated towards the back (**Figure 2**). Symmetry is a typical feature of the oral cavity, where the teeth on the right and left sides mirror each other in appearance. Consequently, the median sagittal plane is the dividing line, splitting the jaw into two halves.

Utilising this median sagittal plane as a reference, directional terms are employed to describe specific locations within the oral cavity. For instance, "mesial" designates a direction towards the median sagittal plane or the centre of the dental arch. Conversely, "distal" refers to the opposite direction, away from the median sagittal plane. "Lingual" indicates the direction towards the tongue, while in the upper jaw, "palatal" denotes the direction towards the palate. In the anterior region, the term "labial" describes the direction towards the lips, and "buccal" represents the direction towards the cheeks. The surfaces of adjacent teeth that are in close contact are referred to as "approximal" surfaces, and the surface the teeth get in contact with during chewing is denoted as "occlusal" (Hillson, 2005).

A complete dentition is composed of four primary types of teeth: incisors (I), canines (C), premolars (P), and molars (M). To make identification and description easier, abbreviations and additional notations are used to denote their location. First, an "L" indicates the lower jaw (mandible), and a "U" is used for the upper jaw (maxilla). For the left half of the jaw, "L" is added, while "R" is used for the right half. Furthermore, Incisors can be classified as "1" or "2". The central incisor on each side is denoted as "1", and the lateral incisor is designated as "2". Humans have only one canine on each side of the dental arch. Therefore, "1" or no number is assigned since it is unique in the dentition. Typically, mammals have four premolars, but the first two premolars are reduced in humans, resulting in only the latter two remaining. These are labelled "3" and "4". The group of molars usually makes up to three teeth. The first molar is marked as "1", the second as "2", and the third as "3". For instance, LLM1 refers to the lower left first molar, which is the first (1) molar (M) on the mandible's (L) left (L) side (Irish, 2015).

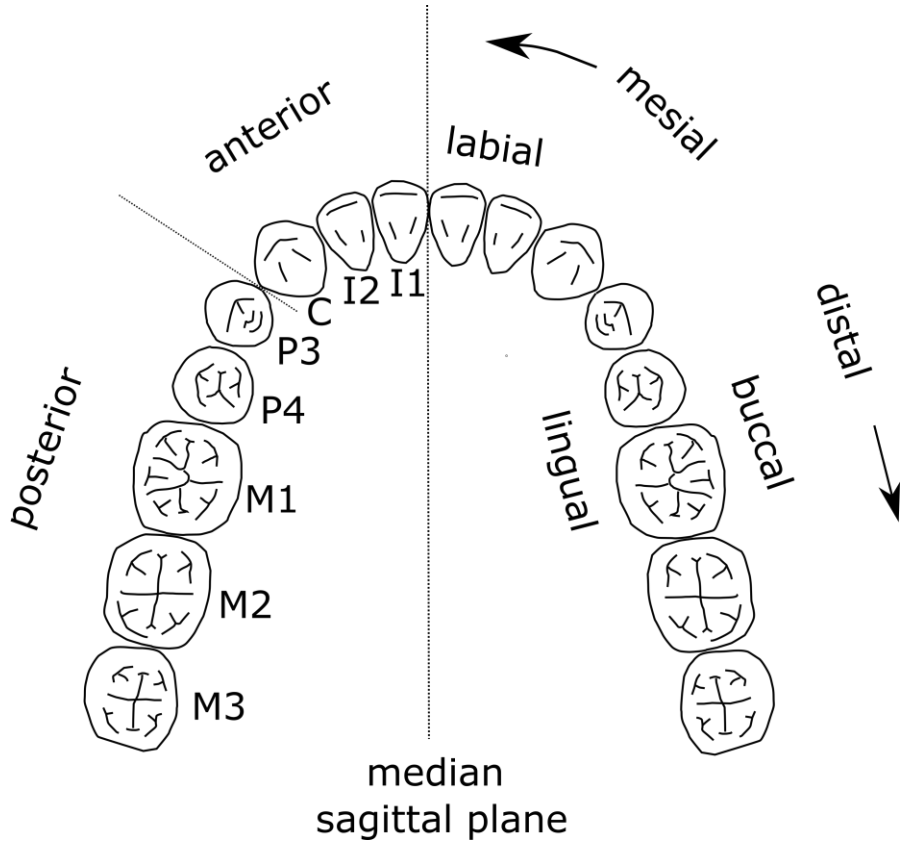

Figure 2 Terminology and directions of orientation in the oral cavity.

2.3 Tooth wear

Tooth wear can be classified into two main types: abrasion, which occurs when teeth come into contact with food or other materials, and attrition, which results from tooth-on-tooth contact (Kay and Hiiemae, 1974).

When we eat, our teeth are used to grind various types of food, including hard, tough, fibrous, and soft items. The wear and the signs of wear on teeth differ depending on the type of food consumed, as well as the speed at which wear occurs. However, not only does the mechanical strength of the mastication play a role, but the abrasive impurities in the food, such as dirt, sand or stone abrasion from grain grinding, can also contribute to tooth wear (Grupe et al., 2015, Kullmer, 2015).

Individuals of advanced age from historical populations show a strong and uniform abrasion on their occlusal surfaces. This is due to the combined effect of the non-processed food and the strong chewing motion necessary to grind it. The speed of abrasion is high in juvenile and

adult age and slowly decreases in old age, as does the strength of the masticatory muscles. Therefore, the determination of age at death with the help of tooth wear should only be done with caution. In addition, the tooth type also plays a role. Small teeth with thinner enamel wear out faster than larger teeth (Grupe et al., 2015).

Wear facets develop as a natural result of the teeth coming into contact during dentition closure. Over time, these facets become more noticeable due to regular chewing movements. The formation and characteristics of these facets are also influenced by the types of food consumed, which can provide valuable insights into an individual's eating habits, potential tooth misalignment, or even using the teeth as a tool (Fiorenza et al., 2018, Grupe et al., 2015).

A precise analysis of the occlusal surface is essential to examine wear facets comprehensively. This complex examination allows for a deeper understanding of the patterns and implications of tooth wear (Kullmer et al., 2009). However, it is important to note that such a detailed analysis was not conducted in this study, so a more in-depth explanation is omitted here.

Since the enamel does not abrade evenly, incisors and canines, premolars and molars must be examined separately. The work of Murphy (1959), which was further developed by Smith (1984), serves as a basis. The stages of wear listed here range from no wear (wear stage 1) to minor enamel wear, such as the beginning reduction of cusp height and slight dentine exposure (wear stages 2-3) to pronounced complete dentine exposure (wear stages 4-8) (**Figure 3**).

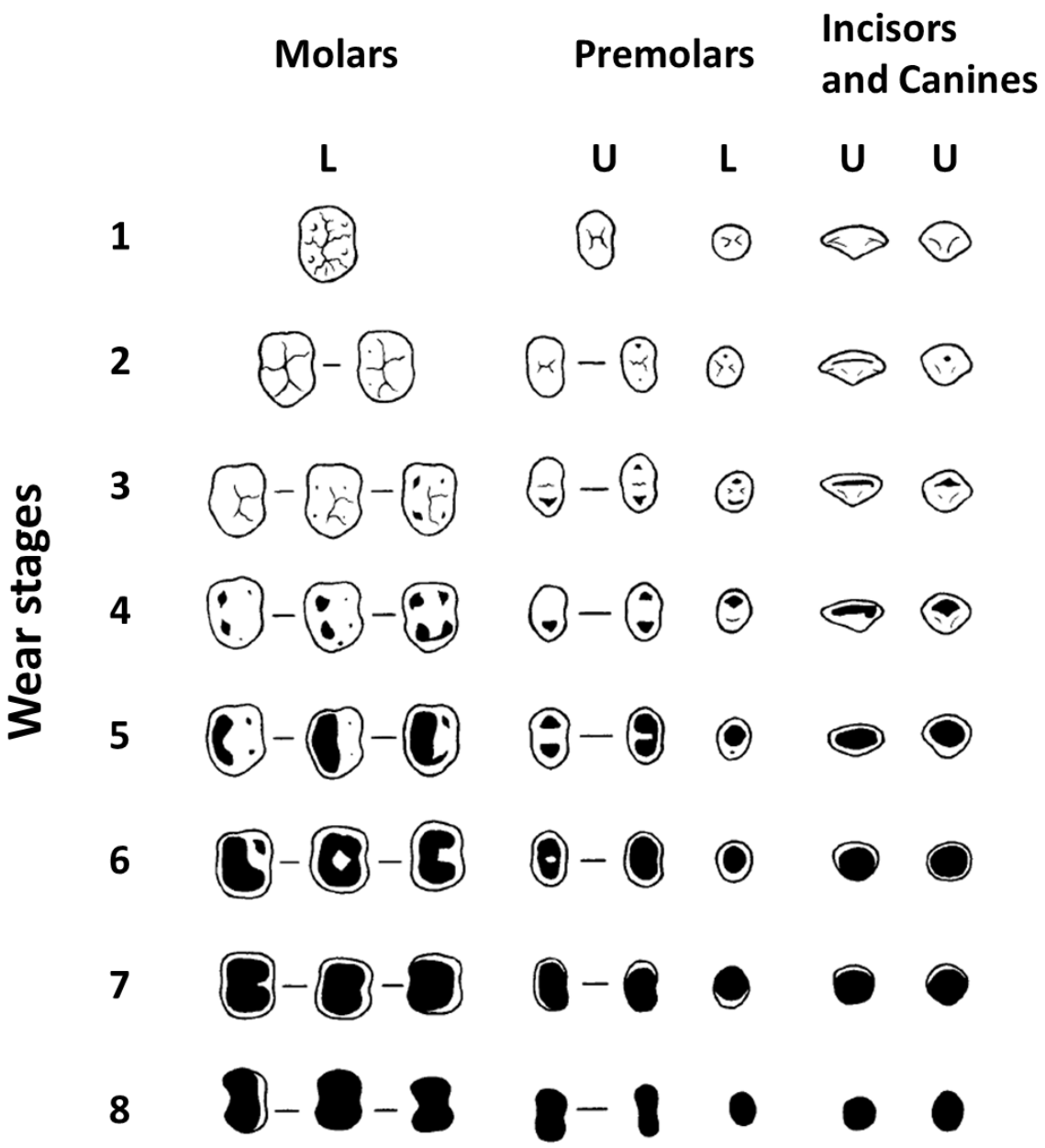

Figure 3 Diagram of wear stages after Murphy (1959), modified by Smith (1984). Crown surfaces and the degrees of wear that are typical for these stages. L (lower jaw) and U (upper jaw). White parts display intact enamel, black parts exposed dentine. For stages 1 to 3, the focus is on evaluating the extent of cusp removal. For stages 4 to 8, the evaluation centres around examining the crown's proportion of dentin versus enamel. Modified after Smith (1984).

2.4 Tooth enamel development

Tooth development takes place in different stages. It begins with the initiation stage in the sixth to the seventh week of human embryogenesis. The ectomesenchyme and the dental lamina start to grow. In the bud stage (eighth week), the dental lamina grows into the shape of a bud and penetrates the growing ectomesenchyme. During the cap stage (ninth to tenth week), the former bud-shaped tooth germ forms into a cap-shaped enamel organ surrounded by the dental follicle filled with dental papilla. In the eleventh to twelfth week, the enamel organ differentiates into a bell shape with four cell types (one of them is the ameloblasts), while the dental papilla forms two different cell types. In the apposition stage (varies with tooth), the hard dental tissues such as enamel, dentine, and cementum are formed (Bath-Balogh and Fehrenbach, 2011, Hillson, 2005, Nanci, 2018).

Ameloblasts (enamel-secreting cells) develop a protrusion called the Tomes process which secretes the prismatic and interprismatic enamel matrix (**Figure 4**). Ameloblasts and odontoblasts (dentine-secreting cells) have their excretory ends facing each other so that they are moving further apart, the more enamel matrix and predentine are deposited, forming the enamel-dentine junction (Maas and Dumont, 1999, Schwarzbach et al., 2010). Ameloblasts start from the future tip of the dentine horn. They move outwards to increase the thickness of the crown. Ameloblasts at the crown's lateralities begin later, and the ameloblasts at the cervix start last. However, they are all active for about the same amount of time of matrix secretion. The odontoblasts begin at the same point and move inwards. During the maturation phase, ameloblasts regress, the accumulated enamel matrix proteins are cleaved, and apatite crystallites are formed (Hillson, 2005, Lacruz et al., 2012, Maas and Dumont, 1999, Nanci, 2018).

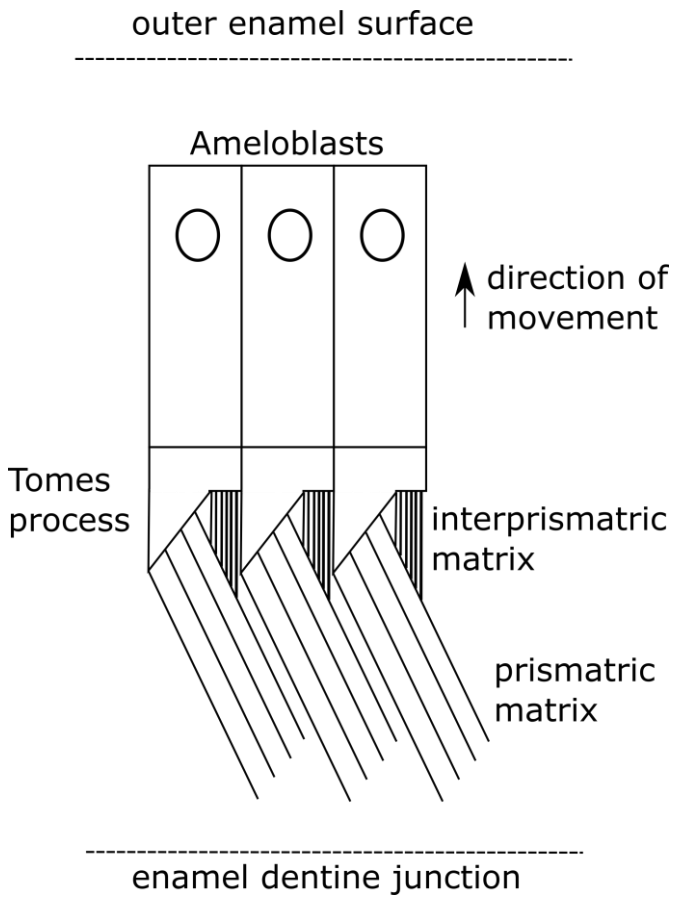

Figure 4 Ameloblasts during enamel secretion. Tomes processes secrete prismatic enamel matrix at the distal end and interprismatic enamel matrix at the proximal end.

Human tooth development takes place over the course of years. As mentioned above it starts during embryogenesis and ends with the eruption of the third molar at 16 to 23 years of age (AlQahtani et al., 2010). During that time the development starts and ends at different ages, depending on the developing tooth type. All deciduous teeth start their development in uterus. However, the main focus here is on the development of permanent teeth.

The development of permanent teeth begins with the first molar around birth. The second tooth to develop is the central incisor and lateral incisor of the mandible at around three months of age. This is followed by the canine at ten months and the lateral incisor of the maxilla, followed by the third premolar at 18 months and the fourth premolar at 24 months of age. The second molar starts the development around seven years of age and the third molar at around eigth (AlQahtani et al., 2010, Logan and Kronfeld, 1933).

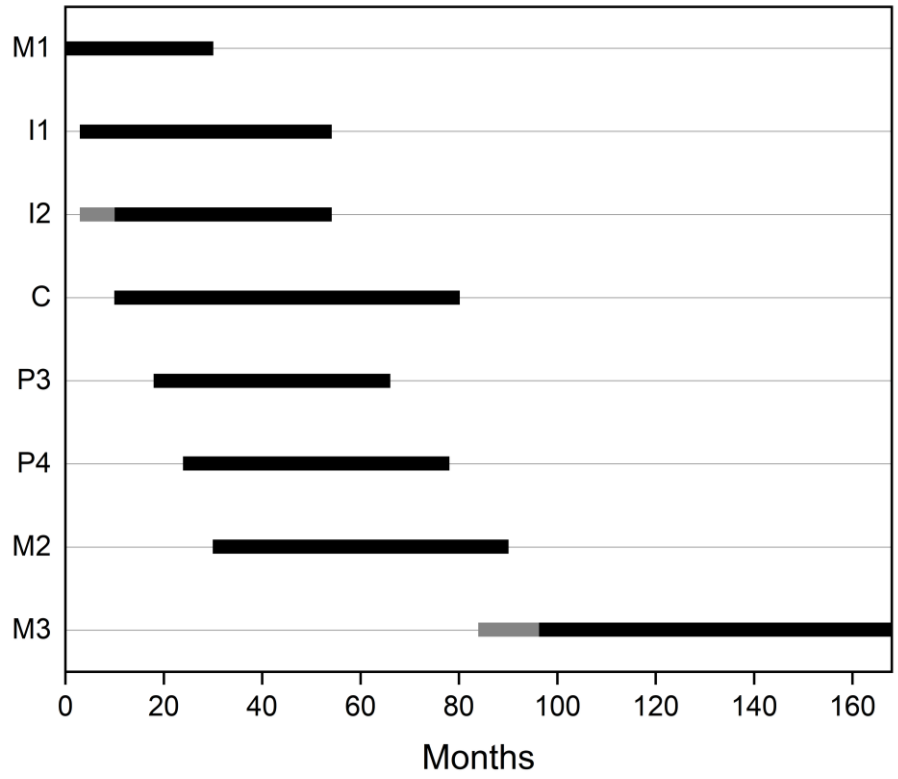

Figure 5 Average Crown formation times of permanent teeth after (AlQahtani et al., 2010) and (Logan and Kronfeld, 1933). M1 (first molar), I1 (central incisor), I2 (lateral incisor), C (canine), P3 (third premolar), P4 (fourth premolar), M2 (second molar), M3 (third molar). Grey bars show a different beginning in the mandible and maxilla. The development of the lateral incisor starts around three months in the mandible and at ten months in the maxilla. The third molar of the maxilla starts at seven years, whereas the third molar of the mandible usually starts at around eight years of age.

The completion of the dental crown of permanent teeth varies between 30-36 months in the first molar. Both incisors are completed at around four to five years of age. The premolars end their development between five and seven years followed by the second molars at seven to eight years. The third molars vary in their developmental time and therefore complete the crown from 16 up to the mid-twenties.

Table 1 Average crown formation times of permanent teeth from begin of calcification until of the crown formation. M1 (first molar), I1 (central incisor), I2 (lateral incisor), C (canine), P3 (third premolar), P4 (fourth premolar), M2 (second molar), M3 (third molar). Values combined from (AlQahtani et al., 2010) and (Logan and Kronfeld, 1933).

Tooth type	Start of calcification	End of crown formation
M1	Birth – 4.5 months	30-36 months
I1	3-4 months	4-5 years
I2	Maxilla: 10-12 months Mandible: 3-4 months	4-5 years
C	4-5 months	6-7 years
P3	18-24 months	5-6 years
P4	24-30 months	6-7 years
M2	30-36 months	7-8 years
M3	Maxilla: 7-9 years Mandible: 8-10 years	N/A

2.5 Tooth enamel structures

The basic structures of the enamel are prisms. These structures developed from the prismless enamel types in more primitive enamel and are defined as bundles (prisms) of carbonated apatite crystallites that are elongated and oriented in the same direction. Prisms are around 5 to 6 µm in diameter and extend without interruption from the enamel-dentine junction (EDJ) to the outer enamel surface. Furthermore, they are separated from other prisms by the interprismatic enamel or a prism sheath, which are planar crystallite discontinuities resulting from the sharp break between the proximal and distal end of the Tomes process. Compared to the crystallites from the prism, they show a different orientation (Dean, 2012, Mao et al., 2015). The dimension of a typical crystal in a prism lies around 50 nm in width and 10 µm in length (Beniash et al., 2019). While prisms run from the EDJ to the outer enamel surface they do not run in a straight line but oscillate in horizontal planes, which are approximately perpendicular to the longitudinal axis of the tooth (**Figure 6**). From one layer to the next, the prisms oscillate out of phase. The oscillation amplitude of humans is highest in the enamel dentine interface and decreases towards the enamel surface so that the prisms are almost linear. Usually, the prisms hit the enamel surface at right angles or a slight angle (Dean, 2012, Schwarzbach et al., 2010).

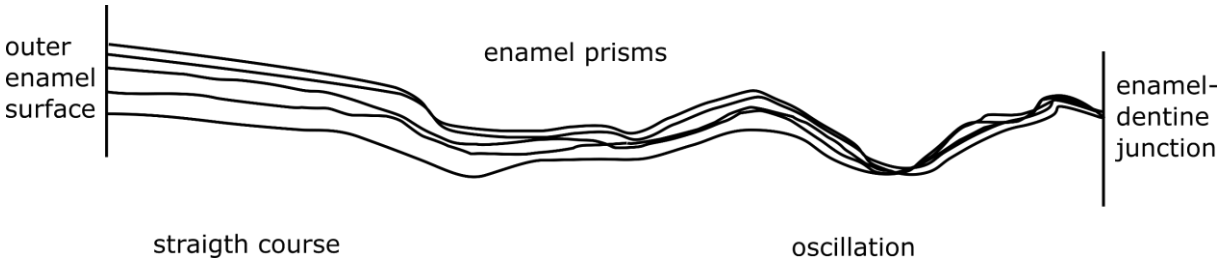

Figure 6 Course of a bundle of prisms. Beginning at the enamel-dentine junction they oscillate in a sinusoidal wave-like form. When reaching the outer enamel surface the prisms are almost linear. Adapted from (Tafforeau et al., 2012).

These sinusoidal wave-like forms of the prisms produce an additional cyclic variation passing down the crowns lateralities. This phenomenon is called decussation and can be seen by the naked eye in the Hunter-Schreger bands (HSB, **Figure 7**). In longitudinal tooth cuts, groups of prisms in a different point of their undulation are shown by light and dark bands. These bands appear this way depending on how the light hits the prism layer. If the layer is hit at right angles to the plane of the longitudinal cut, these prism groups appear darker (diazones). Whereas if the layer is hit parallel to their course, they show up bright (parazones) (Hillson, 1996, Myoung et al., 2009, Wood, 2011). The undulating arrangement of prisms and the connection between horizontal layers among themselves prevents the prisms' separation from each other under load as well as the splintering of enamel. Furthermore, the enamel must cover a larger area on the tooth surface rather than at the EDJ. Since the cross-section of the enamel prisms to the tooth surface does not increase, a larger enamel surface can only be achieved by the prisms hitting the tooth surface at an oblique angle (Schwarzbach et al., 2010).

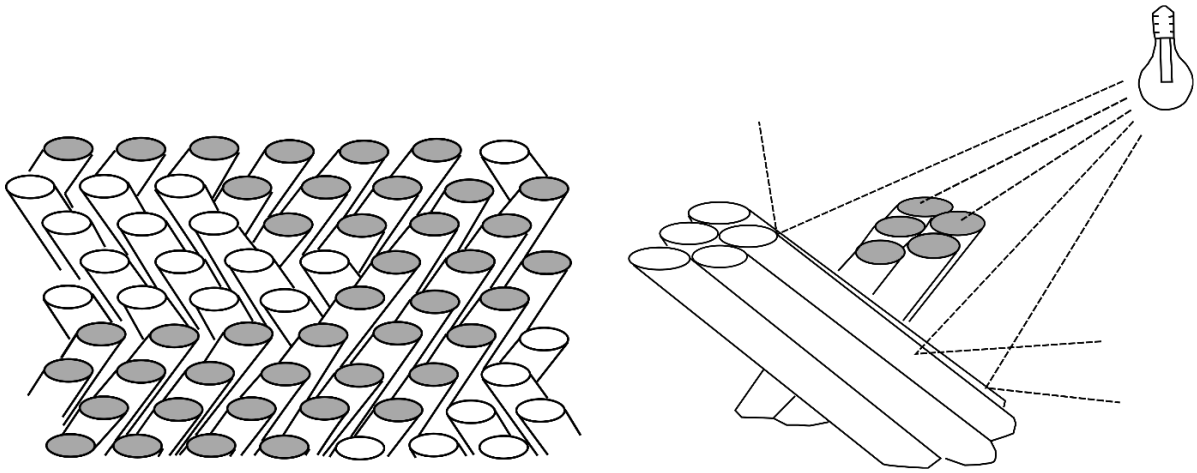

Figure 7 Hunter-Schreger bands appear light or dark, depending on the angle at which the light hits the prisms of different orientations. Diazones appear dark, whereas parazones appear bright. Adapted from Koenigswald and Pfretzschner (1987).

Periodic increments are formed due to biological rhythms (Bromage, 1991, Bromage et al., 2009, Smith, 2006). Ameloblasts secrete enamel in a daily manner, which creates incremental markings along the length of the prism, the so-called cross striations (CS). They represent the amount of enamel deposited in one day (Antoine et al., 2009, Lacruz et al., 2012). This rhythm has been examined experimentally in several studies with injected markers in laboratory animals and macaque dentitions (Bromage, 1991, Mimura, 1939, Molnar et al., 1981, Smith, 2006). In a microscopic image, the CS appear as two parts, light and dark. Both parts together show the thickness of enamel secreted in a single day. By counting these, they can be used to determine the daily secretion rate (DSR) or the crown formation time (CFT) (Dean, 2009, Dean, 2012, Mahoney, 2008, Reid and Dean, 2006).

Another periodic increment is the striae of Retzius or Retzius line (RL). These lines also appear periodically, but counts of CS between adjacent lines reveal a longer rhythm of four to ten days. The rhythm can vary between individuals but remains constant in one individual (Bath-Balogh and Fehrenbach, 2011, Reid and Ferrell, 2006, Smith, 2006). When well-developed RL meet the surface, a shallow depression, a perikymata pit can be seen. The RL are not equally distinct in all areas. They are particularly indistinct under the cusps and become clearer towards the sides. They run concentrically, one above the other at the top of the cusp. On the sides of the cusp toward the cervix, they run parallel to each other from the EDJ to the surface (Hillson, 2014).

Dental enamel can be very sensitive to physiological and environmental changes, and, therefore, amelogenesis can be disrupted by systemic external disturbances, which leads to permanent enamel defects. These stressors are recorded as accentuated lines (AL) (Nava et al., 2019). Unlike intrinsic rhythm-related incremental features, these lines are associated with non-specific stressor events. One well-known example is the neonatal line, which forms in teeth just before, during, and immediately after birth. Accentuated lines can sometimes be observed alongside enamel hypoplasia, but they may also occur without any surface indications of developmental stress (Wood, 2011). Metabolic disturbances resulting from various stresses have been linked to several childhood morbidities, encompassing conditions such as malnutrition, low birth weight, maternal infections during pregnancy, diseases, and undernourishment during the weaning stages, as well as common febrile childhood illnesses (Birch and Dean, 2014, Hillson, 2014, Schultz et al., 1998, Witzel et al., 2008).

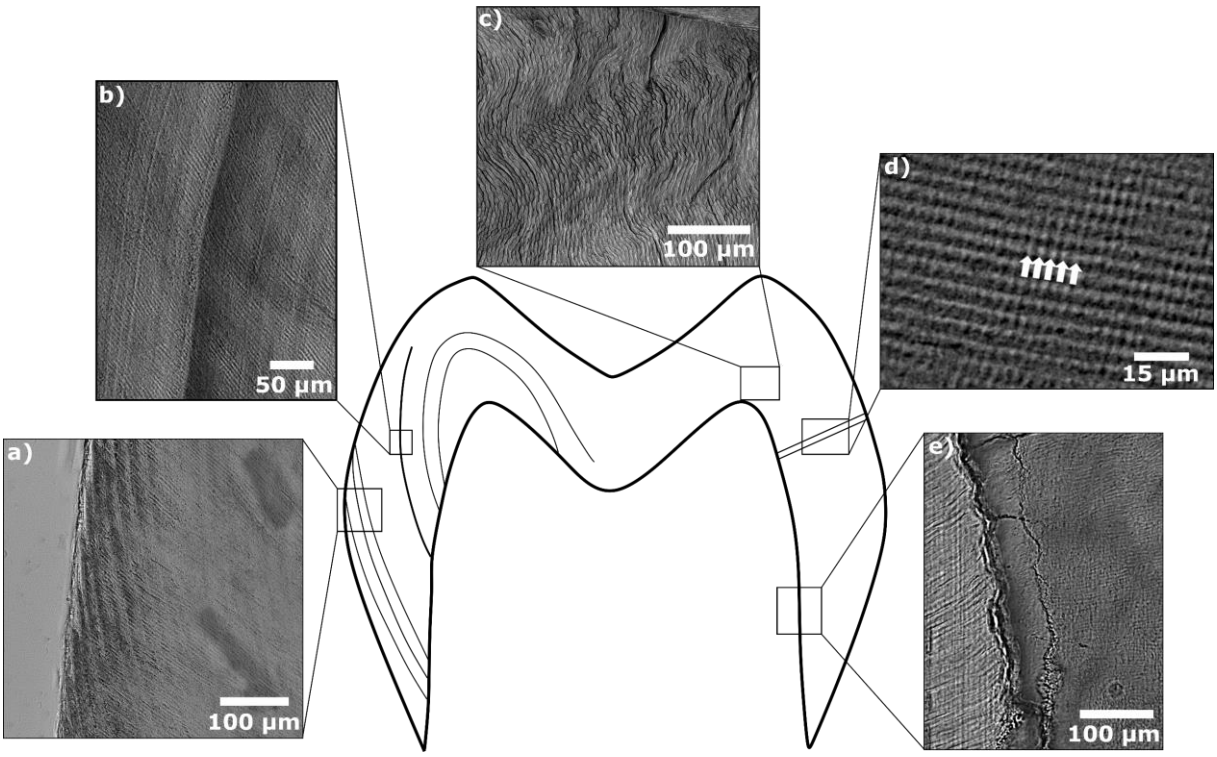

Figure 8 Overview of enamel microstructures. Depicting a) striae of Retzius (RL), b) accentuated lines (AL), c) decussation of enamel prisms, d) cross striations (CS) and e) the enamel-dentine junction (EDJ).

2.6 Chemical composition of teeth

Teeth consist of different components: The tooth crown is made of highly mineralised enamel which envelops the softer dentine. Dentine comprises 70-75% calcium phosphate, 5-10% water and 20% organic matter. Dental enamel, on the other hand, is one of the hardest materials in the mammalian body. It consists of 96% calcium phosphate, 3% water and 1% organic matter (Dorozhkin and Epple, 2002). It is built from carbonated hydroxyapatite crystallites. The crystallographic nature is based on hydroxyapatite with some structural substitution of the dominant phosphate (PO_4^{3-}) ions by carbonate ions (CO_3^{2-}) (Daculsi et al., 1990, LeGeros, 1981, LeGeros et al., 1968). This biologically altered apatite is often called bioapatite. It contains between 3 wt% and 7 wt% carbonate (Dorozhkin and Epple, 2002). Enamel is a dense and compact tissue with minimal pore space, featuring a distinct prismatic microstructure and long hydroxyapatite crystallites measuring over 1 µm. Its compact nature contributes to its exceptional hardness and resistance to geochemical alterations. It also shows low susceptibility to structural changes related to diagenetic origin. On the other hand, dentine is a more porous tissue, containing smaller crystallites measuring less than 0.1 µm and a higher proportion of organic matter (collagen). Due to its porosity and organic content, dentine is comparatively less resistant to geochemical alterations than enamel (Kohn et al., 1999, Tabuce et al., 2007). However, these different properties complement each other very well. The hardness of enamel withstands chewing forces, while the elasticity of dentine protects enamel from fracture and supports the tooth structure (Maas and Dumont, 1999).

2.7 Fluoride in dental care

Caries is a widespread dental condition affecting adults and children worldwide (Fejerskov et al., 2015, Listl et al., 2015, Meyer et al., 2018). Several established methods exist to prevent this disease effectively. One factor in preventing caries is maintaining a diet with reduced sugar intake, as sugar consumption contributes to its development (Sheiham and James, 2015).

In addition to dietary adjustments, implementing various preventive strategies can make a substantial difference in caries prevention at home and under professional care. To control

plaque, chemical compounds like chlorohexidine or cetylpyridinium chloride can be used (Cieplik et al., 2018, Kensche et al., 2017, Marsh, 2012, Meyer and Enax, 2019). Regular plaque removal through consistent tooth brushing, professional tooth cleaning, and flossing are also essential (Needleman et al., 2015, Terezhalmy et al., 2008, van Loveren, 2013).

Moreover, remineralising agents are another valuable method for preventing caries (Fejerskov et al., 2015). These agents help to strengthen and repair weakened enamel, protecting teeth from further damage.

Human tooth enamel consists of the inorganic mineral hydroxyapatite ($Ca_5(PO_4)_3OH$), with minor ionic substitutions, commonly referred to as "bioapatite" (Dorozhkin and Epple, 2002). As an acid-soluble mineral, hydroxyapatite is vulnerable to erosion caused by acidic agents, including those secreted by bacteria found in dental caries (Epple et al., 2022).

To increase tooth remineralisation while minimising demineralisation, various products based on fluorides and calcium phosphates are utilised. Among these remineralisation agents, fluoride is the most commonly applied (Fejerskov et al., 2015, van Loveren, 2013). It is incorporated into different dental products such as mouthwashes (Marinho et al., 2016), toothpastes (Walsh et al., 2019), gels (Marinho et al., 2015), and varnishes (Marinho et al., 2013) in varying concentrations to prevent caries effectively (Zanatta et al., 2020).

Oral care products encompass a range of fluoride sources, including sodium fluoride (NaF), sodium monofluorophosphate (Na_2PFO_3), tin(+II)fluoride (SnF_2), and amine fluorides ($R_4N^+F^-$) (Epple and Enax, 2018, van Loveren, 2013). In Germany, fluoride mouthwashes for adults typically contain around 250 ppm fluoride (e.g. SENSODYNE Cool und Fresh, GSK GmbH, 217 ppm F^-) while fluoride toothpaste for adults typically has 1450 ppm fluoride (e.g. Colgate Total Original, Colgate-Palmolive, 1450 ppm F^-) (both considered as cosmetic products for daily use). However, products with higher fluoride concentrations, classified as drugs, are used in special cases. For example, fluoride gels contain 12,500 ppm fluoride (e.g. Elmex Gelée, CP-GABA GmbH, 12,500 ppm F^-) and are applied once per week, while fluoride varnishes (applied approximately once or twice per year) may contain even higher fluoride concentrations, varying by manufacturer, such as 22,600 ppm fluoride (e.g. Profluorid® Varnish, VOCO GmbH, 22,600 ppm F^-) (Amaechi et al., 2019, Scholz et al., 2019).

It is essential to be aware that the presence of calcium-containing abrasives, like calcium carbonate, in toothpaste can reduce the availability of fluoride due to the precipitation of calcium fluoride (CaF_2) (Eggert and Neubert, 1999, Enax and Epple, 2018). Various modes of action of fluorides on teeth have been proposed, including the formation of protective layers such as fluorapatite ($Ca_5(PO_4)_3F$) and calcium fluoride (CaF_2) (Buzalaf et al., 2011, Cate, 1997, Fejerskov et al., 2015). However, it should be noted that fluoridation is limited to the outermost surface of the tooth (Badiola et al., 2015).

Despite the protective effects of fluoride, there have been discussions about whether a very thin fluoride-rich layer can adequately shield teeth from acid attacks (Mueller et al., 2010). While fluoride remains a valuable tool in caries prevention, ongoing research and reviews aim to further our understanding of its precise mechanisms and effectiveness in promoting oral health.

3 Materials and Methods

3.1 Materials

3.1.1 Recent human tooth sample for comparison

Recent human teeth were obtained from different private sources and were used to establish a comparison for the studied teeth. The structure and chemical composition of unaltered human teeth with known origin was conducted on various teeth. Three of these teeth were used as an example for this work (**Table 2**).

Age and sex are random, as both factors have no influence on the analyses performed. Only the condition of the teeth (minor wear, no caries) was a selection criterion.

Table 2 Recent human tooth sample used for comparison.

Sample number	Sex	Age at extraction	Tooth type	Source
Hs01	f	17	LLM3	Private practice
Hs14-2	N/A	N/A	LRM1	Private practice
Hs18	m	22	LLM3	Private donation

3.1.2 Medieval human tooth samples from Gevensleben

3.1.2.1 Site

The Gevensleben site is located approximately 37 km southeast of Braunschweig in Lower Saxony, Germany. It falls within the fertile Loess region, known for its favourable living conditions for various communities during prehistoric times. The area's agriculture thrived, enabling people not only to survive but also to engage in increasingly intensive agricultural activities in the centuries following the Roman Iron Age (Wieckowska-Lüth and Heske, 2019). During the medieval period (700-1000 AD), the site served as an early Christian cemetery (Geschwinde and Röckelein, 2018, Heske, 2018). Modern excavations were conducted in March 2016, covering an area of approximately 400 m^2. The excavation yielded a total of 63 burials, oriented in the west-east or northwest-southeast direction. The excavated individuals include 17 males, 21 females, 1 of unknown sex, 4 adolescents, and 20 children, representing the rural population of the Braunschweig area. Detailed analyses of the archaeological and

anthropological findings have been conducted and are published in the summary work by Grefen-Peters (2018, 2020). The Department of Prehistory and Early History at Georg August University Goettingen houses the skeletal series.

3.1.2.2 Teeth

The teeth selected for preliminary examination by Scanning electron microscopy (SEM) and Energy dispersive X-ray spectroscopy (EDX) were first and third molars of three male individuals (11 LLM1, 18 LLM3 and 41b LRM1; marked with asterisks in **Table 3**). These were not used in the subsequent enamel histology study.

The sample used for the enamel histology study consisted of 27 teeth obtained from ten individuals, as shown in Table 1. To ensure an adequate amount of enamel for examination, two to three teeth were selected per individual based on their state of preservation. Priority was given to teeth with minimal abrasion.

The selection primarily focused on the first to third lower molars due to their potential to provide insights into a child's development over a significant period. This decision was made to maintain consistency across the sample. In cases where these molars were missing or poorly preserved, upper molars, premolars, or, in exceptional cases, a canine tooth were chosen as substitutes. However, it is important to note that the main objective of the study was to cover the period from birth to puberty.

Both male and female individuals were included in the study without differentiation, as previous research conducted by Bernatzky et al. (2018) suggested similar living conditions for both sexes.

Table 3: List of all individuals and teeth analysed in this study U (upper), L (lower); R (right), L (left); C (canine), P3 (third premolar), P4 (fourth premolar), M1 (first molar), M2 (second molar), M3 (third molar). Asterisks mark the teeth used for SEM, EDX and PXRD and are not included in histological analyses.

Individual number	Sex	Age at death (years)	Teeth analysed
11	m	N/A	LLM1*
12	m	35-40	LLM2, LLM3
18	m	N/A	LLM3*
22	m	45-55	LLM2, LLM3
30	f	55-65	LLC, LLP3, LRM3
33	f	50-60	LLM1, LLM2, LLM3
38a	f	25	URM1, URM2, URM3
39	f	50	LRP3, LRP4, ULM2
41b	m	16-17	LRM1*
43	f	19-20	LLM1, LLM2, LLM3
45	f	20	LLM1, LLM2, LLM3
53	m	55-65	LLM2, LRM3
63a	f	40-50	LLP4, LLM1, LLM2

3.1.3 Recent Human tooth samples for fluoride immersion

A total of 16 extracted teeth from 11 patients were used for these experiments. The teeth were obtained from private dentistry practices after medically caused extraction. The teeth were cleaned and dry stored. The known patient information included their regular dental care habits. The selection of the teeth was based on their preservation state. The teeth were mostly free of caries and had no dental fillings. The tooth types did not matter for these experiments since only the enamel and its composition were analysed.

For immersion, solutions with different potassium fluoride concentrations and pH values were made. To adjust the pH of around 4.6 to 4.7, a citrate buffer (citric acid 54.1 mM/sodium citrate 46 mM) was used. Potassium fluoride, sodium citrate dihydrate and citric acid were used. Distilled water served as a solvent in all cases. To mount the teeth on the sample holder, the adhesive Crystalbond™ 509 was used.

3.1.4 Chemicals

Table 4 Chemicals used in experiments conducted in this work.

Chemical	Manufacturer
Acetone (99.5%)	Bernd Kraft, Duisburg, Germany
Acheson Silver DAG	Plano GmbH, Wetzlar, Germany
Citric acid (99.5%)	Honeywell-Fluka, Schwerte, Germany
Crystalbond™ 509	Plano GmbH, Wetzlar, Germany
Diamond Suspension polycrystalline 0.1 µm	ATM Qness GmbH, Mammelzen, Germany
Diamond Suspension polycrystalline 1 µm	ATM Qness GmbH, Mammelzen, Germany
Diamond Suspension polycrystalline 3 µm	ATM Qness GmbH, Mammelzen, Germany
EpoThin™ Hardener 2	Buehler Ltd., Illinois Tool Works Inc., Lake Bluff, IL, USA
EpoThin™ Resin 2	Buehler Ltd., Illinois Tool Works Inc., Lake Bluff, IL, USA
Hydrochloric acid (37%)	VWR International, Rosny-sous-Bois, France
Potassium fluoride (99%)	Acros Organics—Fisher Scientific, Schwerte, Germany
Sodium citrate dihydrate (99%)	AppliChem, Darmstadt, Germany

3.2 Methods

3.2.1 Scanning electron microscopy (SEM)

Scanning electron microscopy (SEM) is used to visualise the surface of a sample by scanning it with a focused beam of electrons, creating images with magnifications ranging from a few times to several hundred thousand times. This method can be used to analyse samples with structures smaller than half the wavelength of visible light (400-700 nm) and are therefore not suitable for light microscopy due to the Abbé diffraction limit (Equation 1) with the resolution *d*, the wavelength *λ*, the refraction index of the immersion medium *n*, the aperture angle *α*, and numerical aperture *NA*.

$$d = \frac{\lambda}{2n \bullet sin\,\alpha} = \frac{\lambda}{2 \bullet NA} \quad (1)$$

The SEM operates in vacuum to avoid any potential interaction of the electron beam with air. The initial electron beam of primary electrons (PE) is generated by using a tungsten filament or a field emission source. The beam then passes through a series of electromagnetic lenses to be focussed and projected onto the sample in a scanning pattern. As the electron beam interacts with the atoms within the sample, it creates several signals. The secondary electrons (SE) are low-energy electrons that are inelastically scattered and emitted from the surface (**Figure 9 a**). The backscattered electrons (BSE) are highly energetic electrons originating from the primary electron beam and are elastically scattered within the sample (**Figure 9 b**). A detector located at an angle above the sample collects the emitted electrons, amplifies their intensity and converts the signal into an electrical signal. The electrical signals are then processed and used to generate an image of the sample on a monitor.

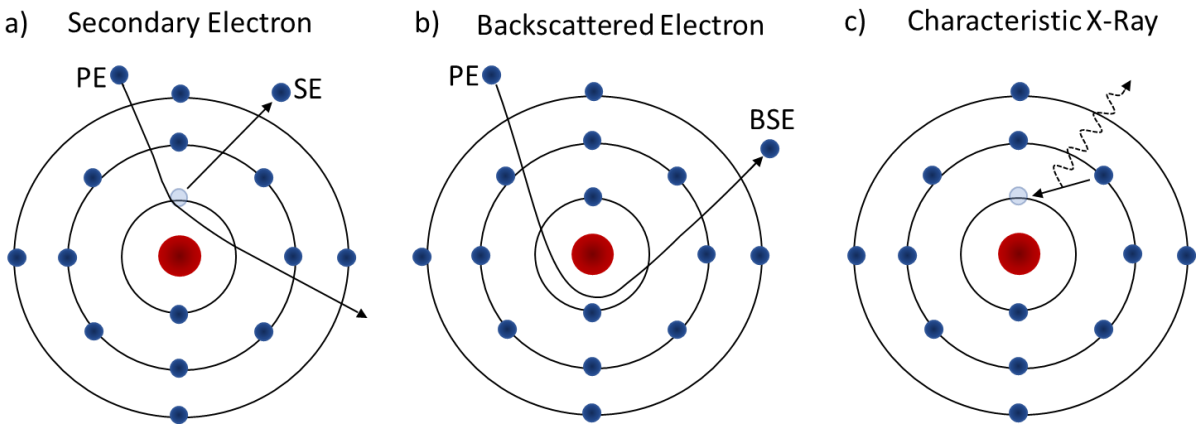

Figure 9 Illustration depicting electrons generated through Scanning Electron Microscopy (SEM). **a)** Secondary electrons inelastically scattered and emitted**. b)** Backscattered electrons elastically scattered. **c)** Energy release in form of characteristic X-rays. PE= primary electrons, SE= secondary electrons, BSE= backscattered electrons.

The secondary electrons are most commonly used to yield topographic images of the sample. The contrast of the picture depends on the amount of SE reaching the detector from certain parts of the surface of the sample. The amount varies strongly dependent on the topography. SE emitted on edges of the surface are less likely to be reabsorbed by the sample material and therefore reach the detector in larger amounts resulting in a brighter spot on the image.

The sample usually needs a special preparation for this method to prevent charging effects caused by the electron beam. Depending on the material, it needs to be conductive itself or coated by a conductive material such as gold, palladium or carbon (Goldstein et al., 2017).

All scanning electron microscopy examinations were performed with an Apreo S LoVac instrument (Thermo Fisher Scientific, Waltham, MA, USA).

3.2.2 Energy-dispersive X-ray spectroscopy (EDX)

Energy-dispersive X-Ray spectroscopy (EDX) is a technique for quantitative and semi-quantitative analysis of the elemental constitution of a solid sample. It provides information on the elemental composition and distribution within a sample.

A high-energy electron beam hits the atoms in the sample, releasing electrons of the inner shell from the atoms (**Figure 9 a**). This creates vacancies in the inner shells, which are then filled by the electrons from the outer shell. In general, electrons located further away from the atom core exhibit higher values of potential energy than those on lower shells. This is why any vacancies on the inner shell of an atom are instantly targeted by electrons in higher shells. During the transition of the electrons, the difference in potential energy is emitted in the form of X-ray photons.

The energy and the number of released X-ray photons can be measured by an X-ray detector which is positioned close to the sample. The energy of these X-rays is characteristically for each element because of their individual orbital energy values and can therefore be used for identification. When the X-rays hit the detector, they interact with the detector material and generate electrical pulses proportional to their energy. These electrical pulses are processed and converted into an energy spectrum, which represents the distribution of X-ray energies detected. To identify the elements, this spectrum is compared to known X-ray energy signatures of different elements in a database. The intensity of the individual peaks in the spectrum corresponds to the relative abundances of the detected elements, so it is possible to determine the relative concentration or weight percentage of the present elements.

Various analyses in combination with SEM images were used: EDX spectrum, EDX line scan for elemental composition along a pre-determined line, and EDX mapping for an elemental distribution in a pre-determined area (Goldstein et al., 2017).

Energy-dispersive X-ray spectroscopy (EDX) was performed with an UltraDry EDS detector, Thermo Fisher Scientific (Thermo Fisher Scientific, Waltham, MA, USA).

3.2.3 X-ray powder diffraction (PXRD)

X-ray powder diffraction (PXRD) is a method to determine the crystallographic structure of isotropic samples such as crystalline powders. It utilises X-ray with wavelengths ranging from 0.1 to 100 Å. The wavelength of X-rays is in the same order of magnitude as interatomic distances, enabling the determination of atomic structures in crystalline materials. By analysing the angles and intensities of the diffracted X-rays, information such as atomic

positions, bond lengths, and angles within the unit cell can be obtained. This analysis is based on the principle of constructive interference of monochromatic X-rays and a crystalline sample.

The X-rays are generated by an X-ray tube, which emits X-rays with a specific wavelength or energy. When the radiation interacts with the crystal lattice of the powdered sample, there will be constructive interference under certain conditions according to Bragg's law:

$$n \cdot \lambda = 2d \cdot sin\theta \tag{2}$$

where n is a positive integer, λ is the wavelength, d is the spacing between crystal lattice planes, and θ is the diffraction angle. As the only variable in the Bragg equation, θ is responsible for conditional constructive interference, which can be observed. Constructive interference of diffracted radiation occurs only if the Bragg equation is met. For this, the path difference $2dsin\theta$ of two individually diffracted X-rays must equal to an integer multiple of the wavelength.

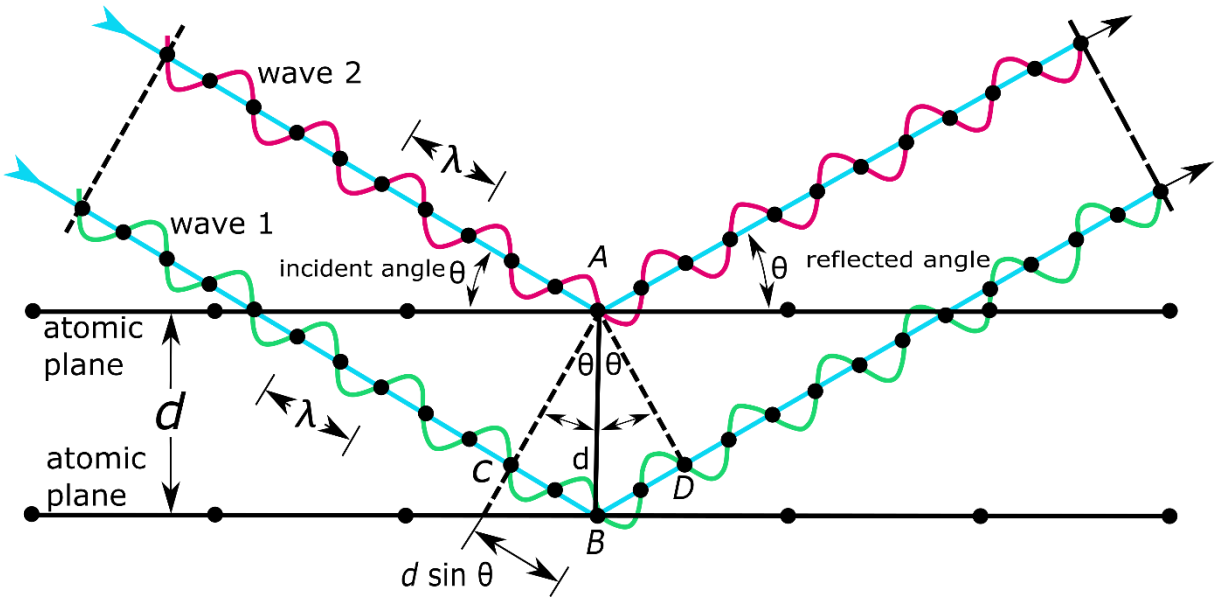

Figure 10 Bragg diffraction in a crystal. Waves 1 and 2, in phase, interact with atoms A and B, respectively, in a crystal with lattice planes separated by distance d. The diffracted angle θ is equal to the incident angle θ. To stay in phase, the path length CBD must be an integer multiple (n) of the wavelength (λ). By geometry, CB and BD equal d times the sinus of θ, or $d\ sin\ \theta$. Thus, $n\ \lambda = 2d\ sin\ \theta$, known as the Bragg law.

Following the entrance into the sample, the X-rays get diffracted at the crystal lattice planes. A detector captures the diffracted X-rays at certain angles where constructive interference occurs, which are then converted into electrical signals and processed to obtain a diffraction pattern. This pattern consists of a series of reflexes representing the different crystal lattice planes within the material. The diffraction pattern is analysed to obtain information about the crystal structure. The positions and intensities of the reflexes are used to determine the lattice parameters, the crystal symmetry and the orientation of the crystal planes in the material. This information is compared to known reference patterns to identify and characterise the sample material (Dinnebier and Billinge, 2008).

All X-ray powder diffractograms were measured by a Bruker D8d Advance powder diffractometer (Bruker Corporation, Billerica, MA, USA) in Bragg-Brentano reflection mode with Cu K_α radiation (λ = 1.54 Å). For qualitative analysis, the Bruker software Diffrac.suite Eva (V6) V1 and the diffraction pattern of synthetic hydroxyapatite (ICDD PDF No. 000-09-0432) were used as a reference.

3.2.4 Optical microscopy

Optical Microscopy, also known as light microscopy, utilises visible light and a combination of lenses to magnify and resolve fine details of the sample under investigation. It allows the visualisation and study of various specimens, including cells, tissues, microorganisms, and histological samples. One commonly used technique is bright-field microscopy, which was also used in this work.

In bright-field microscopy, a halogen or LED lamp is employed to illuminate the sample with a bright and uniform light, ensuring an even and diffused illumination. This method relies on differences in light absorption, reflection and scattering between the sample and the surrounding medium to create a contrast. Objective lenses collect and focus the transmitted light and come in different magnifications, typically ranging from 4x to 100x. The choice of objectives determines the resolution and image quality.

A condenser lens system collects and focuses light onto to specimen and helps to ensure a uniform illumination and an optimal contrast. Adjusting the condenser lens controls the amount of light passing through the sample, affecting brightness and contrast in the image.

The sample is placed on the specimen holder, such as a glass slide, which is then attached to the stage. The stage serves as a platform which is vertically adjustable for focussing and can be controlled horizontally in x and y directions to position the sample. Classical light microscopes have ocular lenses to observe the magnified image of the specimen produced by the optical lens. But modern microscopes can be fully or partially digital, so the image can be viewed on a monitor. This enables capturing of high-resolution images and videos of the specimen for documentation and analysis. Image processing and analysis software can be used to enhance, measure, and quantify features in the acquired images (Girkin, 2019).

All light microscopic images were obtained using a Keyence BZ 9000 microscope (Keyence, Neu Isenburg, Germany) with an integrated digital camera.

4 Experimental

4.1 Recent Tooth

In addition to the studies on the historical teeth from Gevensleben and the recent teeth used for the fluoride immersion experiments, several recent teeth from different sources were used. As these were included for verification and comparison of the studies, they were treated the same way as the studied teeth. A detailed description of the procedure (SEM and EDX, histological thin sectioning, digital analyses and PXRD) can be found in the following subchapters.

4.2 Gevensleben

Thirty teeth from 13 individuals were used for this study. Two to three teeth were selected per individual based on their state of preservation. Priority was given to teeth with minimal abrasion.

All jaws were photographed before the teeth were removed. Then all extracted teeth were photographed from all sites (mesial, distal, lateral, buccal and occlusal). After that, all teeth were cleaned using demineralised water and an ultrasonic bath. Then they were again photographed from all sites.

The preparation process, which involved embedding the samples in epoxy resin and cutting them using a low-speed saw, remained consistent for all subsequent analyses.

4.2.1 Preparation for SEM analyses and histological thin sectioning

To prevent damage to the teeth in the following processing work, they were coated in Crystalbond™ 509. Crystalbond is heated in a petri dish on a heating plate until liquified. The tooth was submerged, covered entirely and placed on a silicon base for hardening, providing a flat underside for a more precise embedding.

The tooth was then embedded in epoxy resin in Buehler EpoThin™ 2 (Buehler Ltd., Illinois Tool Works Inc., Lake Bluff, IL, USA) to prevent it from breaking during cutting and for easier handling. For that, 1/3 of Buehler EpoThin™ 2 Hardener was mixed with 2/3 Buehler EpoThin™

2 Resin and thoroughly stirred. The tooth was placed in a silicon mould and aligned. The resin was then poured onto the tooth. If it moved during that process, it was realigned with a spatula. Curing the resin requires at least 9 hours, but it is best if the resin is cured for around 24 hours to be fully hardened.

The resin block with the tooth inside was removed from the silicon mould for further work. It was inspected for the best longitudinal cutting plane through the tip of a cusp. The mesiolingual cusp was chosen, but if that was not suitable for analysis, e.g. because of abrasion or splintering, a longitudinal cut of the mesiobuccal cusp was chosen instead. The bucco-lingual cutting plane was drawn onto the resin block with a waterproof pen. For cutting, the tooth was clamped in a specimen holder (Single Saddle Chuck, Buehler Ltd.) and aligned so that the previously drawn cutting plane was parallel to the edge of the holder. The holder was attached to a low-speed saw (Buehler IsoMet™ Low speed saw) and aligned so that the saw blade (4" IsoMet Diamond Wafering Blade 15HC, Buehler) was 300 µm away from the drawn plane (**Figure 11**). Due to the material loss caused by the thickness of the blade (300 µm), cutting right on the desired cutting plane is not recommended. Demineralised water was used as a lubricant for the cutting process. To prevent the tooth from splintering during cutting, the rotating speed was adjusted to 60-90 rpm. After the first cut, the cutting surface was polished with polycrystalline diamond suspension (1 µm) and demineralised water on a grinding and polishing machine (Saphir 520, ATM) with a polishing cloth (Epsilon, ATM) until the surface was free of scratches from the cutting process.

4.2.2 SEM and EDX

For the SEM analysis, the tooth was etched with 5% hydrochloric acid in water to increase the visibility of the ultrastructure of the dental enamel. For that, the tooth was immersed in the acidic solution for 15 seconds. After that, it was cleaned with demineralised water in an ultrasonic bath and dried afterwards. The epoxy block was electrically contacted on the specimen holder using a carbon adhesive band and grounded to the holder with conductive silver paint on the base of the block. However, they were not sputter-coated with a conductive metal as commonly used for SEM preparation to avoid an effect on the elemental composition.

The etched surface was then analysed using SEM images of the whole cutting surface, and details of the enamel and the ultrastructure were captured. Afterwards, the elemental composition was analysed by EDX. This initial work was done to rule out any change in the tooth before the histological examinations.

4.2.3 Histological thin sectioning

The histological thin sections of teeth were created by the following process. The low thickness of the section (around 100 µm) allows the detection of microscopic enamel defects.

The tooth was handled as described in chapter 4.2.1 but without SEM and EDX analyses. After polishing, the tooth was glued using Buehler EpoThin™ 2 with the cutting surface onto a microscopic slide that was cleaned with demineralised water. For the second cut, the slide was mounted on a vacuum specimen holder (Vacuum Chuck for glass slides, Buehler Ltd.). The holder was aligned on the saw so that the cut was made around 600 µm next to the slide. This distance was again chosen because of the loss of material due to the blade.

From the second cut (**Figure 11**), a section with a thickness of around 300 µm was received and ground down using silicon carbide grinding paper (P1200 and P2500; ATM) to a thin section with a thickness of around 100 µm. For this, the section was placed in a hand holder and ground to a thickness of about 200 µm using P1200 grinding paper. Afterwards, a finer-grained grinding paper (P2500) was chosen, and the section was ground until a thickness of about 100 µm was reached. Since the surface was scratched by cutting and grinding, the final step is polishing the section with diamond suspension (1 µm, ATM). A microscope and a calliper were used between steps to check for progress.

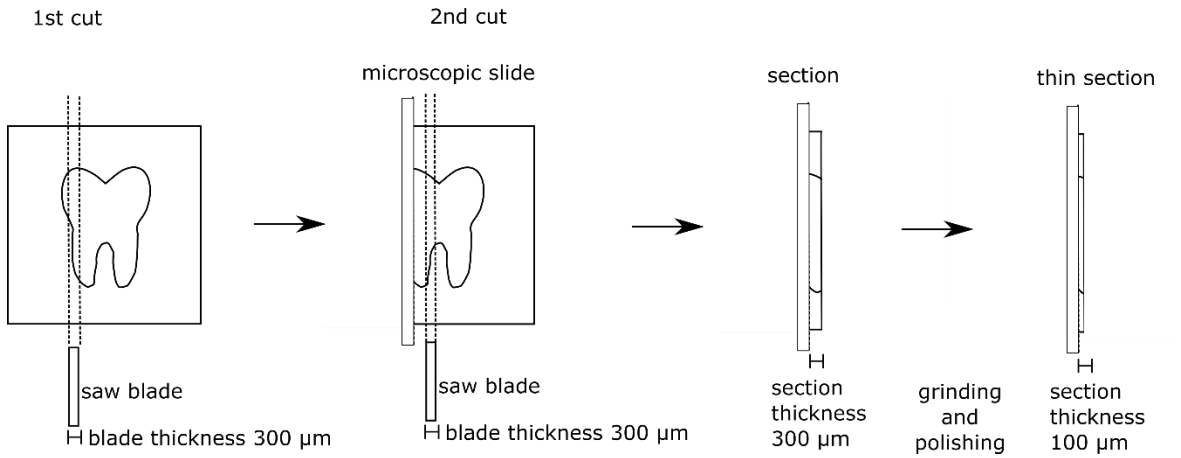

Figure 11 Process of thin sectioning. The first cut was made 300 µm next to the desired sectioning plane due to the thickness of the blade (300 µm) and the resulting loss of material. The specimen was then glued to a microscopic slide and cut for the second time 600 µm to the selected plane. The obtained section of 300 µm thickness was then ground and polished to a thin section of 100 µm thickness.

4.2.4 Digital analyses

A Keyence BZ 9000 light microscope with an integrated camera was used to digitise the sections. To get an overview of the whole crown, a magnification of 4x was used. Images for the chronology were taken in 20x magnification, and details for the cross striations (CS) analyses were captured in 40x magnification. The individual pictures were merged using the Image Composite Editor (ICE, Microsoft Research).

The histological analyses were done using Adobe Photoshop CS5 Portable software (Adobe Inc.). The studied structures were identified on the micrograph and were drawn in and measured.

At first, enamel and dentine were identified, and a line along the enamel-dentine junction (EDJ) was drawn to differentiate between those two parts.

The daily secretion rate (DSR) describes the amount of enamel matrix in micrometres (µm) that was secreted by the ameloblasts in 24 hours. The rate represents the distance between an enamel prism's adjacent cross striations (CS). To determine the DSR, areas where the CS could easily be detected were examined. The total length of the CS was measured and divided

by the number of CS (Smith, 2008, Wood, 2011). The tooth crown was divided into cuspal and lateral enamel, and both parts were again divided into inner, mid and outer parts (Dean, 2009). In each section, five locations were selected where the CS could be identified (Mahoney, 2011). The DSR was used as a basis for the other calculations.

The crown formation time (CFT) describes the time the tooth crown secretion takes to form the tooth crown. It is determined by the counts of CS and striae of Retzius (RL) in the enamel (Wood, 2011). The method by Dean (2012) was employed: A 200 µm long line was drawn along a prism at the dentine horn (Figure line AC). From the end of this line, another line along or parallel to RL was tracked until it reached the EDJ (**Figure 12** A to B). This procedure was repeated and continued until the end of the EDJ at the cervix of the tooth. Since the ameloblasts differentiate into active secretory cells along the EDJ from the tip of the dentine horn to the cervix at different rates, the triangular sections drawn are different in length. However, each segment is secreted in the same amount of time. With the DSR, the time required to secrete 200 µm of prisms could be calculated by division of 200 µm by the DSR. Since ameloblasts enlarge the thickness as well as the length of the tooth crown simultaneously, the same time was necessary to cover the distance along the EDJ (**Figure 12** A to B) as well as along the prism. With this, the triangular sections along the EDJ could be counted and multiplied with the time taken to cover an equal number of 200 µm prisms.

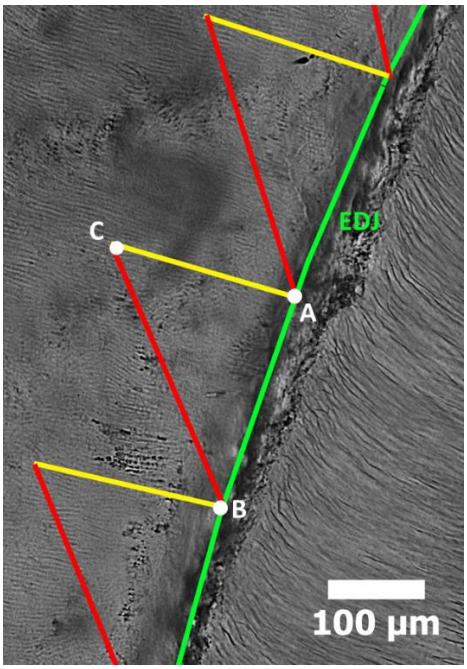

Figure 12 A 200 µm line (A to C, yellow) was drawn along a prism. A second line along or parallel to a striae of Retzius was drawn (C to B, red). The distance from A to C was covered at the same time as the distance from A to B.

As a last analysis, the AL were identified, and their course was tracked until they reached the EDJ. The length of the EDJ was measured beginning at the tip of the dentine horn up to the point where the AL met the EDJ. This length was then divided by the DSR, so the time of emergence of this AL could be calculated.

4.2.5 PXRD

Three teeth (33 LLM2, 45 LLM2 and 63a LLM2) were also analysed crystallographically via PXRD, for that one remaining half of the epoxy block was chosen and immersed in acetone so that the Crystalbond™ 509 was dissolved. Thereby the tooth was detached from the epoxy resin. The tooth enamel was then pulverised using a fine grinding device (Proxxon FBS 230/E), and the obtained powder was analysed via PXRD.

4.3 Fluoride immersion of recent teeth

The samples were randomly divided into five groups, with three teeth assigned to each group for the immersion experiment. The following solutions were made to simulate oral care products.

- 250 ppm potassium fluoride (KF) in water (pH = 5.85)
- 250 ppm potassium fluoride (KF) in citrate buffer (pH = 4.60)
- 18,998 ppm potassium fluoride (1 mol L^{-1} KF) in water (pH = 7.76)
- 18,998 ppm potassium fluoride (1 mol L^{-1} KF) in citrate buffer (pH = 4.70)
- fluoride-free citrate buffer (pH = 4.60)
- water (pH ca. 7; one tooth as control)

To prevent surface alteration or contamination after treatment, the teeth were mounted on the sample holder before immersion. The thermoplastic polymer Crystalbond™ 509 was used for this purpose.

The teeth were immersed for 1 min at 37° Celsius. The temperature was obtained with a water bath and ensured with a thermometer. After the immersion, the teeth were rinsed with distilled water and air-dried.

Prior to and after the treatment, the tooth surface morphology of each tooth was examined by SEM. The teeth were electrically contacted and grounded with conductive silver paint to avoid electric charge accumulation. However, they were not coated with a conductive metal as commonly done for SEM preparation in order to avoid an effect of the immersed elements.

The chemical composition, particularly the fluoride content, of the tooth surface was analysed using EDX. For this purpose, 5 to 10 randomly selected spots on the dental enamel surface were examined.

After the treatment with the fluoride solution, the tooth surface was analysed again for the surface morphology as well as the chemical composition at 5 to 10 randomly selected spots.

The effects of the immersion were statistically investigated using SPSS (IBM for Windows, version 26, Armonk, NY, USA).

5 Results and Discussion

5.1 Recent Human Tooth

A foundational context for the discussion and a comparison of the sample in this study was established by conducting all experiments with recent human teeth. The structure and chemical composition of unaltered human teeth with known origin is shown in the following as an example. These analyses were done on different recent human teeth, but only a selection for every analysis is shown due to similar results.

5.1.1 SEM

Teeth from individual Hs01 served as the basis for the SEM analyses. The enamel microstructure is depicted in **Figure 13**.

An overview of the longitudinal cut tooth crown is given in **Figure 13 a.** For this purpose, an SEM mode was employed, which scanned the entire sample at 40x magnification and combined the images to form a complete overview. The white part represents the dental enamel and the dark part in the middle shows the dentine. A crack runs from the enamel surface down through the dentine. This might come from the cleaning or cutting process, but it did not affect the analyses.

The typical human enamel structure is represented in **Figure 13 b** and **c**. As described in chapter 2.5, enamel prisms run parallel from the enamel-dentine junction to the outer enamel surface. During the course of that, they undulate up and down regularly while simultaneously following a long curve in the vertical plane of the section. See chapter 2.5 for a detailed description of the prism course and decussation.

The decussation can also be seen as Hunter-Schreger bands in **Figure 13 c** and **d.** These light and dark bands are also visible to the naked eye and result from the different orientations of the prisms. Depending on the light that hits a group of prisms, they appear as light bands (parazones) or dark bands (diazones) (Myoung et al., 2009, Wood, 2011).

Single prisms can be seen in **Figure 13 e**. The prisms are encased by interprismatic enamel, which shows a different orientation than the prismatic enamel. Nevertheless, they do not differ in the chemical composition. Both are made of elongated, carbonated hydroxyapatite crystallites (**Figure 13 f**) (Maas and Dumont, 1999, Mao et al., 2015).

All structures can be seen as described in the literature. This tooth was used as a reference for further investigations.

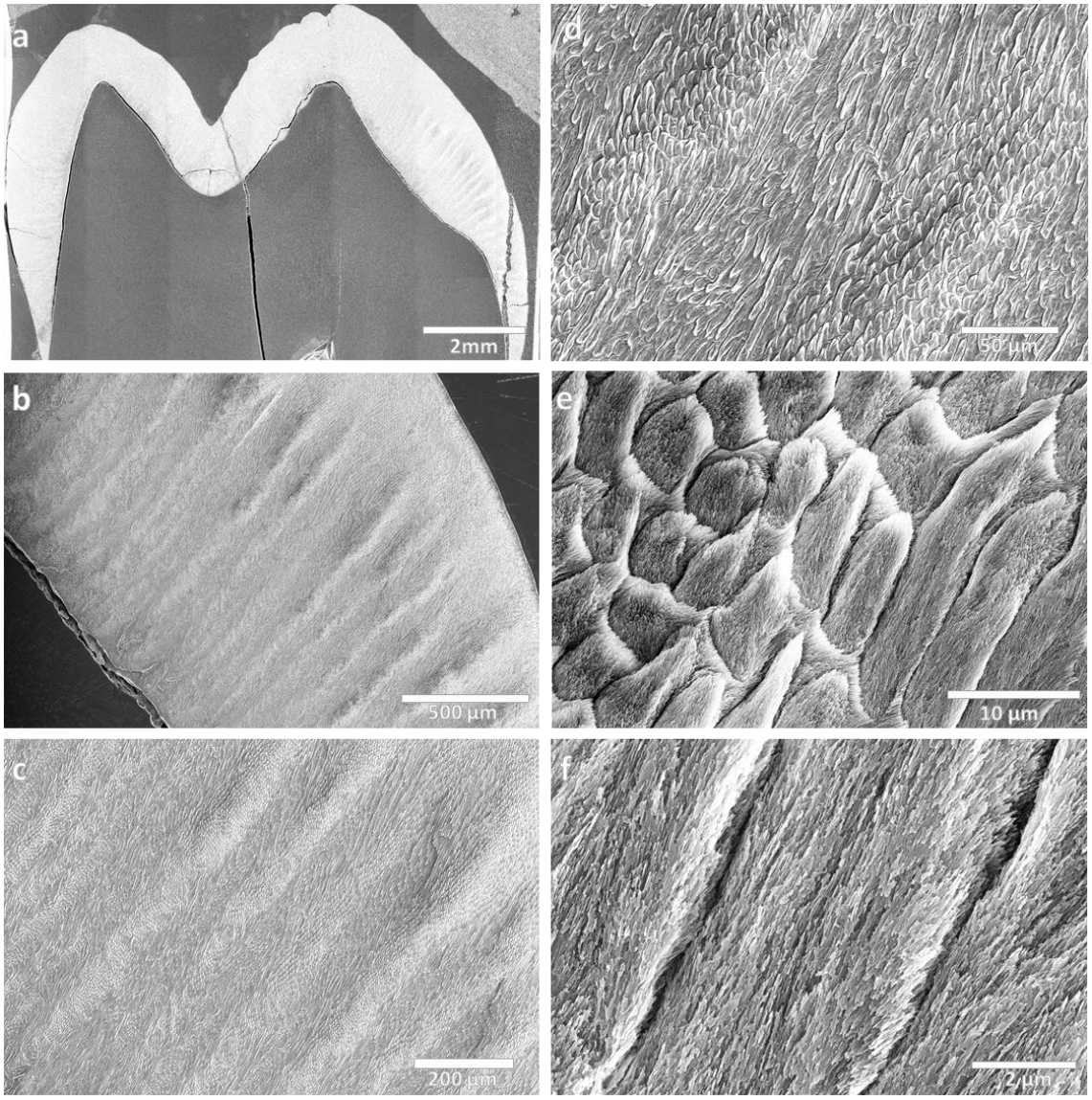

Figure 13 SEM images of the dental enamel microstructure of a recent human tooth (Hs01) at different magnifications. a) Tooth section of a whole tooth crown combined from single pictures at 40x magnification, b) dental enamel at 200x magnification, c) dental enamel at 400x magnification, d) Hunter-Schreger bands at 1.500x magnification, e) prisms with interprismatic enamel at 10.000x magnification, f) crystallites of enamel prism at 40.000x magnification.

5.1.2 EDX

The elemental composition of the dental enamel of Hs01 was analysed using EDX. This tooth showed the typical elements expected in tooth enamel: carbon, oxygen, sodium, magnesium, phosphorus and calcium (**Figure 14**).

Stoichiometric hydroxyapatite contains calcium, oxygen, hydrogen and phosphate ($Ca_5(OH)(PO_4)_3$). Biological hydroxyapatite often deviates from this strict stoichiometric composition with ionic substitutions due to the flexibility within the crystal structure. For example, this allows the substitution of calcium and phosphate ions. Therefore, carbon is contained in a small amount of 0.8 wt% (**Table 5**), which comes from the substitution of phosphate ions (PO_4^{3-}) with carbonate ions (CO_3^{2-}). Calcium can be substituted by sodium and magnesium, which explains the small amounts of contained sodium (0.9 wt%) and magnesium (0.3 wt%) (Daculsi et al., 1990, LeGeros, 1981, LeGeros et al., 1968).

The calcium-phosphorous ratio was 1,62, corresponding to the biological hydroxyapatite ratio in dental enamel (Epple, 2003). Consequently, the integration of ions into the hydroxyapatite lattice varies naturally, leading to differences in composition. Therefore, the EDX results here can only give an example of the dental enamel composition, but other recent human teeth are expected to show a similar composition.

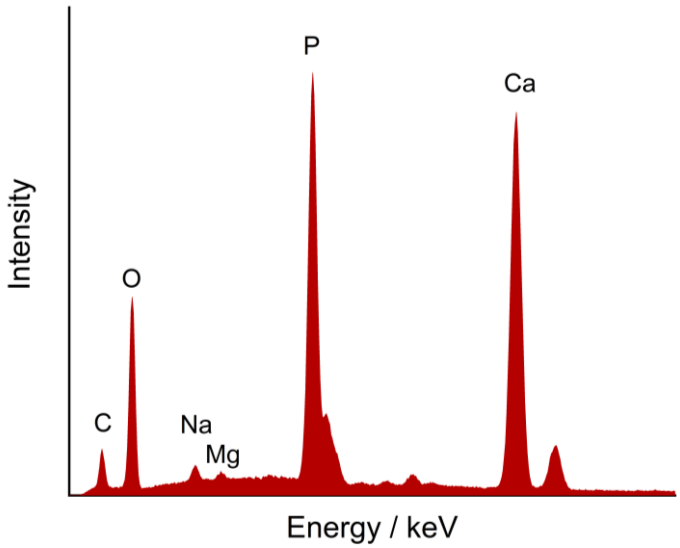

Figure 14 EDX spectra of dental enamel from a recent human tooth (Hs01).

Table 5 Quantitative results from EDX analyses of dental enamel from a recent human tooth (Hs01) in weight percent (wt%) and atomic percent (at%).

Element	Wt%	± Error	At%	± Error
C	0.8	± 0.3	1.5	± 0.6
O	40.4	± 0.3	59.9	± 0.4
Na	0.9	± 0.1	0.9	± 0.1
Mg	0.3	± 0.0	0.3	± 0.0
P	18.7	± 0.2	14.3	± 0.1
Ca	39.0	± 0.2	23.1	± 0.1

5.1.3 PXRD

To confirm the results obtained with EDX, X-ray powder diffraction was used. The recent human tooth sample (Hs14-2) was compared to synthetic hydroxyapatite (ICDD PDF No. 00-009-0432), as displayed in **Figure 15**.

The strongest reflexes of the sample at 25.911°, 31.696°, 32.192°, 32.853° and 49.466° compared to the corresponding positions in the reference at 25.879°, 31.774°, 32.197°, 32.902° and 49.469° (**Table 6**) indicate a strong similarity.

This analysis showed that the crystalline structure of the recent dental enamel is very similar to that of synthetic hydroxyapatite. Minor differences are due to the substitutions in biological apatite, as described before.

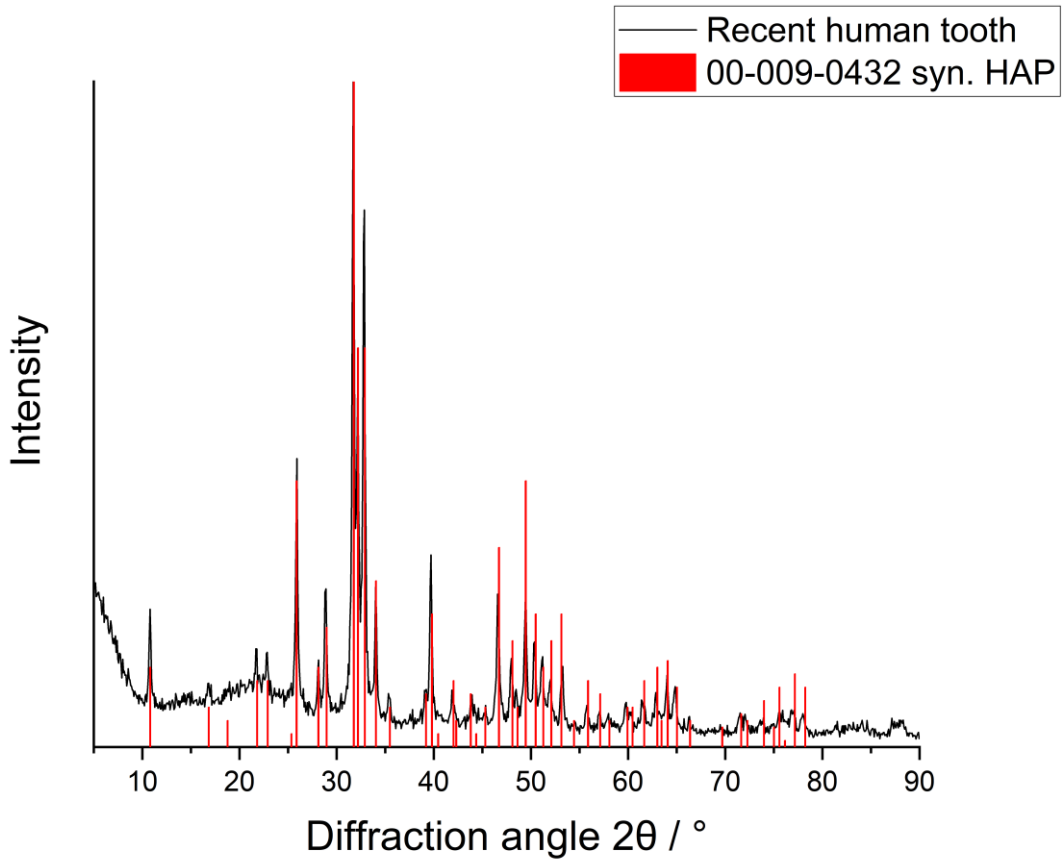

Figure 15 X-ray powder diffractogram of recent human tooth enamel of Hs14-2. The black line shows the reflexes of the sample. The red bars correspond to the reference of synthetic hydroxyapatite (ICDD PDF No. 00-009-0432).

Table 6 Comparison of the strongest observed reflex positions in the recent human sample (Hs14-2) and the positions of the corresponding reflexes of the reference (ICDD PDF No. 00-009-0432), including the lattice plane.

Reflex position (observed) 2θ/°	**Reflex position (reference) 2θ/°**	**Lattice plane (hkl)**
25.911	25.879	(002)
31.696	31.774	(211)
32.192	32.197	(112)
32.853	32.902	(300)
49.466	49.469	(213)

5.1.4 Microstructural analysis

A microstructural analysis was done to establish a chronology of stressful events during the development of the dental enamel. Since a person with a known history donated this tooth, a comparison could be made with events during this time.

The tooth shows no abrasion since it is a third molar and was extracted before it erupted and could get into contact during occlusion. This equals a wear stage 1 (Smith, 1984). The dental enamel on the mesiolingual side was damaged and detached during extraction (**Figure 16 a**). Therefore, the distobuccal cusp was chosen for analysis (**Figure 16 c**).

The examination revealed an EDJ length of 5900 µm and a CFT of 1.82 years, indicating tooth enamel development from 8 to 9.82 years (96-118 months).

Four AL formed between 8.17 and 8.78 years (**Table 7**). Since the person's history is known, these dates were compared to events in that age. The first three lines could not be traced back to any known cause. However, the fourth line lies around the age of 8.78 years; during that time, the person had bursitis. Whether this inflammation put such a strain on the body that AL formed cannot be definitively answered, but it can be seen as a possible reason.

The DSR ranges from 2.62 µm/day in the cuspal inner enamel to 3.39 µm/day in the lateral outer enamel.

Table 7 Number of Accentuated Lines (AL) in tooth LLM3 Hs18 and age at time of appearance in months and years.

AL No.	Age (months)	Age (years)
1	98	8.17
2	100	8.35
3	104	8.63
4	105	8.78

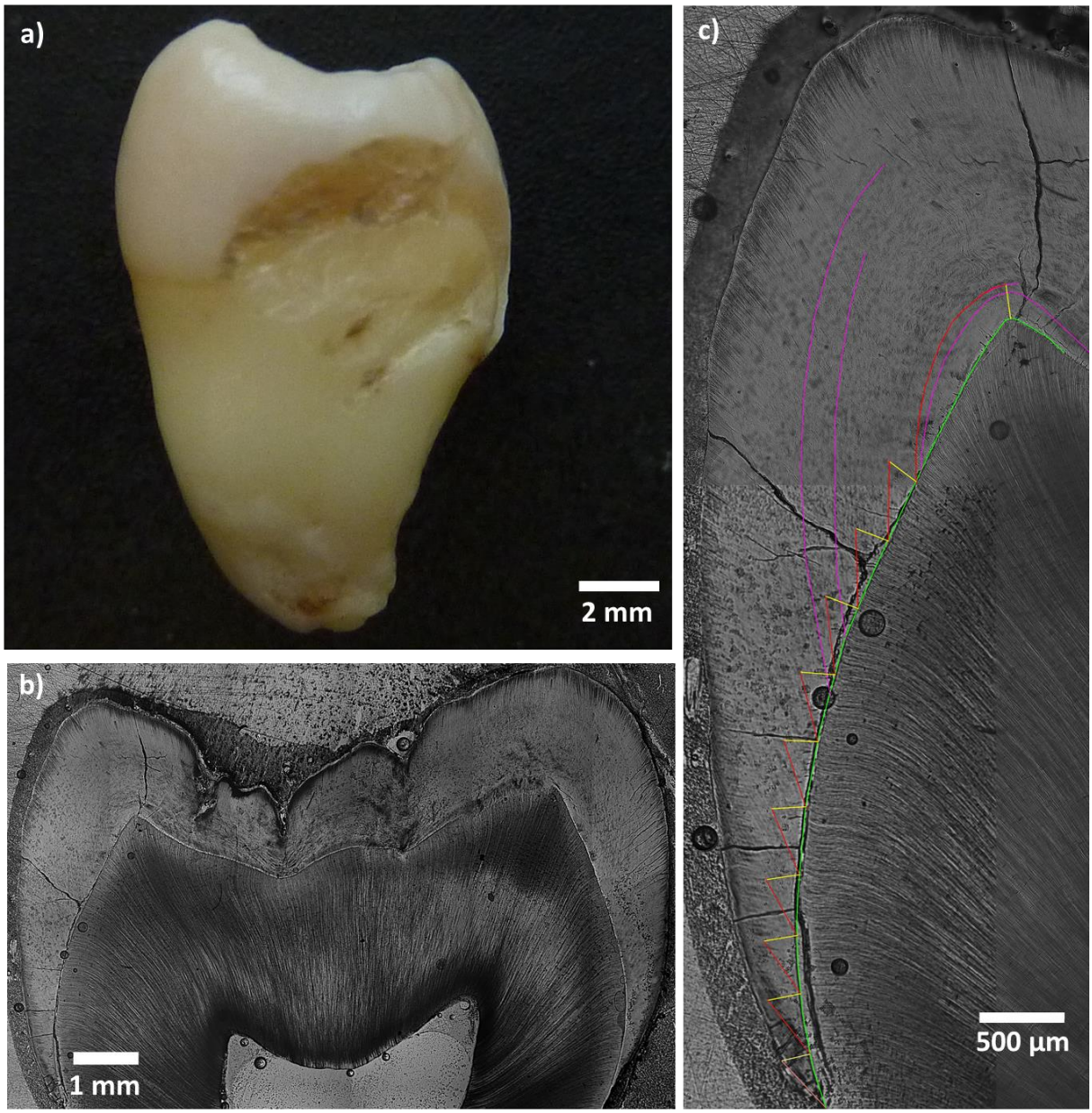

Figure 16 Various views of tooth Hs18 LLM3. a) Tooth in mesial view, b) longitudinal section of the distal cusps, c) distobuccal cusp with analysis (green: EDJ, yellow: 200 µm prism, red: RL, and purple: AL).

5.2 Gevensleben

The Gevensleben teeth were examined using SEM and EDX in order to assess potential structural and chemical alterations over time. This was followed by a detailed morphological and histological examination of 10 individuals, including a total of 27 teeth.

The conclusions drawn from this comprehensive investigation shed light on the broader population of Gevensleben, adding valuable insights to our understanding of this medieval community, their way of life, and important phases during their youth.

5.2.1 Individual 41b – SEM and EDX

The first individual examined was individual 41b, a male who died at age 16-17. This tooth (LRM1) is used as a representative in terms of enamel structure. It mainly remained unchanged over time. The tooth enamel microstructure of sample 41b is depicted in varying magnifications in **Figure 17**.

Initially, a comprehensive overview of the longitudinal tooth section is provided (**Figure 17 a**). For this purpose, an SEM mode was employed, which scanned the entire sample at minimal magnification (x19) and combined the images to form a complete overview. In this representation, the dental enamel is portrayed in lighter shades, while the inner dark regions correspond to the dentine, with the dental pulp embedded within it.

The typical structure is represented in **Figure 17 b** and **c**. Enamel prisms run parallel from the enamel-dentine junction to the outer enamel surface. During the course of that, they follow a long curve in the vertical plane of the section and undulate up and down regularly at the same time, which is the so-called decussation (Hillson, 2014).

The decussation can also be seen as Hunter-Schreger bands (HSB, **Figure 17 b** to **d)**. These result from prisms in different orientations of their undulation. HSB are also visible to the bare eye. Depending on the angle of the light hitting on the group of prisms, they can appear as dark bands (diazones) or show up bright (parazones) (Myoung et al., 2009, Wood, 2011).

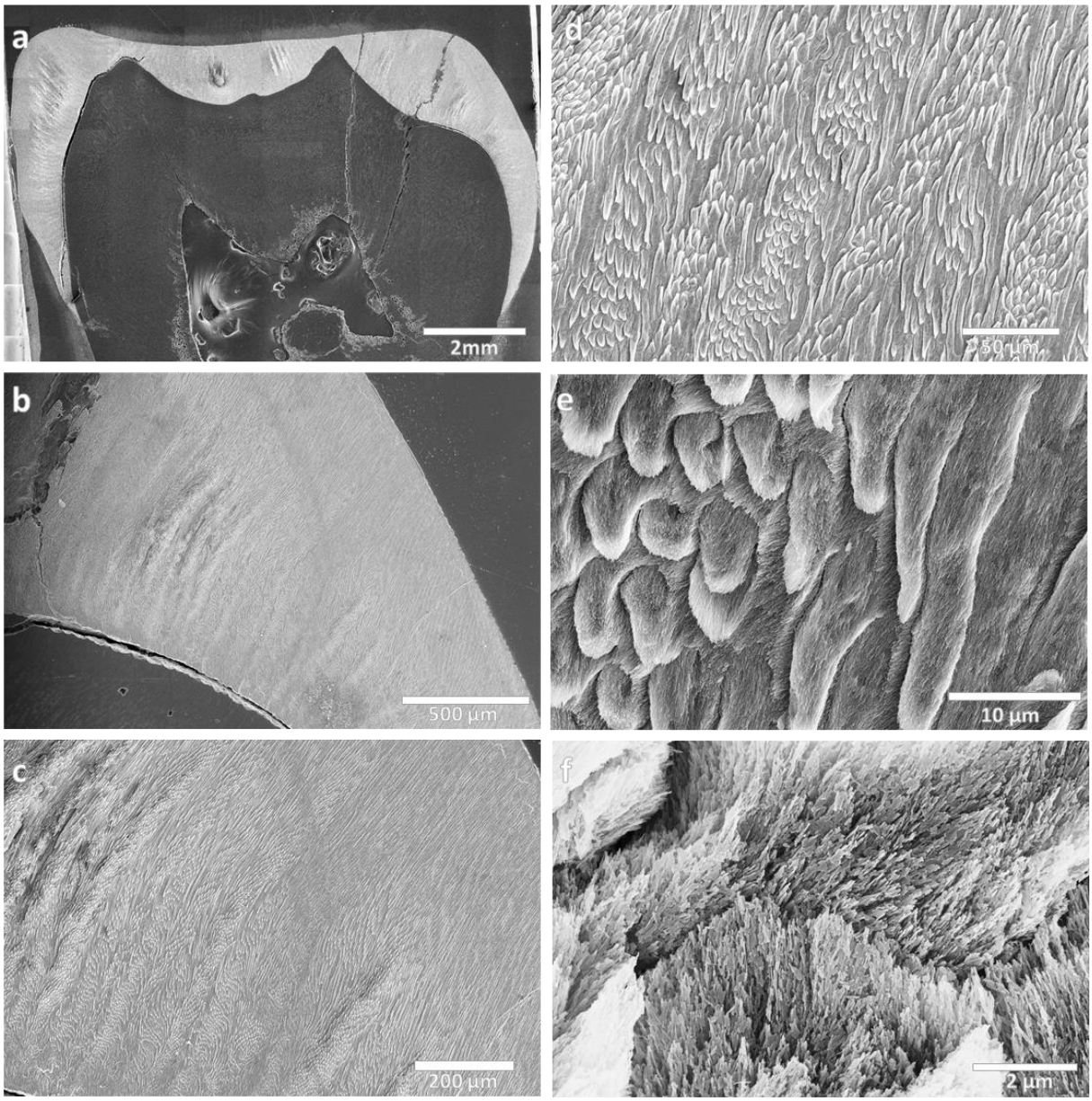

Figure 17 SEM images of the dental enamel microstructure of tooth 41b LRM1 (male, 16-17 years old) at different magnifications. a) Tooth section of a whole tooth crown combined from single pictures at 19x magnification, b) dental enamel at 200x magnification, c) dental enamel at 400x magnification, d) Hunter-Schreger bands at 1.500x magnification, e) prisms with interprismatic enamel at 10.000x magnification, f) crystallites of enamel prism at 40.000x magnification.

The single prisms are encased by interprismatic enamel (**Figure 17 f**). Prismatic and interprismatic enamel differ in the organisation of the crystallites but not in their composition since both are made out of hydroxyapatite (Maas and Dumont, 1999).

Not only that, all structures described in the literature can be found in this tooth; compared to the enamel microstructure of the recent human tooth sample described in the previous chapter (5.1) the Gevensleben sample's structure seems unchanged over time.

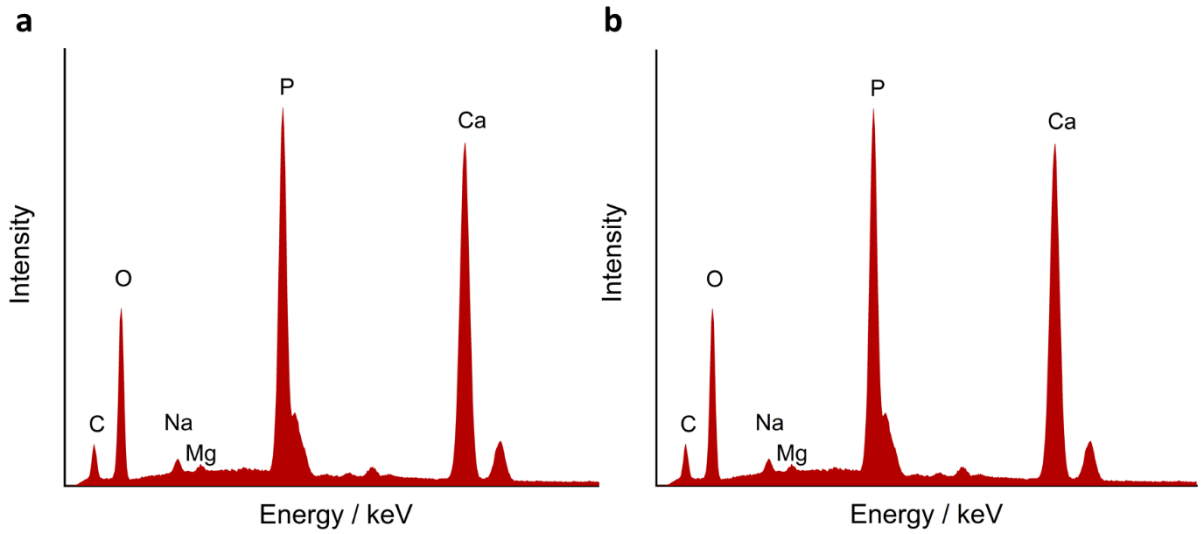

Figure 18 EDX spectra of dental enamel. (a) Spectrum of the Gevensleben sample (41b LRM1) and (b) spectrum of a recent human tooth.

To verify the elemental composition, EDX spectra of tooth 41b LRM1 and a recent reference tooth were taken. Both teeth showed a very high similarity in their composition (**Figure 18**). Minor differences can be found when comparing the elemental composition in **Table 8**. The molar calcium-phosphorous ratio was 1.61 in the Gevensleben sample and 1.60 in the recent samples. This corresponds to the ratio that prevails in calcium-deficient hydroxyapatite between 1.50 and 1.67 (Epple, 2003).

Biological hydroxyapatite in bones and teeth is always non-stoichiometric since the structure in all ionic sites (calcium, phosphate, hydroxide) is flexible that other ions can easily be incorporated. Therefore, a natural variation of these elements can be found in teeth. For more examples of slightly different elemental composition in enamel, see EDX analyses in chapter 5.3.

Aside from natural variation, no significant changes in composition between historic teeth from Gevensleben and recent teeth were expected. The mean calcium-phosphorous ration in

both tooth samples is 1.60 corresponding to the biological hydroxyapatite ratio in dental enamel (Epple, 2003). Dental enamel does not change much, undergoing only minimal alterations. Due to its high mineralisation, it possesses a heightened resilience to external influences when compared to other biological tissue like bone. Consequently, no substantial modifications were expected within this relatively short time frame of around 1000 years (Kendall et al., 2018, Parker et al., 1974).

Table 8 Quantitative results from EDX analyses of dental enamel of a sample from Gevensleben (41b LRM1) and a recent human tooth in weight percent (wt%) and atomic percent (at%). Calculated mean values are shown here with the standard deviation (SD). Nine measurements at different positions on the tooth were performed for the Gevensleben sample and three for the recent tooth sample.

	41b LRM1 tooth enamel				Recent tooth enamel			
Element	**Wt%**	**SD**	**At%**	**SD**	**Wt%**	**SD**	**At%**	**SD**
C	2.7	0.1	1.7	0.1	1.0	0.0	2.6	2.0
O	44.1	1.8	61.8	3.1	39.7	0.1	59.1	1.3
Na	0.7	0.1	0.7	0.1	0.9	0.1	0.9	0.0
Mg	0.3	0.0	0.3	0.0	0.3	0.1	0.3	0.1
P	16.7	0.3	12.1	0.4	17.8	0.1	14.3	0.1
Ca	34.7	0.7	19.4	0.6	36.8	0.2	22.9	0.3

5.2.2 Individual 63a – PXRD

In order to confirm these findings on a crystalline level, X-ray powder diffraction was used to compare the enamel of a Gevensleben sample (63a LLM2) and that of recent human enamel as well as a reference of synthetic hydroxyapatite (ICDD number 00-009-0432). This analysis revealed that the enamel, indeed, did not change in its composition over time. Both samples showed reflexes characteristic for the reference of synthetic hydroxyapatite (**Figure 19**). In summary, it can be stated that the composition of the tooth enamel remained unaffected for over 1000 years, after burial, reinforcing the persistent nature of dental enamel as a reliable bioarchive.

After these preliminary examinations, the histological examination of the teeth was carried out.

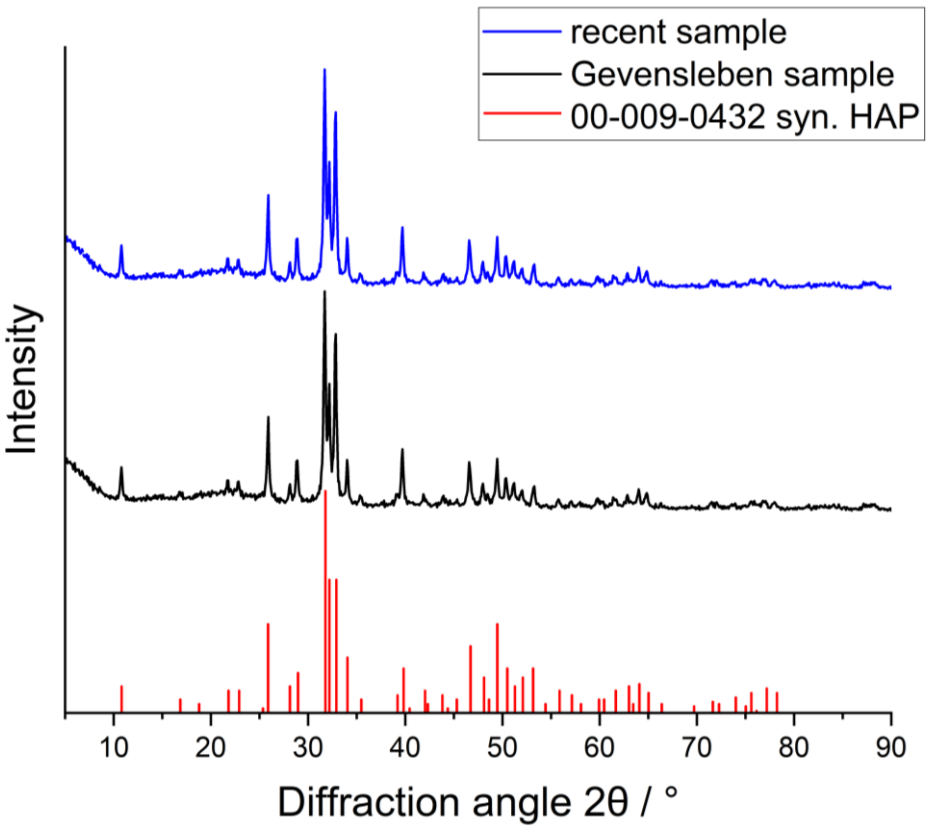

Figure 19 X-ray powder diffractogram of tooth enamel of a recent human sample (blue) and the Gevensleben sample (black; 63a LLM2). The red bars correspond to the reference of synthetic hydroxyapatite (ICDD PDF No. 00-009-0432).

5.2.3 Individual 12

Individual 12 was a male who died at age 35-40. He was buried in a single grave along with several grave goods, including a belt buckle, a knife, and an iron spike known as the "*Schulzenstab*." The *Schulzenstab* is a rare artefact primarily associated with male burials in Carolingian-era cemeteries in northern Germany, the northern Netherlands, and the northern Harz foreland. It is believed that this rod was possessed by individuals entrusted with legal leadership roles, such as village heads called "*Schulzen*" and "*Schultheiß*" (Blaich, 2013).

Individuals holding such official positions were likely from socially privileged families within their communities. They may have experienced a comparatively less stressful childhood than individuals from lower-income households. This observation aligns with previous anthropological analyses conducted on the remains. Notably, the tooth surfaces revealed only

few stress markers, such as enamel hypoplasia (enamel defects) on the premolars, which indicate a period of stress experienced around 5-6 years of age (Grefen-Peters, 2020). Unfortunately, the available teeth for this study did not cover this period.

Three teeth were extracted from the lower jaw and analysed: LLM1, LLM2 and LLM3 (**Figure 20**). During the preparation, the enamel of LLM1 became detached from the tooth, and despite efforts to reattach it, the tooth had to be excluded from the analysis.

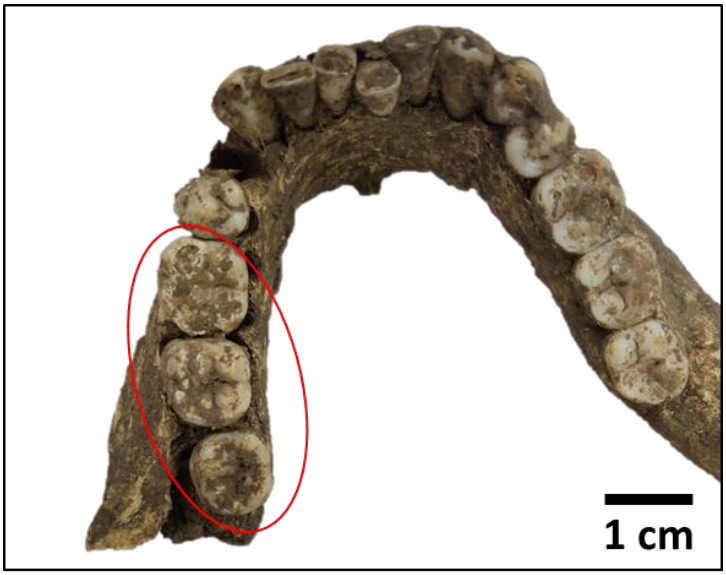

Figure 20 Lower jaw of individual 12. The complete dentition is preserved. The left canine appears missing but has only fallen out of the dental socket. The red circle indicates which teeth have been extracted (LLM1, LLM2, LLM3).

5.2.3.1 LLM2

The first tooth analysed from individual 12 was the lower left second molar (LLM2). When received, it was covered by dirt, but after cleaning, the tooth could be adequately analysed. The abrasion shows a wear stage of 4 (Smith, 1984) since the dentine is exposed to some extent. The tooth is also decayed and has some areas of demineralisation. Furthermore, there is discolouration, especially in the root area (**Figure 21 a**). The exposition of the dentine can be seen in **Figure 21 b** on the mesiobuccal cusp, as well as a carious lesion, which already extends into the dentine.

The mesiolingual cusp was used to analyse the microstructures of the enamel. It revealed an EDJ length of 8089 µm and a CFT of 2.16 years, leading to a development time from age 2.50 to 4.66 (30-56 months).

Eight AL appeared between 2.82 years and 3.68 years (**Table 9**). The stressful events that might have caused these AL to emerge might be weaning since it fits in that time period.

The DSR ranges from 4.26 ± 0.33 µm in the lateral inner enamel to 4.82 ± 0.11 µm in the cuspal outer enamel (Appendix 8.2, **Table 55**). The lateral inner DSR with 4.26 µm/day was used to calculate the chronology.

Table 9 Number of Accentuated Lines (AL) in tooth 12 LLM2 and age at time of appearance in months and years.

AL No.	Age (months)	Age (years)
1	34	2.82
2	35	2.94
3	39	3.22
4	41	3.40
5	41	3.43
6	42	3.53
7	44	3.65
8	44	3.68

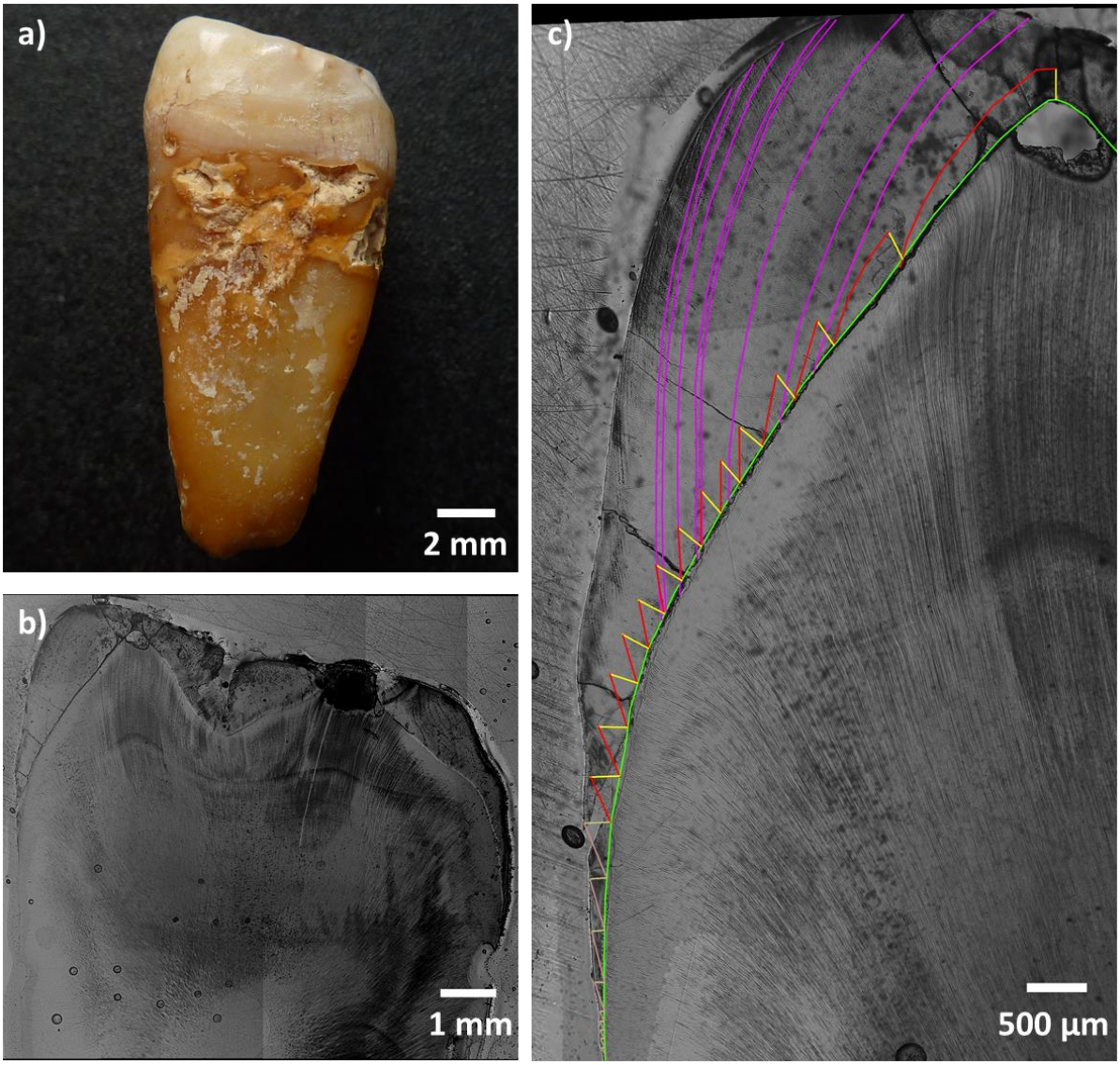

Figure 21 Various views of tooth 12 LLM2. a) Tooth after cleaning in mesial view, b) longitudinal section of the mesial cusps, c) mesiolingual cusp with analysis (green: EDJ, yellow: 200 µm prism, red: RL, and purple: AL).

5.2.3.2 LLM3

The second tooth from individual 12 was the lower left third molar (LLM3). This tooth was cleaned as well to analyse it properly. It shows comparatively lower levels of abrasion, categorising it as wear stage 2 (Smith, 1984). Like LLM2, LLM3 exhibited caries lesions and discolouration, with the tooth cervix significantly affected by these conditions.

The analyses of microstructure were performed on the mesiolingual cusp. It revealed an EDJ length of 4894 µm and a CFT of 1.72 years, leading to a development time from 8.00 to 9.71 years (96-117 months).

During that time, four AL emerged between 8.61 and 9.25 years (**Table 10**). The presence of these lines may be attributed to a growth spurt that typically occurs during this period, coinciding with the transition to the second developmental stage in children, marked by various physical and cognitive changes (Arnold, 1986).

The DSR are lowest at 3.79 ± 0.27 µm/day in the lateral outer enamel and highest at 4.38 ± 0.14 µm/day in the cuspal outer enamel (Appendix 8.2, **Table 55**). The lateral inner DSR with 3.86 µm/day was used to calculate the chronology.

Table 10 Number of Accentuated Lines (AL) in tooth 12 LLM3 and age at time of appearance in months and years.

AL No.	Age (months)	Age (years)
1	103	8.61
2	105	8.74
3	106	8.84
4	111	9.25

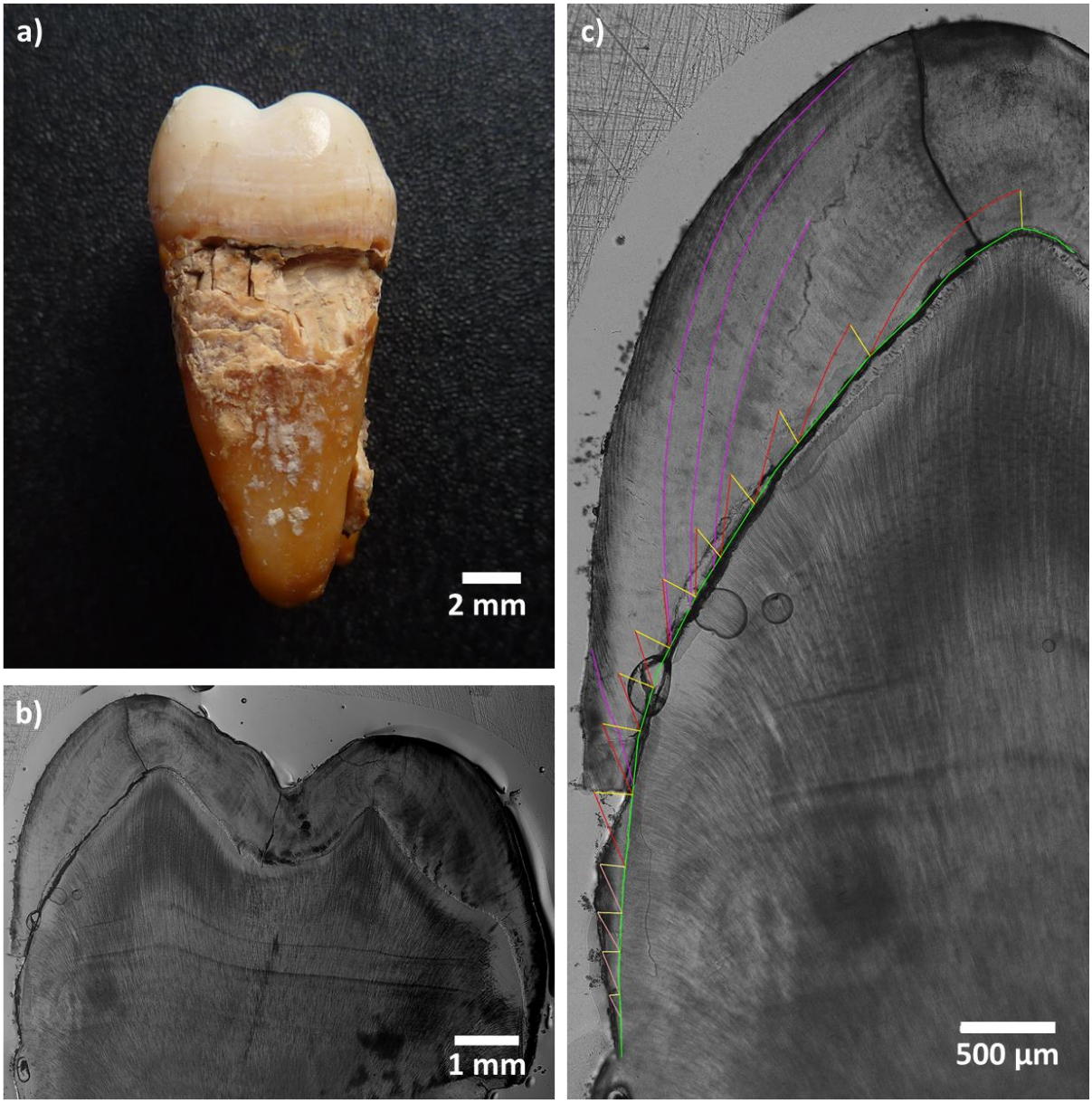

Figure 22 Various views of tooth 12 LLM3. a) Tooth after cleaning in mesial view, b) longitudinal section of the mesial cusps, c) mesiolingual cusp with analysis (green: EDJ, yellow: 200 µm prism, red: RL, and purple: AL).

5.2.4 Individual 22

Individual 12 was a male who died at age 35-55.

Due to the high abrasion of nearly all teeth, only two teeth were suitable for analysis and were extracted from the lower jaw: LLM2 and LLM3 (**Figure 23**). Crossbite and overbite probably led to high tooth wear. This also caused numerous pulp openings and inflammation of the alveoli. There is no evidence of a particular position in society, as in individual 12. However, it is worth mentioning that he had a striking physiognomy with a large mandibular angle and a pointed chin.

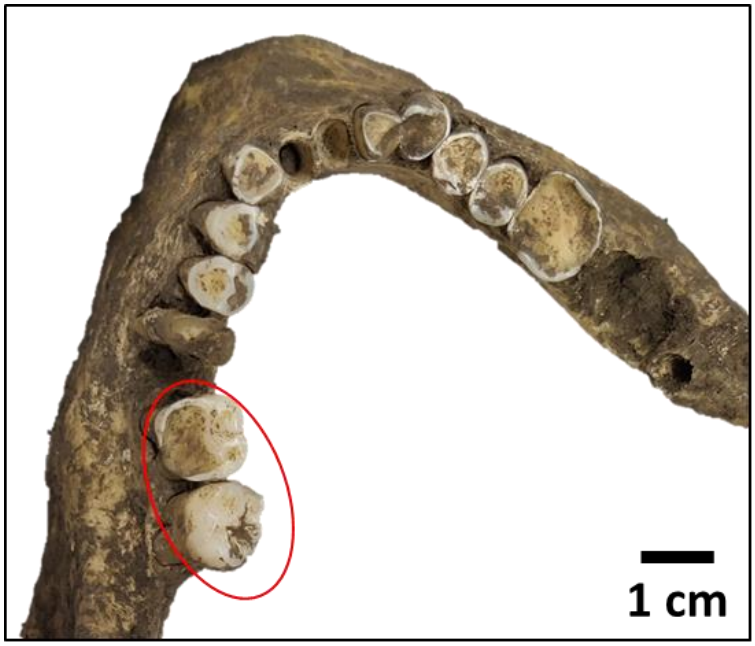

Figure 23 Lower jaw of individual 22. The dentition is not complete. The red circle indicates which teeth have been extracted (LLM2, LLM3).

5.2.4.1 LLM2

The first tooth analysed of individual 22 was the lower left second molar (LLM2). The vast abrasion could be seen even without cleaning. Almost half of the tooth crown is absent due to the crossbite, and some part of the dentine is also missing. This leads to a wear stage of 5 (Smith, 1984). Due to this, the analysis was only possible on the mesiolingual cusp. Contrary to the mesiobuccal cusp, this was well preserved and showed less abrasion (**Figure 24**).

The microstructure analyses of the enamel revealed an EDJ length of 4441 µm and a CFT of 1.74 years, meaning that the tooth enamel was developed between the age of 2.50 and 4.22 (30-51 months old).

Eight AL emerged between the ages of 2.82 and 3.57 (**Table 11**). There are numerous lines around the age of 3 years, which fits with the assumed weaning process at that time (Bernatzky et al., 2018). The most intense lines are AL 1 and 2 which might be connect with a longer stress period, since the enamel between these lines appears different.

The DSR ranges from 3.07 ± 0.21 µm/day in the cuspal inner enamel to 4.11 ± 0.32 µm/day in the lateral outer enamel (Appendix 8.2, **Table 55**). The lateral inner DSR with 3.38 µm/day was used to calculate the chronology.

Table 11 Number of Accentuated Lines (AL) in tooth 22 LLM2 and age at time of appearance in months and years. Especially pronounced lines are printed in bold type.

AL No.	Age (months)	Age (years)
1	**34**	**2.82**
2	**34**	**2.87**
3	38	3.17
4	38	3.19
5	39	3.22
6	40	3.32
7	40	3.36
8	41	3.45
9	43	3.57

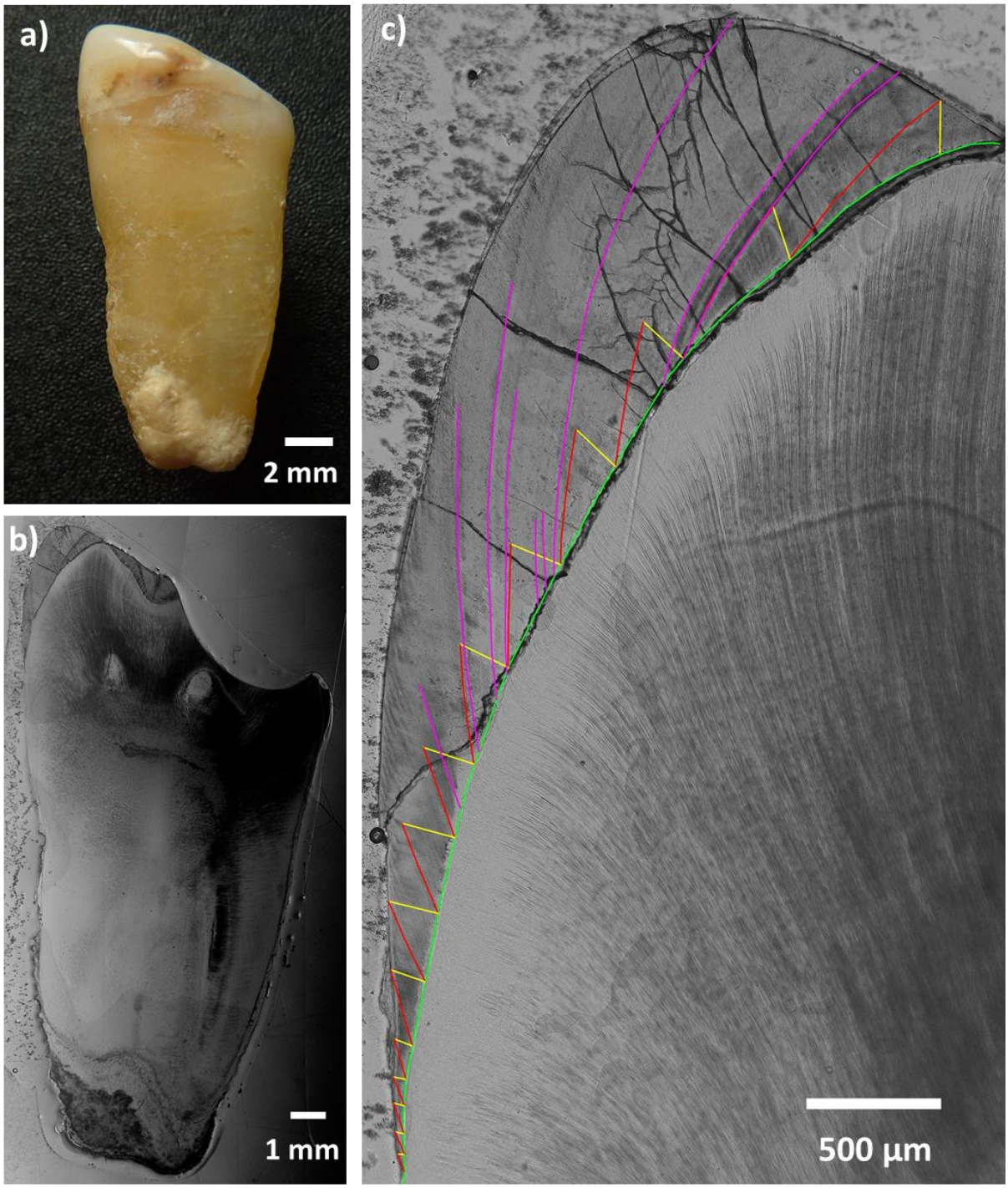

Figure 24 Various views of tooth 22 LLM2. a) Tooth after cleaning in mesial view, b) longitudinal section of the mesial cusps, c) mesiolingual cusp with analysis (green: EDJ, yellow: 200 µm prism, red: RL, and purple: AL).

5.2.4.2 LLM3

The second tooth analysed for individual 22 was the lower left third molar (LLM3). It shows less abrasion than LLM2 but still has great enamel loss with a little exposed dentine on the mesiobuccal cusp due to the crossbite. This tooth is categorised as a wear stage 3 (Smith, 1984).

The mesiolingual cusp was used for a microstructure analysis of the tooth enamel (**Figure 25 c**). It revealed an EDJ length of 5025 µm and a CFT of 1.31 years, leading to a developmental time from 8.00 to 9.31 years (96-112 months).

There were fourteen AL formed between the age of 8.06 to 8.76 (**Table 12**), at least one line per month between 97 and 105 months old. These AL may be attributed to a growth spurt typically occurring during that period and the transition to the second developmental stage in children, which is accompanied by various physical and cognitive changes (Arnold, 1986).

The DSR ranges from 3.71 ± 0.21 µm/day in the lateral mid enamel to 4.71 ± 0.20 µm/day in the cuspal outer enamel (Appendix 8.2, **Table 55**). The lateral inner DSR with 4.31 µm/day was used to calculate the chronology.

Table 12 Number of Accentuated Lines (AL) in tooth 22 LLM3 and age at time of appearance in months and years.

AL No.	Age (months)	Age (years)
1	97	8.09
2	97	8.12
3	98	8.16
4	98	8.21
5	99	8.29
6	100	8.33
7	100	8.37
8	101	8.42
9	101	8.45
10	102	8.49
11	102	8.52
12	103	8.55
13	104	8.67
14	105	8.76

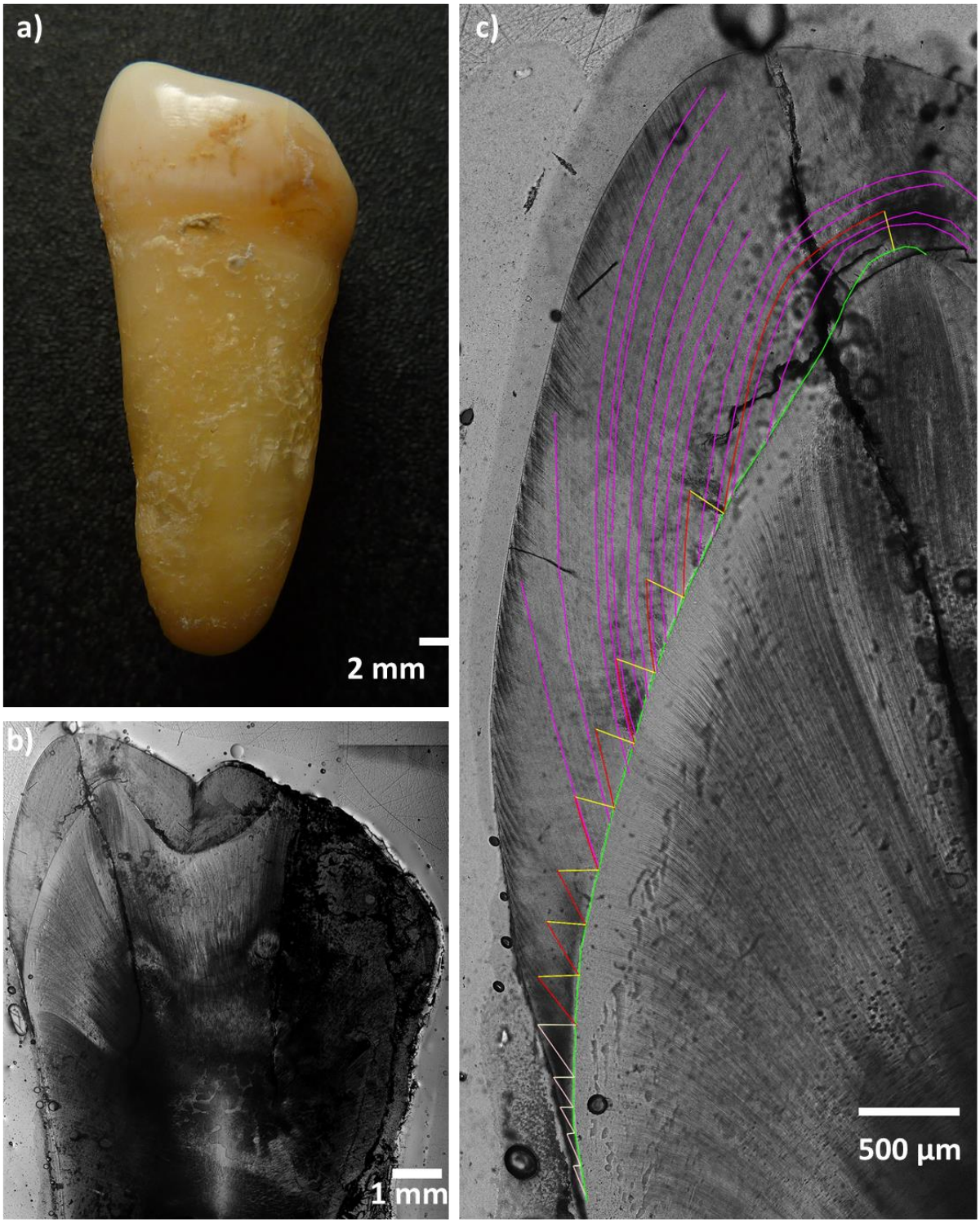

Figure 25 Various views of tooth 22 LLM3. a) Tooth after cleaning in mesial view, b) longitudinal section of the mesial cusps, c) mesiolingual cusp with analysis (green: EDJ, yellow: 200 µm prism, red: RL, and purple: AL).

5.2.5 Individual 30

Individual 30 was identified as a female who died at the age of 55 to 65. Alongside individual 53, it represents one of the oldest specimens examined. The lower jaw is fractured into two parts, while most teeth exhibit significant abrasion. Inflammatory changes are evident in the alveoli, and calculus is present in the cervical area of each tooth. Additionally, certain teeth display irregular abrasion patterns, likely from a crossbite.

Figure 26 Lower jaw of individual 30. The red circles indicate which teeth have been extracted (LLC, LLP3, LRM3).

5.2.5.1 LLC

The first tooth analysed is the lower left canine (LLC). Like many teeth from this individual, it shows high abrasion on the tip of the crown, categorised as wear stage 3-4 (Smith, 1984). The calculus described above is visible in **Figure 27 a**, although parts have been removed during the cleaning process. The inflammatory changed alveoli also changed the roots of this tooth.

The labial enamel was used for a microstructure analysis of the tooth enamel (**Figure 27 c**). The examination revealed an EDJ length of 8184 µm and a CFT of 4.93 years, indicating tooth enamel development between the ages of 0.88 to 5.80 (11-70 months).

During this period, eleven AL formed between the ages of 1.10 and 2.42 (**Table 13**). However, the tooth section became indistinct for later stages of development due to the preparation process, preventing reliable results beyond this timeframe.

The DSR varied across different regions of the enamel, ranging from 3.11 ± 0.21 µm/day in the lateral mid enamel to 4.21 ± 0.11 µm/day in the cuspal outer enamel (Appendix 8.2, **Table 55**). The lateral inner DSR with 3.34 µm/day was used to calculate the chronology.

Table 13 Number of Accentuated Lines (AL) in tooth 30 LLC and age at time of appearance in months and years.

AL No.	Age (months)	Age (years)
1	13	1.10
2	16	1.36
3	17	1.42
4	19	1.58
5	19	1.62
6	21	1.74
7	25	2.08
8	27	2.24
9	27	2.26
10	28	2.37
11	29	2.42

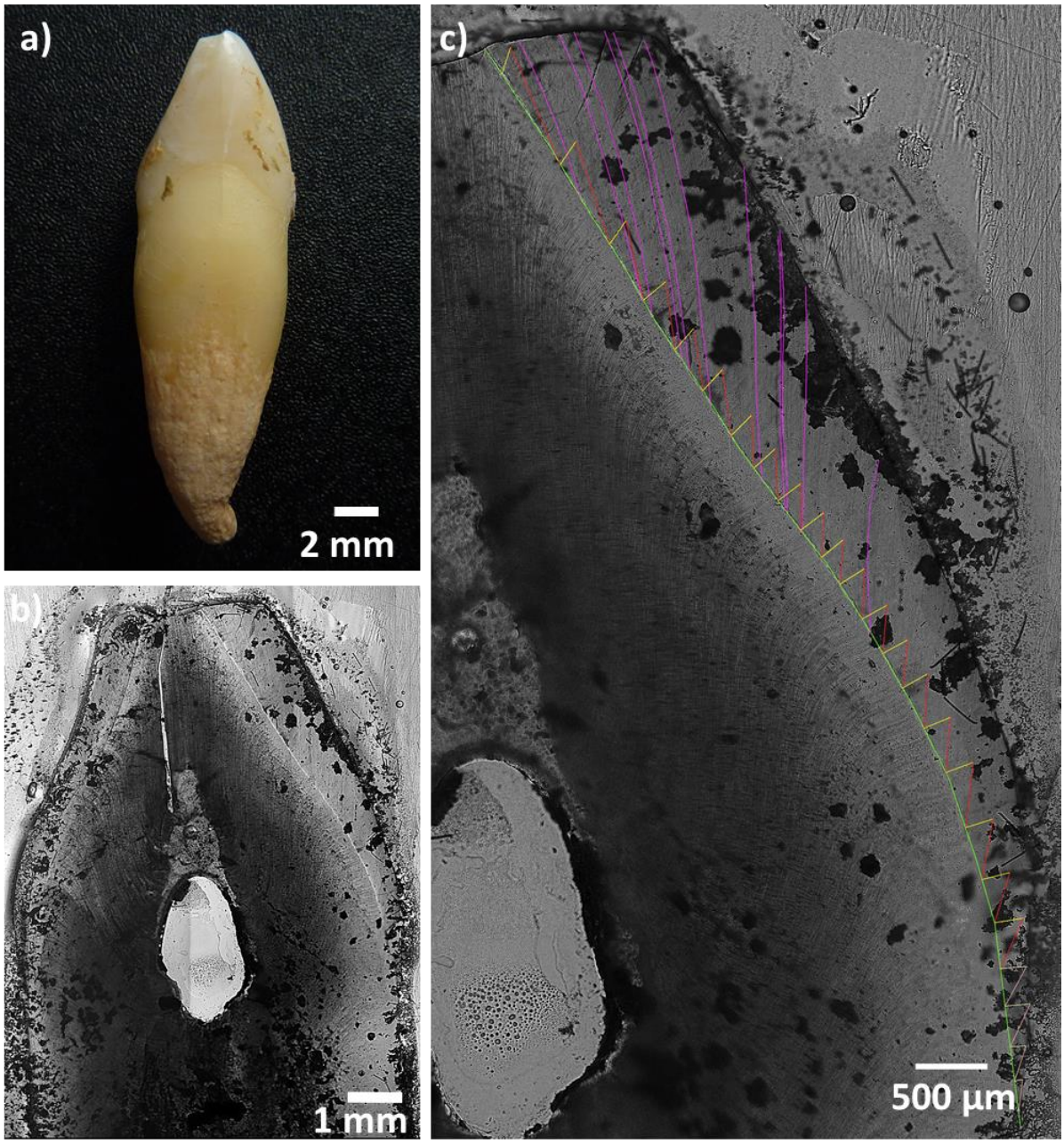

Figure 27 Various views of tooth 30 LLC. a) Tooth after cleaning in mesial view, b) longitudinal section of the tooth, c) labial enamel with analysis (green: EDJ, yellow: 200 µm prism, red: RL, and purple: AL).

5.2.5.2 LLP3

The second tooth analysed was the lower left third premolar (LLP3). It shows an abrasion of a wear stage 3 (Smith, 1984). The inflammatory changes in the alveoli are also visible here at the roots of the teeth (**Figure 28 a**).

The buccal enamel was used for microstructure analyses of the tooth enamel (**Figure 28 c**). The examination revealed an EDJ length of 6618 µm and a CFT of 4.56 years, indicating tooth enamel development between the ages of 1.55 to 6.05 years (18-73 months).

During this period, five AL formed between the ages of 1.90 and 3.08 years (**Table 14**). AL 2 at age 2.29 (27 months) can also be found on the previous tooth (LLC, **Table 13**, AL 8 and 9). However, the tooth section became indistinct for later stages of development due to the preparation process, preventing reliable results beyond this timeframe.

The DSR varies comparatively less than in other teeth, ranging from 3.08 µm/day in the lateral inner enamel to 3.76 µm/day in the cuspal outer enamel (Appendix 8.2, **Table 55**). The lateral inner DSR with 3.08 µm/day was used to calculate the chronology.

Table 14 Number of Accentuated Lines (AL) in tooth 30 LLP3 and age at time of appearance in months and years.

AL No.	Age (months)	Age (years)
1	23	1.90
2	27	2.29
3	32	2.70
4	35	2.96
5	37	3.08

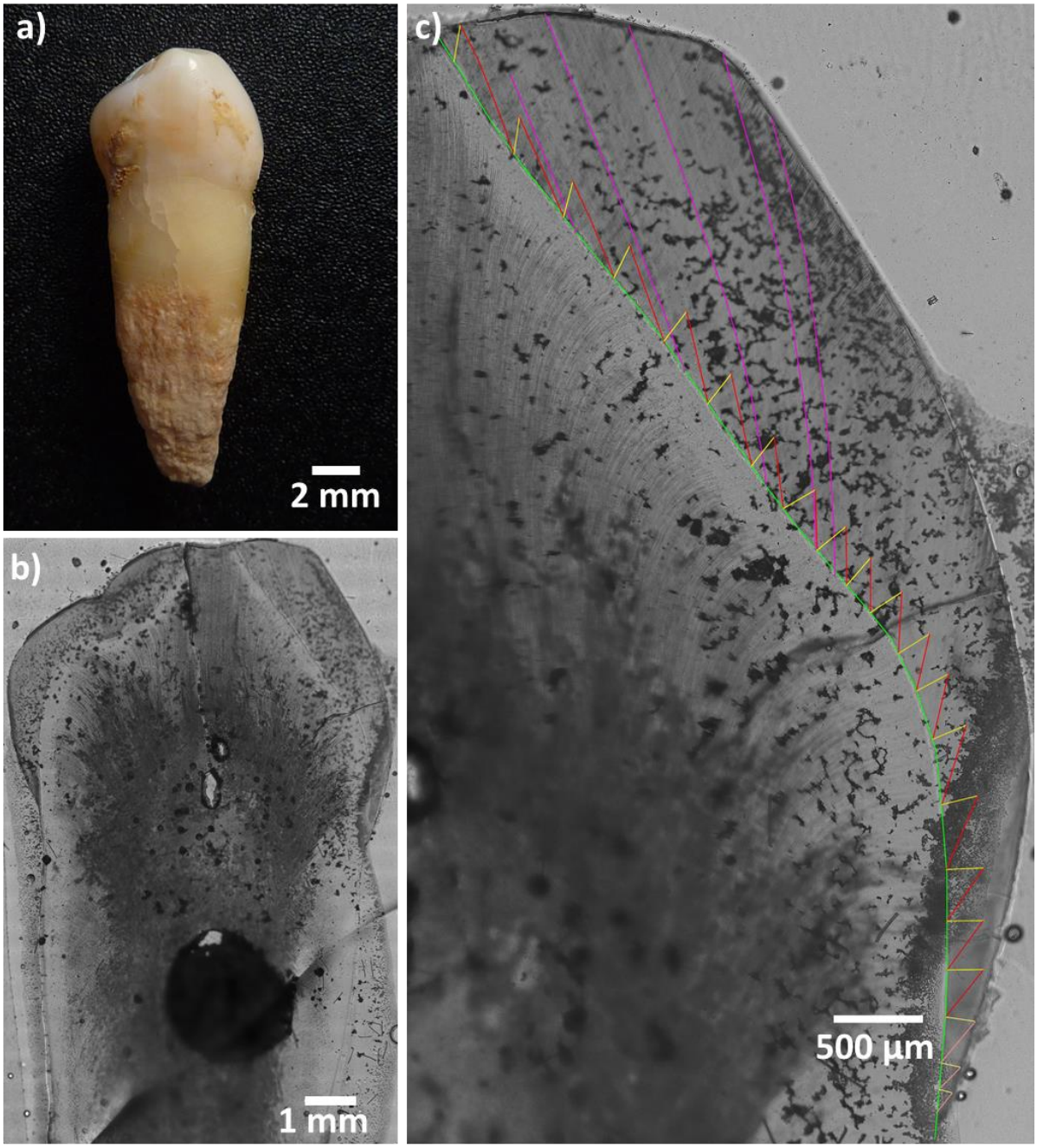

Figure 28 Various views of tooth 30 LLP3. a) Tooth after cleaning in mesial view, b) longitudinal section of the tooth, c) buccal cusp with analysis (green: EDJ, yellow: 200 µm prism, red: RL, and purple: AL).

5.2.5.3 LRM3

The third tooth analysed of individual 30 was the lower right third molar (LRM3). Preferably teeth from one side of the jaw should be used, but since the third molar of the lower left side was severely worn down, this tooth was chosen.

Similar to the other teeth from this individual, but unusual for a third molar, this tooth is also worn down to a great extent and is therefore categorised as wear stage 5 (Smith, 1984). In addition, the buccal cusps of the tooth are damaged from demineralisation. Since this did not affect the mesiolingual side, the mesiolingual cusp was chosen for analysis (**Figure 29**).

The examination revealed an EDJ length of 4685 µm and a CFT of 0.95 years, indicating tooth enamel development between the ages of 8.00 to 8.95 years (96-107 months).

Eight AL formed between 8.14 and 8.46 years (**Table 15**). These lines may come from a growth spurt that usually happened during that time and the shift to the second developmental stage in children accompanied by other physical and cognitive changes (Arnold, 1986).

Since no other tooth from this individual was formed during this time, there can be no comparison as in the previous teeth (LLC and LLP3).

The DSR varies comparatively less than in other teeth, ranging from 3.73 µm/day in the cuspal inner enamel to 4.29 µm/day in the cuspal outer enamel (Appendix 8.2, **Table 55**). The lateral inner DSR with 4.12 µm/day was used to calculate the chronology.

Since the enamel of this tooth is abraded to a great extent, these results do not reflect accurate times and rates and can, therefore, only be used as estimates.

Table 15 Number of Accentuated Lines (AL) in tooth 30 LRM3 and age at time of appearance in months and years.

AL No.	Age (months)	Age (years)
1	98	8.14
2	98	8.15
3	98	8.16
4	99	8.27
5	100	8.31
6	100	8.34
7	101	8.40
8	102	8.46

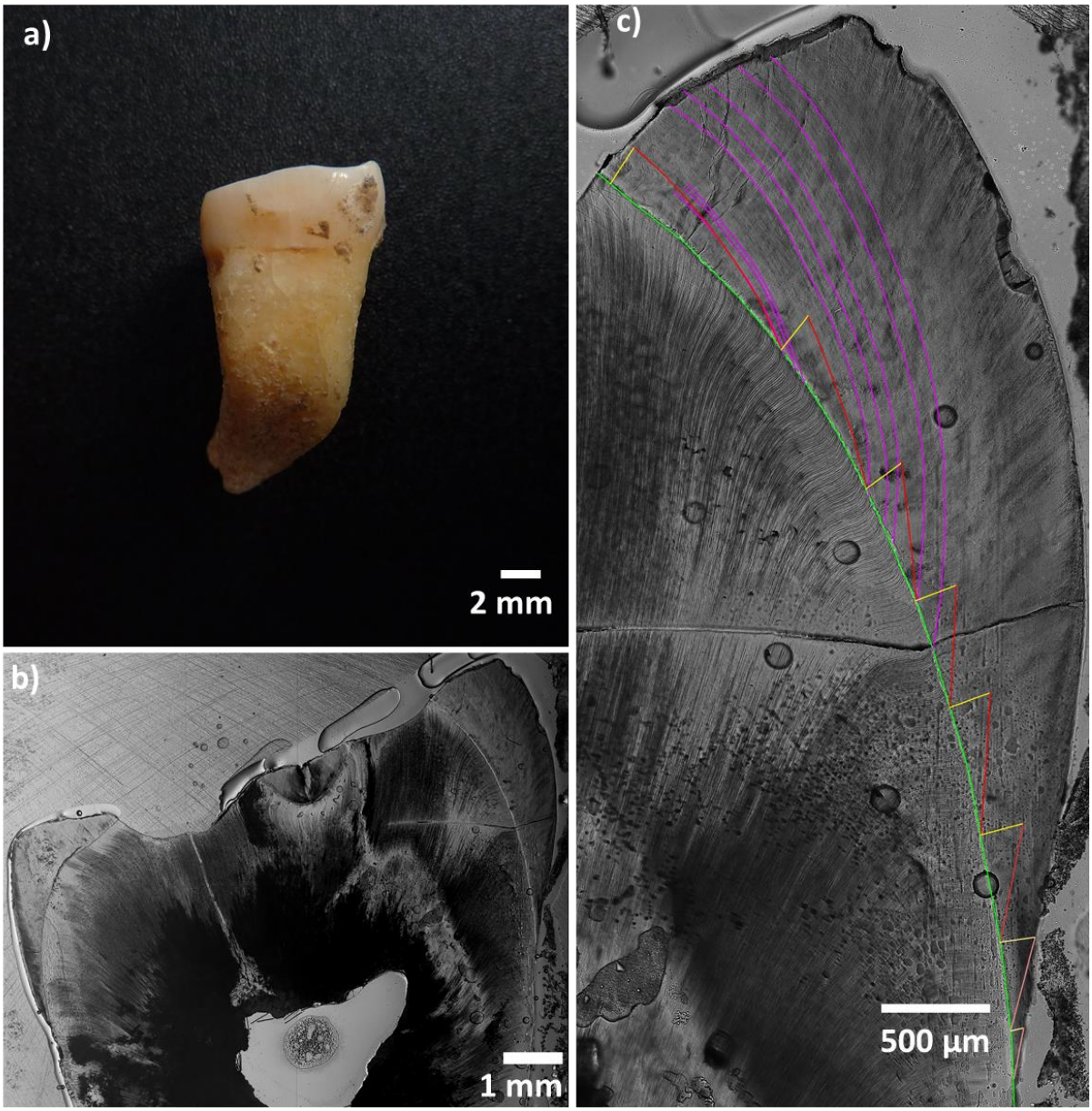

Figure 29 Various views of tooth 30 LRM3. a) Tooth after cleaning in mesial view, b) longitudinal section of the mesial cusps, c) mesiolingual cusp with analysis (green: EDJ, yellow: 200 µm prism, red: RL, and purple: AL).

5.2.6 Individual 33

Individual 33 was a female who died at age 50-60. The jaw is fractured into two parts. The teeth show a moderate abrasion for the high age this individual reached. Some teeth display calculus build-up at the tooth cervix, while others show cavities. However, considering her age, the overall condition of the teeth is remarkably good.

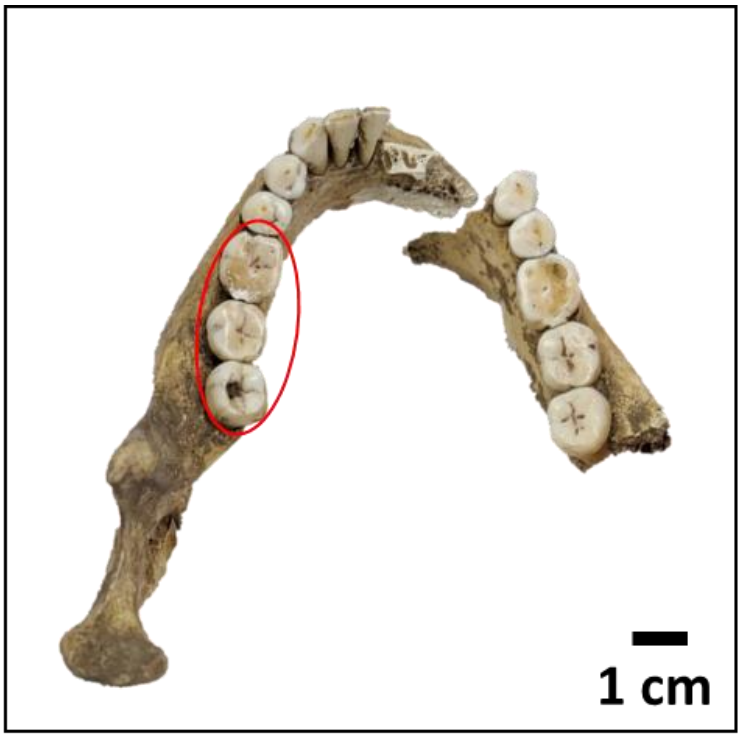

Figure 30 Lower jaw of individual 33. The red circle indicates which teeth have been extracted (LLM1, LLM2, LLM3).

5.2.6.1 LLM1

The first tooth analysed was the lower left first molar (LLM1). This tooth is the most worn, which is expected since it is the first permanent tooth to erupt (AlQahtani et al., 2010).

The tooth exhibits a significant degree of wear, falling into wear stage 4 (Smith, 1984) since some dentine is exposed (**Figure 31 b**). It has also been damaged on the mesial side of the cusp (**Figure 31 a**).

For the microstructure analysis, the mesiolingual cusp was used (**Figure 31 c**). It revealed an EDJ length of 4959 µm and a CFT of 2.02 years, indicating tooth enamel development between 0 to 2.02 years (0-24 months).

During this period, seventeen AL formed between 0.25 and 1.88 years (**Table 16**). There are two phases, with around one AL every month from 6 to 12 months old and from 17 to 23 months, which may come from the first contact of children with their environment and, therefore, pathogens (Jenni, 2021). Another event might be the start of weaning around that age.

The DSR varies in different parts of the enamel, ranging from 3.45 ± 0.29 µm/day in the lateral inner enamel to 4.71 ± 0.26 µm/day in the lateral outer enamel (Appendix 8.2, **Table 56**). For the calculation of the chronology, the lateral inner DSR was used.

Table 16 Number of Accentuated Lines (AL) in tooth 33 LLM1 and age at time of appearance in months and years.

AL No.	Age (months)	Age (years)
1	3	0.25
2	6	0.52
3	7	0.61
4	8	0.65
5	8	0.69
6	9	0.73
7	10	0.83
8	11	0.90
9	11	0.93
10	12	0.96
11	17	1.41
12	18	1.48
13	19	1.55
14	20	1.66
15	20	1.69
16	22	1.86
17	23	1.88

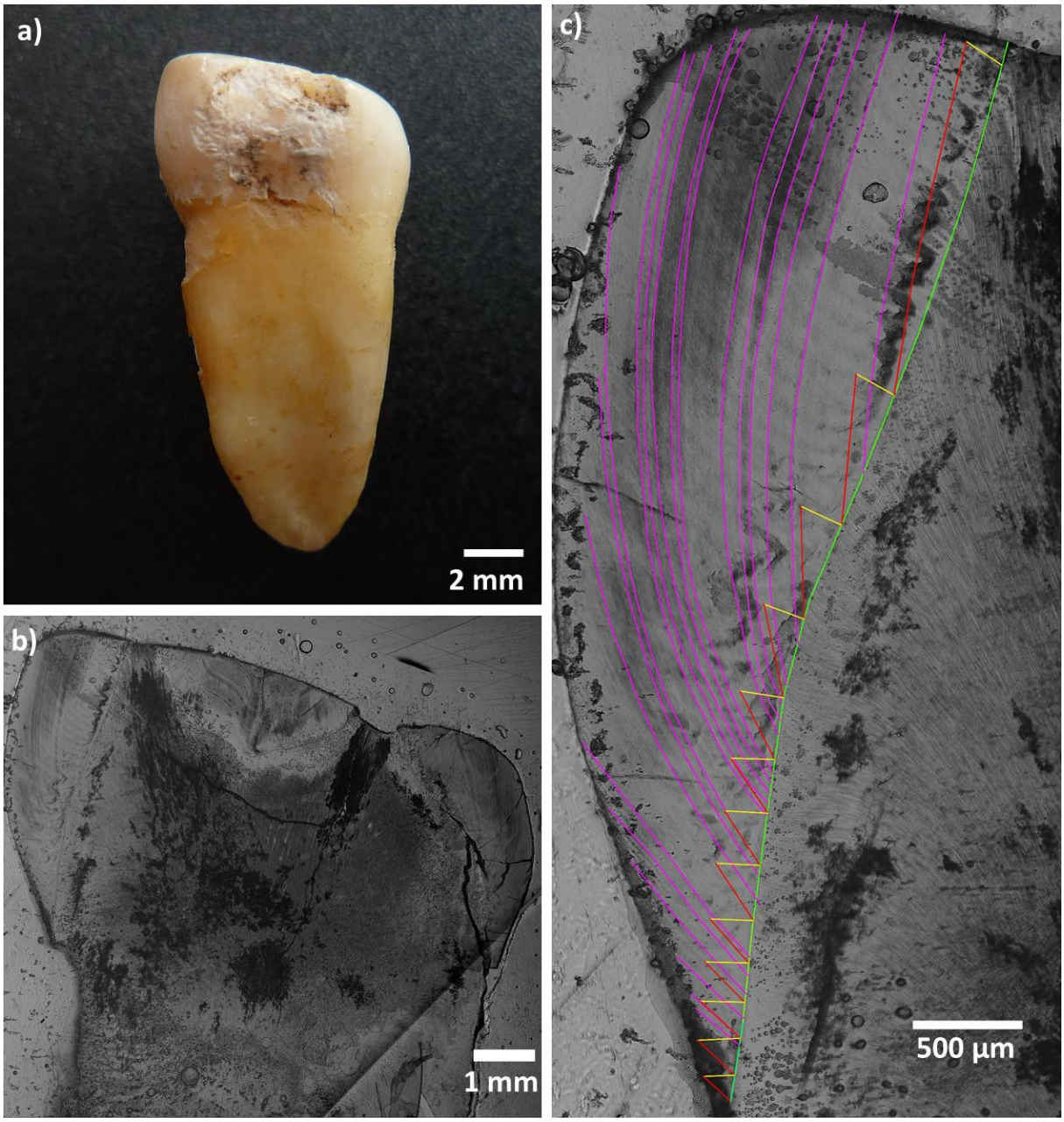

Figure 31 Various views of tooth 33 LLM1. a) Tooth after cleaning in mesial view, b) longitudinal section of the mesial cusps, c) mesiolingual cusp with analysis (green: EDJ, yellow: 200 µm prism, red: RL, and purple: AL).

5.2.6.2 LLM2

The second tooth analysed of individual 33 is the lower left second molar (LLM2). The tooth shows some wear but less excessive than LLM1 of this individual. It only shows some wear facets and one spot of open dentine. Therefore, the tooth falls into wear stage 3 (Smith, 1984).

The mesiolingual cusp was used for microstructure analyses (**Figure 32 c**). The EDJ had a length of 4563 µm and a CFT of 2.14 years, indicating tooth enamel development between the ages of 2.5 to 4.64 years (30-56 months).

During this time, eight AL formed between 2.61 and 3.38 years (**Table 17**). There are alone 3 AL around 32 months of age. These might have resulted from weaning as previous studies by archaeologists suggested for this population (Bernatzky et al., 2018).

The DSR varies in different parts of the enamel, ranging from 3.13 ± 0.12 µm/day in the cuspal inner enamel to 4.43 ± 0.20 µm/day in the cuspal outer enamel (Appendix 8.2, **Table 56**). The lateral inner DSR with 3.31 µm/day was used to calculate the chronology.

Table 17 Number of Accentuated Lines (AL) in tooth 33 LLM2 and age at time of appearance in months and years.

AL No.	Age (months)	Age (years)
1	31	2.61
2	32	2.63
3	32	2.68
4	32	2.70
5	36	3.01
6	38	3.14
7	39	3.27
8	41	3.38

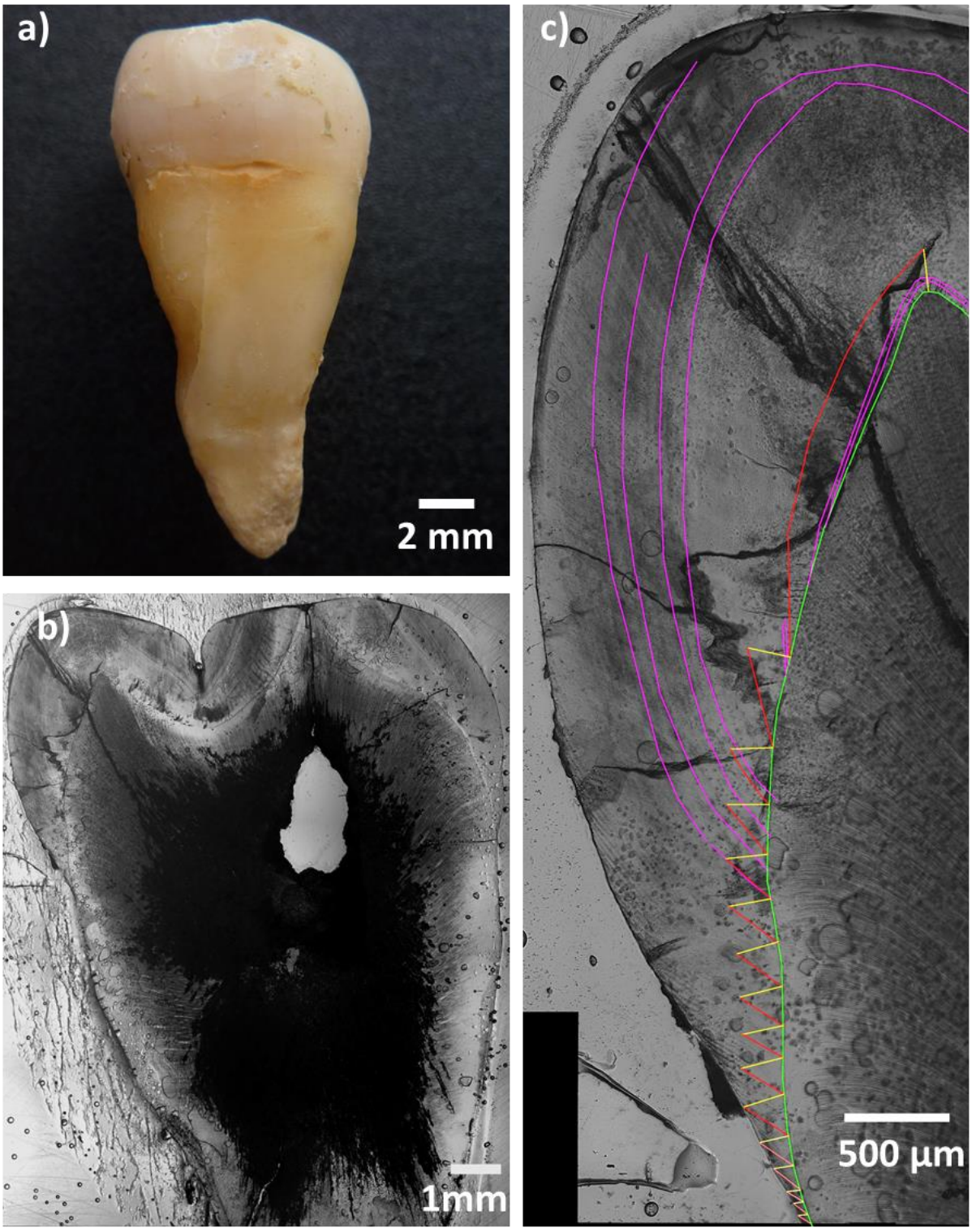

Figure 32 Various views of tooth 33 LLM2. a) Tooth after cleaning in mesial view, b) longitudinal section of the mesial cusps, c) mesiolingual cusp with analysis (green: EDJ, yellow: 200 µm prism, red: RL, and purple: AL).

5.2.6.3 LLM3

The third tooth of individual 33 that was analysed was the lower left third molar (LLM3). This tooth shows calculus at the lateral parts of the crown (**Figure 33 a**). The occlusal surface has very little tooth wear considering this person's high age. However, it has a large cavity between the mesiobuccal and distobuccal cusps. But this did not affect the mesiolingual cusp, allowing it to be used for further analysis (**Figure 33 c**).

The EDJ length was 4640 µm and a CFT of 1.39 years. Considering the estimated starting times, this leads to tooth enamel development between the ages of 8.00 to 9.39 years (96-116 months).

During this time, five AL formed between 8.31 and 8.97 years (**Table 18**). The presence of these lines between the ages of 8 and 9 years aligns with the developmental stage characterised by growth spurts in children. It is plausible that these lines were influenced by the rapid growth and other physical and cognitive changes occurring during this period (Arnold, 1986).

The DSR varies in different parts of the enamel, ranging from 3.54 ± 0.32 µm/day in the cuspal inner enamel to 4.81 ± 0.16 µm/day in the cuspal outer enamel (Appendix 8.2, **Table 56**). For the calculation of the chronology, the lateral inner DSR was used.

Table 18 Number of Accentuated Lines (AL) in tooth 33 LLM3 and age at time of appearance in months and years.

AL No.	Age (months)	Age (years)
1	100	8.31
2	102	8.46
3	103	8.56
4	105	8.71
5	108	8.97

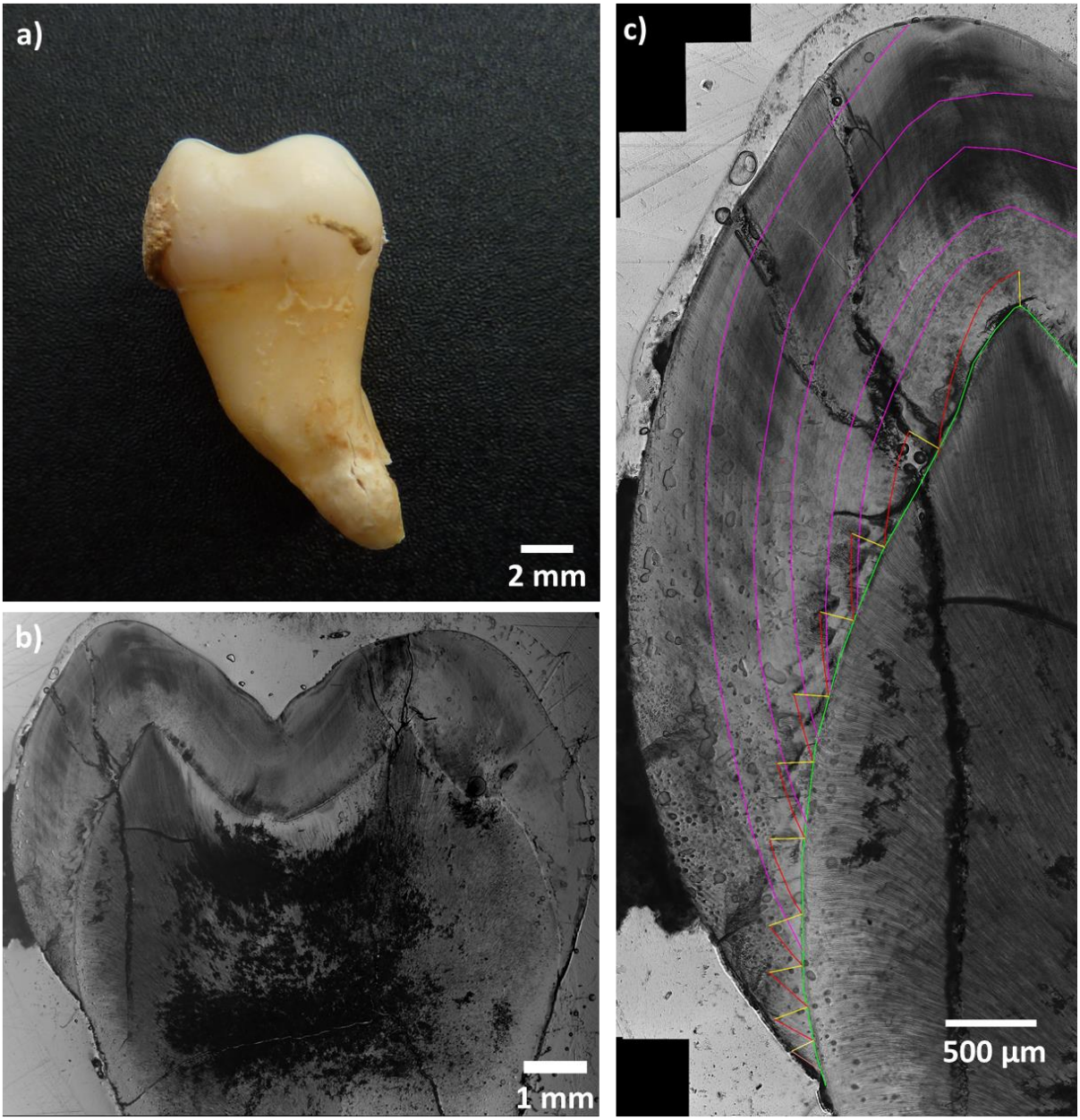

Figure 33 Various views of tooth 33 LLM3. a) Tooth after cleaning in mesial view, b) longitudinal section of the mesial cusps, c) mesiolingual cusp with analysis (green: EDJ, yellow: 200 µm prism, red: RL, and purple: AL).

5.2.7 Individual 38a

Individual 38a was a 25-year-old female. The upper jaw is fragmented, and only the right part was available for analysis. The first, second and third upper right molars (URM1, URM2, URM3) were extracted for analyses (**Figure 34**). Some teeth were loose after cleaning but have been secured in place using adhesive film.

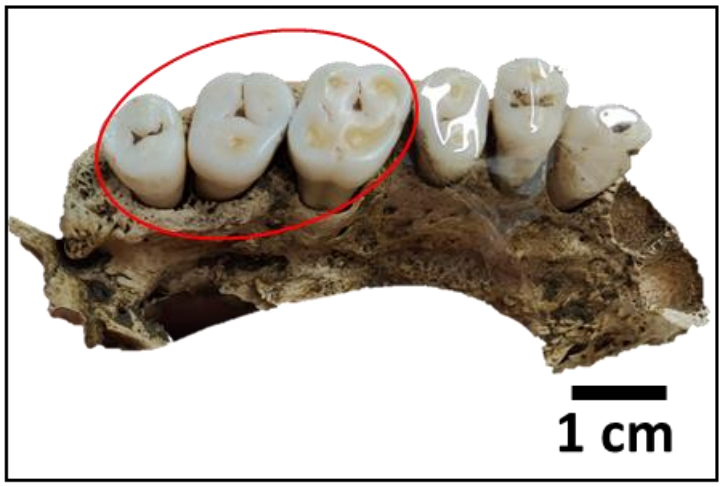

Figure 34 Upper jaw fragment of individual 38a. The red circle indicates which teeth have been extracted (URM1, URM2, URM3).

5.2.7.1 URM1

The first tooth examined was the upper right first molar (URM1). Remarkably, this tooth displays significant abrasion, with exposed dentin on each cusp. The level of wear observed, including the merging of some dentin pits, indicates an exceptionally high wear stage of 4-5 (Smith, 1984), given the individual's age at the time of death, estimated to be around 25 years. The flat tooth crown and exposed dentine can be seen in **Figure 35 a** and **b.**

For the microstructure analysis, the mesiobuccal cusp was used (**Figure 35 c**). The EDJ length was measured to be 4123 µm with a CFT of 1.81 years. This leads to an estimated tooth enamel development from birth to 1.81 years (0-22 months).

During that time, fifteen AL emerged between the age of 0.25 and 1.50 years (**Table 19**). Nine of those lines developed between the age of 5 to 10 months. During that time, a child starts

to get into contact with the environment and, therefore, with potential pathogens (Jenni, 2021).

The DSR varies in different parts of the enamel, ranging from 3.35 ± 0.24 µm/day in the cuspal outer enamel to 4.40 ± 0.32 µm/day in the lateral mid enamel (Appendix 8.2, **Table 56**). This is unusual since the DSR typically increases from the enamel's inner to outer parts (Nava et al., 2017). Compared with other samples, the highest rate is not found in the mid portion of the lateral enamel. The lateral inner DSR with 3.96 µm/day was used to calculate the chronology.

Since the enamel of this tooth is abraded to a great extent, these results may not reflect accurate times and rates and can, therefore, only be used as estimates.

Table 19 Number of Accentuated Lines (AL) in tooth 38a URM1 and age at time of appearance in months and years.

AL No.	Age (months)	Age (years)
1	3	0.25
2	3	0.28
3	5	0.45
4	6	0.50
5	7	0.54
6	7	0.62
7	8	0.66
8	9	0.75
9	9	0.78
10	10	0.81
11	10	0.86
12	12	1.00
13	14	1.15
14	14	1.15
15	18	1.50

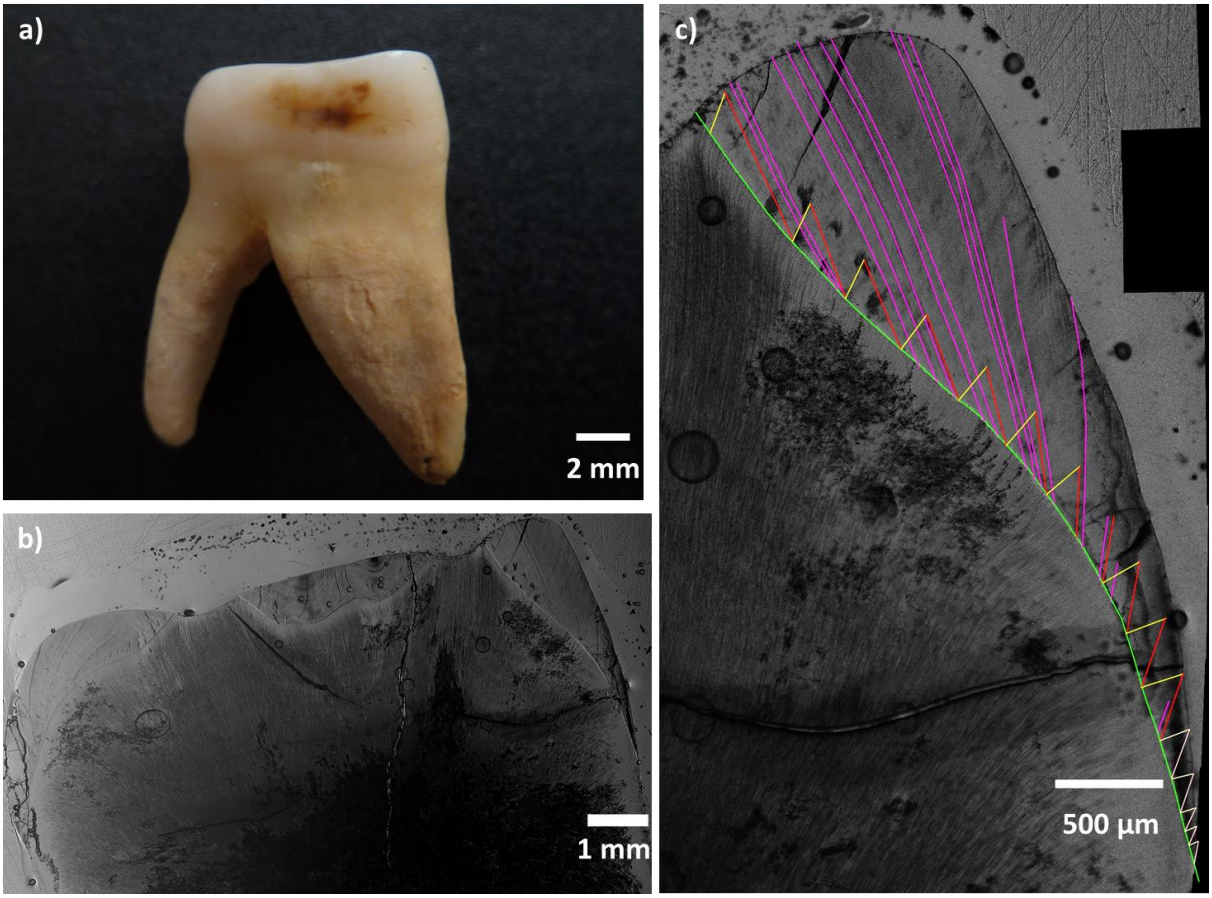

Figure 35 Various views of tooth 38a URM1. a) Tooth after cleaning in mesial view, b) longitudinal section of the mesial cusps, c) mesiobuccal cusp with analysis (green: EDJ, yellow: 200 µm prism, red: RL, and purple: AL).

5.2.7.2 URM2

The second tooth analysed from individual 38a was the upper right second molar (URM2). While this tooth exhibits some degree of cusp abrasion, the level of exposed dentin is comparatively lower than that observed in URM1 (**Figure 36 a** and **b**). It aligns with wear stage 3 (Smith, 1984).

The mesiobuccal cusp was used for the microstructural analyses (**Figure 36 c**) due to the lesser degree of abrasion than the other cusps. This analysis revealed an EDJ length of 5492 µm and a CFT of 2.50 years, resulting in a development time from 2.50 to 5.00 years (30-60 months).

Between the ages of 2.64 and 3.96, twelve AL emerged (**Table 20**). There appears to be a noticeable increase in the formation of AL around the age of 3 years. During that time, weaning took place, which might have caused these lines.

The DSR varies in different parts of the enamel, ranging from 3.78 ± 0.37 µm/day in the lateral inner enamel to 4.86 ± 0.22 µm/day in the cuspal outer enamel (Appendix 8.2, **Table 56**). For the calculation of the chronology, the lateral inner DSR was used.

Table 20 Number of Accentuated Lines (AL) in tooth 38a URM2 and age at time of appearance in months and years.

AL No.	Age (months)	Age (years)
1	32	2.64
2	33	2.76
3	36	2.97
4	36	3.03
5	37	3.07
6	37	3.09
7	38	3.13
8	40	3.31
9	40	3.36
10	42	3.50
11	43	3.58
12	48	3.96

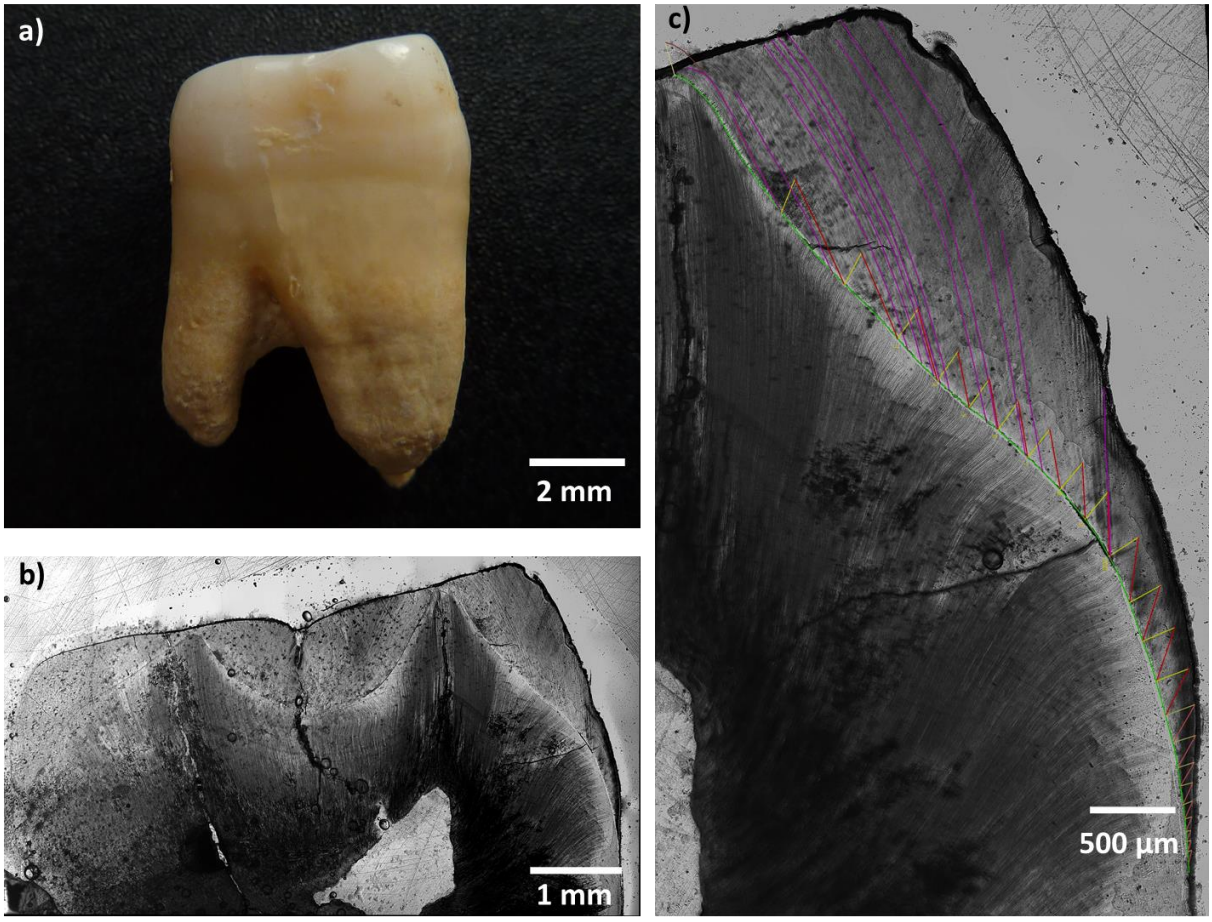

Figure 36 Various views of tooth 38a URM2. a) Tooth after cleaning in mesial view, b) longitudinal section of the mesial cusps, c) mesiobuccal cusp with analysis (green: EDJ, yellow: 200 µm prism, red: RL, and purple: AL).

5.2.7.3 URM3

The last tooth analysed of individual 38a was the upper right third molar (URM3). It was well preserved and showed the least abrasion compared to URM1 and URM2. However, during the cleaning and drying process, the tooth sustained a crack extending from the root tip to the cusp (**Figure 37 a** and **b**). Despite this, the tooth remained intact without complete splitting, allowing it to be used for further analyses.

For the microstructure analysis, the mesiolingual cusp was used. It was planned to use the mesiobuccal cusp for continuity (as in URM2), but the structures could be seen more clearly at the mesiolingual cusp. Therefore, this area was chosen to ensure optimal visualisation and analysis.

The EDJ length was 4809 µm and was formed from age 7.00 to 8.90 (84-107 months), leading to a CFT of 1.91 years.

During that time, six AL emerged between 7.53 and 7.98 years, with around one AL per month (**Table 21**). These lines observed may arise from a growth spurt that commonly occurred during that period, coinciding with the transition to the second developmental stage in children, accompanied by various physical and cognitive changes (Arnold, 1986).

The DSR varies in different parts of the enamel, ranging from 3.55 ± 0.31 µm/day in the cuspal inner enamel to 4.12 ± 0.22 µm/day in the cuspal outer enamel (Appendix 8.2, **Table 56**). The lateral inner DSR with 3.87 µm/day was used to calculate the chronology.

Table 21 Number of Accentuated Lines (AL) in tooth 38a URM3 and age at time of appearance in months and years.

AL No.	Age (months)	Age (years)
1	90	7.53
2	91	7.59
3	92	7.64
4	93	7.77
5	94	7.83
6	96	7.98

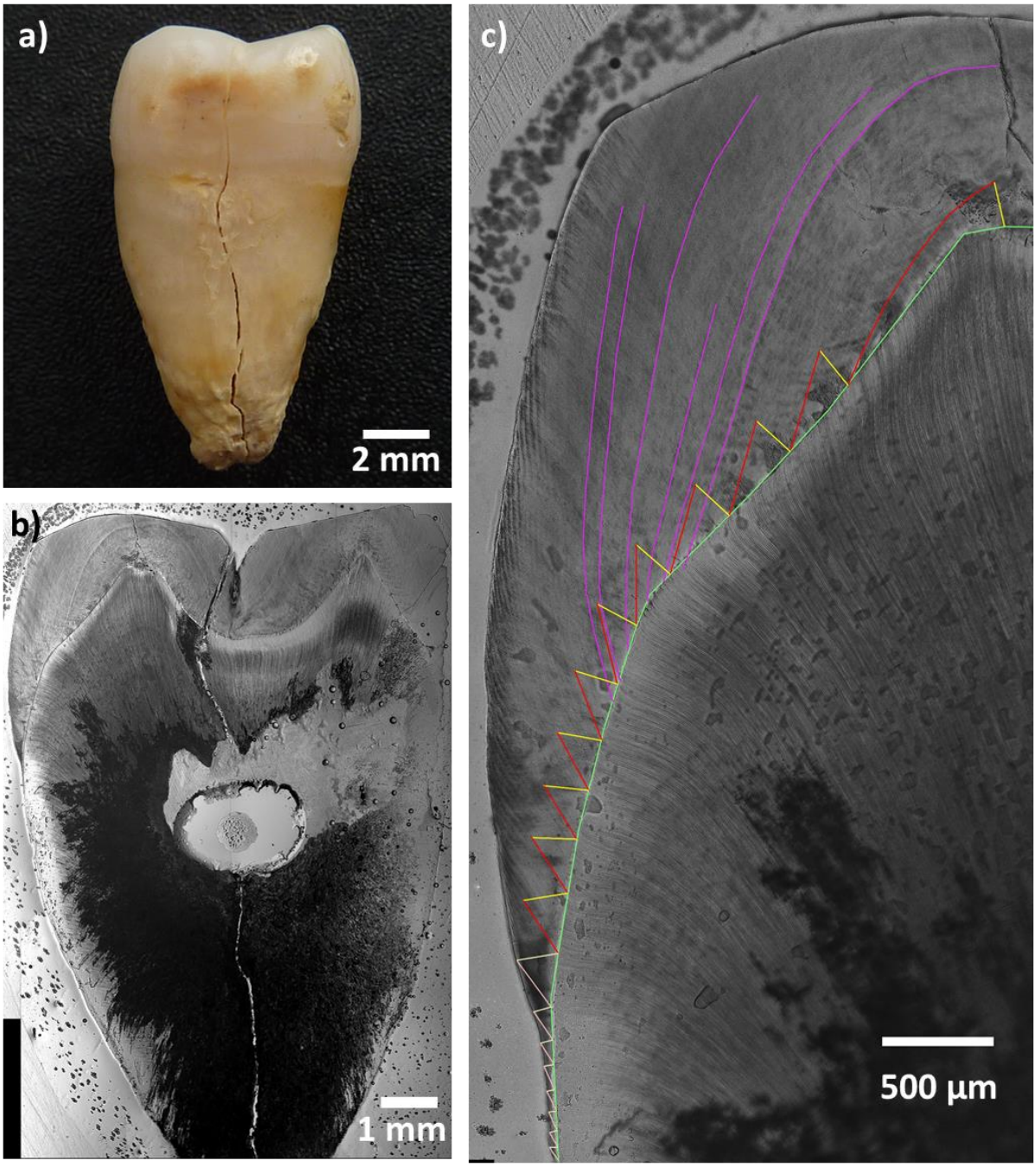

Figure 37 Various views of tooth 38a URM3. a) Tooth after cleaning in mesial view, b) longitudinal section of the mesial cusps, c) mesiolingual cusp with analysis (green: EDJ, yellow: 200 µm prism, red: RL, and purple: AL).

5.2.8 Individual 39

Individual 39 was a female who died at age 50. The jaw bones are well preserved, although the teeth are highly abraded with wear stages of 5-7 (Smith, 1984). The severe wear seems to be caused by malocclusion, probably a crossbite. The teeth in the upper jaw have inclined abrasion facets that slope down palatally. On the second incisor, the entire lingual surface is abraded. The abrasion facets of the first premolars and the first and second molars are obliquely inclined labially in the mandible. The alveoli are reduced and inflamed. Calculus is found circularly on all upper and lower teeth. In the lower jaw, the lingual surfaces of the incisor crowns are entirely covered with calculus. The third molars are developed on both sides of the upper jaw, but the alveoli are empty, and the teeth went missing post-mortem. Their miniature form is, however, recognisable from the shape and size of the alveoli. In the lower jaw, the alveolus of the third molar on the left side is empty as well. This appears to have happened post-mortem, too. In addition, the right mandibular canine is distally rotated, and the mandibular anterior tooth roots are fenestrated.

The lower right premolars exhibit the best preservation among the available teeth, making them the preferred choice for analysis (**Figure 38**, right). Similarly, among the molars, the upper left second molar stands out as the best-preserved tooth and has been selected for further analysis (**Figure 38**, left).

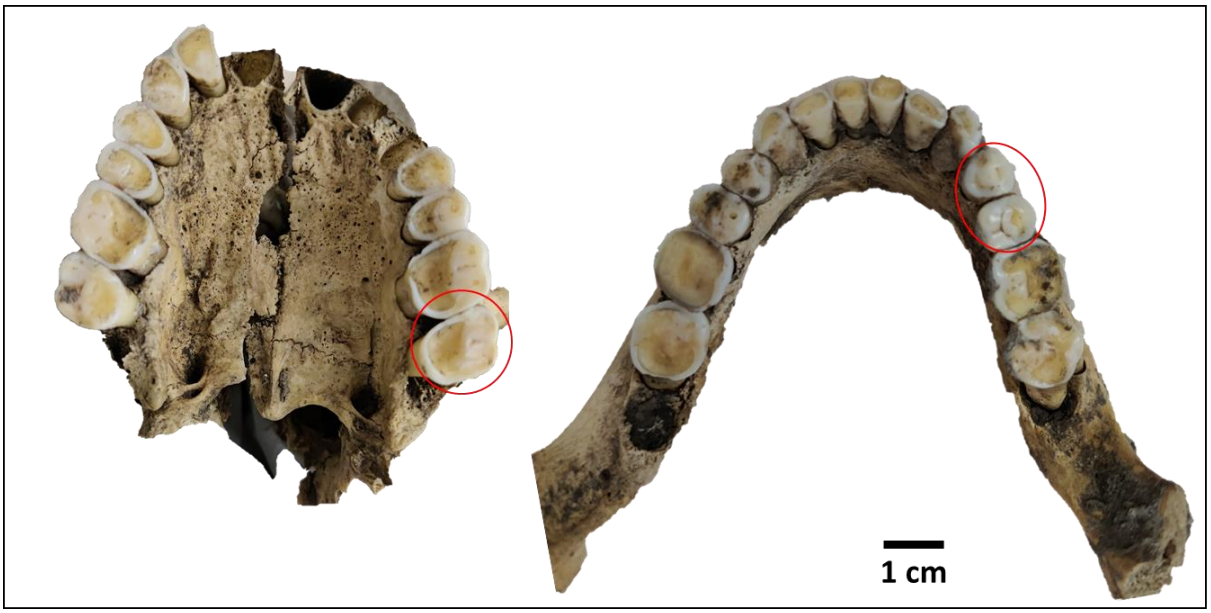

Figure 38 Upper (left) and lower (right) jaw of individual 39. The red circles indicate which teeth have been extracted (ULM2, LRP3, LRP4).

5.2.8.1 LRP3

The first tooth to be analysed of individual 39 is the lower right third premolar (LRP3). The buccal tip of the cusp is abraded with a wear stage 3 (Smith, 1984). Calculus is present around the tooth cervix, and during cleaning, some of it was detached (**Figure 39 a** and **b**).

The buccal cusp of LRP3 was chosen for microstructural analyses (**Figure 39 c**). An EDJ length of 6843 µm was measured with a CFT of 3.89 years. This leads to a developmental time of 1.5 to 5.39 years (18-65 months).

This tooth shows twenty AL, which is the highest amount of AL in all analysed teeth from Gevensleben (**Table 22**). The lines emerged between 1.64 years and 3.42 years. The lines AL 10 and 11 are very prominently developed. Those lines emerged at the age of approximately 2.5 years old. Both lines build a nearly inseparable big line. This leads to the assumption that this person had a very stressful event. Weaning usually happens at this age, but a prominent line like this was found in none of the other teeth of this person. After that age, no AL were detected. A possible explanation for this might be the susceptibility of ameloblasts to record stress. Over the tooth crown this varies, with a lower likelihood of recording stress in the cervical region of the enamel than in the central parts (Nava et al., 2019).

The DSR varied along the enamel from 3.63 µm/day in the lateral inner parts to 4.40 µm/day in the lateral outer portion of the enamel (Appendix 8.2, **Table 56**). The lateral inner DSR with 3.63 µm/day was used to calculate the chronology.

Table 22 Number of Accentuated Lines (AL) in tooth 39 LRP3 and age at time of appearance in months and years. Especially pronounced lines are printed in bold type.

AL No.	Age (months)	Age (years)
1	20	1.64
2	20	1.70
3	23	1.90
4	23	1.91
5	26	2.20
6	27	2.25
7	29	2.41
8	29	2.42
9	29	2.45
10	**30**	**2.52**
11	**31**	**2.54**
12	32	2.66
13	33	2.75
14	34	2.87
15	35	2.94
16	36	3.02
17	37	3.11
18	38	3.13
19	38	3.15
20	41	3.42

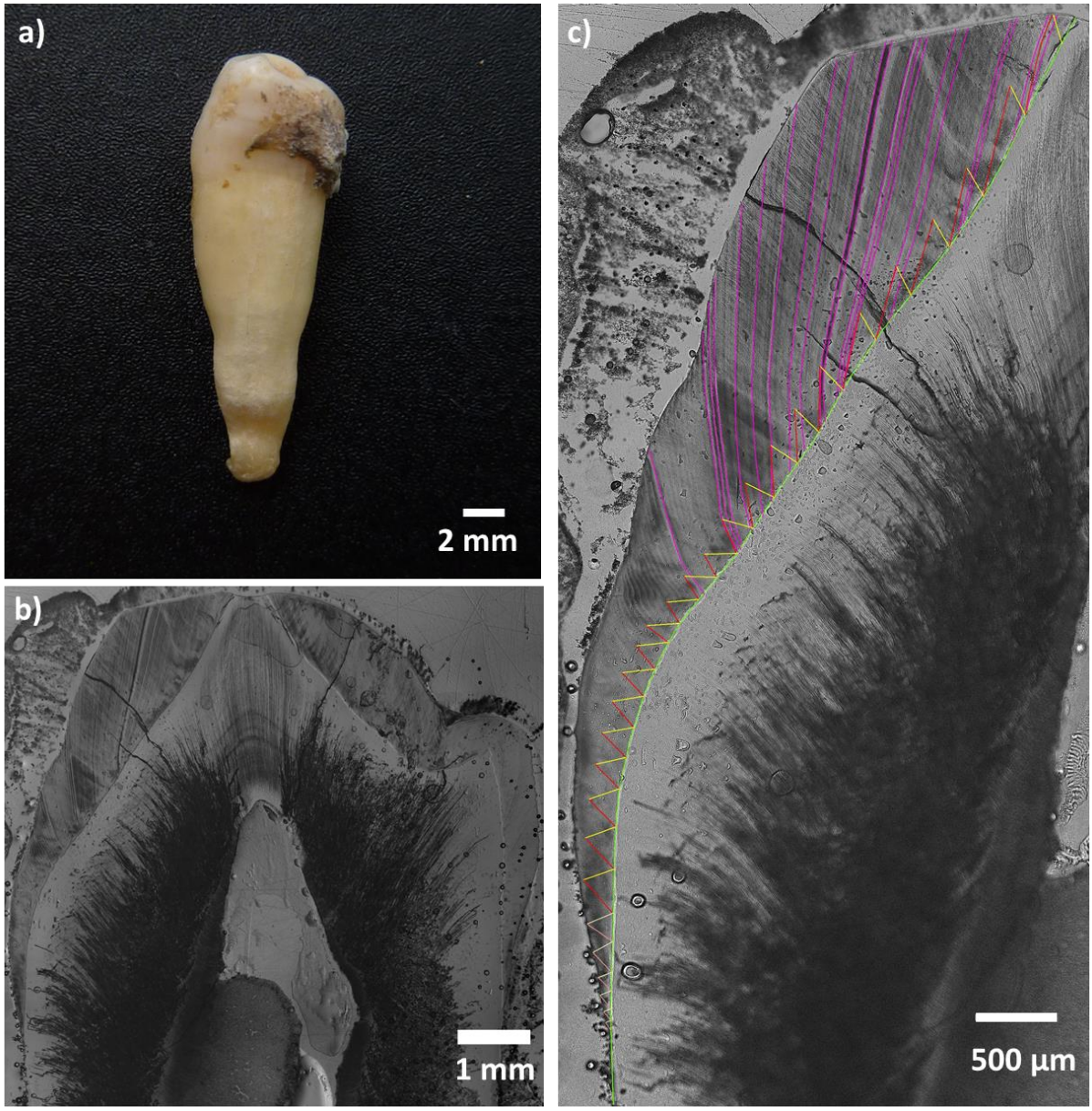

Figure 39 Various views of tooth 39 LRP3. a) Tooth after cleaning in mesial view, b) longitudinal section of the tooth, c) buccal cusp with analysis (green: EDJ, yellow: 200 µm prism, red: RL, and purple: AL).

5.2.8.2 LRP4

The second tooth analysed of individual 39 was the lower right fourth premolar (LRP4). It shows some wear on the buccal cusp, which falls in wear stage 3 (Smith, 1984). LRP4 also showed some calculus, of which some was detached during cleaning (**Figure 40 a** and **b**).

For microstructural analysis, the lingual cusp was chosen (**Figure 40 c**). An EDJ length of 3857 µm was measured with a CFT of 1.48 years. Considering the estimated developmental onset, this leads to a developmental time from age 2.0 to 3.48 (24-42 months).

LRP4 shows ten AL, which emerged from age 2.15 to 2.91 (**Table 23**). At this time, the event resulted in the very prominent line on tooth LRP3. Lines 5 to 7 in LRP4 lie around this timeframe (2.5 years of age) but are not as prominently developed as in LRP3. But AL 9 and 10 at 33 and 35 months of age appear at the same time as in the next tooth (ULM2) from this individual.

The DSR varies from 3.65 µm/day in the cuspal inner enamel to 4.60 µm/day in the lateral outer enamel (Appendix 8.2, **Table 56**). The lateral inner DSR with 4.20 µm/day was used to calculate the chronology.

Table 23 Number of Accentuated Lines (AL) in tooth 39 LRP4 and age at time of appearance in months and years. Asterisk marks lines that appear at the same time in tooth ULM2 from the same individual.

AL No.	Age (months)	Age (years)
1	26	2.15
2	27	2.28
3	29	2.39
4	29	2.43
5	30	2.47
6	30	2.49
7	30	2.53
8	32	2.68
9*	33	2.78
10*	35	2.91

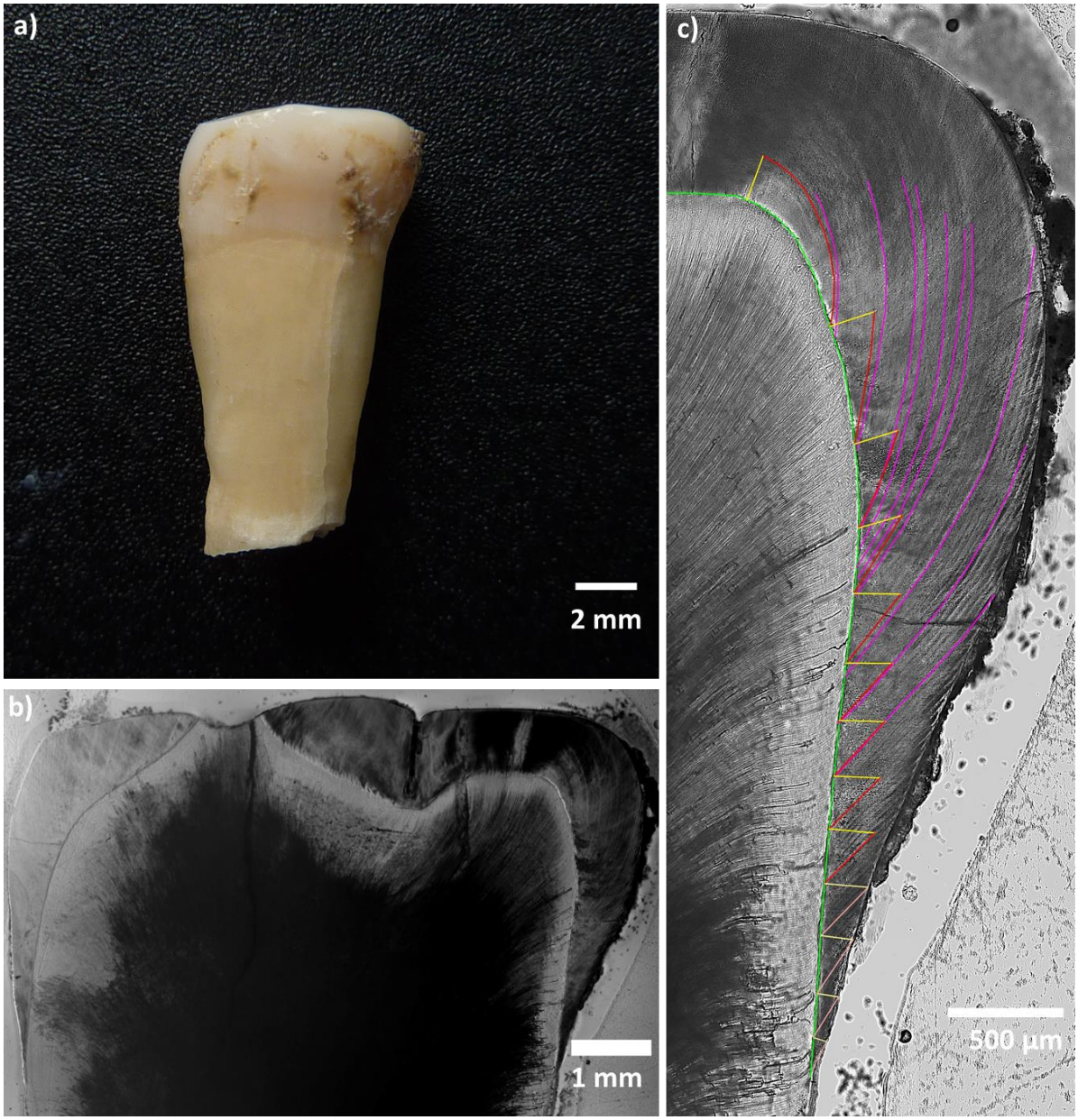

Figure 40 Various views of tooth 39 LRP4. a) Tooth after cleaning in mesial view, b) longitudinal section of the tooth, c) lingual cusp with analysis (green: EDJ, yellow: 200 µm prism, red: RL, and purple: AL).

5.2.8.3 ULM2

The third tooth analysed from individual 39 is the upper left second molar (ULM2). It is highly abraded, especially at the palatial cusps. This classifies at wear stage 5 (Smith, 1984). It also shows some calculus at the tooth cervix and a caries lesion on the distal tooth cervix (**Figure 41 a** and **b**).

The mesiobuccal cusp was chosen for microstructural analysis (**Figure 41 c**). This revealed an EDJ length of 4695 µm and a CFT of 2.35 years. Considering the estimated starting time, this leads to a developmental time from age 2.50 to 4.85 (30-58 months).

Eleven AL can be found over the enamel, which emerged between 2.64 and 3.74 years. Two lines are identical with LRP4: in LRP4 lines 9 and 10 at age 2.78 and 2.91, and in ULM2 3 and 6 at age 2.78 and 2.92 (see **Table 23** and **Table 24**). However, it cannot be said with certainty that the lines result from the same stress events. Since no neonatal line could be found to date this individual's development precisely, the chronology is based on the estimated times of tooth development (AlQahtani et al., 2010).

The DSR varies from 3.58 µm/day in the lateral inner enamel to 4.23 µm/day in the lateral outer enamel (Appendix 8.2, **Table 56**). For the calculation of the chronology, the lateral inner DSR was used.

Table 24 Number of Accentuated Lines (AL) in tooth 39 ULM2 and age at time of appearance in months and years. Asterisk marks lines that appear at the same time in tooth LRP4 from the same individual.

AL No.	Age (months)	Age (years)
1	32	2.64
2	33	2.71
3*	33	2.78
4	34	2.83
5	34	2.87
6*	35	2.92
7	36	3.00
8	37	3.11
9	38	3.15
10	43	3.54
11	45	3.74

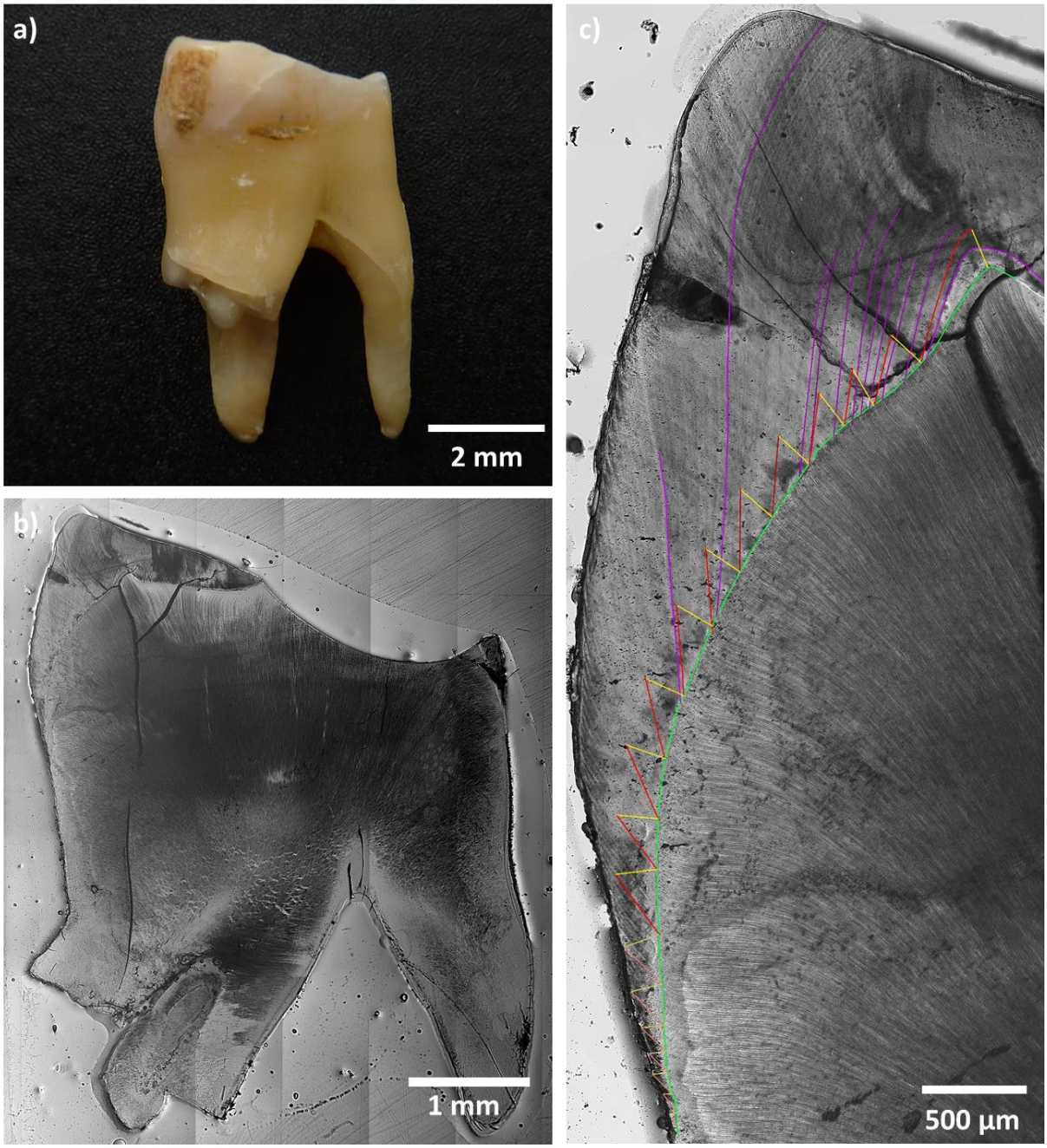

Figure 41 Various views of tooth 39 ULM2. a) Tooth after cleaning in mesial view, b) longitudinal section of the mesial cusps, c) mesiobuccal cusp with analysis (green: EDJ, yellow: 200 µm prism, red: RL, and purple: AL).

5.2.9 Individual 43

Individual 43 was a female who died at age 19-20. The mandible is fragmented into two parts (**Figure 42**). The front teeth of the lower jaw are missing post-mortem. The first to third molars on the left side were chosen for the analyses (LLM1, LLM2, LLM3). Due to the young age, these are well preserved and show, except for the first molar, minor abrasion.

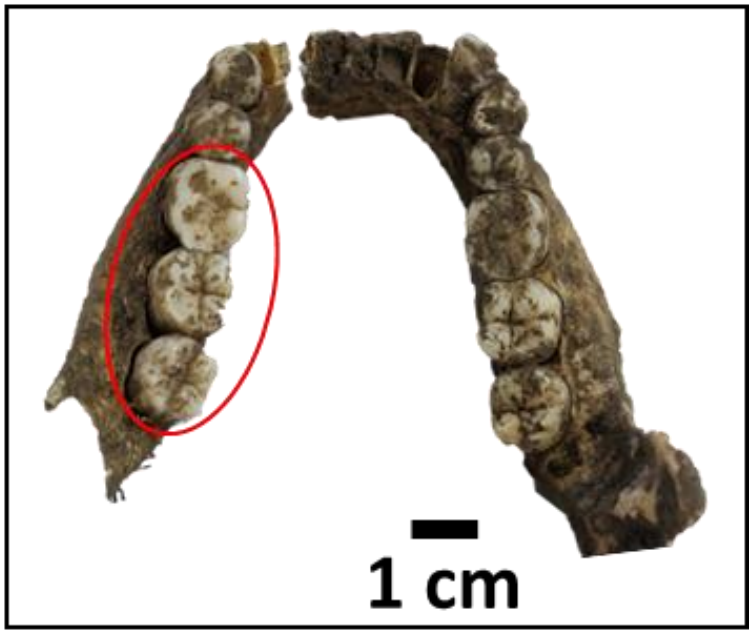

Figure 42 Lower jaw fragments of individual 43. The red circle indicates which teeth have been extracted (LLM1, LLM2, LLM3).

5.2.9.1 LLM1

The first tooth analysed was the lower left first molar (LLM1). It is well preserved but shows some wear of stage 4 (Smith, 1984), especially at the buccal cusps (**Figure 43 a** and **b)**. Due to this, the mesiolingual cusp was chosen for microstructural analyses (**Figure 43 c).**

The analyses revealed an EDJ length of 4819 µm and a CFT of 1.85 years. With the estimated starting time, the tooth enamel development occurred from 0 to 1.85 years (0-22 months).

Fourteen AL can be found, which developed from 0.16 to 1.67 years (**Table 25**). A prominent line is AL6 at age 0.58. During this time, children start interacting with their environment,

which can cause developmental stress for the body or possible infections with pathogens (Jenni, 2021).

The DSR ranges from 3.35 µm/day in the lateral inner enamel to 4.82 µm/day in the cuspal outer enamel (Appendix 8.2, **Table 57**). For the calculation of the chronology, the lateral inner DSR was used.

Table 25 Number of Accentuated Lines (AL) in tooth 43 LLM1 and age at time of appearance in months and years. Especially pronounced lines are printed in bold type.

AL No.	Age (months)	Age (years)
1	2	0.16
2	4	0.33
3	5	0.38
4	5	0.41
5	6	0.50
6	**7**	**0.58**
7	8	0.63
8	9	0.79
9	11	0.88
10	12	1.01
11	13	1.04
12	15	1.25
13	15	1.28
14	20	1.67

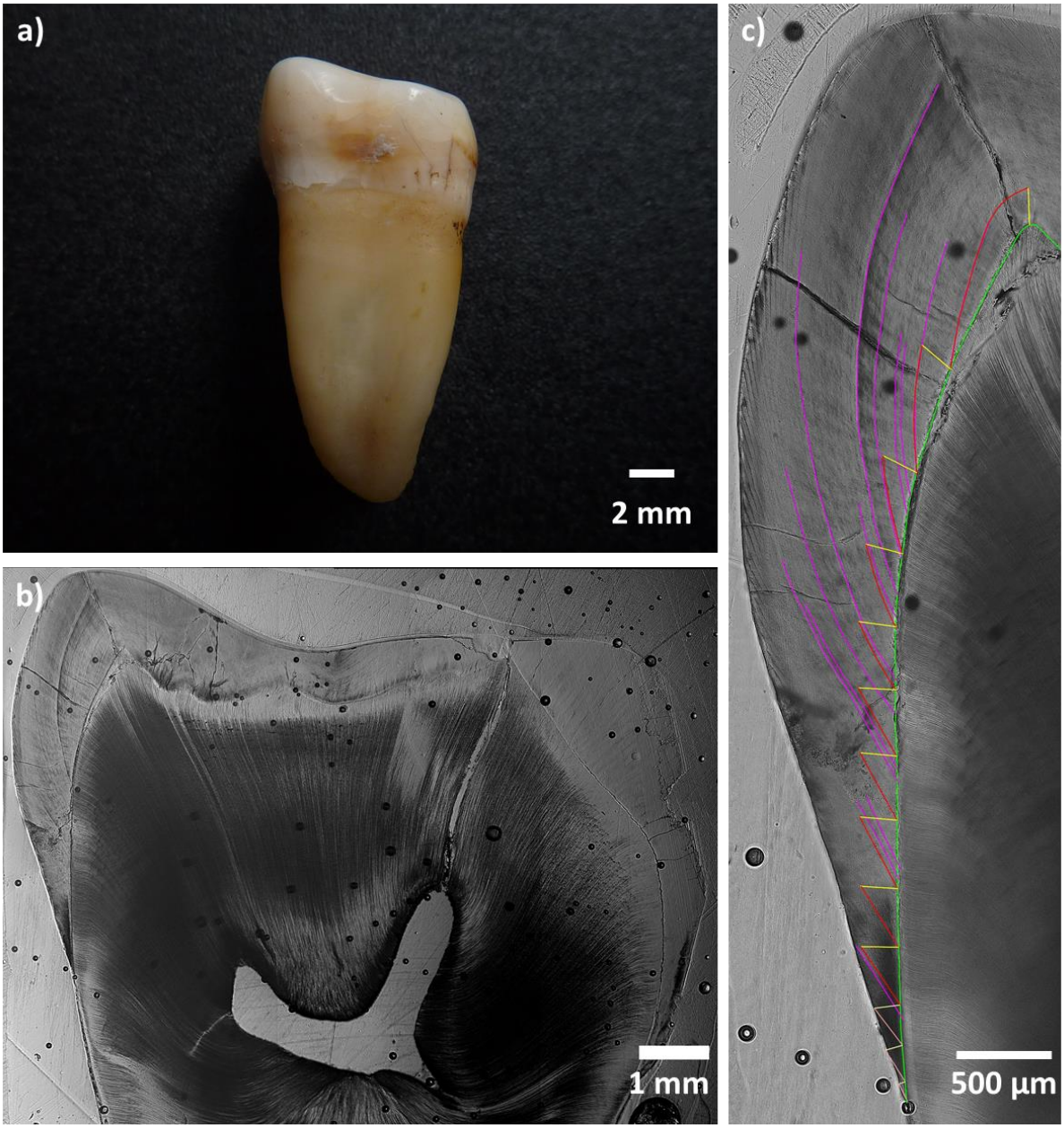

Figure 43 Various views of tooth 43 LLM1. a) Tooth after cleaning in mesial view, b) longitudinal section of the mesial cusps, c) mesiolingual cusp with analysis (green: EDJ, yellow: 200 µm prism, red: RL, and purple: AL).

5.2.9.2 LLM2

The second tooth to be analysed for individual 43 was the lower left second molar (LLM2). It is less abraded than LLM1 and only has some pronounced wear facets but no exposed dentine. It fits a wear stage of 2 (Smith, 1984). Both mesial cusps are well preserved, but some enamel has been detached around the cervix. The mesiolingual cusp shows only minor abrasion and is, therefore, chosen for analysis (**Figure 44**).

The microstructural analyses lead to an EDJ length of 5123 µm and a CFT of 2.21 years. With an estimated starting time, the developmental time of this tooth ranges from 2.50 to 4.70 years (30-56 months).

Only six AL can be found on this tooth (**Table 26**). They developed between 2.65 and 3.30 years. During this time, it is expected that weaning took place, which can be a possible explanation for these lines. The particularly prominent line (AL6, **Table 25**) from the previous tooth LLM1 cannot be found because it developed around age 0.58 years. LLM2 starts forming at around 2.50 years, so any stressful event that happened before this age cannot show up. The prominent line on this tooth is AL5 which emerged at 3.2 years.

The DSR varied along the enamel from 3.60 µm/day in the cuspal inner parts to 4.07 µm/day in the lateral outer portion of enamel (Appendix 8.2, **Table 56**). The lateral inner DSR with 3.75 µm/day was used to calculate the chronology.

Table 26 Number of Accentuated Lines (AL) in tooth 43 LLM2 and age at time of appearance in months and years. Especially pronounced lines are printed in bold type.

AL No.	Age (months)	Age (years)
1	32	2.65
2	35	2.90
3	36	3.01
4	38	3.14
5	**38**	**3.20**
6	40	3.30

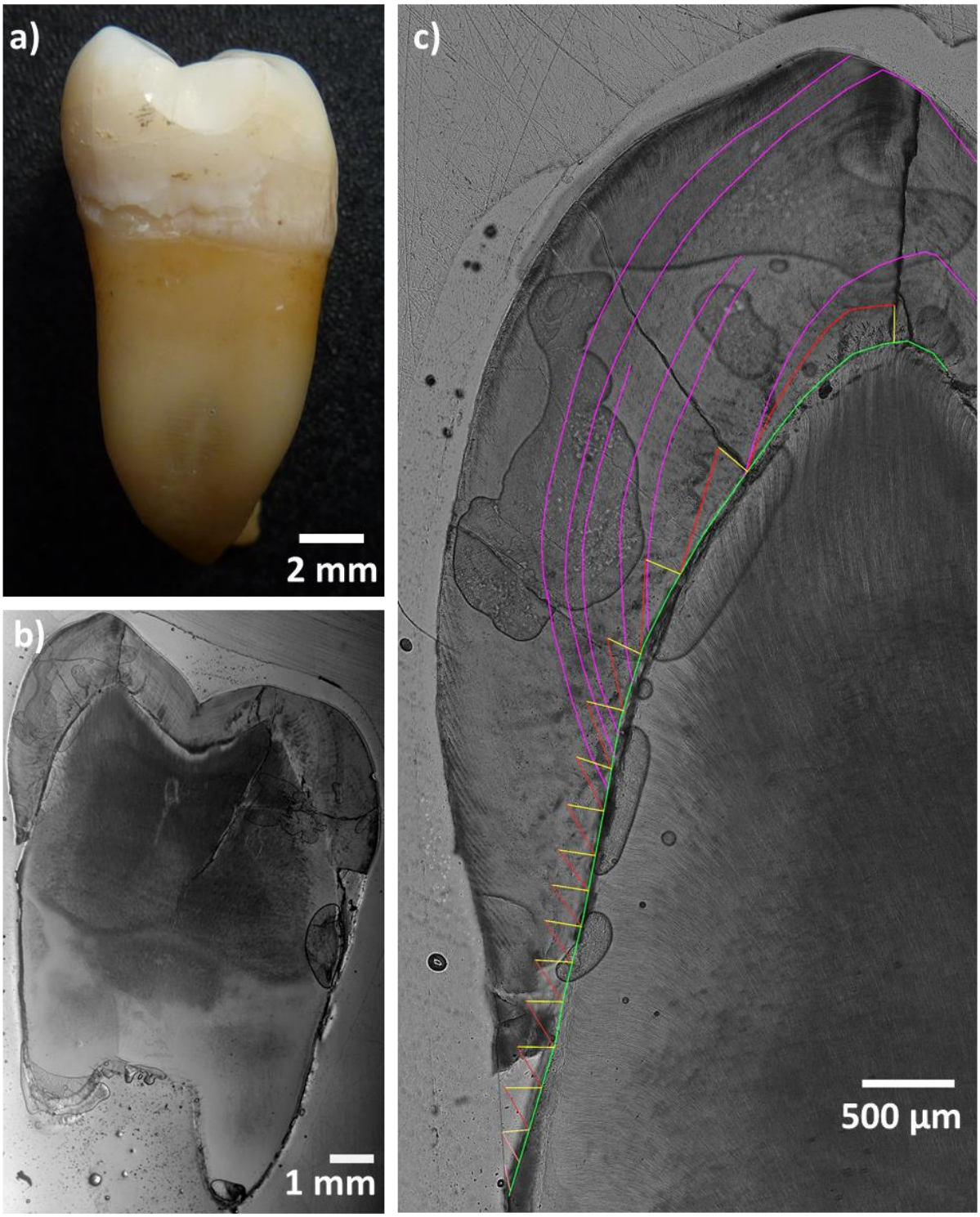

Figure 44 Various views of tooth 43 LLM2. a) Tooth after cleaning in mesial view, b) longitudinal section of the mesial cusps, c) mesiolingual cusp with analysis (green: EDJ, yellow: 200 µm prism, red: RL, and purple: AL).

5.2.9.3 LLM3

The third tooth analysed for individual 43 was the lower left third molar (LLM3). This tooth shows minor abrasion (**Figure 45**) and has a wear stage 2 (Smith, 1984).

Both mesial cusps are well preserved, but in the mesiobuccal cusps, the structures can be detected more clearly (**Figure 45 c**).

The microstructural analyses revealed an EDJ length of 6006 µm and a CFT of 3 years. Considering the estimated starting time of the tooth, the development took place from 8 to 11 years (96-132 months).

Seven AL can be found, which developed from 8.29 to 9.11 years (**Table 27**). The most prominent line is AL 6, at the age of 9.02 years. These accentuated lines may be attributed to a growth spurt typically occurring during that period, coinciding with the transition to the second developmental stage in children, which is accompanied by various physical and cognitive changes (Arnold, 1986). Since this is the only tooth from the extracted sample that develops during this time, this line cannot be found on another tooth.

The DSR changed along the enamel from 3.46 µm/day in the lateral inner parts to 4.60 µm/day in the cuspal outer parts of enamel (Appendix 8.2, **Table 56**). For the calculation of the chronology, the lateral inner DSR was used.

Table 27 Number of Accentuated Lines (AL) in tooth 43 LLM3 and age at time of appearance in months and years. Especially pronounced lines are printed in bold type.

AL No.	Age (months)	Age (years)
1	100	8.29
2	100	8.30
3	100	8.33
4	102	8.50
5	104	8.70
6	**108**	**9.02**
7	109	9.11

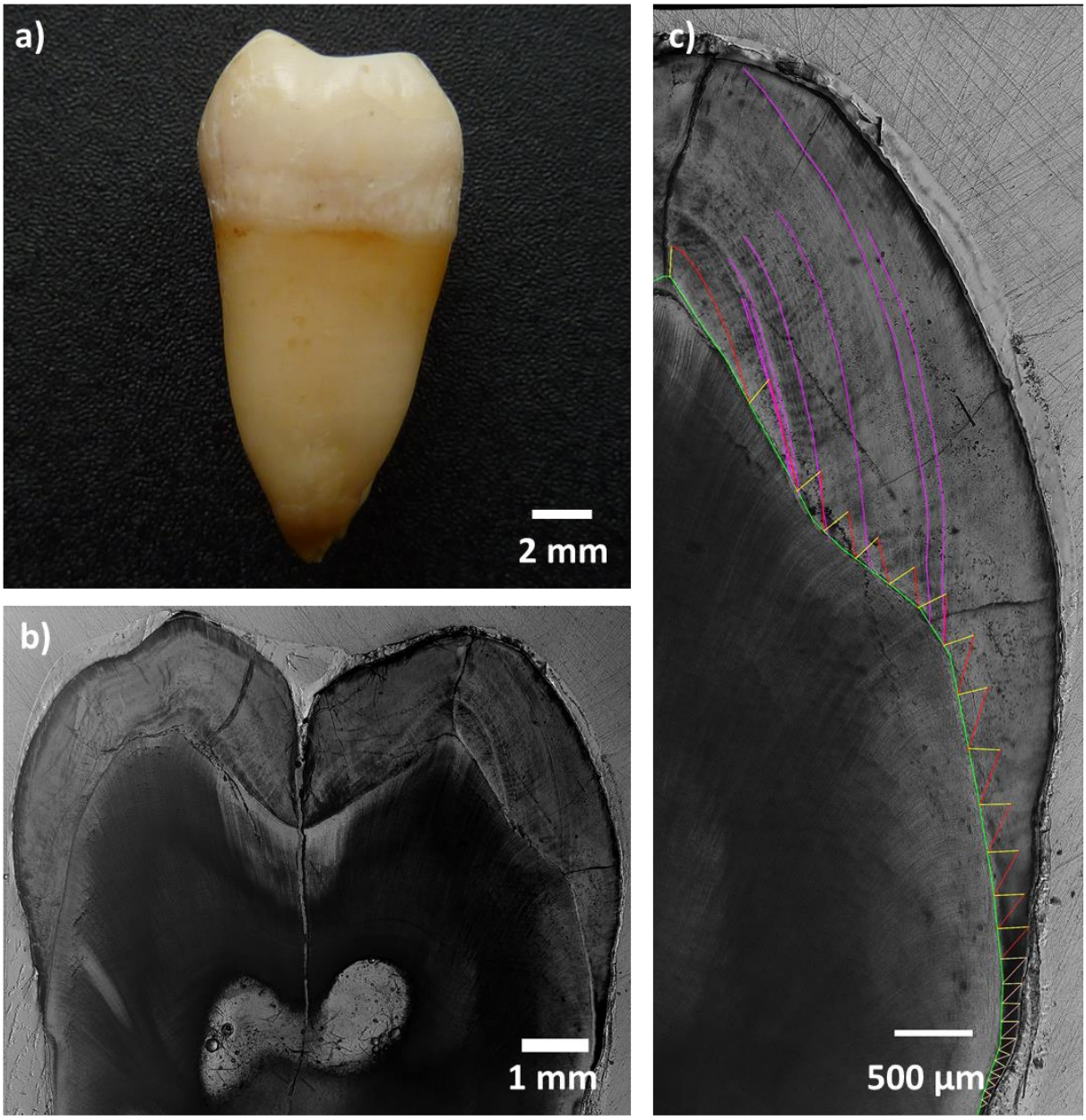

Figure 45 Various views of tooth 43 LLM3. a) Tooth after cleaning in mesial view, b) longitudinal section of the mesial cusps, c) mesiobuccal cusp with analysis (green: EDJ, yellow: 200 µm prism, red: RL, and purple: AL).

5.2.10 Individual 45

Individual 45 was a female who died at age 20. The dentition is in good condition and only shows minor abrasion. Some teeth have small cavities.

The mandible is in very good condition. However, the shape characteristics of this mandible are unusual within this series. The dental arch has an almost perfect shape, and the chin is slightly pointed. None of these characteristics can be found in the other individuals.

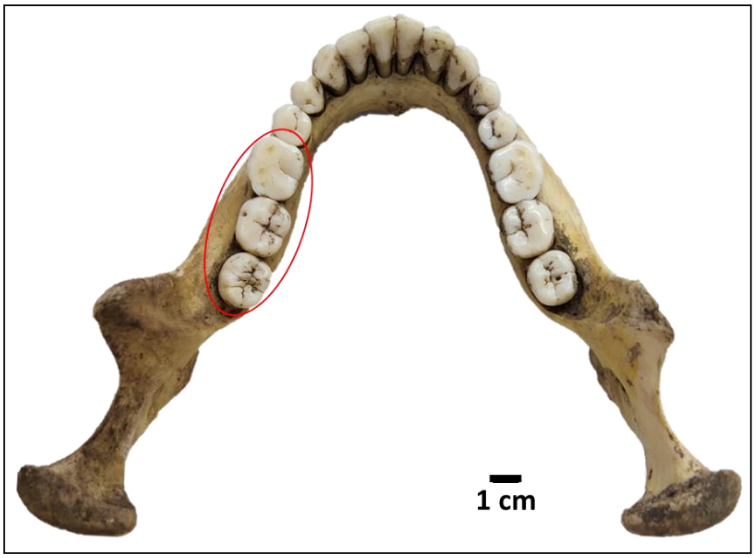

Figure 46 Lower jaw of individual 45. The red circle indicates which teeth have been extracted (LLM1, LLM2, LLM3).

5.2.10.1 LLM1

The first tooth analysed from individual 45 is the lower left first molar (LLM1). This tooth is, caused by the early eruption time, the most abraded tooth from the analysed array of this individual. It has a wear stage of 4 (Smith, 1984).

The mesiolingual cusp has minor abrasion. Nevertheless, the mesiobuccal cusp was better suited for analyses since the structure could be identified more clearly (**Figure 47**). Although the mesiobuccal cusp has a crack that reaches from the enamel down to the pulp, it did not affect the analyses.

The microstructural analyses revealed an EDJ of 6072 µm and a CFT of 2.48 years. The estimated starting time at birth leads to a developmental time from 0 to 2.48 years of age (0-30 months).

During that time, eight AL developed with the first at 0.77 and the last at 2.05 years old (**Table 28**). There is no very prominent line, and no other examined tooth from this individual showed a line at the same time.

The DSR varied along the enamel from 3.66 ±0,32 µm/day in the cuspal mid parts to 4.35 ± 0.36 µm/day in the cuspal outer parts of enamel (Appendix 8.2, **Table 57**). For the calculation of the chronology, the lateral inner DSR of 3.95 µm/day was used.

Table 28 Number of Accentuated Lines (AL) in tooth 45 LLM1 and age at time of appearance in months and years.

AL No.	Age (months)	Age (years)
1	9	0.77
2	10	0.80
3	10	0.86
4	13	1.09
5	15	1.24
6	16	1.37
7	23	1.93
8	25	2.05

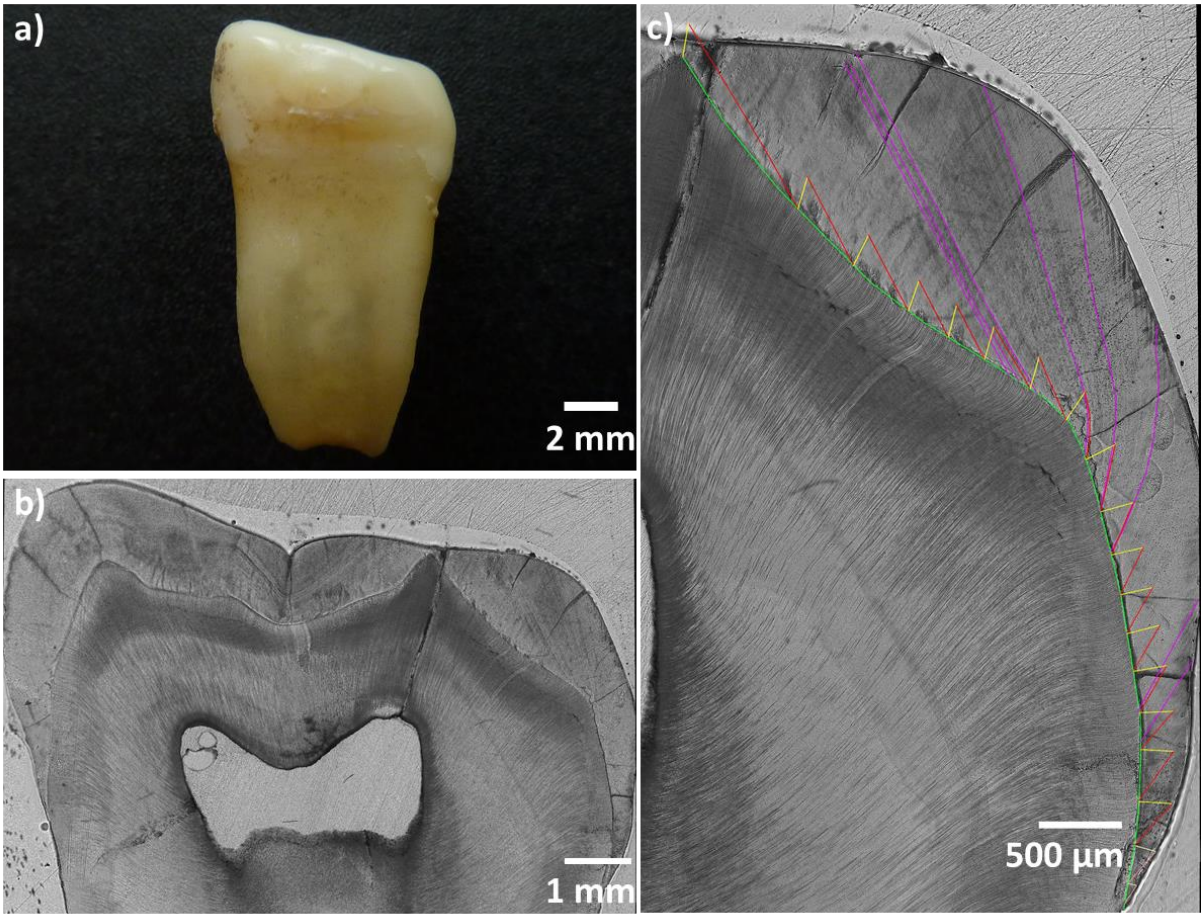

Figure 47 Various views of tooth 45 LLM1. a) Tooth after cleaning in mesial view, b) longitudinal section of the mesial cusps, c) mesiobuccal cusp with analysis (green: EDJ, yellow: 200 µm prism, red: RL, and purple: AL).

5.2.10.2 LLM2

The second tooth analysed of individual 45 was the lower left second molar (LLM2). It shows a few abrasion facets and no exposed dentine (**Figure 48 a** and **b**). Therefore, it has a wear stage of 2 (Smith, 1984).

The mesiolingual cusp was chosen for the examination. It has a crack (**Figure 48 c**) through the enamel, but this did not affect the examination.

The microstructural analyses revealed an EDJ length of 3480 µm and a CFT of 2.08 years. With the estimated starting time, the development took place from 2.50 to 4.58 years (30-55 months).

During this time, only three AL emerged from age 3.04 to 3.47. These are especially few lines for that time since most of the other individuals experienced more stress during weaning.

The DSR varied along the enamel from 3.04 ± 0.24 µm/day in the cuspal outer parts to 4.65 ± 0.27 µm/day in the lateral outer enamel (Appendix 8.2, **Table 57**). For the calculation of the chronology the lateral inner DSR of 3.24 µm/day was used.

Table 29 Number of Accentuated Lines (AL) in tooth 45 LLM2 and age at time of appearance in months and years.

AL No.	Age (months)	Age (years)
1	36	3.04
2	38	3.19
3	42	3.47

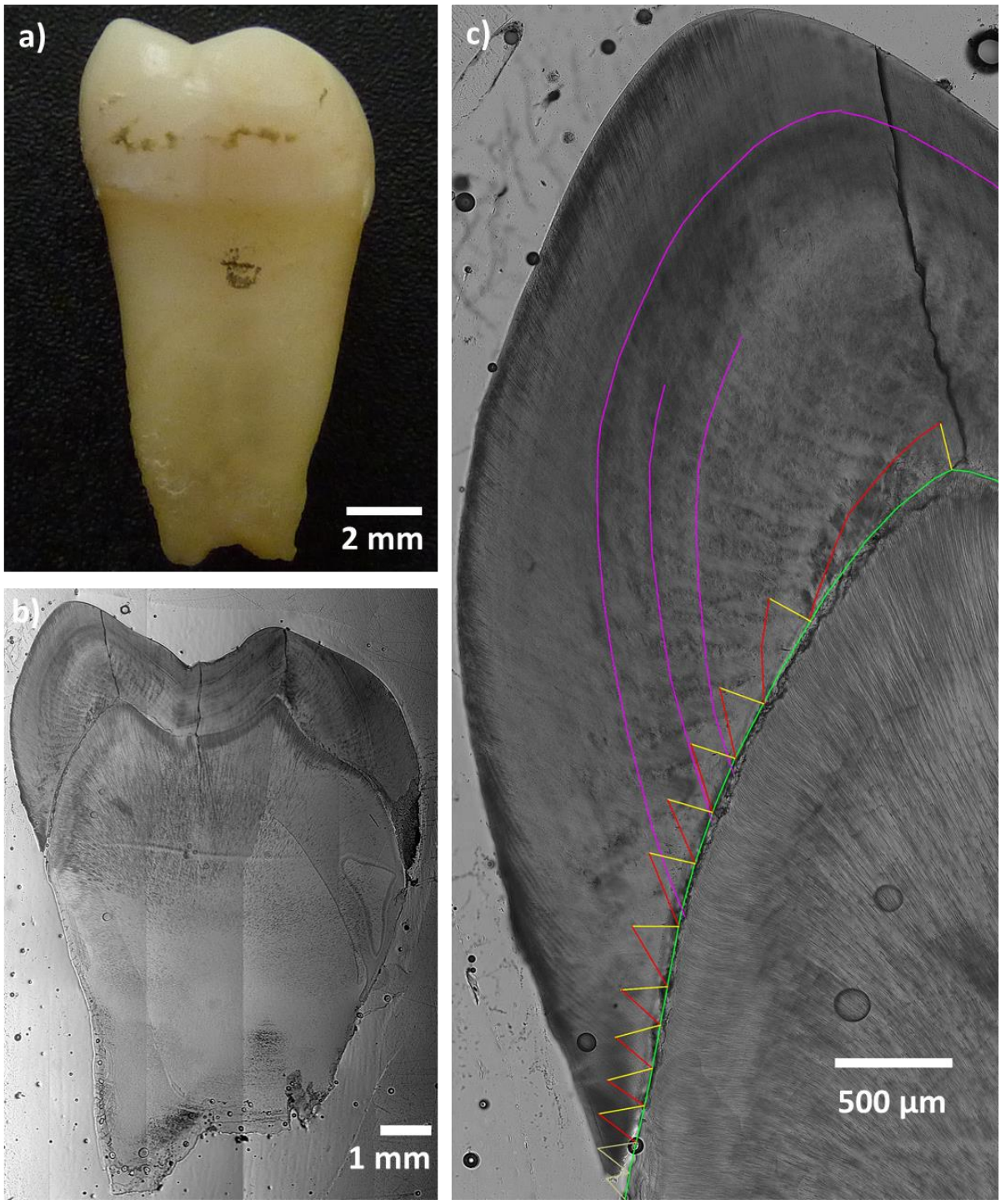

Figure 48 Various views of tooth 45 LLM2. a) Tooth after cleaning in mesial view, b) longitudinal section of the mesial cusps, c) mesiolingual cusp with analysis (green: EDJ, yellow: 200 µm prism, red: RL, and purple: AL).

5.2.10.3 LLM3

The third tooth analysed from individual 45 was the lower left third molar (LLM3). Two of the three roots have grown together to a large extent (**Figure 49**). The open root tips show the young age of this individual.

The occlusal surface is well-preserved and shows nearly no abrasion. The primary tooth structure of all cusps and fissures is nearly completely preserved. This leads to a wear stage of 1-2 (Smith, 1984).

The mesiolingual cusp was chosen for analyses since it is the preferred cusp for continuity in analysis, and the structures can be seen clearly (**Figure 49 c**).

The microstructural analyses revealed an EDJ length of 4867 µm and a CFT of 2.31 years. With the estimated start time, tooth enamel development occurred at the age of 8.00 to 10.31 (96-124 months).

During that time, eleven AL emerged between 8.52 to 9.15 years old. There are a few prominent lines. The first sequence is lines 1 to 3, which lie very close together, forming one nearly inseparable line. The following lines are AL 5 and 8, with the less prominent lines 6 and 7 between them. All these lines occurred between 8.5 to 9 years old. The presence of these lines may be attributed to a growth spurt that typically occurs during this period, coinciding with the transition to the second developmental stage in children, marked by various physical and cognitive changes (Arnold, 1986).

The DSR varied along the enamel from 3.33 ± 0.23 µm/day in the cuspal inner parts to 4.72 ± 0.20 µm/day in the cuspal outer enamel (Appendix 8.2, **Table 57**). For the calculation of the chronology the lateral inner DSR of 3.94 µm/day was used.

Table 30 Number of Accentuated Lines (AL) in tooth 45 LLM3 and age at time of appearance in months and years. Especially pronounced lines are printed in bold type.

AL No.	Age (months)	Age (years)
1	**102**	**8.52**
2	**102**	**8.53**
3	**102**	**8.54**
4	105	8.73
5	**106**	**8.83**
6	106	8.84
7	106	8.86
8	**106**	**8.87**
9	108	9.03
10	109	9.12
11	110	9.15

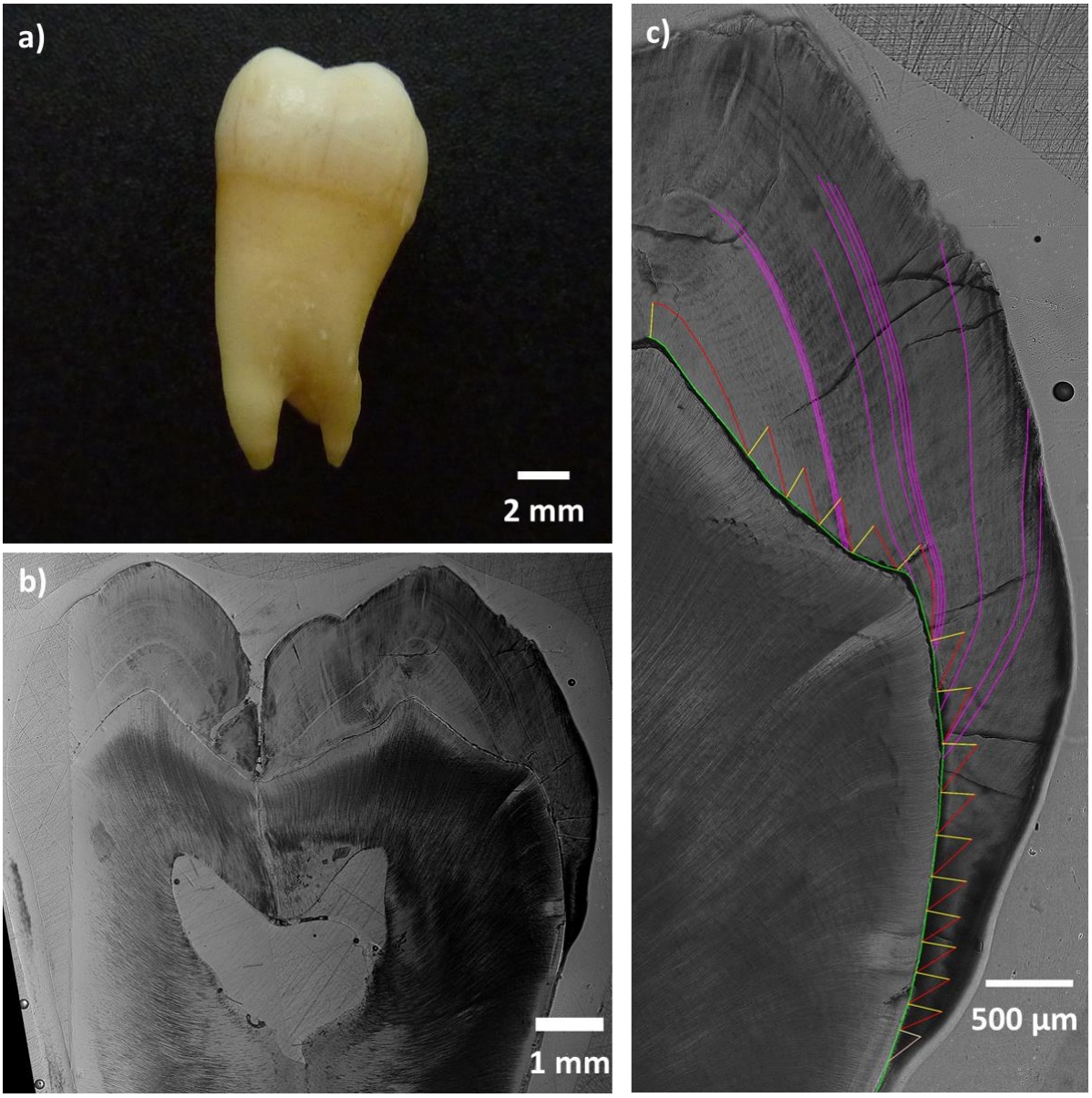

Figure 49 Various views of tooth 45 LLM3. a) Tooth after cleaning in mesial view, b) longitudinal section of the mesial cusps, c) mesiobuccal cusp with analysis (green: EDJ, yellow: 200 µm prism, red: RL, and purple: AL).

5.2.11 Individual 53

Individual 53 was a male who died at age 55-65. The mandible is fractured into two parts (**Figure 50**). Given the advanced age of this individual, most teeth exhibit significant abrasion. The skeletal remains display various pathological changes, including arthrosis and inflammations. Furthermore, evidence of a healed epidural hematoma suggests a cranial roof

trauma likely resulting from a fall. Additionally, anatomical variations in muscle markers and femurs suggest a possible history of horseback riding for this individual (Grefen-Peters, 2018).

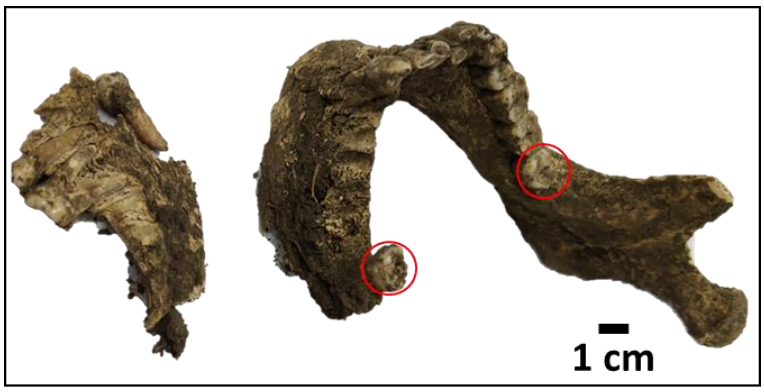

Figure 50 Lower jaw fragments of individual 53. The red circles indicate which teeth have been extracted (LLM2 and LRM3).

5.2.11.1 LLM2

The first tooth examined was the lower left second molar (LLM2). Unfortunately, this tooth was not well preserved, as the mesial enamel was detached, and some damage was observed on the buccal side of the cervix (**Figure 51**). The tooth's crown exhibited significant abrasion in multiple areas leading to a wear stage of 5 (Smith, 1984). However, the distolingual cusp remained relatively well-preserved, making it the selected area for the analysis (**Figure 51 c**).

The microstructural analyses revealed an EDJ length of 4874 µm and a CFT of 2.94 years. With the estimated starting times, this leads to a tooth enamel development time of 2.50 to 5.44 years (30-65 months).

During that time, seven AL developed. They emerged between 2.84 and 4.41 years (**Table 31**). Especially around 3 years ALs 2 and 3 are very pronounced. Weaning probably took place at that time, showing a connection between the weaning process and stress marker.

The DSR varied along the enamel from 3.27 ± 0.33 µm/day in the lateral inner parts to 4.58 ± 0.82 µm/day in the cuspal outer enamel (Appendix 8.2, **Table 57**). For the calculation of the chronology, the lateral inner DSR was used.

Table 31 Number of Accentuated Lines (AL) in tooth 53 LLM2 and age at time of appearance in months and years. Especially pronounced lines are printed in bold type.

AL No.	Age (months)	Age (years)
1	34	2.84
2	**37**	**3.08**
3	**38**	**3.21**
4	39	3.23
5	44	3.70
6	52	4.34
7	53	4.41

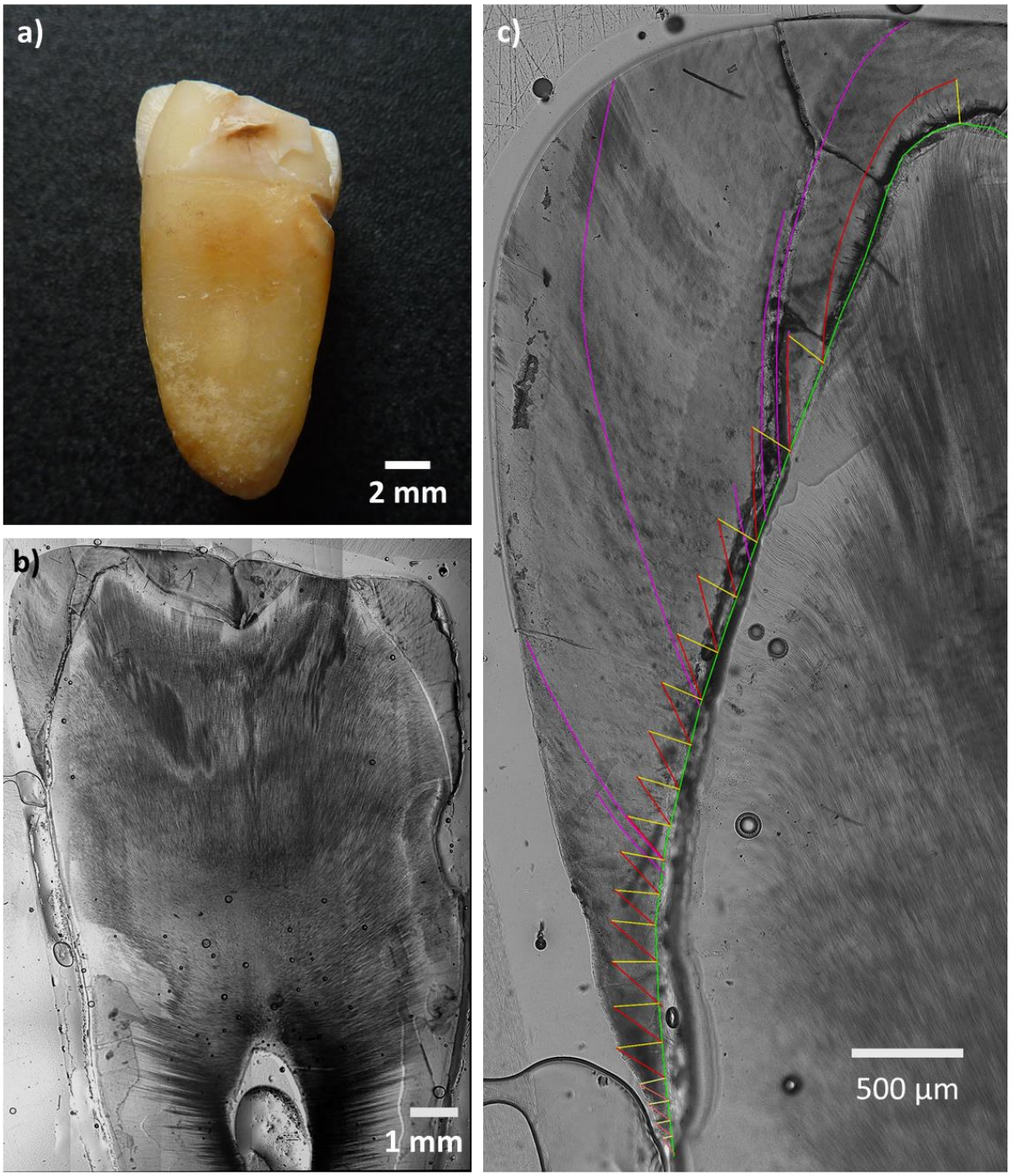

Figure 51 Various views of tooth 53 LLM2. a) Tooth after cleaning in mesial view, b) longitudinal section of the distal cusps, c) distolingual cusp with analysis (green: EDJ, yellow: 200 µm prism, red: RL, and purple: AL).

5.2.11.2 LRM3

The second tooth analysed of individual 53 was the lower right third molar (LRM3). The enamel is better preserved than in the previous tooth LLM2, but it shows some discolouration in the enamel and the root (**Figure 52**). The occlusal surface shows flattened cusps but nearly no exposed dentine and is, therefore, a wear stage of 3 (Smith, 1984). The roots exhibit merging and signs of inflammatory changes. For our analyses, the mesiolingual cusp was selected (**Figure 52 c**) since it is in the best-preserved condition, with no exposed dentine.

The examination revealed an EDJ length of 5126 µm and a CFT of 2.54 years. With the estimated starting times, this leads to a developmental time between ages 8.00 and 10.54 (96-126 months).

Only three AL between 8.30 and 8.62 years emerged (**Table 32**). The presence of these lines could be attributed to a growth spurt that typically occurs during that period, coinciding with the transition to the second developmental stage in children, marked by various physical and cognitive changes (Arnold, 1986).

The DSR varied along the enamel from 3.18 ± 0.29 µm/day in the lateral inner parts to 4.72 ± 0.15 µm/day in the lateral outer enamel (Appendix 8.2, **Table 57**). For the calculation of the chronology, the lateral inner DSR was used.

Table 32 Number of Accentuated Lines (AL) in tooth 53 LRM3 and age at time of appearance in months and years.

AL No.	Age (months)	Age (years)
1	100	8.30
2	101	8.38
3	103	8.62

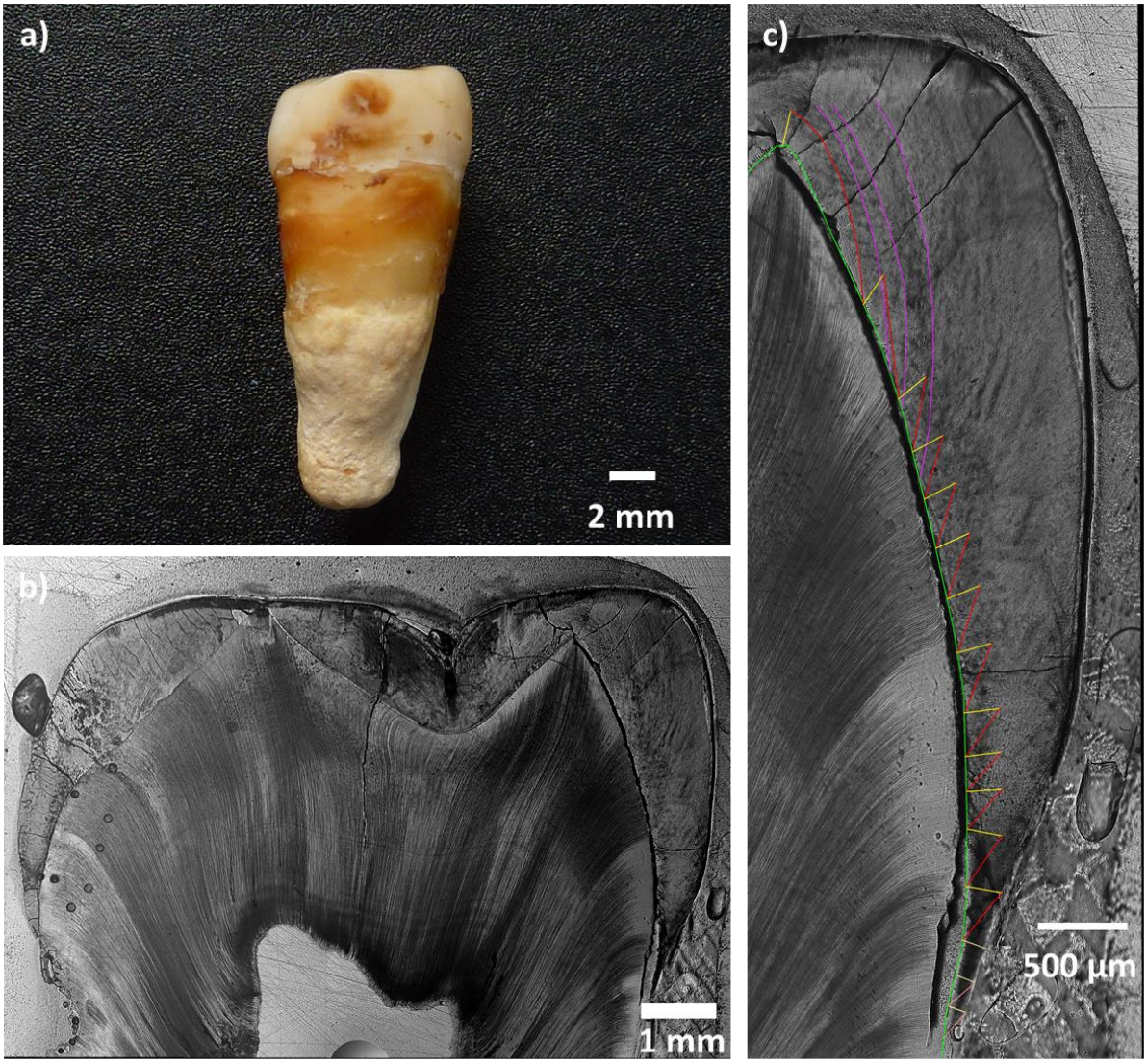

Figure 52 Various views of tooth 53 LRM3. a) Tooth after cleaning in mesial view, b) longitudinal section of the mesial cusps, c) mesiolingual cusp with analysis (green: EDJ, yellow: 200 µm prism, red: RL, and purple: AL).

5.2.12 Individual 63a

Individual 63a was identified as a female who died at age 40-50. The preservation of the mandible is not optimal. Some teeth detached from the alveoli but are still present and stored separately (**Figure 53**). The lower left fourth premolar (LLP4), lower left first molar (LLM1), and lower left second molar (LLM2) were selected for examination. These teeth exhibit significant abrasion, indicating extensive wear. Furthermore, the second molar has been affected by severe caries on the distobuccal cusp. However, the mesial cusps of the teeth remain largely intact, allowing them to be used for analysis.

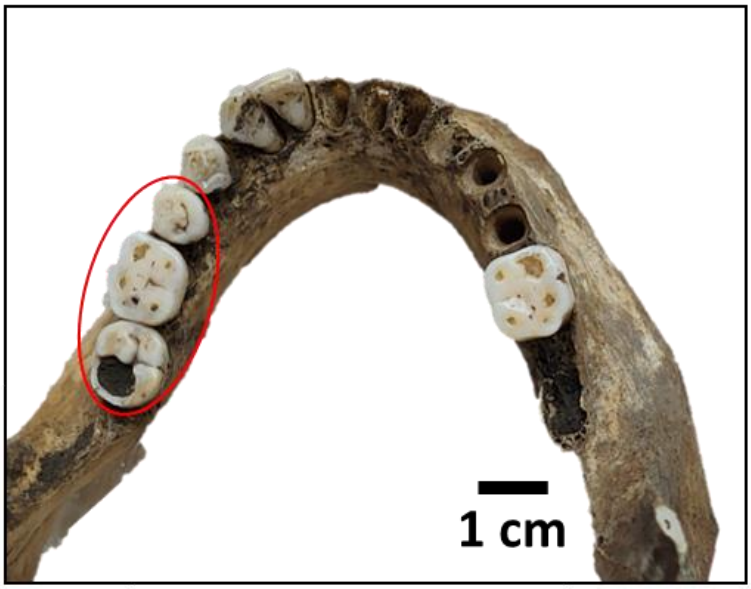

Figure 53 Lower jaw of individual 63a. The red circle indicates which teeth have been extracted (LLP4, LLM1, LLM2).

5.2.12.1 LLP4

The first tooth analysed was the lower left fourth premolar (LLP4). This tooth was analysed from the distal view, as it was deemed more suitable for analysis based on the specific cut made. However, it is important to note that this choice of view does not impact the analysis process or results because the analysed structures are the same just viewed from the opposite direction.

The tooth shows wear facets on both cusps, but no dentine is exposed (**Figure 54**), which leads to a wear stage of 2 (Smith, 1984).

The microstructural analysis was conducted on the lingual cusp (**Figure 54 c**). It revealed an EDJ length of 3281 µm and a CFT of 1.51 years. With the estimated starting time, this leads to a development between 2.00 and 3.51 years.

During this time, nine AL emerged from 2.13 to 2.83 years (**Table 33**). The most prominent line is AL 5, followed by AL 6, which is similar in intensity. The less prominent AL 7 lies very close. Those lines have developed at the age of 2.49, 2.51 and 2.53 years, respectively, in the 30th month of age. It is assumed that during that time, weaning took place, and these lines most likely originated from that stressful process (Bernatzky et al., 2018).

The DSR varied along the enamel from 3.29 ± 0.32 µm/day in the cuspal inner enamel to 4.02 ± 0.22 µm/day in the lateral outer enamel (Appendix 8.2, **Table 58**). For the calculation of the chronology, the lateral inner DSR of 3.61 µm/day was used.

Table 33 Number of Accentuated Lines (AL) in tooth 63a LLP4 and age at time of appearance in months and years. Especially pronounced lines are in bold type. Asterisk marks lines that appear at the same time in tooth LLM2 from the same individual.

AL No.	Age (months)	Age (years)
1	26	2.13
2	26	2.18
3	27	2.28
4	28	2.33
5	**30**	**2.49**
6	**30**	**2.51**
7	30	2.53
8*	31	2.61
9	34	2.83

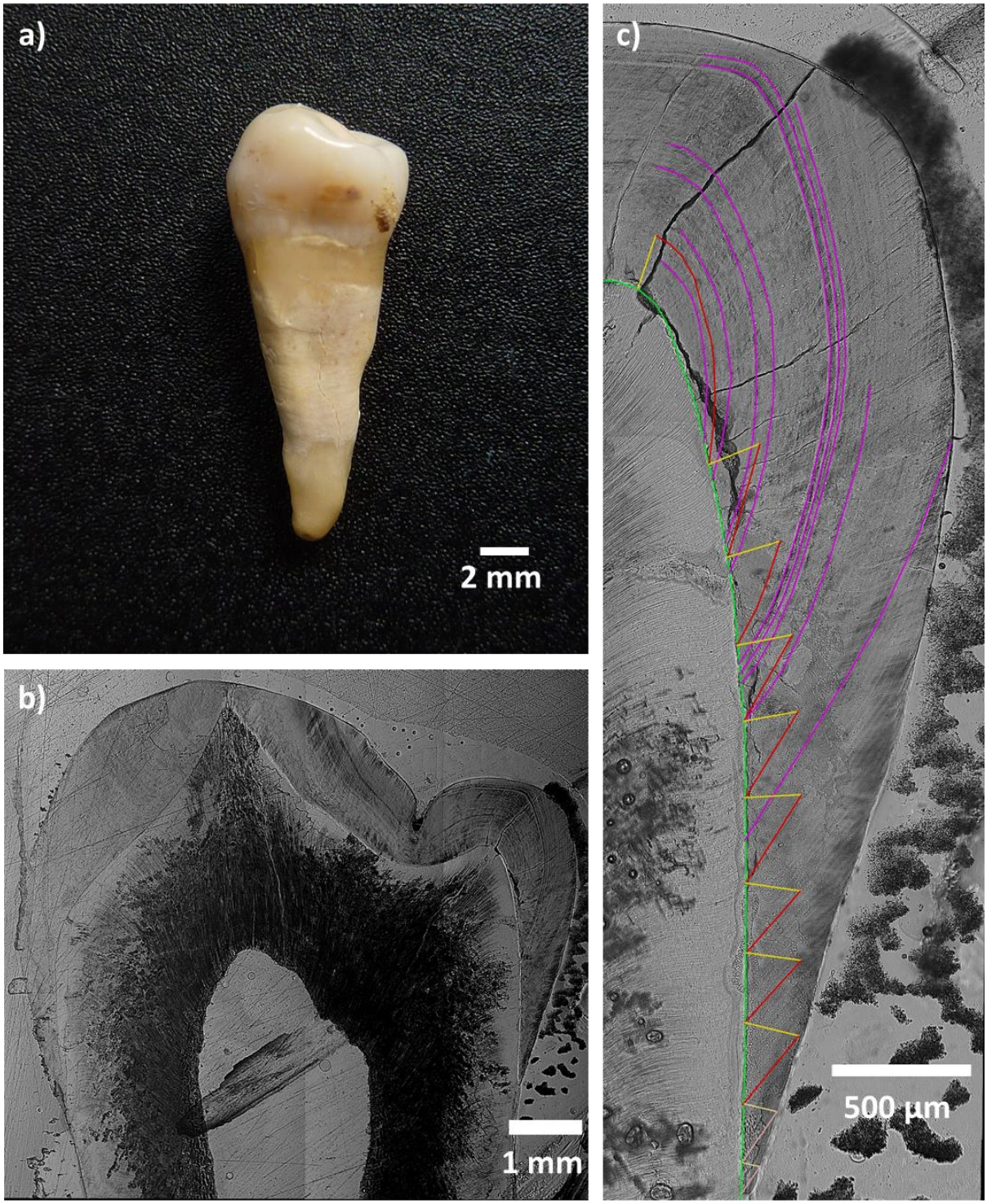

Figure 54 Various views of tooth 63a LLP4. a) Tooth after cleaning in distal view, b) longitudinal section of the tooth, c) lingual cusp with analysis (green: EDJ, yellow: 200 µm prism, red: RL, and purple: AL).

5.2.12.2 LLM1

The second tooth analysed was the lower left first molar (LLM1). It is well preserved but shows extensive wear with exposed dentine in several places, leading to a wear stage of 4 (Smith, 1984). Moreover, the tooth shows some damage on the mesial tooth crown and root (**Figure 55**), but this does not affect the analysis.

For the microstructural analysis, the mesiolingual cusp was used (**Figure 55 c**). It revealed an EDJ of 4649 µm and a CFT of 1.77 years. Considering the estimated starting days, this leads to a developmental time between birth and 1.77 years (0-21 months).

During that time, eight AL emerged between the ages of 0.10 and 0.99 (**Table 34**). On this tooth, none of the lines is particularly intense. The most prominent is AL 7, which lies at the age of 0.92. No comparison can be made with the other examined teeth from this individual, as the teeth were formed later.

The DSR varied along the enamel from 3.55 ± 0.46 µm/day in the lateral mid enamel to 4.32 ± 0.43 µm/day in the cuspal inner enamel (Appendix 8.2, **Table 58**). For the calculation of the chronology, the lateral inner DSR of 3.55 µm/day was used.

Table 34 Number of Accentuated Lines (AL) in tooth 63a LLM1 and age at time of appearance in months and years. Especially pronounced lines are in bold type.

AL No.	Age (months)	Age (years)
1	1	0.10
2	2	0.14
3	2	0.15
4	6	0.49
5	7	0.57
6	10	0.80
7	**11**	**0.92**
8	12	0.99

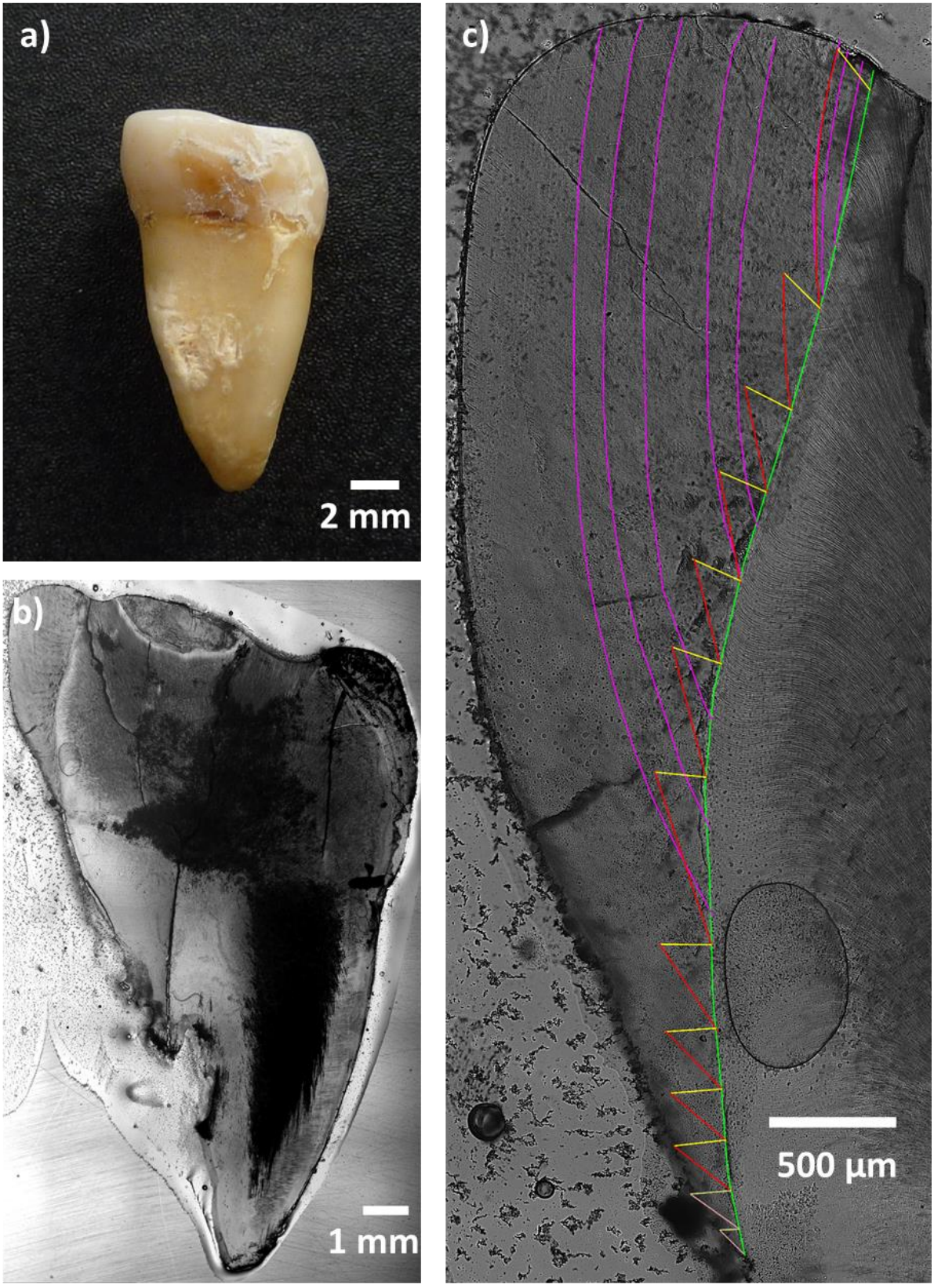

Figure 55 Various views of tooth 63a LLM1. a) Tooth after cleaning in mesial view, b) longitudinal section of the mesial cusps, c) mesiolingual cusp with analysis (green: EDJ, yellow: 200 µm prism, red: RL, and purple: AL).

5.2.12.3 LLM2

The third tooth examined from individual 63a was the lower left second molar (LLM2). Unfortunately, the distobuccal cusp of this tooth is entirely missing due to severe caries. The extent of the cavity reaches the entire pulp and root, resulting in the distal side of the tooth being completely hollow. The mesial cusps are preserved and have a wear stage 3 (Smith, 1984).

The microstructural analysis was conducted on the mesiolingual cusp (**Figure 56 c**). It revealed an EDJ length of 4541 µm and a CFT of 1.59 years. The estimated starting time leads to a developmental time from 2.50 to 4.09 years (30-49 months).

During that time, eight AL emerged between 2.63 and 4.07 years (**Table 35**). The most prominent lines in this time are AL 2 and 3, which lie close together at 2.88 and 2.90 years, respectively, in month 35. AL9 of tooth LLP4 occurred at a similar time at age 2.83 years. Furthermore, the first line from LLM2 (2.63 years) and the eighth line of LLP4 (2.61) are similar, too. Since this method is based on estimates in some places, they can be considered to originate from the same stressful event even if they have not the exact same value.

The DSR varied along the enamel from 3.16 ± 0.14 µm/day in the cuspal mid enamel to 4.64 ± 0.24 µm/day in the lateral outer enamel (Appendix 8.2, **Table 58**). For the calculation of the chronology the lateral inner DSR of 3.89 µm/day was used.

Table 35 Number of Accentuated Lines (AL) in tooth 63a LLM2 and age at time of appearance in months and years. Especially pronounced lines are in bold type. Asterisk marks lines that appear at the same time in tooth LLP4 from the same individual.

AL No.	Age (months)	Age (years)
1*	32	2.63
2*	**35**	**2.88**
3	**35**	**2.90**
4	37	3.06
5	38	3.15
6	40	3.37
7	45	3.77
8	49	4.07

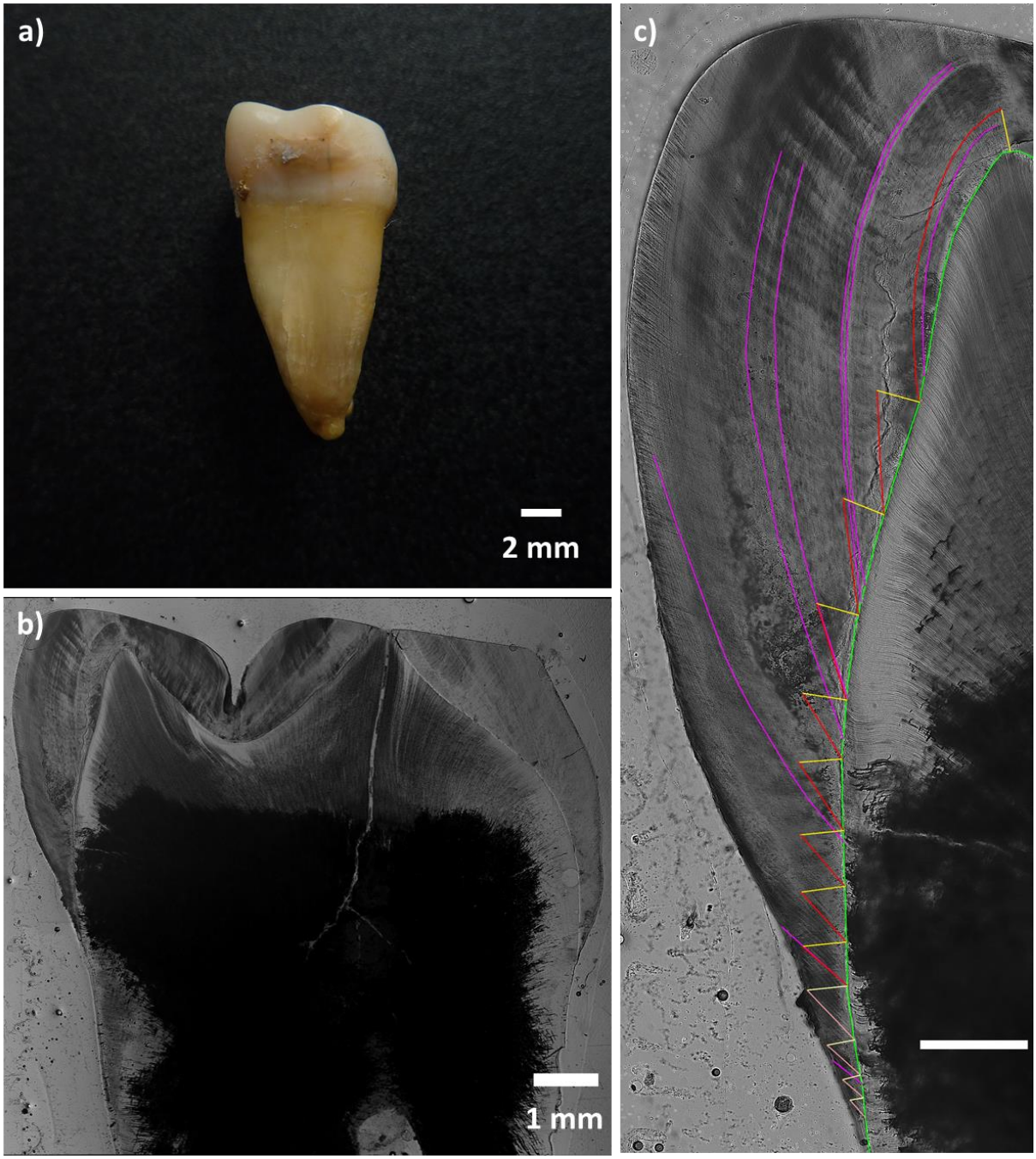

Figure 56 Various views of tooth 63a LLM2. a) Tooth after cleaning in mesial view, b) longitudinal section of the mesial cusps, c) mesiolingual cusp with analysis (green: EDJ, yellow: 200 µm prism, red: RL, and purple: AL).

5.2.13 Combined Results

The previous chapters have provided detailed information on each tooth from every individual in the study. To gain insights into the way of life of the Gevensleben population, the data were combined and analysed from a broader societal perspective, considering the prevailing customs of the time and integrating findings from previous archaeological investigations.

5.2.13.1 Daily secretion rate (DSR)

The daily secretion rate (DSR) was calculated at different places in the tooth crown. The tooth crown was divided into cuspal and lateral enamel, and both parts were again divided into inner, mid and outer regions. At every section, five locations where the cross striations (CS) were seen clearly were selected, the CS were counted, measured, and the length was divided by the counts. This led to the DSR of individual places over the enamel. To compare these rates, means were calculated for every part in every tooth and every part in all teeth combined. These means and their standard deviations are displayed in **Figure 57**.

A detailed comparison of the mean values and the standard deviation can be found in **Table 36**. In the cuspal enamel, the DSR starts in the inner part at 3.8 µm/day, increases to 3.9 µm/day in the mid and ends at 4.2 µm/day in the outer section. In the lateral parts, a similar increase can be seen. The DSR starts at the slowest rate of 3.7 µm/day in the inner enamel, gradually increases to 3.9 µm/day and ends at 4.2 µm/day in the outer portion of the enamel.

For temporal comparison, data from a late Anglo-Saxon population in Newcastle-Upon-Tyne (800-1200 AD), Great Britain, as investigated by Aris et al. (2020b), was employed. The tooth crown of both populations was divided into the same regions, enabling a comparison of the DSR within these regions. However, unlike in Aris et al. (2020a), a sex-based comparison was not performed in this study due to an uneven distribution of males and females in the sample.

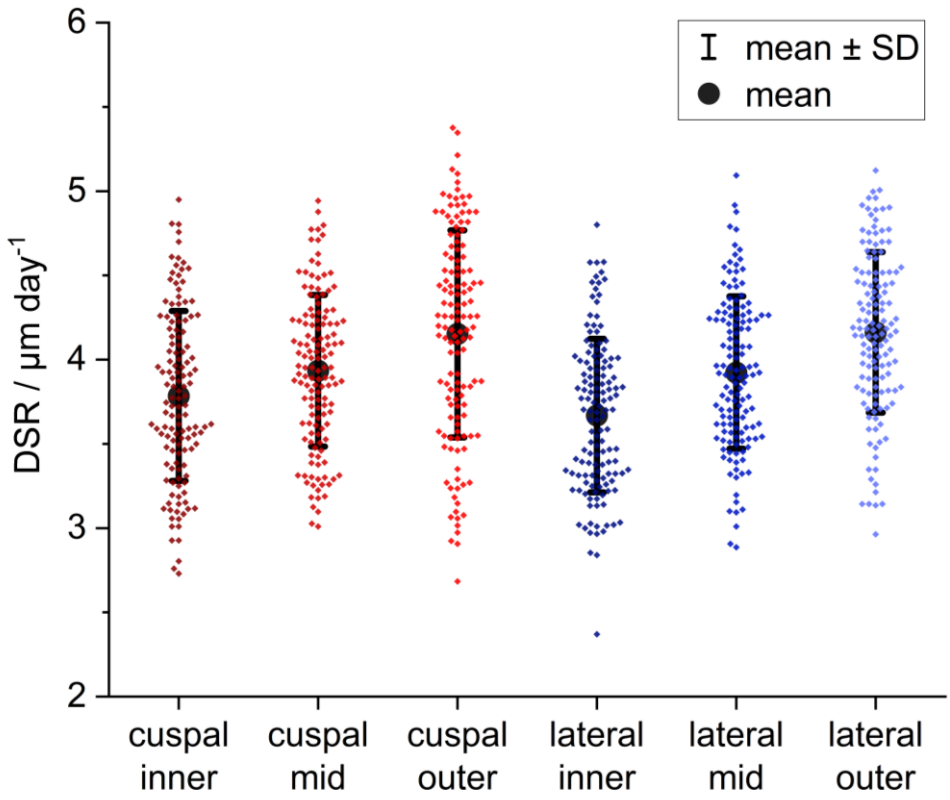

Figure 57 Mean daily secretion rate (DSR) for all Gevensleben individuals. Circles depict the mean rate by enamel regions from inner to outer in cuspal and lateral parts. The error bars display the standard deviation (SD). Diamonds depict single values.

Aris et al. (2020b) reported that the DSR showed a lower rate at the enamel-dentine junction (EDJ), progressively increasing as it moved outward in both enamel parts. Similarly, the Gevensleben population displayed a comparable pattern in their DSR rates. Other investigations demonstrated a decline in DSR over time, with older populations showing higher DSR values than modern ones. For instance, Nava et al. (2017) observed a lower DSR in deciduous incisors of present-day individuals compared to a sample from Imperial Rome.

In a comprehensive study by Aris et al. (2020b), comparisons were made among various sample groups from Great Britain, including Romans (Cirencester, 70-400 AD), early Anglo-Saxons (Ozengell Grange, 500-600 AD), late Anglo-Saxons (Newcastle-Upon-Tyne, 800-120 AD), medieval (St Gregory's Prior and Fishergate House, 1000-1600 AD), and a present sample (Newcastle-Upon-Tyne and Glasgow, modern-day). This investigation revealed a gradual decrease in DSR across the sample groups, from the oldest to the most recent. The

comparison first focused on the late Anglo-Saxon population of Newcastle-Upon-Tyne (800-1200 AD), Great Britain, as it overlaps with the time of the Gevensleben population. Notably, the DSR rates of the Gevensleben sample slightly surpass those of the late Anglo-Saxon population and align more closely with the early Anglo-Saxon sample (**Table 36**). This alignment is reasonable, considering that the Anglo-Saxons are descendants of people from Lower Saxony, Germany, establishing a plausible similarity between the two populations.

Table 36 Comparison of daily secretion rates (DSR) obtained for Gevensleben (700-1000 AD), early Anglo-Saxon of Ozengell Grange (500-600 AD) and late Anglo-Saxon sample of Newcastle-Upon-Tyne (800-1200 AD), Great Britain, analysed in the study of Aris et al. (2020b). N is the number of teeth in the sample. SD is the standard deviation.

	Gevensleben (700-1000 AD) (This study)			**Early Anglo-Saxon (500-600 AD) (Aris et al. 2020a)**			**Late Anglo-Saxon (800-1200 AD) (Aris et al. 2020a)**		
Enamel region	**N**	**DSR (µm/day)**	**SD**	**N**	**DSR (µm/day)**	**SD**	**N**	**DSR (µm/day)**	**SD**
cuspal inner	26	**3.8**	0.5	7	**3.7**	0.2	17	**3.3**	0.3
cuspal mid	27	**3.9**	0.4	7	**4.0**	0.3	18	**3.7**	0.3
cuspal outer	27	**4.2**	0.6	6	**4.4**	0.3	18	**4.0**	0.3
lateral inner	27	**3.7**	0.5	12	**3.4**	0.2	19	**3.4**	0.3
lateral mid	27	**3.9**	0.5	12	**3.9**	0.2	19	**3.6**	0.3
lateral outer	27	**4.2**	0.5	12	**4.2**	0.2	19	**3.9**	0.4

5.2.13.2 Crown formation times (CFT)

The primary approach of this study aimed to establish a chronology of childhood development for the Gevensleben individuals. Two to three teeth from each individual were selected to achieve this, with tooth types overlapping in their formation periods. A total of 27 permanent teeth from 11 individuals were examined. However, it became evident that only a few individuals had sufficient overlapping teeth to create a seamless chronology. Moreover, estimating tooth formation times proved challenging as the neonatal line, a valuable indicator, was absent in all teeth. Therefore, reference values from AlQahtani et al. (2010) and the growth rates listed in *The Reference Manual of Pediatric Dentistry* from the American Academy of Pediatric Dentistry (Logan and Kronfeld, 1933) were utilised for the start of the tooth formation times in the Gevensleben sample.

Concerning these values, however, there are always discussions about which values are correct. Various authors have conducted other studies and proposed different values as guidelines for the onset of calcification. Most authors agree on the initiation of the first molar at birth (Christensen and Kraus, 1965, Logan and Kronfeld, 1933, Reid and Dean, 2006), while others see a time around birth up to an age of 4.5 months (AlQahtani et al., 2010). Different possible starting times are proposed for the second molar. The earliest start is around 2.5 years as a potential outset (AlQahtani et al., 2010, Logan and Kronfeld, 1933). Others consider three years the most probable (Reid and Dean, 2006). Due to the relatively short formation time of the first molar, an estimated initial time of 2.5 years was chosen for this analysis. For third molars, the range of incepting formation is even wider since it can vary between 7 and 9 years in different populations (Fanning and Moorrees, 1969, Reid and Dean, 2006, Tompkins, 1996). For this study, the estimated starting times of upper third molars of 7 years and lower third molars of 8 years were chosen (Logan and Kronfeld, 1933).

The crown formation times were calculated using the DSR and the EDJ length, as described in chapter 4.2.4. These timespans were compared with reference values from the literature ((AlQahtani et al., 2010, Logan and Kronfeld, 1933), **Table 37**). As reference values, the lower limit of the CFTs was used. Generally, the end CFTs of most of the examined teeth slightly precede those of the references. Only two teeth show a CFT like in literature: LLM1 of individual 33 (0-33 months, literature: 0-30 months) and LRP3 of individual 39 (calculated: 18-65 months, literature: 18-66 months) It is essential to recognise that the tooth sections became progressively indistinct towards the tooth neck, making precise analyses error-prone.

The CFT can vary between cusps and also between teeth or individuals. Therefore, this only gives approximate values and cannot be considered absolute.

Table 37 Calculated crown formation times (CFT) of examined teeth from Gevensleben compared to CFT values from literature (AlQahtani et al., 2010, Logan and Kronfeld, 1933).

Individual	Tooth type	CFT (months) Gevensleben	CFT (months) (AlQahtani et al., 2010, Logan and Kronfeld, 1933)
12	LLM2	30-56	30-90
	LLM3	96-117	96-168
22	LLM2	30-51	30-90
	LLM3	96-112	96-168
30	LLC	11-70	10-80
	LLP3	18-73	18-66
	LRM3	96-107	96-168
33	LLM1	0-33	0-30
	LLM2	30-56	30-90
	LLM3	96-113	96-168
38a	URM1	0-22	0-30
	URM2	30-60	30-90
	URM3	84-107	84-168
39	LRP3	18-65	18-66
	LRP4	24-42	24-78
	ULM2	30-58	30-90
43	LLM1	0-22	0-30
	LLM2	30-56	30-90
	LLM3	96-132	84-168
45	LLM1	0-30	0-30
	LLM2	30-55	30-90
	LLM3	96-124	84-168
53	LLM2	30-65	30-90
	LRM3	96-126	84-168
63a	LLM1	0-19	0-30
	LLP4	24-45	24-78
	LLM2	30-48	30-90

5.2.13.3 Accentuated Lines (AL)

Accentuated Lines are used as a general health indicator during childhood (Larsen, 2015, Simpson, 1999, Żądzińska et al., 2015). The data of the AL of the Gevensleben sample were collected for individual teeth by examining the histological thin sectioning. The AL were drawn in, and their course was tracked down to the EDJ, where the time of emergence was calculated using the previously established chronology (see chapter 4.2.4).

Every tooth had at least 3 (45 LLM2) but a maximum of 20 AL (39 LRP3). Per individual, a total number of 10 (individual 53) to 41 AL (individual 39) could be found (**Table 38**). However, these numbers depend on the number of teeth analysed. Individual 53 only had two teeth examined, whereas individual 39 had three. Furthermore, it depends on the tooth type analysed because a longer CFT leads to a broader timespan in the life of the individual in that AL can emerge.

However, it has to be considered that in teeth with overlapping development timelines (30 LLC and LLP3, 33 LLM1 and LLM2, 39 LRP3 and LRP4, 63a LLP4 and LLM2), the actual count of enamel lines (AL) may be slightly reduced. This is due to the simultaneous development of different tooth types, which means that AL originating from the same stressful event might manifest on two adjacent teeth. Nevertheless, matching these AL was only possible with a few teeth and even there it could not be determined with certainty that the AL came from the same stress event. Therefore, all of the AL were included in the calculation.

Table 38 Number of AL in the teeth of all individuals from Gevensleben. The total number of enamel lines (AL) in teeth undergoing overlapping development may be reduced. AL resulting from a single stress event can appear on two teeth simultaneously undergoing development.

Individual	Sex	Tooth type	Number of AL per tooth	Total number of ALs
12	m	LLM2	8	12
		LLM3	4	
22	m	LLM2	9	23
		LLM3	14	
30	f	LLC	11	24
		LLP3	5	
		LRM3	8	
33	f	LLM1	17	30
		LLM2	8	
		LLM3	5	
38a	f	URM1	15	33
		URM2	12	
		URM3	6	
39	f	LRP3	20	41
		LRP4	10	
		ULM2	11	
43	f	LLM1	14	27
		LLM2	6	
		LLM3	7	
45	f	LLM1	8	22
		LLM2	3	
		LLM3	11	
53	m	LLM2	7	10
		LRM3	3	
63a	f	LLM1	8	25
		LLP4	9	
		LLM2	8	

The mean count of AL on different tooth types was calculated (**Table 39**). The appearance of AL on one tooth type was added and then divided by the number of examined teeth belonging to that tooth type. For the first molar, this gives a mean count of 12.5 AL with a minimum of 8 to a maximum of 17. These were calculated with five teeth. The second molar shows less AL with a mean of 8 AL, a most minor of 3, and a maximum of 12. Also, the second molar is the most commonly extracted tooth in this study. The third molar shows the fewest number of AL on all teeth analysed. A possible explanation for that can be that children at higher age

experience less stress or are more stress resilient. However, this varies greatly between individuals with a minimum of 3 AL and a maximum of 14 on the eight teeth examined. Considering the CFT of the different tooth types, the mean number of AL is not related to the length of the developing time of the tooth since the teeth with longer CFT do not show more than those with shorter CFT. It appears to be the other way around, but this might be due to the stressful events happening during that time and their effect on the children's development and not related to the length of CFT.

The data of the other teeth are not very reliable since only one canine, and only two third and two fourth premolars were included in this study. Nevertheless, since they cover an extended period, they often include more AL than the other teeth.

Table 39 Cumulated occurrence of Accentuated lines (AL) by tooth type. Displayed with approximated crown formation time by literature (AlQahtani et al., 2010, Logan and Kronfeld, 1933), number of teeth from this tooth type analysed (N), the mean count of AL occurring on this tooth type and the minimum (Min) and maximum (Max) of AL occurring on this tooth type in the Gevensleben sample.

Tooth type	CFT (years) (AlQahtani et al., 2010, Logan and Kronfeld, 1933)	N	Mean count of AL	Min	Max
C	0.8 – 6.6	1	11.0	-	-
P3	1.5 – 5.5	2	12.5	5	20
P4	2 – 6.5	2	9.5	9	10
M1	0 – 2.5	5	12.4	8	17
M2	2.5 – 7.5	9	8.0	3	12
M3	7 – 14	8	7.3	3	14

Approximately 30 km west of Gevensleben lies Werlaburgdorf, another early medieval burial ground (700-1000 AD), which is thoroughly characterised archaeologically and anthropologically. On this site, an extensive collection of 236 individuals in 234 graves were excavated. The relative mortality rates, depicted in **Figure 58** and reported by Grefen-Peters (2013), revealed an average life expectancy of approximately 29 years for females and 31 years for males at birth. Notably, the early years exhibited high mortality rates, with 44% of

the population not surviving to adulthood. Another significant mortality peak was observed among females aged 15 to 19, likely attributed to first-time pregnancies (Bernatzky et al., 2018). For adults, the average life expectancy was estimated to be around 41 years for females and 47 years for males (Grefen-Peters, 2013). Given the substantial sample size from Werlaburgdorf, which corresponds to a similar time period to Gevensleben, these data serve as valuable benchmarks for comparison with the Gevensleben sample.

Figure 58 Relative mortality per mille of the population found in the neighbouring population of Werlaburgdorf (data taken from Grefen-Peters (2013)). Blue squares show the age at death in male individuals, and respectively red circles show those of females.

To gain a comprehensive understanding of the childhood experiences of the Gevensleben population, the number and time of emergence of all AL was aggregated from all teeth of each individual and then divided by the number of individuals in whom AL were present. This approach allows for a collective assessment of AL occurrence and duration across the entire sample, providing valuable insights into the population's overall childhood health and stress patterns. With this method, the AL prevalence was calculated and plotted against the age of the children in months (**Figure 59**). AL that had only emerged on one tooth, with this tooth being the only developing one during that specific time, would falsely display a prevalence of 100 and were, therefore, not considered.

During the initial month after birth, infants benefit from the protection provided by maternal antibodies (Glezen, 2003). However, as this protection gradually declines, there is a notable increase in the prevalence of AL to 83 to 100 %. This rise is particularly prominent between 7 and 10 months of age (**Figure 59**) when children begin to sit, experience the eruption of their first teeth, and actively engage with their environment (Jenni, 2021). As their activity level grows, they are more susceptible to encountering potential pathogens, which might have played a role in the heightened occurrence of AL during this developmental phase.

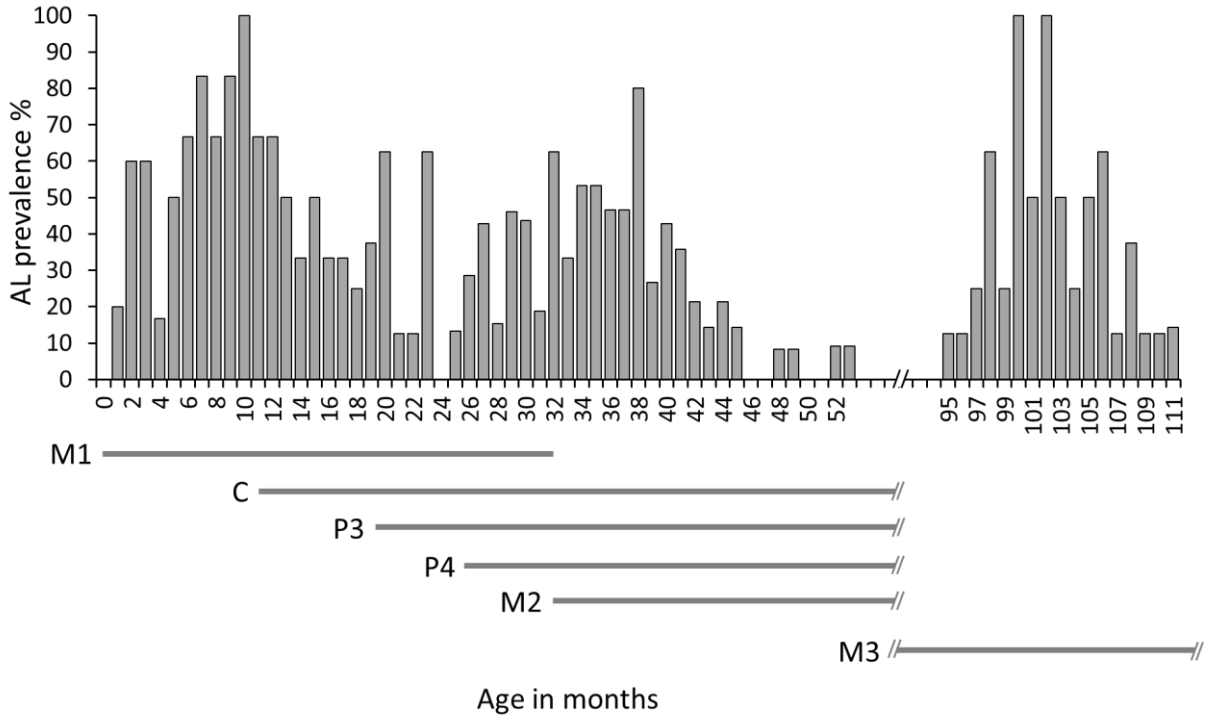

Figure 59 Cumulative distribution of AL prevalence in the Gevensleben sample from birth to 53 months and 95 to 111 months old with approximated developmental times of all used tooth types. M1: first molar, C: canine, P3: third premolar, P4: fourth premolar, M2: second molar, M3: third molar.

The low tooth abrasion observed in the Gevensleben individuals up to three years of age indicates an extended breastfeeding period, suggesting a gradual weaning process. However, weaning during this period posed risks to children, as they were unaccustomed to non-infant diets and exposed to partially spoiled food and unhygienic cooking utensils. Such conditions

frequently result in gastrointestinal diseases that could be life-threatening (Bernatzky et al., 2018).

Analysing the nearby site of Werlaburgdorf, the highest mortality occurred around three years of age (**Figure 58**). It is suggested that the same conditions also apply to the situation in Gevensleben (Bernatzky et al., 2018). This period of high mortality corresponds to the presence of stress markers in the teeth of individuals between 32 and 38 months (2.7-3.2 years, **Figure 59**), which may reflect the challenging conditions experienced by children during this time. Not all children could withstand these difficulties, and among those who survived, a higher prevalence of AL (up to 80%) was observed in their teeth. Increased enamel hypoplasia in the teeth of surviving children suggests that they endured significant physiological stress, disease, or nutritional deficiencies during the weaning phase (Birch and Dean, 2014, Goodman and Rose, 1991, Witzel et al., 2008), which might have started around the first period of stress at 7 months and ended at the second increase in AL prevalence at around 3 years of age.

The third period shows a higher prevalence of AL was observed between 98 to 106 months (8.2 to 8.8 years, **Figure 59**), reaching a high of 100 %. In medieval times, child development was divided into three distinct stages, and the transition from "infantia" to "puerita" typically occurred around the age of 7 years (Arnold, 1986). During the "pueritia" stage, children experienced the change from deciduous to permanent teeth, accompanied by the completion of language development. Additionally, this stage marked another growth spurt, leading to various physical and cognitive changes. Evidently, these transitional processes, along with the associated stressors, likely contributed to the higher prevalence of AL during this period. Increased social pressure and other stress factors during this developmental stage could also have played a role in the formation of AL (Enwonwu, 1973, Hillson, 2014).

Anthropological analyses of children's bones from Gevensleben provide compelling evidence to support this conclusion. For instance, muscle markers found on the bones of a 12 to 13-year-old boy from grave 55 suggest that he was already walking long distances, indicating early engagement in laborious activities at a young age (Grefen-Peters, 2020).

Furthermore, historical records reveal that the overall health situation of the population was far from optimal. Most inhabitants suffered from malnutrition and anaemia due to periodic

food shortages and infectious diseases. Chronic middle ear infections and inflammation of the meninges contributed to reduced immune competence. Additionally, the poor quality of housing, characterised by inadequate heating, dampness, and poor ventilation, aggravated mucous membranes and increased the incidence of infections, particularly affecting young children (Bernatzky et al., 2018). These factors could also account for some of the observed stress markers.

Even if all work has been carried out according to the same precise procedure, errors can still occur. Since no neonatal line was found in any tooth, all age assignments are based on estimates. The actual value may be slightly offset in reality. However, with several sources used for estimation, the error was tried to be kept low. Since much of the work in the digital analyses was performed manually, human error cannot be ruled out here either. The quality of the cuts as well as the resolution of the digital images may favour errors.

But natural variations also contribute to errors. Ameloblasts, for example, are not equally susceptible to stress at all stages of excretion. The likelihood of recording stress is higher in the lateral parts of the tooth crown than in the cuspal and cervical region (Nava et al., 2019). Different tooth types were chosen to get a broad coverage of all ages and overcome this bias.

However, since the greatest care was taken and the results can, for the most part, have been successfully compared with the literature and the previous results of the archaeological and anthropological investigations, it can be assumed that the results are plausible.

5.3 Fluoride Immersion

For this study, 16 extracted teeth from 11 patients were used. They were examined and, based on their preservation, chosen for the experiments. They were then given a sample code consisting of Hs for *Homo sapiens* and a number. Different teeth from one individual have the same code but differentiate in the second number. The use of a numbering system ensured the study's blinding, maintaining a level of confidentiality regarding patient information throughout the teeth-receiving process. This approach effectively shielded the experiments from any potential biases or external influences.

Five solutions with different fluoride content and pH were prepared: 250 ppm fluoride in water, 250 ppm fluoride in citrate buffer, 18,998 ppm fluoride in water, 18,998 ppm fluoride in citrate buffer, fluoride-free citrate buffer and as a control demineralised water. After that, the teeth were randomly divided into groups of three teeth per solution (**Table 40**).

As an illustrative example of our approach, one specific tooth and its corresponding results are shown. This example will demonstrate the effects of the solution applied. For a conclusive results section, all teeth are taken into account.

Table 40 Overview of solutions and samples used in this study.

Solution	Sample code
250 ppm fluoride in water (pH 5.85)	Hs01
	Hs05-2
	Hs10-1
250 ppm fluoride in citrate buffer (pH 4.6)	Hs04
	Hs12-3
	Hs14
18,998 ppm fluoride in water (pH 7.76)	Hs05 -1
	Hs06
	Hs11-2
18,998 ppm fluoride in citrate buffer (pH 4.7)	Hs03
	Hs12-2
	Hs13
Fluoride-free citrate buffer (pH 4.6)	Hs12-1
	Hs15-1
	Hs15-2
Water (pH 7)	Hs16

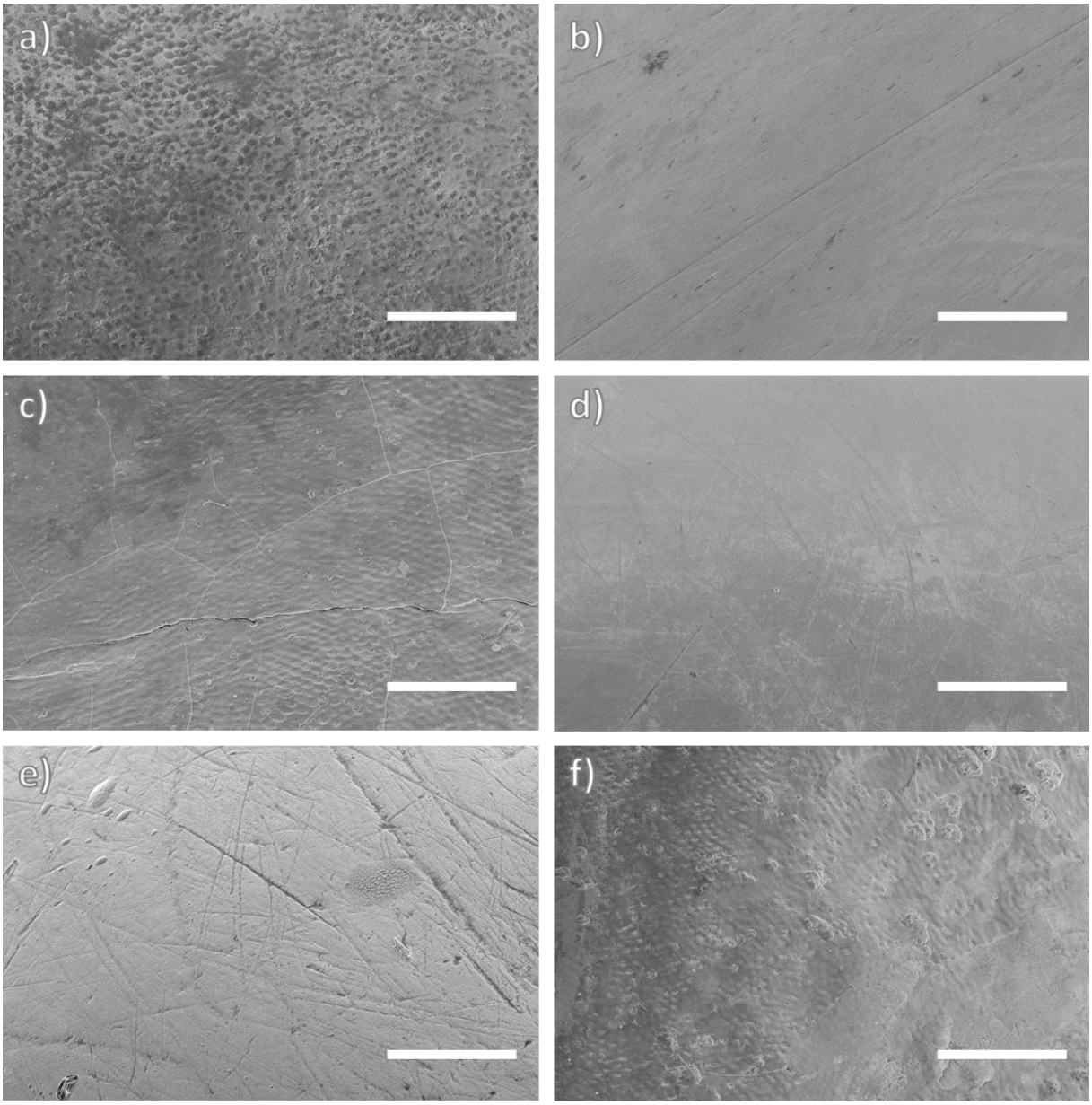

Figure 60 Representative SEM images of dental enamel surface at a magnification of 1000x. a) Without treatment, b) after immersion in aqueous 250 ppm fluoride (pH 5.85), c) after immersion in 250 ppm fluoride in citrate buffer (pH 4.6), d) after immersion in aqueous 18,998 ppm fluoride (pH 7.76), e) after immersion in 18,998 ppm in citrate buffer (pH 4.7), and f) after immersion in fluoride-free citrate buffer (pH 4.6). Scale bars 100 µm.

SEM images (**Figure 60**) were recorded to identify any morphological alterations in the enamel. It was observed that the enamel surface exhibited a wide range of variability in terms of its topography. This included the presence of cracks, scratches, and irregularities, likely resulting from activities such as tooth brushing or chewing.

A comparison was made between the enamel surface before and after immersion, but no significant differences were observed. In addition, the formation of calcium fluoride (CaF_2) globules was tested for, as it is assumed that the fluoride can also precipitate as such (Cate, 1997, Epple et al., 2022, Kiesow et al., 2021). Interestingly, no calcium fluoride globules were detected, neither morphologically through SEM nor crystallographically via PXRD analysis. These findings align with previous research by Lelli et al. (2014), which also reported the absence of any phase other than apatite. It appears that the formation of these globules requires a longer immersion time or a more etched surface.

5.3.1 250 ppm fluoride solution

The concentration of fluoride used in this experiment represents the one in commercial mouthwashes. To investigate if these have an impact on the incorporation of fluoride into enamel, the teeth were examined before and after the treatment as described in 4.3.

5.3.1.1 EDX analysis

EDX analyses have been conducted before and after the treatment with an aqueous 250 ppm fluoride solution (pH 5.85) to investigate if this concentration of fluoride leads to significant changes in the tooth enamel composition and thus validates an incorporation of fluoride. 35 spectra of 3 teeth were recorded before immersion and 32 after, of which one of each is shown in **Figure 61** as an example.

Both spectra show a similar composition, with the main elements consisting of calcium, phosphorus and oxygen. Carbon is also found, which probably originates from the organic matrix or impurities on the tooth that can still be found after cleaning. In addition, traces of sodium and magnesium were examined.

However, the focus of this study is on fluoride, which could only be detected in minimal quantities.

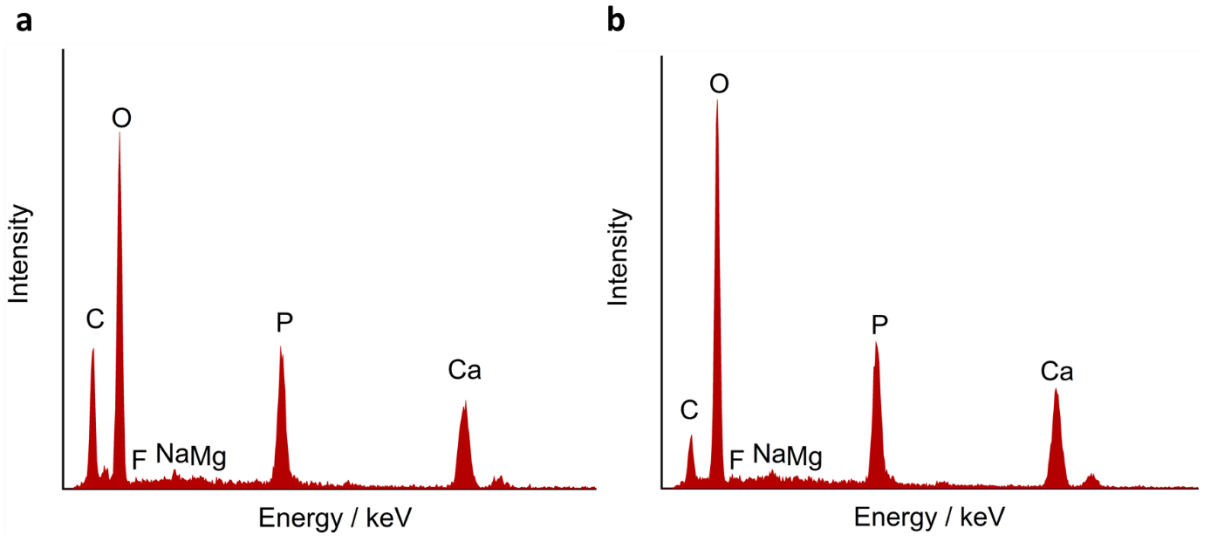

Figure 61 EDX spectra of the tooth enamel surface of sample Hs05-2 (a) before and (b) after treatment with an aqueous fluoride solution of 250 ppm fluoride (pH 5.85).

The quantitative results of the EDX analysis conducted on the enamel surface of sample Hs05-2 are shown in **Table 41**. The analysis compares the composition before and after treatment with an aqueous solution of 250 ppm fluoride. The focus is on selected elements present in hydroxyapatite, calcium (Ca), phosphorus (P), oxygen (O), and the introduced fluoride (F). It provides detailed information on the relative concentrations of these elements in weight percent (wt%) and atomic percent (at%), highlighting any changes resulting from the fluoride treatment.

The portions of all elements increased after the treatment. Since dental enamel is a natural material, it varies in its composition. The measurements provided in this analysis represent a single spot on the tooth crown and may not be representative of the entire enamel structure. Variations in composition can be expected throughout the entire tooth crown.

In this example, the values of fluoride increased from 0.1 wt% to 0.4 wt%. This leaves the impression that the treatment impacted the composition of the enamel, but when the measurement is repeated on several spots over the surface of the tooth crown, it shows that

the increase is not given everywhere and, most importantly, is not statistically significant (see chapter 5.3.7, **Table 53**).

Table 41 Quantitative results of the EDX analysis of the enamel surface of Hs05-2 before and after treatment with a solution of 250 ppm fluoride in water. Selected elements contained in hydroxyapatite are shown: calcium (Ca), phosphorus (P), oxygen (O) as well as fluoride (F).

	Before immersion in 250 ppm fluoride				**After immersion in 250 ppm fluoride**			
Element	**Wt%**	**± Error**	**At%**	**± Error**	**Wt%**	**± Error**	**At%**	**± Error**
Ca	21.9	± 0.4	10.0	± 0.2	25.0	± 0.6	12.3	± 0.3
P	10.7	± 0.3	6.3	± 0.2	12.5	± 0.2	7.9	± 0.2
O	44.2	± 1.0	50.8	± 1.1	51.4	± 0.9	63.2	± 1.0
F	0.1	± 0.3	0.1	± 0.3	0.4	± 0.3	0.4	± 0.4

The calcium-phosphorous ratio before immersion is 1.59 and after immersion 1.56, corresponding to the ratio that prevails in calcium-deficient hydroxyapatite, which is between 1.50 and 1.67. The biological hydroxyapatite in bones and teeth is always non-stoichiometric. Since the structure in all ionic sites (calcium, phosphate, hydroxide) is so flexible that other ions can easily be incorporated. This includes, for example, sodium, potassium, magnesium and strontium, which are incorporated instead of calcium. This explains the small amount of these elements found, as described earlier. Carbonate is incorporated for phosphorus and fluoride, chloride and carbonate for hydroxide (Epple, 2003).

5.3.1.2 PXRD analysis

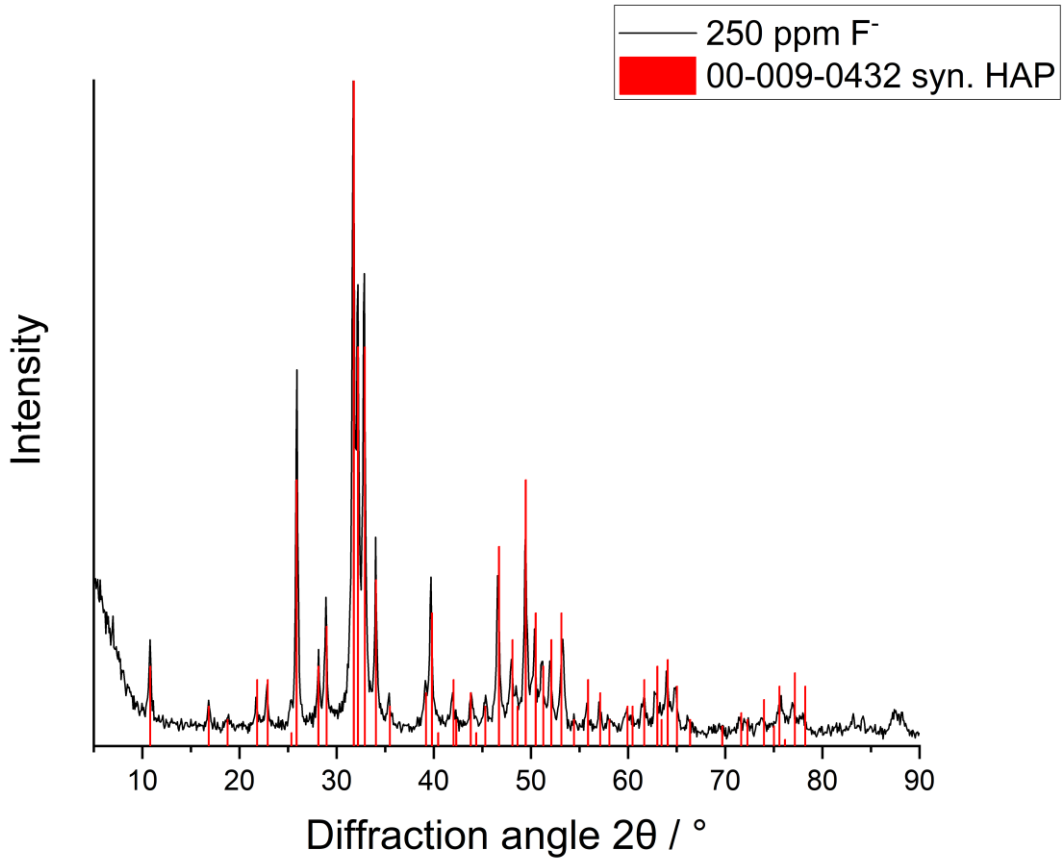

Figure 62 X-ray powder diffractogram of tooth enamel of Hs05-2 after the treatment with 250 ppm fluoride (F^-) in water. The black line shows the reflexes of the sample. The red bars correspond to the reference of synthetic hydroxyapatite (ICDD PDF No. 00-009-0432).

An X-ray powder diffractogram is shown in **Figure 62** of dental enamel of Hs05-2 after immersion in 250 ppm fluoride solution. The diffractogram was compared to the synthetic hydroxyapatite reference (ICDD PDF No. 00-009-0432). It shows a high level of agreement, which is also displayed in **Table 42**. The most notable reflexes of the sample at 25.911°, 31.696°, 32.192°, 32.853° and 49.466° and their corresponding positions in the reference at 25.879°, 31.774°, 32.197°, 32.902° and 49.469° were compared, indicating a strong similarity. These observations strongly suggest that the hydroxyapatite phase of dental enamel was not altered by the immersion in a fluoride solution.

Table 42 Comparison of the strongest observed reflex positions measured in HS05-2 treated with 250 ppm fluoride in water and the positions of the corresponding reflexes of the reference, including the lattice plane.

Reflex position (observed) 2θ/°	Reflex position (reference) 2θ/°	Lattice plane (hkl)
25.911	25.879	(002)
31.696	31.774	(211)
32.192	32.197	(112)
32.853	32.902	(300)
49.466	49.469	(213)

5.3.2 250 ppm fluoride solution (pH 4.6)

Following the immersion in a 250 ppm fluoride solution in water that resulted in no significant alteration of the enamel, a new solution was prepared with the same concentration of fluoride but at a lower pH value of 4.6. The pH value, in this case, was adjusted with citrate buffer. The purpose behind this adjustment was to mimic the acidic nature of some oral care products for which a higher fluoride uptake has been reported (Epple et al., 2022, Scholz et al., 2019).

5.3.2.1 EDX analysis

EDX analysis was conducted before and after treatment with a 250 ppm fluoride solution at pH 4.6 to investigate whether this combination of fluoride and pH value leads to significant changes in tooth enamel composition and fluoride incorporation. A total of 43 spectra before and 41 after immersion were recorded, with one example shown before and after treatment in **Figure 63**.

Both spectra exhibit a similar composition, with the primary elements being calcium, phosphorus, and oxygen. Additionally, the presence of carbon is observed, likely originating from the organic matrix and residual impurities on the tooth surface after cleaning. Sodium and magnesium elements were also examined, albeit in minor quantities.

However, it is important to note that the primary focus of this study is on fluoride. Although detected, fluoride was found only in small amounts within the enamel, indicating a very limited level of fluoride incorporation.

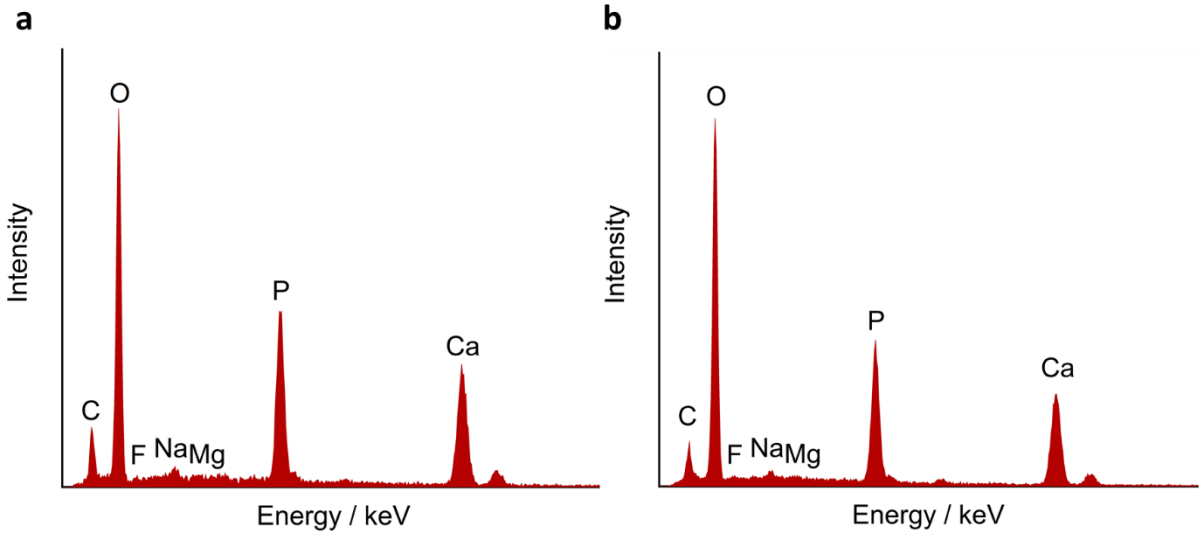

Figure 63 EDX spectra of the tooth enamel surface of HS12-3 (a) before and (b) after treatment with a fluoride solution of 250 ppm fluoride at a pH value of 4.6.

A comprehensive overview of the quantitative results obtained from the EDX analysis performed on the enamel surface of Hs12-3 is provided in **Table 43**. It compares the composition before and after treatment with a solution containing 250 ppm fluoride (pH 4.6). The analysis focuses on the elements found in hydroxyapatite, including calcium (Ca), phosphorus (P), oxygen (O), and the introduced fluoride (F).

There are changes in the distribution of atomic and weight percentages. These are probably related to the natural variation in tooth enamel, as described in chapter 5.3.1.1.

During the initial measurement before immersing the sample in the fluoride solution, either no fluoride was detected, or the fluoride content was below the detection limit of the EDX technique, and, therefore, no fluoride content is listed. After the treatment, the measured value increased to 0.3 wt%. Nevertheless, a statistical analysis (see chapter 5.3.7, **Table 53**) demonstrates that this increase is not statistically significant.

Table 43 Quantitative results of the EDX analysis of the enamel surface of Hs12-3 before and after treatment with a solution of 250 ppm fluoride (pH 4.6). Selected elements contained in hydroxyapatite are shown: calcium (Ca), phosphorus (P), oxygen (O) as well as fluoride (F).

	Before immersion in 250 ppm fluoride (pH 4.6)				**After immersion in 250 ppm fluoride (pH 4.6)**			
Element	**Wt%**	**± Error**	**At%**	**± Error**	**Wt%**	**± Error**	**At%**	**± Error**
Ca	28.5	± 0.6	14.5	± 0.3	25.9	± 0.4	12.9	± 0.2
P	13.7	± 0.2	9.0	± 0.2	12.5	± 0.2	8.0	± 0.1
O	47.9	± 0.7	61.0	± 0.9	52.6	± 0.6	65.5	± 0.8
F	0.0	N/A	0.0	N/A	0.3	± 0.3	0.3	± 0.3

The calcium-phosphorous ratio before and after immersion is 1.61, corresponding to the ratio that prevails in calcium-deficient hydroxyapatite, which is between 1.50 and 1.67. As described in chapter 5.3.1.1, this is due to the natural ionic substitution (Epple, 2003).

5.3.2.2 PXRD analysis

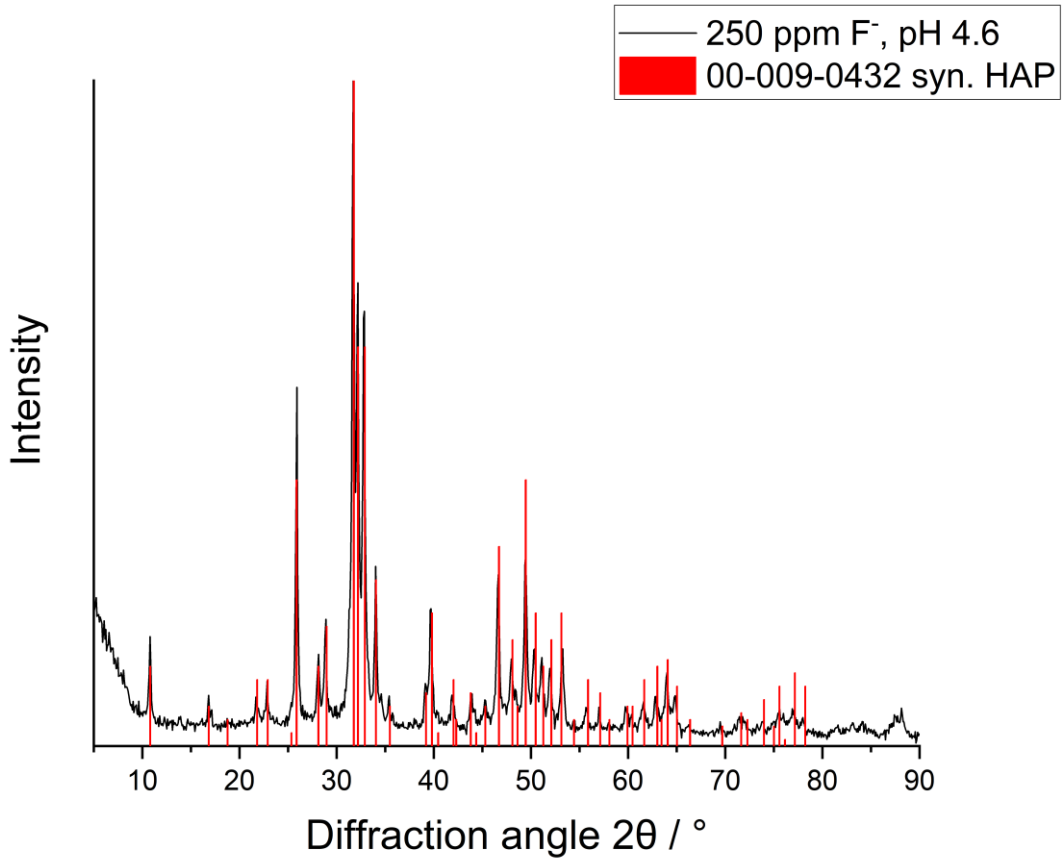

Figure 64 X-ray powder diffractogram of tooth enamel of Hs04 after the treatment with 250 ppm fluoride (pH 4.6). The black line shows the reflexes of the sample. The red bars correspond to the reference of synthetic hydroxyapatite (ICDD PDF No. 00-009-0432).

An X-ray powder diffractogram of dental enamel of sample Hs04 following immersion in a 250 ppm fluoride solution (pH 4.6) is depicted in **Figure 64**. The diffractogram was compared to the synthetic hydroxyapatite reference (ICDD PDF No. 00-009-0432). Notably, a remarkable level of agreement is observed, which is further illustrated in **Table 44**. By comparing the strongest reflexes of the sample at 25.911°, 31.696°, 32.192°, 32.853° and 49.466° and their corresponding positions in the reference at 25.879°, 31.774°, 32.197°, 32.902° and 49.469°, a high similarity can be observed. These findings strongly indicate that the hydroxyapatite phase of dental enamel remained unaffected by the immersion in the fluoride solution.

Table 44 Comparison of the strongest observed reflex positions for the sample Hs04 treated with 250 ppm fluoride in citrate buffer (pH 4.6) and the positions of the corresponding reflexes of the reference, including the lattice plane.

Reflex position (observed) 2θ/°	Reflex position (reference) 2θ/°	Lattice plane (hkl)
25.911	25.879	(002)
31.696	31.774	(211)
32.192	32.197	(112)
32.853	32.902	(300)
49.466	49.469	(213)

5.3.3 18,998 ppm fluoride solution

Since the concentration of 250 ppm fluoride did not lead to an increase of fluoride in dental enamel, a higher concentration of 18,889 ppm (1 mol L^{-1}) was chosen. This concentration is similar to professional fluoride varnishes (Weyant et al., 2013).

5.3.3.1 EDX analysis

EDX analysis was performed to examine the effects of the treatment with the 18,998 ppm fluoride solution in water (pH 7.76) on the tooth enamel of Hs05-1 composition and fluoride incorporation. A comprehensive set of 31 spectra before immersion and 32 after was recorded for analysis, **Figure 65** shows an example of spectra before and after the treatment.

The primary elements observed in both spectra are calcium, phosphorus, and oxygen, which are the characteristic elements of dental enamel. Additionally, the presence of carbon is detected, which may likely originate from the organic matrix or residual impurities on the tooth surface, that may remain on the tooth surface even after cleaning. In relatively minimal quantities, the elements sodium and magnesium were identified.

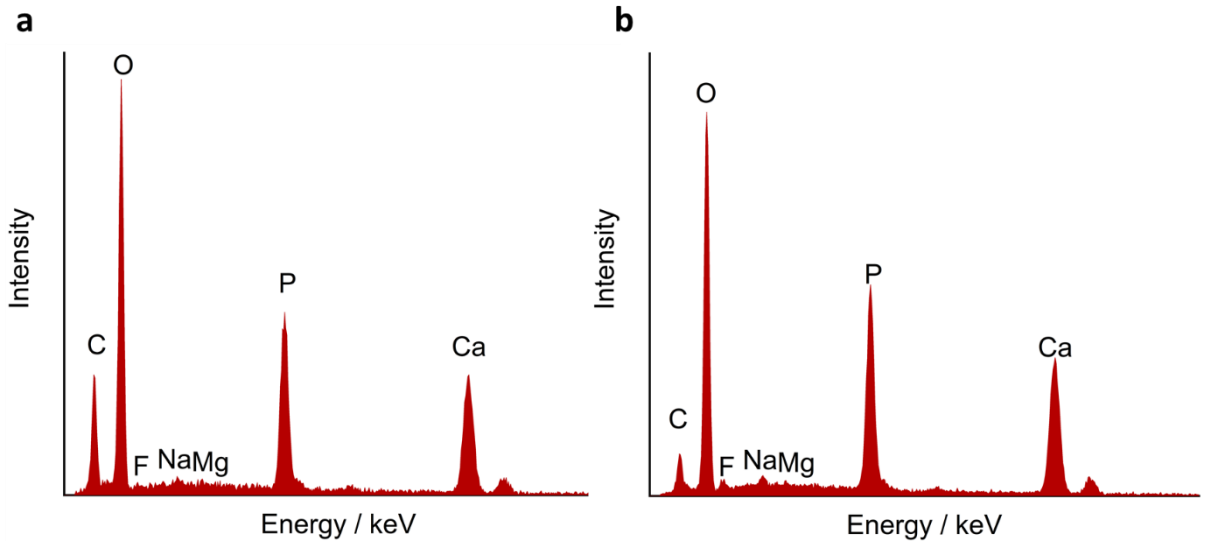

Figure 65 EDX spectra of the tooth enamel surface of Hs05-1 (a) before and (b) after treatment with a fluoride concentration of 18,998 ppm fluoride in water (pH 7.76).

A comprehensive overview of the quantitative results obtained from the EDX analysis performed on the enamel surface is provided in **Table 45**. The table compares the composition before and after treatment with a solution containing 18,998 ppm fluoride. The analysis focuses on the elements found in hydroxyapatite, including calcium (Ca), phosphorus (P), oxygen (O), and the introduced fluoride (F).

As in the previous analyses, the focus lies on fluoride. An increase in fluoride can be observed in the spectrum. During the initial measurement before immersing the sample in the fluoride solution, 0.2 wt% fluoride was detected. After the treatment, the measured value increased to 1.2 wt%.

This observation can be confirmed with the quantitative data obtained from the EDX analysis, displayed in **Table 45**. It should be noted that it appears that the content of all elements has increased. But if we consider further examinations carried out on the teeth, the assumption that the introduction of 18.998 ppm fluoride leads to a significant increase in the fluoride content is confirmed (see chapter 5.3.7, **Table 53**).

Table 45 Quantitative results of the EDX analysis of the enamel surface of Hs05-1 before and after treatment with a concentration of 18,998 ppm fluoride. Selected elements contained in hydroxyapatite are shown: calcium (Ca), phosphorus (P), oxygen (O) as well as fluoride (F).

	Before immersion in 18,998 ppm fluoride				**After immersion in 18,998 ppm fluoride**			
Element	**Wt%**	**± Error**	**At%**	**± Error**	**Wt%**	**± Error**	**At%**	**± Error**
Ca	25.4	± 0.4	12.2	± 0.2	30.0	± 0.5	15.6	± 0.2
P	12.1	± 0.2	7.5	± 0.2	14.2	± 0.2	9.5	± 0.1
O	45.4	± 0.9	54.8	± 1.0	47.2	± 0.6	62.0	± 0.8
F	0.2	± 0.3	0.2	± 0.3	1.09	± 0.25	1.2	± 0.3

The calcium-phosphorous ratio before immersion is 1.62 and after 1.64, corresponding to the ratio that prevails in calcium-deficient hydroxyapatite, which is between 1.50 and 1.67. As described in chapter 5.3.1.1, this is due to the natural ionic substitution (Epple, 2003).

5.3.3.2 PXRD analysis

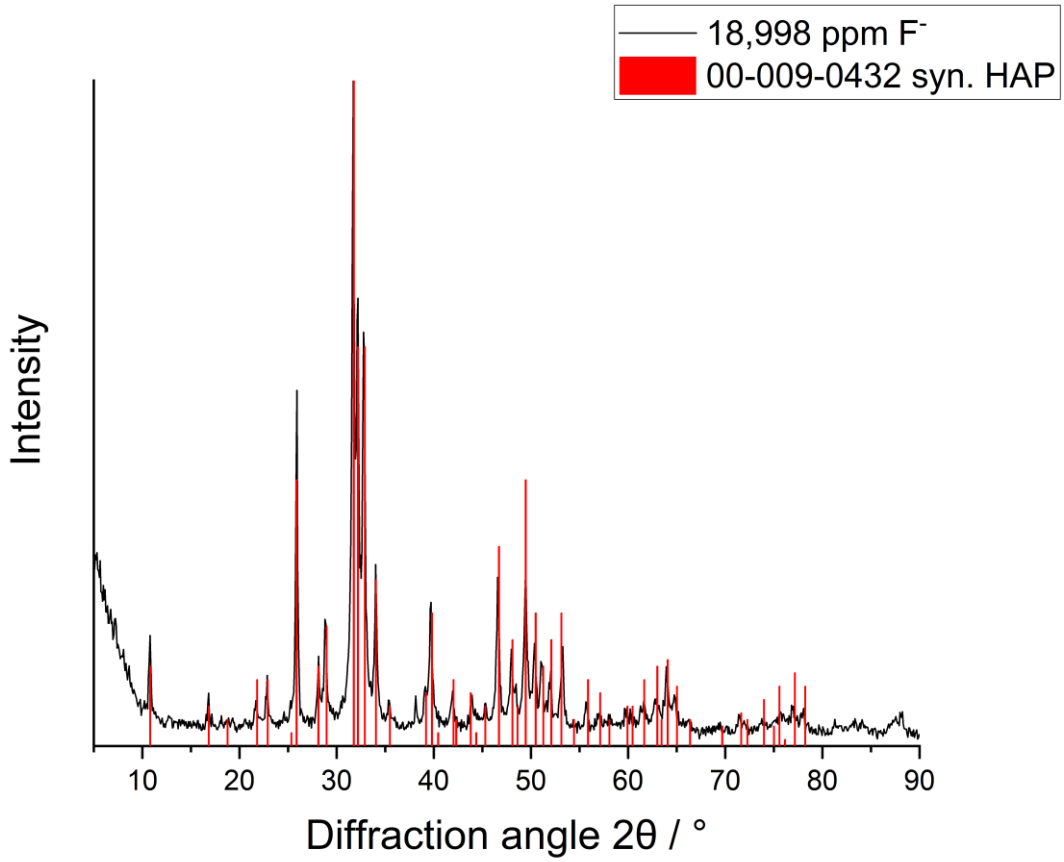

Figure 66 Representative X-ray powder diffractogram of tooth enamel of Hs06 after the treatment with 18,998 ppm fluoride in water (pH 7.76). The black line shows the reflexes of the sample. The red bars correspond to the reference of synthetic hydroxyapatite (ICDD PDF No. 00-009-0432).

An X-ray powder diffractogram of dental enamel subsequent to immersion in an 18,998 ppm fluoride solution is shown in **Figure 66**. A comparative analysis was performed by aligning the diffractogram with the synthetic hydroxyapatite reference (ICDD PDF No. 00-009-0432). Notably, a remarkable level of agreement is observed, as demonstrated in **Table 46**.

By examining the strongest reflexes of the sample, specifically at 25.911°, 31.696°, 32.192°, 32.771°, and 49.466°, and comparing them to their corresponding positions in the reference at 25.879°, 31.774°, 32.197°, 32.902°, and 49.469°, a high degree of similarity becomes

evident. These findings strongly support the conclusion that the hydroxyapatite phase of dental enamel remained unaltered following immersion in the fluoride solution.

Table 46 Comparison of the strongest observed reflex positions of the sample treated with 18,998 ppm fluoride in water (pH 7.76) and the positions of the corresponding reflexes of the reference, including the lattice plane.

Reflex position (observed) 2θ/°	Reflex position (reference) 2θ/°	Lattice plane (hkl)
25.911	25.879	(002)
31.696	31.774	(211)
32.192	32.197	(112)
32.771	32.902	(300)
49.466	49.469	(213)

5.3.4 18,998 fluoride solution (pH 4.7)

The previous experiment (chapter 5.3.3) led to the conclusion that the fluoride concentration is high enough to incorporate fluoride in tooth enamel. To increase the amount of fluoride incorporated, another experiment with the same concentration of fluoride (18,998 ppm) but with a slightly acidic pH value of 4.7 (adjusted with citrate buffer) was carried out. With this, the nature of highly concentrated fluoride gels and vanishes with acidic pH (e.g. Elmex Gelée, CP-GABA GmbH, 12,500 ppm fluoride, pH 4.75) is mimicked.

5.3.4.1 EDX analysis

EDX analysis was conducted to investigate the impact of composition and fluoride incorporation after treating the tooth enamel with an 18,998 ppm fluoride solution in citrate buffer (pH 4.7). A comprehensive collection of 50 spectra before and 37 after immersion was recorded for detailed examination. **Figure 67** illustrates an example of spectra before and after the treatment.

In both spectra, the primary elements observed are calcium, phosphorus, and oxygen, which are characteristic components of dental enamel. Additionally, the presence of carbon is

detected, likely originating from the organic matrix or residual impurities that may persist on the tooth surface even after cleaning procedures. The elements sodium and magnesium were identified, although in relatively small quantities.

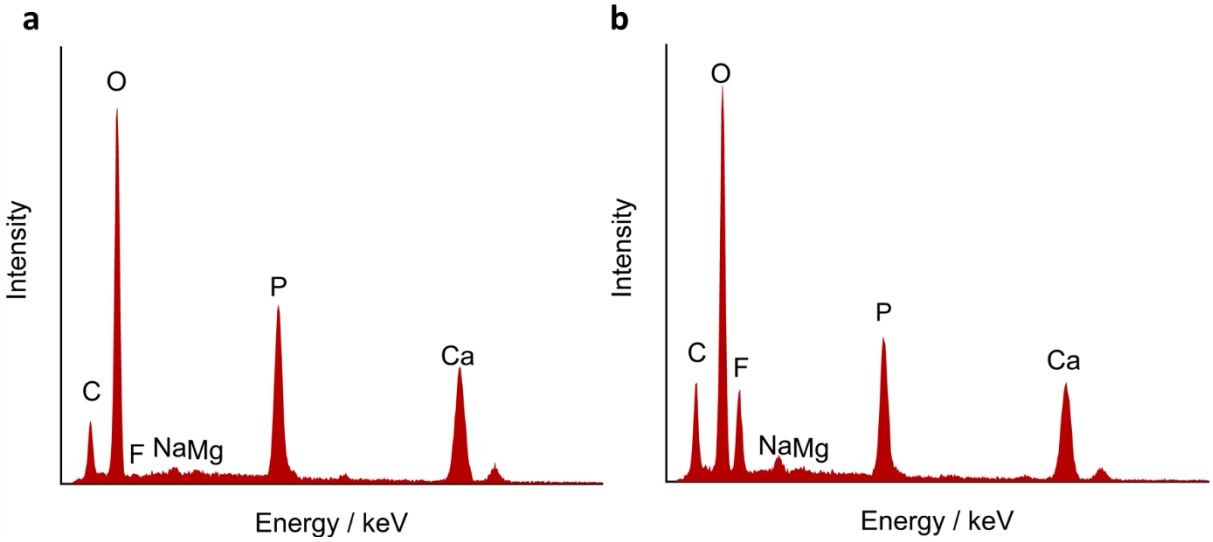

Figure 67 EDX spectra of the tooth enamel surface of Hs12-2 (a) before and (b) after treatment with a fluoride concentration of 18,998 ppm fluoride in citrate buffer (pH 4.7).

A comprehensive summary of the quantitative results from the EDX analyses of Hs12-2 conducted on the enamel surface is represented in **Table 47**. The table compares the composition of the tooth enamel before and after treatment with the 18,998 ppm fluoride solution in citrate buffer at a pH value of 4.7. The analyses focus on the elements calcium (Ca), phosphorus (P) and oxygen (O), which are commonly found in hydroxyapatite, as well as the introduced fluoride (F).

Notable changes in the distribution of atomic and weight percentages are observed. These are probably due to natural variation, as in the previous experiments.

The fluoride content increased from 0.1 wt% up to 10.3 wt%, which is a significant difference (see chapter 5.3.7, **Table 53**).

Table 47 Quantitative results of the EDX analysis of the enamel surface of Hs12-2 before and after treatment with a solution of 18,998 ppm fluoride (pH 4.7). Selected elements contained in hydroxyapatite shown: calcium (Ca), phosphorus (P), oxygen (O) as well as fluoride (F).

	Before immersion in 18,998 ppm fluoride (pH 4.7)				**After immersion in 18,998 ppm fluoride (pH 4.7)**			
Element	**Wt%**	**± Error**	**At%**	**± Error**	**Wt%**	**± Error**	**At%**	**± Error**
Ca	27.3	± 0.3	13.7	± 0.2	21.8	± 0.3	10.4	± 0.1
P	13.5	± 0.2	8.7	± 0.1	10.1	± 0.2	6.2	± 0.1
O	48.4	± 0.6	60.8	± 0.8	42.9	± 0.8	51.2	± 0.9
F	0.1	± 0.2	0.1	± 0.3	10.2	± 0.5	10.3	± 0.5

The calcium-phosphorous ratio before immersion is 1.57 and 1.68. The ratios correspond to the ratio that prevails in calcium-deficient hydroxyapatite, which is between 1.50 and 1.67. As described in chapter 5.3.1.1, this is due to the natural ionic substitution (Epple, 2003).

5.3.4.2 PXRD analysis

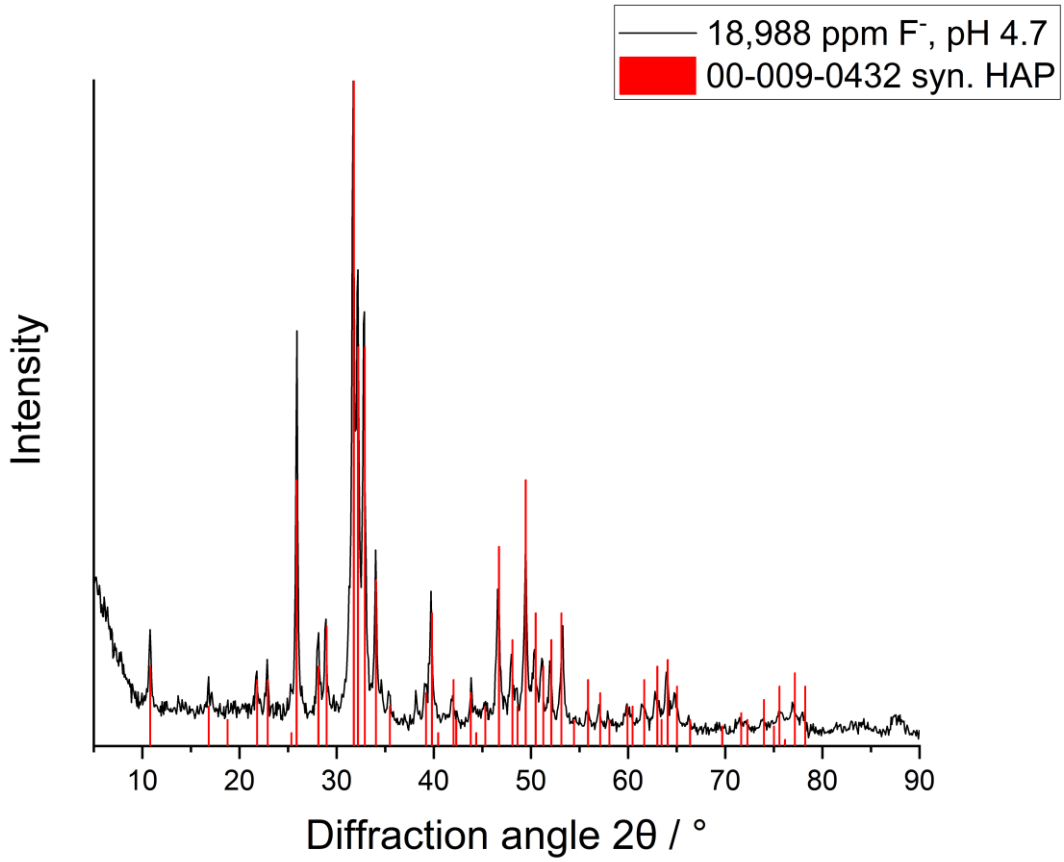

Figure 68 X-ray powder diffractogram of tooth enamel Hs03 after the treatment with 18,998 ppm fluoride in citrate buffer (pH 4.7). The black line shows the reflexes of the sample. The red bars correspond to the reference of synthetic hydroxyapatite (ICDD PDF No. 00-009-0432).

An X-ray powder diffractogram of the dental enamel of Hs03 after being immersed in an 18,998 ppm fluoride solution at pH 4.6 is illustrated in **Figure 68**. To assess the similarity between the diffractogram and the synthetic hydroxyapatite reference (ICDD PDF No. 00-009-0432), a comparative analysis was conducted. Remarkably, a high level of agreement is observed, as corroborated by **Table 48**.

By examining the most prominent reflexes of the sample at 25.911°, 31.696°, 32.192°, 32.853°, and 49.466° and comparing them to the corresponding positions in the reference at 25.879°, 31.774°, 32.197°, 32.902°, and 49.469°, a strong similarity is evident. These findings provide

compelling evidence that the hydroxyapatite phase of dental enamel remained unaffected following the immersion in the fluoride solution.

Table 48 Comparison of the strongest observed reflex positions in the sample Hs03 treated with 18,998 ppm fluoride in citrate buffer and the positions of the corresponding reflexes of the reference, including the lattice plane.

Reflex position (observed) 2θ/°	Reflex position (reference) 2θ/°	Lattice plane (hkl)
25.911	25.879	(002)
31.696	31.774	(211)
32.192	32.197	(112)
32.853	32.902	(300)
49.466	49.469	(213)

5.3.5 Solution without fluoride (pH 4.6)

To investigate the potential impact of pH alteration on the tooth surface, a comparative solution was prepared without fluoride but adjusted pH to 4.6 using citrate buffer. This control solution was specifically designed to assess whether changes in pH alone would lead to significant modifications on the tooth surface.

5.3.5.1 EDX analysis

EDX analysis was performed to investigate the effects of treating tooth enamel with a pH adjusted solution on its composition and the fluoride content. A comprehensive set of 38 spectra before and 15 after was recorded to provide a thorough examination, and **Figure 69** shows an example of spectra obtained before and after the treatment.

In both spectra, the primary elements observed are calcium, phosphorus, and oxygen, which are characteristic constituents of dental enamel. Additionally, the presence of carbon is detected, likely originating from the organic matrix or residual impurities that may persist on

the tooth surface even after cleaning procedures. Also, traces of the elements sodium and magnesium are found.

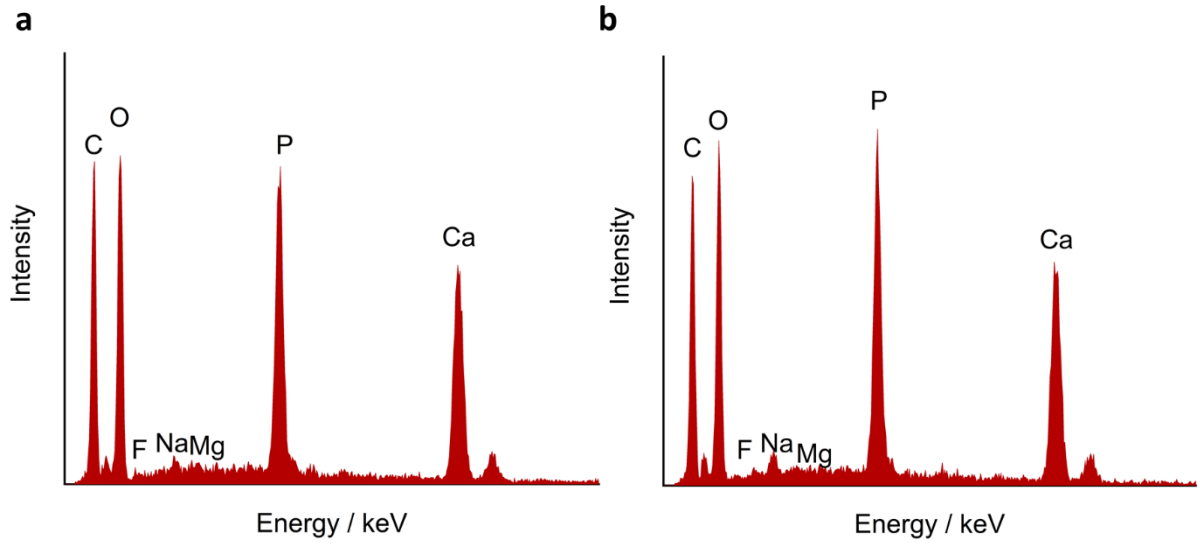

Figure 69 EDX spectra of the tooth enamel surface of Hs15-1 (a) before and (b) after treatment with a solution with no fluoride and a pH value of 4.6.

A comprehensive summary of the quantitative results obtained from the EDX analysis conducted on the enamel surface of Hs15-1 is provided in **Table 49**. The table compares the composition of tooth enamel before and after treatment with a solution at a pH value of 4.6. The analysis focuses on the elements typically found in hydroxyapatite, including calcium (Ca), phosphorus (P), oxygen (O), and fluoride (F), although the latter was not part of the solution.

Changes in the composition were minor and might as well be due to natural variation. Since the solution did not contain fluoride, it was expected that the fluoride content would not change. But in fact, it appears that fluoride was completely removed from the tooth or at least reduced to an amount that was not detectable by the EDS technique. This removal of fluoride is likely attributed to the acidic nature of the solution, which facilitated the dissolution of surface material. It is known from literature that fluoride from dental care products primarily remains on the surface and does not penetrate deeply (Faidt et al., 2017, Loskill et al., 2013, Mueller et al., 2010, Sternitzke et al., 2012). Therefore, during the immersion process, the fluoride content dissolved into the solution, resulting in its removal from the tooth enamel.

Table 49 Quantitative results of the EDX analysis of the enamel surface of Hs15-1 before and after treatment with a solution at pH 4.7. Selected elements contained in hydroxyapatite shown: calcium (Ca), phosphorus (P), oxygen (O) as well as fluoride (F).

	Before immersion in solution of pH 4.6				**After immersion in solution of pH 4.6**			
Element	**Wt%**	**± Error**	**At%**	**± Error**	**Wt%**	**± Error**	**At%**	**± Error**
Ca	28.1	± 0.6	13.4	± 0.3	30.2	± 0.6	14.7	± 0.3
P	13.2	± 0.2	8.1	± 0.1	14.0	± 0.3	8.8	± 0.2
O	30.7	± 0.8	36.6	± 1.0	29.0	± 0.7	35.3	± 0.9
F	0.5	± 0.2	0.5	± 0.2	0.0	N/A	0.0	N/A

The calcium-phosphorous ratio before immersion is 1.65 and after 1.67, corresponding to the ratio that prevails in calcium-deficient hydroxyapatite, which is between 1.50 and 1.67. As described in chapter 5.3.1.1, this is due to the natural ionic substitution (Epple, 2003).

5.3.5.2 PXRD analysis

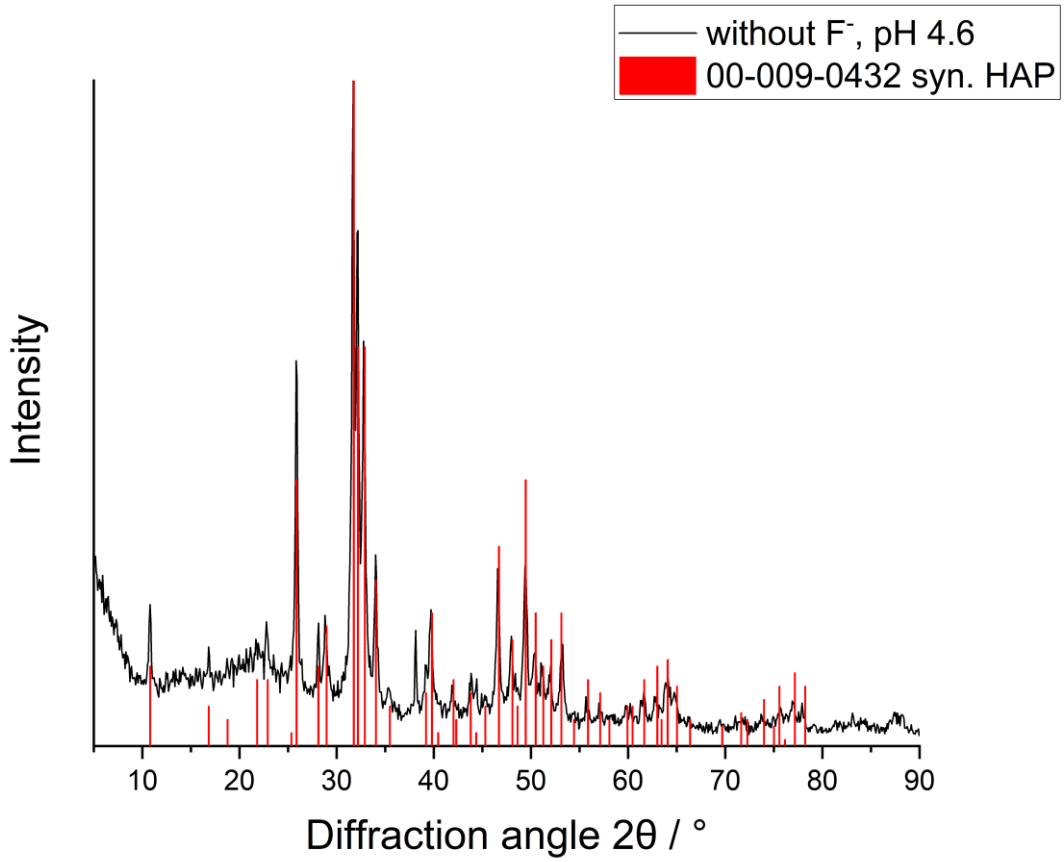

Figure 70 X-ray powder diffractogram of tooth enamel of Hs15-1 after the treatment with a fluoride-free solution at pH 4.6. The black line shows the reflexes of the sample. The red bars correspond to the reference of synthetic hydroxyapatite (ICDD PDF No. 00-009-0432).

An X-ray powder diffractogram of tooth enamel of Hs15-1 after the treatment with a solution of pH 4.6 is displayed in **Figure 70**. The reflexes of the sample are compared to the reference of synthetic hydroxyapatite (ICDD PDF No. 00-009-0432).

The diffractogram in **Figure 70** demonstrates a high level of agreement when compared to the synthetic hydroxyapatite reference, as further supported by **Table 50**. The most notable reflexes of the sample, occurring at 25.828°, 31.771°, 32.192°, 32.771°, and 49.466°, were compared to their corresponding positions in the reference at 25.879°, 31.774°, 32.197°, 32.902°, and 49.469°. This comparison reveals a strong similarity, providing evidence that the hydroxyapatite phase of dental enamel remained unaltered following immersion in the fluoride solution.

Table 50 Comparison of the strongest observed reflex positions in sample Hs15-1 treated with a solution at pH 4.7 and the positions of the corresponding reflexes of the reference, including the lattice plane.

Reflex position (observed) 2θ/°	Reflex position (reference) 2θ/°	Lattice plane (hkl)
25.828	25.879	(002)
31.771	31.774	(211)
32.192	32.197	(112)
32.771	32.902	(300)
49.466	49.469	(213)

5.3.6 Water

To further compare and rule out any other step of the treatment altering the composition, the teeth were placed in distilled water precisely as before with the fluoride solutions.

5.3.6.1 EDX analysis

EDX analysis was performed to investigate the effects of treating tooth enamel with water. One spectrum was conducted before and after the treatment.

Both spectra in **Figure 71** exhibit the presence of calcium, phosphorus, and oxygen as the primary elements, which are characteristic constituents of dental enamel. The detection of carbon suggests its origin from the organic matrix and residual impurities that can remain on the tooth surface despite cleaning procedures. Sodium and magnesium are observed in minimal quantities in the spectra.

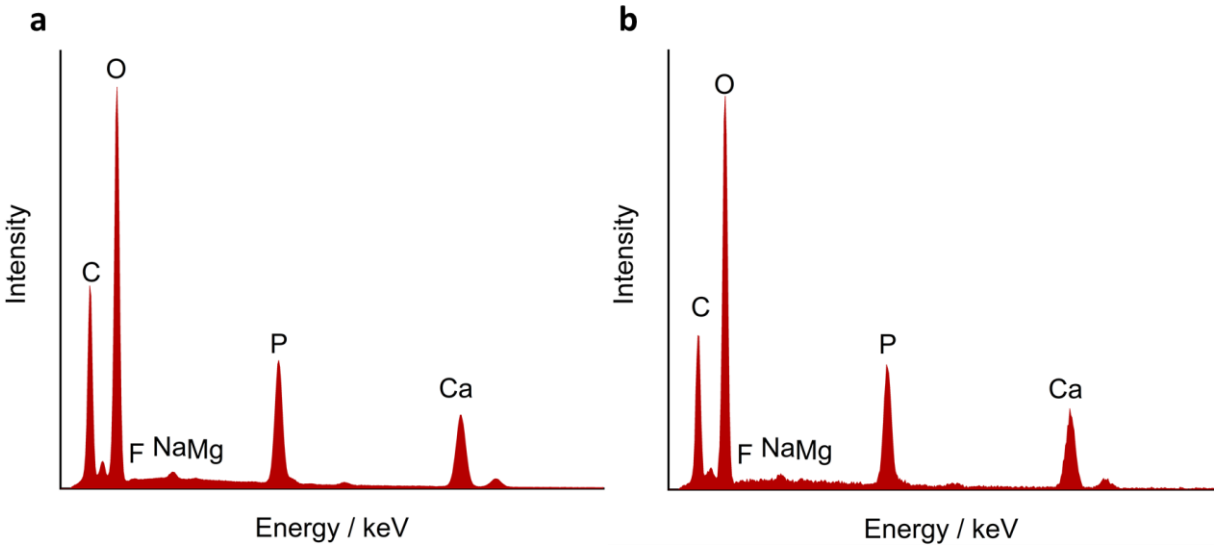

Figure 71 EDX spectra of the tooth enamel surface of Hs08 (a) before and (b) after treatment with water.

A comprehensive summary of the quantitative results obtained from the EDX analysis conducted on the enamel surface of Hs08 is provided in **Table 51**. The table compares the composition of tooth enamel before and after treatment with a solution at a pH value of 4.6. The analysis focuses on the elements typically found in hydroxyapatite, including calcium (Ca), phosphorus (P), oxygen (O), and fluoride (F), while the latter was not contained in the solution.

Changes in the composition were marginal and might as well be due to natural variation. Since the solution did not contain fluoride, a change was not expected.

Table 51 Quantitative results of the EDX analysis of the enamel surface of Hs08 before and after treatment with a water (pH 7). Selected elements contained in hydroxyapatite are shown: calcium (Ca), phosphorus (P), oxygen (O) as well as fluoride (F).

	Before immersion in water				**After immersion in water**			
Element	**Wt%**	**± Error**	**At%**	**± Error**	**Wt%**	**± Error**	**At%**	**± Error**
Ca	17.8	± 0.4	7.9	± 0.2	16.8	± 0.1	7.3	± 0.0
P	9.6	± 0.2	5.5	± 0.1	9.4	± 0.1	5.3	± 0.0
O	48.7	± 0.6	53.9	± 0.7	47.9	± 0.2	52.0	± 0.3
F	0.0	N/A	0.0	N/A	0.0	N/A	0.0	N/A

The calcium-phosphorous ratio before immersion is 1.43 and after 1.37. The detected ratio is remarkably low, yet it appears to be a natural variation in this individual's teeth. Notably, the values before insertion exhibit similarly low levels, showing minimal change after immersion.

5.3.6.2 PXRD analysis

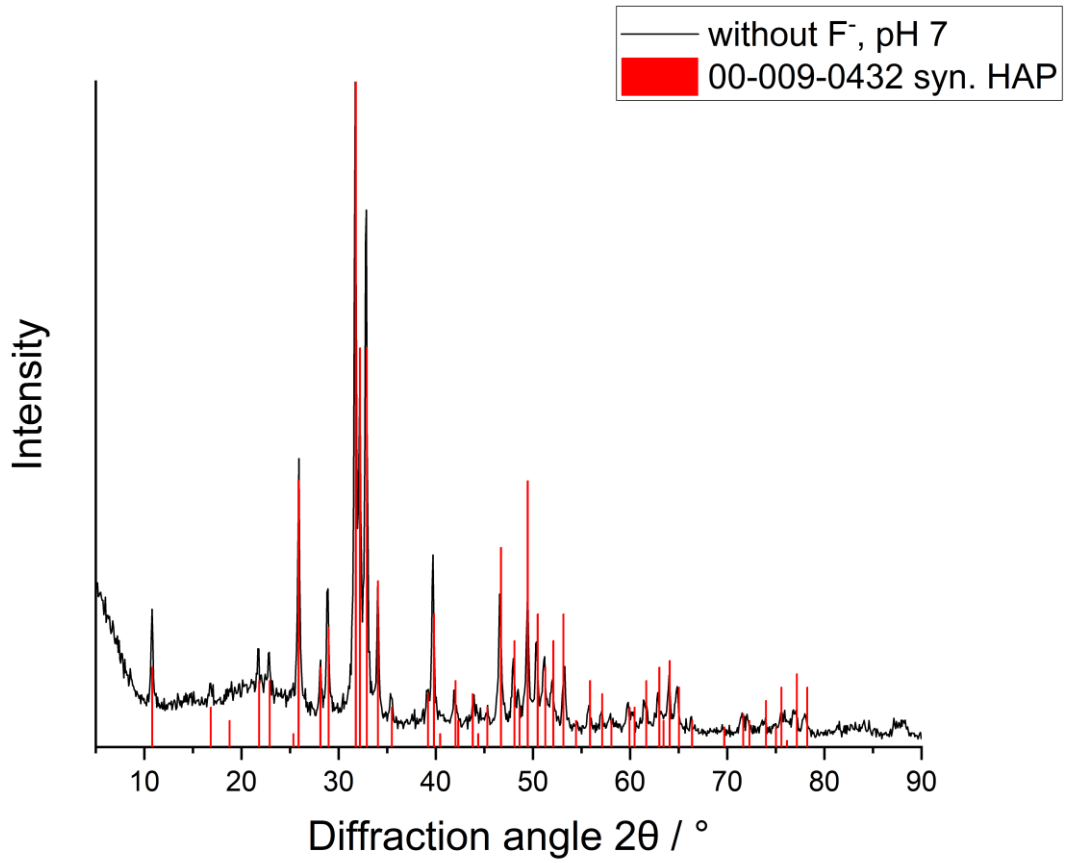

Figure 72 X-ray powder diffractogram of tooth enamel of Hs08 after the treatment with water (no fluoride, pH 7). The black line shows the reflexes of the sample. The red bars correspond to the reference of synthetic hydroxyapatite (ICDD PDF No. 00-009-0432).

An X-ray powder diffractogram of tooth enamel after treatment with water is shown in **Figure 72**. The reflexes of the sample are compared to the reference of synthetic hydroxyapatite (ICDD PDF No. 00-009-0432).

The diffractogram in **Figure 72** demonstrates a high level of agreement when compared to the synthetic hydroxyapatite reference, as further supported by **Table 52**. The strongest reflexes

of the sample, occurring at 25.911°, 31.696°, 32.192°, 32.853°, and 49.466°, were compared to their corresponding positions at 25.879°, 31.774°, 32.197°, 32.902°, and 49.469° in the reference. This comparison reveals a strong similarity, providing compelling evidence that the hydroxyapatite phase of dental enamel remained unaltered following immersion in the water.

Table 52 Comparison of the strongest observed reflex positions in sample Hs08 treated with a solution with no fluoride content at pH 7 and the positions of the corresponding reflexes of the reference, including the lattice plane.

Reflex position (observed) 2θ/°	Reflex position (reference) 2θ/°	Lattice plane (hkl)
25.911	25.879	(002)
31.696	31.774	(211)
32.192	32.197	(112)
32.853	32.902	(300)
49.466	49.469	(213)

5.3.7 Statistical analyses and combined results

As previously described, numerous teeth showed an increase in fluoride after immersion. Nevertheless, not all increases were statistically significant. An overview of the fluoride concentration in wt% of all teeth before and after immersion is given in **Figure 73** and in **Table 53**.

The effects of the immersion were statistically investigated in each tooth separately. For this purpose, the exact non-parametric Mann-Whitney tests (Appendix 8.4, **Table 64**) were performed (as the Wilk-Shapiro test indicated a violation of normal distribution in some teeth). Two-sided p-values are reported. For the sake of completeness, t-tests for independent samples were performed.

The immersion in 250 ppm fluoride solution in water did not or only slightly increase the fluoride concentration in three teeth. A statistically significant increase was solely observed in one tooth (Hs01). Treatment with a 250 ppm fluoride solution in citric acid did not change the fluoride content in the dental enamel (**Table 53**). This goes along with the results of previous studies in which teeth were treated with fluoride-containing toothpaste (Arnold et al., 2006,

Lee et al., 2015, Lelli et al., 2014). It is reported that the fluoride uptake from toothpaste into a thin surface layer of the tooth happens during a few minutes (Faidt et al., 2017). The lack of significant alteration in fluoride content after immersion in an acidic, fluoride-free medium and water highlights the naturally low concentration of fluoride in teeth, confirming previous findings summarised in Epple et al. (2022).

Table 53 Average fluoride concentration after immersion in fluoride solution in weight percent (wt%) and average change of fluoride concentration in a tooth with standard deviation and p-values for statistical significance (Storsberg et al., 2022).

Immersion medium	N	Average fluoride concentration before immersion/wt%	Average fluoride concentration after immersion/wt%	Average change in fluoride concentration compared to the same tooth before immersion/wt%
250 ppm F^- (water, pH 5.85)	3	0.13 ± 0.14	0.20 ± 0.19	+0.09 ± 0.07 (not significant)
250 ppm F^- (citrate buffer, pH 4.6)	3	0.20 ± 0.17	0.24 ± 0.22	+0.04 ± 0.07 (not significant)
18,998 ppm F^- (water, pH 7.76)	3	0.15 ± 0.16	0.83 ± 0.33	+0.68 ± 0.05 (significant, $p < 0.0001$)
18,998 ppm F^- (citrate buffer, pH 4.7)	3	0.15 ± 0.15	9.20 ± 2.77	+9.06 ± 2.77 (significant, $p < 0.0001$)
Fluoride-free citrate buffer (pH 4.6)	3	0.21 ± 0.17	0.05 ± 0.11	−0.16 ± 0.15 (not significant)
Water (pH 7)	1	0.00	0.00	N/A

All teeth that were immersed in solutions of 18,998 ppm fluoride showed a significant ($p<0.0001$) increase in fluoride concentration (**Table 53**). Notably, the fluoride concentration increased by approximately tenfold at a low pH level. This is similar to earlier studies where fluoride gels were applied (Amaechi et al., 2020). Furthermore, it is consistent with earlier findings (Hjortsjo et al., 2015, Scholz et al., 2019), which described that fluoride uptake was notably higher following treatment with a high-fluoride gel at a low pH value. This could be attributed to the surface etching of the dental enamel and the partial dissolution and reprecipitation of fluoride-containing apatite.

Since CaF_2 globules could not be verified, neither morphologically via SEM nor crystallographically via PXRD, the exact chemical and crystallographic nature of the deposited fluoride on the tooth surface remains unknown. However, it should also be considered that

the very thin layer of fluoride on the tooth surface was probably covered by the much higher volume of abraded untreated hydroxyapatite, which was around a couple of 100 µm thick. Fluoride penetrates enamel only for a few ten nanometres, as earlier studies with X-ray photoelectron spectroscopy found (Faidt et al., 2017, Loskill et al., 2013, Mueller et al., 2010, Sternitzke et al., 2012). Therefore, the fluoride-rich surface layer only comprises around 0.1 to 0.2 vol% of the abraded sample used for PXRD. Laboratory X-ray powder diffractometers have a detection limit under which this concentration falls well, especially when detecting poorly crystalline or nanocrystalline phases (Klug and Alexander, 1974). While the presence of CaF_2 cannot be ruled out, there is also no direct indication of its existence, apart from the elevated fluoride content observed by EDX in the surface layer (9 to 10 wt%), which surpasses the maximum fluoride content possible for fluorapatite (3.77 wt%). Additionally, it is worth mentioning that existing evidence in the literature regarding the formation of CaF_2 has predominantly relied on elemental analysis conducted through various methods (Gerth et al., 2007, Mueller et al., 2010, Scholz et al., 2019, Sternitzke et al., 2012) but never on a crystallographic method.

Teeth immersed in fluoride-free solutions (pH 4.6) show a slight decrease in the fluoride concentration. However, it was only statistically significant in one tooth (Hs15-1).

The immersion in water showed no effect. It was expected to get those results since those were only used as a control group.

The uptake of fluoride into enamel depends on the fluoride concentration in the solution as well as on the pH value. In particular, very high fluoride concentrations under acidic conditions favour fluoride uptake.

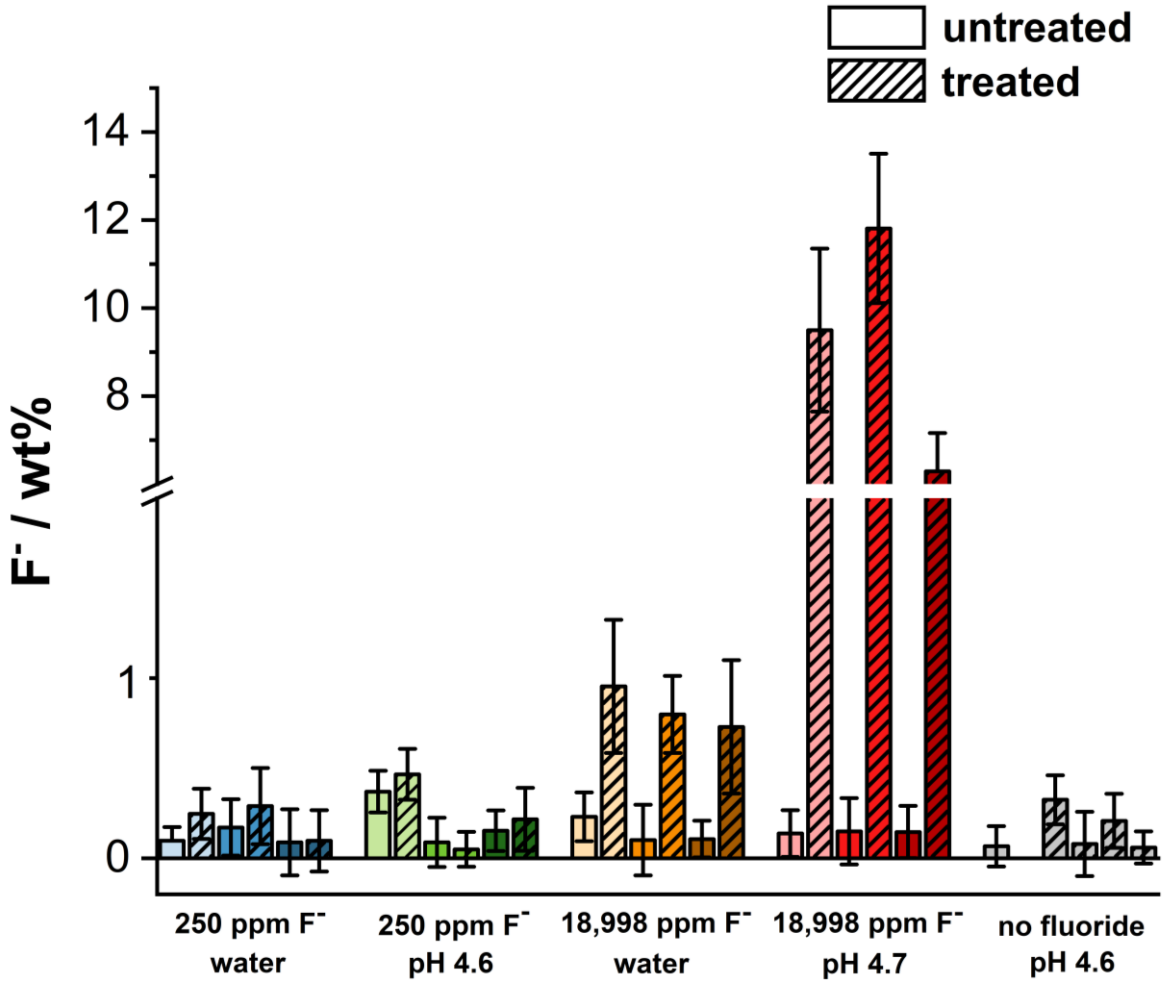

Figure 73 Average fluoride content of different treatment groups as determined by EDX. For every concentration, three teeth were selected and immersed in the indicated concentration of fluoride. Fluoride contents before immersion are depicted with a blank bar, and after immersion, with a hatched one (Storsberg et al., 2022).

6 Summary

The research conducted on the Gevensleben population, an early medieval burial ground in Lower Saxony from 700 to 1000 AD, has provided insights into the childhood development and health of individuals during that period. The study focused on daily secretion rates (DSR) in tooth enamel, crown formation times (CFT) of teeth, and accentuated lines (AL) as indicators of health and stress during childhood.

The daily secretion rate (DSR) was measured at different locations in tooth crowns. It was found to increase from the inner to the outer enamel in both the cuspal and lateral enamel regions. Comparisons were made with other historical populations, and the Gevensleben DSR rates aligned more closely with the early Anglo-Saxon sample than the late Anglo-Saxon one, although the latter were closer in time to Gevensleben.

Crown formation times (CFT) were estimated using reference values due to the absence of neonatal lines in the teeth. The calculated CFT values generally preceded the reference values.

Accentuated lines (AL) were used as indicators of childhood health and stress. The prevalence of AL showed an increase between 7 to 10 months, likely attributed to increased activity and exposure to pathogens. Another peak in AL prevalence was observed around 3 years of age, corresponding to a period of high mortality in nearby populations, possibly related to challenging weaning conditions. A third peak occurred between 8 to 9 years, which coincided with a transitional developmental stage.

Overall, the Gevensleben population experienced challenging living conditions, including malnutrition, infectious diseases, and inadequate housing. These factors likely contributed to the observed stress markers in the teeth and bones of the individuals.

Fluoride is found in human teeth primarily on the tooth surface, albeit in minimal amounts. The study aimed to investigate the uptake of fluoride in human teeth when exposed to different fluoride-containing solutions to simulate dental care treatments. The teeth were immersed in solutions with 250 ppm fluoride, representing mouth rinses, and a highly concentrated potassium fluoride solution (18,998 ppm; 1 mol L^{-1}), representing fluoride

varnishes. The immersion was conducted in water and citrate buffer (pH 4.6 to 4.7) to mimic the acidic nature of some fluoride gels.

This research found that treatment with 250 ppm fluoride did not significantly change the fluoride content of the tooth enamel at both neutral and acidic pH levels. In contrast, teeth exposed to 18,998 ppm fluoride showed a substantial increase in fluoride content, especially at low pH. The fluoride uptake was about ten times higher in the high-concentration fluoride solution compared to the low-concentration solution, indicating that significantly elevated fluoride levels in the surrounding medium (which are beyond the range of most oral care products) are necessary to effectively increase the surface content of fluoride in teeth.

Despite these findings, the exact chemical and crystallographic characteristics of the fluoride-rich surface layer remain a subject of inquiry due to its inherently thin nature. Further research is required to fully understand this layer's properties and composition.

6.1 Zusammenfassung

Die an der Bevölkerung von Gevensleben, einem frühmittelalterlichen Gräberfeld aus dem 8. bis 10. Jahrhundert n. Chr., durchgeführten Untersuchungen haben Einblicke in die kindliche Entwicklung und den Gesundheitszustand der Menschen in dieser Zeit gegeben. Die Studie konzentrierte sich auf die tägliche Sekretionsrate des Zahnschmelzes (*daily secretion rate*, DSR), die Kronenbildungszeiten (*crown formation time*, CFT) der Zähne und die akzentuierten Linien (*accentuated lines*, AL) als Indikatoren für Gesundheit und Stress in der Kindheit.

Die tägliche Sekretionsrate (DSR) wurde an verschiedenen Stellen in den Zahnkronen gemessen und es wurde festgestellt, dass sie sowohl in den Höcker- als auch in den Seitenschmelzregionen vom inneren zum äußeren Schmelz zunimmt. Es wurden Vergleiche mit anderen historischen Populationen gezogen und die DSR von Gevensleben stimmten eher mit der frühangelsächsischen als mit der spätangelsächsischen Probe überein, obwohl letztere zeitlich näherliegend an Gevensleben einzuordnen sind.

Die Kronenbildungszeiten (CFT) wurden anhand von Referenzwerten geschätzt, da die Zähne keine neonatalen Linien aufwiesen. Die berechneten CFT lagen im Allgemeinen vor den Referenzwerten.

Akzentuierte Linien (AL) wurden als Indikatoren für Gesundheit und Stress in der Kindheit verwendet. Die Prävalenz der AL nahm zwischen 7 und 10 Monaten zu, was wahrscheinlich auf die erhöhte Aktivität und den Kontakt mit Krankheitserregern zurückzuführen ist. Eine weitere Spitze der AL-Prävalenz wurde im Alter von etwa 3 Jahren beobachtet, was einer Periode hoher Sterblichkeit in der nahegelegenen Populationen Werlaburgdorf entspricht. Diese Stressperiode hängt möglicherweise mit den schwierigen Bedingungen beim Abstillen der Kinder zusammen. Ein dritter Höhepunkt trat zwischen 8 und 9 Jahren auf, was mit einer Übergangsphase in der Entwicklung und damit einhergehenden körperlichen und kognitiven Veränderungen zusammenfiel.

Insgesamt herrschten in der Gevensleben-Bevölkerung schwierige Lebensbedingungen, welche sich durch Unterernährung, Infektionskrankheiten und chronische Erkrankungen bedingt durch karge Behausungen zeigen. Diese Faktoren trugen wahrscheinlich zu den beobachteten Stressmarkern in den Zähnen und Knochen der Menschen bei.

Fluorid findet sich in den menschlichen Zähnen hauptsächlich auf der Zahnoberfläche, wenn auch in sehr geringen Mengen. Ziel dieser Studie war es, die Aufnahme von Fluorid in die menschlichen Zähne zu untersuchen, wenn diese verschiedenen fluoridhaltigen Lösungen ausgesetzt werden, um eine Zahnbehandlung zu simulieren. Die Zähne wurden in Lösungen mit 250 ppm Fluorid getaucht, diese repräsentieren Mundspülungen, und in eine hochkonzentrierte Kaliumfluoridlösung (18.998 ppm; 1 mol L^{-1}), die professionellen Fluoridlacken entspricht. Die Versuche wurden im wässrigen Medium und in Citratpuffer (pH 4,6 bis 4,7) durchgeführt, um den sauren Charakter einiger Fluoridgele nachzuahmen.

Die Untersuchung ergab, dass die Behandlung mit 250 ppm Fluorid den Fluoridgehalt des Zahnschmelzes sowohl bei neutralen als auch bei sauren pH-Werten nicht signifikant veränderte. Im Gegensatz dazu zeigten Zähne, die 18.998 ppm Fluorid ausgesetzt waren, einen erheblichen Anstieg des Fluoridgehalts, insbesondere bei niedrigem pH-Wert. Die Fluoridaufnahme war in der hochkonzentrierten Fluoridlösung etwa zehnmal höher als in der niedrig konzentrierten Lösung, was darauf hindeutet, dass deutlich erhöhte Fluoridwerte im umgebenden Medium (die über den Bereich der meisten Mundpflegeprodukte hinausgehen) erforderlich sind, um den Oberflächengehalt an Fluorid in den Zähnen wirksam zu erhöhen.

Trotz dieser Erkenntnisse sind die genauen chemischen und kristallografischen Eigenschaften der fluoridreichen Oberflächenschicht aufgrund ihrer dünnen Beschaffenheit nicht abschließend geklärt. Weitere Forschung ist erforderlich, um die Eigenschaften und die Zusammensetzung dieser Schicht vollständig zu verstehen.

7 References

AlQahtani, S.J., Hector, M.P., Liversidge, H.M., 2010. Brief communication: The London atlas of human tooth development and eruption, Am. J. Phys. Anthropol. 142, 481-490.

Amaechi, B.T., AbdulAzees, P.A., Alshareif, D.O., Shehata, M.A., de Carvalho Sampaio Lima, P.P., Abdollahi, A., Kalkhorani, P.S., Evans, V., 2019. Comparative efficacy of a hydroxyapatite and a fluoride toothpaste for prevention and remineralization of dental caries in children, Brit. Dent. J. 5, 18.

Amaechi, B.T., AbdulAzees, P.A., Okoye, L.O., Meyer, F., Enax, J., 2020. Comparison of hydroxyapatite and fluoride oral care gels for remineralization of initial caries: a pH-cycling study, Brit. Dent. J. 6, 9.

Antoine, D., Hillson, S., Dean, M.C., 2009. The developmental clock of dental enamel: a test for the periodicity of prism cross-striations in modern humans and an evaluation of the most likely sources of error in histological studies of this kind, J. Anat. 214, 45-55.

Aris, C., Mahoney, P., Deter, C., 2020a. Enamel growth rates of anterior teeth in males and females from modern and ancient British populations, Am. J. Phys. Anthropol. 173, 236-249.

Aris, C., Mahoney, P., O'Hara, M.C., Deter, C., 2020b. Enamel thickness and growth rates in modern human permanent first molars over a 2000 year period in Britain, Am. J. Phys. Anthropol. 173, 141-157.

Arnold, K., 1986. Kindheit im Europäischen Mittelalter, in: Martin, J., Nitschke, A. (Eds.), Zur Sozialgeschichte der Kindheit, Karl Alber, Freiburg i. Br., pp. 443-467.

Arnold, W.H., Dorow, A., Langenhorst, S., Gintner, Z., Banoczy, J., Gaengler, P., 2006. Effect of fluoride toothpastes on enamel demineralization, BMC Oral Health 6, 8.

Badiola, K.A., Bird, C., Brocklesby, W.S., Casson, J., Chapman, R.T., Coles, S.J., Cronshaw, J.R., Fisher, A., Frey, J.G., Gloria, D., Grossel, M.C., Hibbert, D.B., Knight, N., Mapp, L.K., Marazzi, L., Matthews, B., Milsted, A., Minns, R.S., Mueller, K.T., Murphy, K., Parkinson, T., Quinnell, R., Robinson, J.S., Robertson, M.N., Robins, M., Springate, E., Tizzard, G., Todd, M.H., Williamson,

A.E., Willoughby, C., Yang, E., Ylioja, P.M., 2015. Experiences with a researcher-centric ELN, Chem. Sci. 6, 1614-1629.

Bath-Balogh, M., Fehrenbach, M.J., 2011. Illustrated dental embryology, histology, and anatomy, 3rd ed., Elsevier Saunders, St.Louis, Missouri, USA.

Beniash, E., Stifler, C.A., Sun, C.-Y., Jung, G.S., Qin, Z., Buehler, M.J., Gilbert, P.U.P.A., 2019. The hidden structure of human enamel, Nat. Commun. 10, 4383.

Bernatzky, M., Geschwinde, M., Grefen-Peters, S., Heske, I., Müller, M., Palka, A., Posselt, N., Röckelein, H., 2018. Das Gräberfeld von Gevensleben: Menschen im Braunschweiger Land zwischen 750 und 1150 n. Chr., Isensee Verlag, Oldenburg.

Birch, W., Dean, M.C., 2014. A method of calculating human deciduous crown formation times and of estimating the chronological ages of stressful events occurring during deciduous enamel formation, J. Forensic Leg. Med. 22, 127-144.

Blaich, M.C., 2013. Werla 2. Die Menschen von Werlaburgdorf. Ein Beitrag zur Geschichte des Nordharzvorlandes im 08. bis 10. Jahrhundert, Monographien des Römisch-Germanischen Zentralmuseums, Verlag des Römisch-Germanischen Zentralmuseums, Mainz.

Brickley, M.B., Morgan, B., 2023. Assessing diagnostic certainty for scurvy and rickets in human skeletal remains, Am. J. Biol. Anthropol. 181, 637-645.

Bromage, T.G., 1991. Enamel incremental periodicity in the pig-tailed macaque: A polychrome fluorescent labeling study of dental hard tissues, Am. J. Phys. Anthropol. 86, 205-214.

Bromage, T.G., Lacruz, R.S., Hogg, R., Goldman, H.M., McFarlin, S.C., Warshaw, J., Dirks, W., Perez-Ochoa, A., Smolyar, I., Enlow, D.H., Boyde, A., 2009. Lamellar bone is an incremental tissue reconciling enamel rhythms, body size, and organismal life history, Calcif. Tissue Int. 84, 388-404.

Buzalaf, M.A., Pessan, J.P., Honorio, H.M., Cate, J.M.t., 2011. Mechanisms of action of fluoride for caries control, Monogr. Oral Sci. 22, 97-114.

Cate, J.M.t., 1997. Review on fluoride, with special emphasis on calcium fluoride mechanisms in caries prevention, Eur. J. Oral Sci. 105, 461-465.

Christensen, G.J., Kraus, B.S., 1965. Initial calcification of the human permanent first molar, J. Dent. Res. 44, 1338 - 1342.

Cieplik, F., Kara, E., Muehler, D., Enax, J., Hiller, K.A., Maisch, T., Buchalla, W., 2018. Antimicrobial efficacy of alternative compounds for use in oral care towards biofilms from caries-associated bacteria in vitro, Microbiologyopen e695, 1-10.

Daculsi, G., LeGeros, R.Z., Heughebaert, M., Barbieux, I., 1990. Formation of carbonate-apatite crystals after implantation of calcium phosphate ceramics, Calcif. Tissue Int. 46, 20-27.

Dean, M.C., 2009. Extension rates and growth in tooth height of modern human and fossil hominin canines and molars, Front. Oral. Biol. 13, 68-73.

Dean, M.C., 2012. A histological method that can be used to estimate the time taken to form the crown of a permanent tooth, Methods Mol. Biol., Humana Press, Totowa, pp. 89-100.

Dinnebier, R.E., Billinge, S.J.L., 2008. Powder diffraction: Theory and practice, Royal Society of Chemistry, Cambridge.

Dorozhkin, S.V., Epple, M., 2002. Biological and medical significance of calcium phosphates, Angew. Chem. Int. Ed. 41, 3130-3146.

Eggert, F., Neubert, R., 1999. In vitro investigation of the liberation of fluoride ions from toothpaste compounds in a permeation model, Eur. J. Pharm. Biopharm. 47, 169-173.

Enax, J., Epple, M., 2018. Synthetic hydroxyapatite as a biomimetic oral care agent, Oral Health Prev. Dent. 16, 7-19.

Enwonwu, C.O., 1973. Influence of socio-economic conditions on dental development in Nigerian children, Arch. Oral Biol. 18, 95-107.

Epple, M., 2003. Biomaterialien und Biomineralisation - Eine Einführung für Naturwissenschaftler, Mediziner und Ingenieure, Teubner, Wiesbaden.

Epple, M., Enax, J., 2018. Moderne Zahnpflege aus chemischer Sicht, Chem. Unserer Zeit 52, 218-228.

Epple, M., Enax, J., Meyer, F., 2022. Prevention of caries and dental erosion by fluorides - A critical discussion based on physico-chemical data and principles, Dent. J. 10, 6.

Faidt, T., Zeitz, C., Grandthyll, S., Hans, M., Hannig, M., Jacobs, K., Muller, F., 2017. Time dependence of fluoride uptake in hydroxyapatite, ACS Biomater. Sci. Eng. 3, 1822-1826.

Fanning, E.A., Moorrees, C.F., 1969. A comparison of permanent mandibular molar formation in Australian aborigines and Caucasoids, Arch. Oral. Biol. 14, 999-1006.

Fejerskov, O., Nyvad, B., Kidd, E., 2015. Dental caries: The disease and its clinical management, Third Edition, Wiley Blackwell, Oxford.

Fiorenza, L., Benazzi, S., Oxilia, G., Kullmer, O., 2018. Functional relationship between dental macrowear and diet in Late Pleistocene and recent modern human populations, Int. J. Osteoarchaeol. 28, 153-161.

Fiorenza, L., Kullmer, O., 2013. Dental wear and cultural behavior in Middle Paleolithic humans from the Near East, Am. J. Phys. Anthropol. 152, 107-117.

Forshaw, R., 2015. Unlocking the past: The role of dental analysis in archaeology, Dent. Hist. 60, 51-62.

Gerth, H.U., Dammaschke, T., Schäfer, E., Züchner, H., 2007. A three layer structure model of fluoridated enamel containing CaF2, Ca(OH)2 and FAp, Dent. Mater. 23, 1521-1528.

Geschwinde, M., Röckelein, H., 2018. Transformation und Bedrängnis. Der Friedhof von Gevensleben und das Braunschweiger Land am Ende des 1. Jahrtausends, Das Gräberfeld von Gevensleben. Menschen im Braunschweiger Land zwischen 750 und 1150 n. Chr. Wegweiser zur Vor und Frühgeschichte Niedersachsens, Isensee Verlag Oldenburg, Oldenburg, pp. 9-12.

Girkin, J., 2019. A practical guide to optical microscopy, 1 ed., CRC Press, Taylor and Francis Group, Boca Raton.

Glezen, W.P., 2003. Effect of maternal antibodies on the infant immune response, Vaccine 21, 3389-3392.

Goldstein, J.I., Newbury, D.E., Michael, J.R., Ritchie, N.W.M., Scott, J.H.J., Joy, D.C., 2017. Scanning electron microscopy and X-ray microanalysis, Springer New York.

Goodman, A.H., Rose, J.C., 1991. Dental enamel hypoplasias as indicators of nutritional status, in: Kelley, M.A., Larsen, C.S. (Eds.), Advances in Dental Anthropology, Wiley-Liss, New York, pp. 279-293.

Grefen-Peters, S., 2013. Die menschlichen Skelettreste aus dem frühmittelalterlichen Gräberfeld von Werlaburgdorf, Lkr. Wolfenbüttel, in: Blaich, M.C. (Ed.), Werla 2. Die Menschen von Werlaburgdorf. Ein Beitrag zur Geschichte des Nordharzvorlandes im 08. bis 10. Jahrhundert. Monographien des Römisch-Germanischen Zentralmuseums, Verlag des Römisch-Germanischen Zentralmuseums, Mainz, pp. 29-73.

Grefen-Peters, S., 2018. Die Menschen von Gevensleben und Werlaburgdorf, Das Gräberfeld von Gevensleben - Menschen im Braunschweiger Land zwischen 750 und 1150 n. Chr., Isensee Verlag Oldenburg, Oldenburg, pp. 31-36.

Grefen-Peters, S., 2020. Die Skelette aus dem frühmittelalterlichen Gräberfeld von Gevensleben. Rekonstruktion von Lebenswelten, Archäologie in Niedersachsen, Isensee Verlag Oldenburg, Oldenburg, pp. 118-123.

Grupe, G., Harbeck, M., McGlynn, G.C., 2015. Prähistorische Anthropologie, 1 ed., Springer Spektrum Berlin, Heidelberg.

Heske, I., 2018. Die Christianisierung und das Alter der Gräberfelder, Das Gräberfeld von Gevensleben. Menschen im Braunschweiger Land zwischen 750 und 1150 n. Chr. Wegweiser zur Vor- und Frühgeschichte in Niedersachsen, Isensee Verlag Oldenburg, Oldenburg, pp. 37-44.

Hillson, S., 1996. Dental Anthropology, Cambridge University Press, Cambridge.

Hillson, S., 2005. Teeth, 2 ed., Cambridge University Press, Cambridge.

Hillson, S., 2014. Tooth development in human evolution and bioarchaeology, Cambridge University Press, Cambridge.

Hjortsjo, C., Young, A., Kiesow, A., Cismak, A., Berthold, L., Petzold, M., 2015. A descriptive in vitro electron microscopic study of acidic fluoride-treated enamel: potential anti-erosion effects, Caries Res. 49, 618-625.

Irish, J.D., 2015. Terms and terminology used in dental anthropology, A companion to dental anthropology, pp. 85-93.

Jenni, O., 2021. Das Säuglingsalter – Kontaktaufnahme mit der Welt, Die kindliche Entwicklung verstehen: Praxiswissen über Phasen und Störungen, Springer Berlin Heidelberg, Berlin, Heidelberg, pp. 173-232.

Joannes-Boyau, R., Adams, J.W., Austin, C., Arora, M., Moffat, I., Herries, A.I.R., Tonge, M.P., Benazzi, S., Evans, A.R., Kullmer, O., Wroe, S., Dosseto, A., Fiorenza, L., 2019. Elemental signatures of Australopithecus africanus teeth reveal seasonal dietary stress, Nature 572, 112-115.

Kay, R.F., Hiiemae, K.M., 1974. Jaw movement and tooth use in recent and fossil primates, Am. J. Phys. Anthropol. 40, 227-256.

Kendall, C., Eriksen, A.M.H., Kontopoulos, I., Collins, M.J., Turner-Walker, G., 2018. Diagenesis of archaeological bone and tooth, Palaeogeogr. Palaeoclimatol. Palaeoecol. 491, 21-37.

Kensche, A., Holder, C., Basche, S., Tahan, N., Hannig, C., Hannig, M., 2017. Efficacy of a mouthrinse based on hydroxyapatite to reduce initial bacterial colonisation in situ, Arch. Oral Biol. 80, 18-26.

Kiesow, A., Teuscher, N., Morawietz, M., Eick, S., 2021. In vitro surface investigation of calcium fluoride-like precipitation on human enamel after topical treatment with the organic fluoride nicomethanol hydrofluoride, Oral Health Prev. Dent. 19, 59-65.

Klug, H.P., Alexander, L.E., 1974. X-ray diffraction procedures for polycrystalline and amorphous materials, Wiley-Interscience, New York.

Koenigswald, W.v., Pfretzschner, H.U., 1987. Hunter-Schreger-Bänder im Zahnschmelz von Säugetieren (Mammalia), Zoomorphology 106, 329-338.

Kohn, M.J., Schoeninger, M.J., Barker, W.W., 1999. Altered states: effects of diagenesis on fossil tooth chemistry, Geochim. Cosmochim. Acta 63, 2737-2747.

Kullmer, O., 2015. Der verlorene Biss: Biologische und kulturelle Evolution der Zähne, in: Böhme, H., Kordaß, B., Slomiski, B. (Eds.), Das Dentale - Faszination des oralen Systems in Wissenschaft und Kultur, Qunitessenz, Berlin, pp. 65-86.

Kullmer, O., Benazzi, S., Fiorenza, L., Schulz, D., Bacso, S., Winzen, O., 2009. Technical note: Occlusal fingerprint analysis: quantification of tooth wear pattern, Am. J. Phys. Anthropol. 139, 600-605.

Lacruz, R.S., Hacia, J.G., Bromage, T.G., Boyde, A., Lei, Y., Xu, Y., Miller, J.D., Paine, M.L., Snead, M.L., 2012. The circadian clock modulates enamel development, J. Biol. Rhythms 27, 237-245.

Larsen, C.S., 2015. Bioarchaeology: Interpreting behavior from the human skeleton, 2 ed., Cambridge University Press, Cambridge.

Lee, B.S., Chou, P.H., Chen, S.Y., Liao, H.Y., Chang, C.C., 2015. Prevention of enamel demineralization with a novel fluoride strip: enamel surface composition and depth profile, Sci. Rep. 5, 13352.

LeGeros, R.Z., 1981. Apatites in biological systems, Prog. Cryst. Growth Charact. 4, 1-45.

LeGeros, R.Z., Trautz, O.R., LeGeros, J.P., Klein, E., 1968. Carbonate substitution in the apatite structure, Bull. Soc. Chim. Fr., 1712-1718.

Lelli, M., Putignano, A., Marchetti, M., Foltran, I., Mangani, F., Procaccini, M., Roveri, N., Orsini, G., 2014. Remineralization and repair of enamel surface by biomimetic Zn-carbonate hydroxyapatite containing toothpaste: a comparative in vivo study, Front. Physiol. 5, 333.

Listl, S., Galloway, J., Mossey, P.A., Marcenes, W., 2015. Global economic impact of dental diseases, J. Dent. Res. 94, 1355-1361.

Logan, W., Kronfeld, R., 1933. Development of the human jaws and surrounding structures from birth to the age of fifteen years., J. Am. Dent. Assoc. 20, 379-427.

Loskill, P., Zeitz, C., Grandthyll, S., Thewes, N., Müller, F., Bischoff, M., Herrmann, M., Jacobs, K., 2013. Reduced adhesion of oral bacteria on hydroxyapatite by fluoride treatment, Langmuir 29, 5528-5533.

Lumsden, A.G.S., Osborn, J.W., 1977. The evolution of chewing: A dentist's view of palaeontology, J. Dent. 5, 269-287.

Maas, M.C., Dumont, E.R., 1999. Built to last: The structure, function, and evolution of primate dental enamel, Evol. Anthropol. 8, 133-152.

Mahoney, P., 2008. Intraspecific variation in M1 enamel development in modern humans: implications for human evolution, J. Hum. Evol. 55, 131-147.

Mahoney, P., 2011. Human deciduous mandibular molar incremental enamel development, Am. J. Phys. Anthropol. 144, 204-214.

Maier, W., 1978. Zur Evolution des Säugetiergebisses- Typologische und konstruktionsmorphologische Erklärungen, Natur u. Museum, 288-300.

Mao, F., Wang, Y., Meng, J., 2015. A systematic study on tooth enamel microstructures of Lambdopsalis bulla (Multituberculate, Mammalia) - Implications for multituberculate biology and phylogeny, PLoS One 10, e0128243.

Marinho, V.C., Chong, L.Y., Worthington, H.V., Walsh, T., 2016. Fluoride mouthrinses for preventing dental caries in children and adolescents, Cochrane Database Syst. Rev. 7, Cd002284.

Marinho, V.C., Worthington, H.V., Walsh, T., Chong, L.Y., 2015. Fluoride gels for preventing dental caries in children and adolescents, Cochrane Database Syst. Rev. 2015, Cd002280.

Marinho, V.C., Worthington, H.V., Walsh, T., Clarkson, J.E., 2013. Fluoride varnishes for preventing dental caries in children and adolescents, Cochrane Database Syst. Rev., Cd002279.

Marsh, P.D., 2012. Contemporary perspective on plaque control, Br. Dent. J. 212, 601-606.

Meyer, F., Amaechi, B.T., Fabritius, H.O., Enax, J., 2018. Overview of calcium phosphates used in biomimetic oral care, Open Dent. J. 12, 406-423.

Meyer, F., Enax, J., 2019. Hydroxyapatite in oral biofilm management, Eur. J. Dent. 13, 287-290.

Mimura, F., 1939. The periodicity of growth lines seen in enamel, Kobyo-shi 13, 454-455.

Molnar, S., Przybeck, T.R., Gantt, D.G., Elizondo, R.S., Wilkerson, J.E., 1981. Dentin apposition rates as markers of primate growth, Am. J .Phys. Anthropol. 55, 443-453.

Mueller, F., Zeitz, C., Mantz, H., Ehses, K.H., Soldera, F., Schmauch, J., Hannig, M., Hufner, S., Jacobs, K., 2010. Elemental depth profiling of fluoridated hydroxyapatite: saving your dentition by the skin of your teeth?, Langmuir 26, 18750-18759.

Murphy, T., 1959. The changing pattern of dentine exposure in human tooth attrition, Am. J. Phys. Anthropol. 17, 167-178.

Myoung, S., Lee, J., Constantino, P., Lucas, P., Chai, H., Lawn, B., 2009. Morphology and fracture of enamel, J. Biomech. 42, 1947-1951.

Nanci, A., 2018. Ten Cate's oral histology: development, structure, and function, 9th ed., Elsevier, St. Louis, Missori, USA.

Nava, A., Bondioli, L., Coppa, A., Dean, C., Rossi, P.F., Zanolli, C., 2017. New regression formula to estimate the prenatal crown formation time of human deciduous central incisors derived from a Roman Imperial sample (Velia, Salerno, Italy, I-II cent. CE), PLOS ONE 12, e0180104.

Nava, A., Frayer, D.W., Bondioli, L., 2019. Longitudinal analysis of the microscopic dental enamel defects of children in the Imperial Roman community of Portus Romae (necropolis of Isola Sacra, 2nd to 4th century CE, Italy), J. Archaeol. Sci. Rep. 23, 406-415.

Needleman, I., Nibali, L., Di Iorio, A., 2015. Professional mechanical plaque removal for prevention of periodontal diseases in adults--systematic review update, J. Clin. Periodontol. 42 Suppl 16, S12-35.

Parker, R.B., Murphy, J.W., Toots, H., 1974. Fluorine in fossilized bone and tooth: distribution among skeletal tissues, Archaeometry 16, 98-102.

Reid, D.J., Dean, M.C., 2006. Variation in modern human enamel formation times, J. Hum. Evol. 50, 329-346.

Reid, D.J., Ferrell, R.J., 2006. The relationship between number of striae of Retzius and their periodicity in imbricational enamel formation, J. Hum. Evol. 50, 195-202.

Scholz, K.J., Federlin, M., Hiller, K.A., Ebensberger, H., Ferstl, G., Buchalla, W., 2019. EDX-analysis of fluoride precipitation on human enamel, Sci. Rep. 9, 13442.

Schultz, M., Carli-Thiele, P., Schmidt-Schultz, T.H., Kierdorf, U., Kierdorf, H., Teegen, W.-R., Kreutz, K., 1998. Enamel hypoplasias in archaeological skeletal remains, in: Alt, K.W., Rösing, F.W., Teschler-Nicola, M. (Eds.), Dental anthropology: fundamentals, limits and prospects, Springer, Vienna, pp. 293-311.

Schwarzbach, H., Stachniss, V., Steiniger, B., 2010. Mikroskopische Anatomie der Zähne und des Parodonts, Thieme, Stattgart.

Schweissing, M.M., Grupe, G., 2003. Stable strontium isotopes in human teeth and bone: a key to migration events of the late Roman period in Bavaria, J. Archaeol. Sci. 30, 1373-1383.

Scott, G.R., 2014. Dental Anthropology, in: Smith, C. (Ed.), Encyclopedia of global archaeology, Springer New York, New York, NY, pp. 2107-2113.

Sheiham, A., James, W.P., 2015. Diet and dental caries: The pivotal role of free sugars reemphasized, J. Dent. Res. 94, 1341-1347.

Simpson, S.W., 1999. Reconstructing patterns of growth disruption from enamel microstructure, in: Hoppa, R.D., FitzGerald, C.M. (Eds.), Human growth in the Past: Studies from bones and teeth, Cambridge University Press.

Smith, B.H., 1984. Patterns of molar wear in hunter–gatherers and agriculturalists, Am. J. Phys. Anthropol. 63, 39-56.

Smith, T.M., 2006. Experimental determination of the periodicity of incremental features in enamel, J. Anat. 208, 99-113.

Smith, T.M., 2008. Incremental dental development: methods and applications in hominoid evolutionary studies, J. Hum. Evol. 54, 205-224.

Sternitzke, V., Kaegi, R., Audinot, J.N., Lewin, E., Hering, J.G., Johnson, C.A., 2012. Uptake of fluoride from aqueous solution on nano-sized hydroxyapatite: examination of a fluoridated surface layer, Environ. Sci. Technol. 46, 802-809.

Storsberg, J., Loza, K., Epple, M., 2022. Incorporation of fluoride into human teeth after immersion in fluoride-containing solutions, Dent. J. 10, 1-9.

Tabuce, R., Delmer, C., Gheerbrant, E., 2007. Evolution of the tooth enamel microstructure in the earliest proboscideans (Mammalia), Zool. J. Linn. Soc. 149, 611-628.

Tafforeau, P., Zermeno, J.P., Smith, T.M., 2012. Tracking cellular-level enamel growth and structure in 4D with synchrotron imaging, J. Hum. Evol. 62, 424-428.

Terezhalmy, G.T., Bartizek, R.D., Biesbrock, A.R., 2008. Plaque-removal efficacy of four types of dental floss, J. Periodontol. 79, 245-251.

Tompkins, R.L., 1996. Human population variability in relative dental development, Am. J. Phys. Anthropol. 99, 79-102.

Ungar, P.S., 2010. Mammal Teeth: Origin, Evolution, and Diversity, Johns Hopkins University Press.

Ungar, P.S., 2011. Dental evidence for the diets of Plio-Pleistocene hominins, Am. J. Phys. Anthropol. 146, 47-62.

Ungar, P.S., 2014. Teeth: A very short introduction, Oxford University Press.

van Loveren, C., 2013. Toothpastes, Karger, Basel.

Walsh, T., Worthington, H.V., Glenny, A.M., Marinho, V.C.C., Jeroncic, A., 2019. Fluoride toothpastes of different concentrations for preventing dental caries, Cochrane Database Syst. Rev., CD007868.

Weyant, R.J., Tracy, S.L., Anselmo, T.T., Beltrán-Aguilar, E.D., Donly, K.J., Frese, W.A., Hujoel, P.P., Iafolla, T., Kohn, W., Kumar, J., Levy, S.M., Tinanoff, N., Wright, J.T., Zero, D., Aravamudhan, K., Frantsve-Hawley, J., Meyer, D.M., 2013. Topical fluoride for caries prevention: executive summary of the updated clinical recommendations and supporting systematic review, J. Am. Dent. Assoc. 144, 1279-1291.

Wieckowska-Lüth, M., Heske, I., 2019. On-site palao-ecological investigations at the Hünenburg hillfort-settlement complex, with special reference to non-pollen palynomorphs, in: dal Corso, M., Kirleis, W., Kneisel, J., Taylor, N., Wieckowska-Lüth, M., Zanon, M. (Eds.), How`s life? Living conditions in the 2nd and 1st Millennia BCE. Scales of transformation in prehistoric and archaic societies, Sidestone press Leiden, Leiden, pp. 167-186.

Witzel, C., Kierdorf, U., Schultz, M., Kierdorf, H., 2008. Insights from the inside: histological analysis of abnormal enamel microstructure associated with hypoplastic enamel defects in human teeth, Am. J. Phys. Anthropol. 136, 400-414.

Wood, B., 2011. Wiley-Blackwell Encyclopedia of Human Evolution, in: Wood, B. (Ed.), Wiley-Blackwell, Chester, West Sussex.

Żądzińska, E., Lorkiewicz, W., Kurek, M., Borowska-Strugińska, B., 2015. Accentuated lines in the enamel of primary incisors from skeletal remains: A contribution to the explanation of early childhood mortality in a medieval population from Poland, Am. J. Phys. Anthropol. 157, 402-410.

Zanatta, R.F., Caneppele, T.M.F., Scaramucci, T., El Dib, R., Maia, L.C., Ferreira, D., Borges, A.B., 2020. Protective effect of fluorides on erosion and erosion/abrasion in enamel: a systematic review and meta-analysis of randomized in situ trials, Arch. Oral Biol. 120, 104945.

8 Appendix

8.1 Abbreviations

Table 54 Abbreviations and their meanings used in this work

Abbreviation	Meaning
AL	Accentuated lines
BSE	Backscattered electrons
CS	Cross striations
CFT	Crown formation time
DSR	Daily secretion rate
EDJ	Enamel-dentine junction
EDX	Energy-dispersive X-ray spectroscopy
Hs	*Homo sapiens* used in sample name
HSB	Hunter-Schreger bands
PE	Primary electrons
PXRD	Powder X-ray diffraction
RL	Retzius lines/ Striae of Retzius
SD	Standard deviation
SE	Secondary electrons
SEM	Scanning electron microscopy

8.2 Gevensleben

Table 55 Daily Secretion Rates (DSR) in all enamel regions of individuals 12, 22 and 30. Single measurements and means are displayed with standard deviation (SD).

region	12_LLM2	12_LLM3	22_LLM2	22_LLM3	30_LLC	30_LLP3	30_LRM3
cuspal inner	3.84	4.05	3.12	4.58	3.73	-	3.89
	4.50	4.56	3.12	4.45	3.69	-	3.44
	4.14	3.94	3.06	4.80	4.23	-	3.37
	4.00	4.18	2.73	4.35	3.62	-	3.77
	4.95	4.46	3.31	4.81	3.35	-	4.17
mean	**4.29**	**4.24**	**3.07**	**4.60**	**3.72**	**3.42**	**3.73**
SD	**0.44**	**0.27**	**0.21**	**0.21**	**0.32**	**0.44**	**0.33**
cuspal mid	4.52	3.88	4.09	4.94	3.30	3.62	3.86
	4.09	4.39	3.26	4.74	3.85	4.01	4.14
	4.39	4.59	3.51	4.04	3.42	3.19	4.02
	4.80	4.71	3.29	4.24	3.18	4.01	4.21
	4.77	4.18	3.39	4.52	3.62	3.95	4.21
mean	**4.51**	**4.3495**	**3.51**	**4.50**	**3.47**	**3.76**	**4.09**
SD	**0.29**	**0.33**	**0.34**	**0.37**	**0.26**	**0.36**	**0.15**
cuspal outer	4.77	4.26	3.26	4.74	4.23	3.48	4.44
	4.68	4.59	3.15	4.97	4.32	3.84	4.33
	4.82	4.26	2.97	4.42	4.28	3.77	4.26
	4.97	4.41	3.27	4.74	4.17	3.47	4.19
	4.87	4.39	3.73	4.65	4.04	3.87	4.26
mean	**4.82**	**4.38**	**3.28**	**4.71**	**4.21**	**3.69**	**4.29**
SD	**0.11**	**0.14**	**0.28**	**0.20**	**0.11**	**0.20**	**0.09**
lateral inner	3.87	3.69	3.66	4.39	3.51	3.17	4.02
	3.95	3.46	2.84	4.42	3.25	3.01	3.83
	4.46	4.52	3.33	4.38	3.40	3.14	4.58
	4.46	3.85	3.64	4.58	3.26	3.22	4.11
	4.58	3.77	3.41	3.81	3.30	2.85	4.04
mean	**4.26**	**3.86**	**3.38**	**4.31**	**3.34**	**3.08**	**4.12**
SD	**0.33**	**0.40**	**0.33**	**0.30**	**0.11**	**0.15**	**0.28**
lateral mid	4.77	3.45	4.18	3.76	3.20	4.02	3.69
	4.28	3.66	3.60	3.81	2.89	3.70	4.11
	4.79	4.26	4.33	3.86	2.91	3.86	3.78
	4.68	4.26	3.84	3.79	3.16	3.52	4.31
	4.43	3.92	3.90	3.35	3.39	3.91	4.24
mean	**4.59**	**3.91**	**3.97**	**3.71**	**3.11**	**3.80**	**4.03**
SD	**0.22**	**0.36**	**0.29**	**0.21**	**0.21**	**0.20**	**0.28**
lateral outer	4.77	3.59	3.71	4.34	3.50	3.65	4.19
	4.92	3.48	3.90	4.64	3.14	3.74	3.14
	4.77	4.14	4.29	3.82	3.29	4.14	3.66
	4.23	3.97	4.52	4.11	3.62	3.82	4.09
	4.43	3.80	4.14	3.99	3.14	3.42	3.71
mean	**4.63**	**3.79**	**4.11**	**4.18**	**3.34**	**3.75**	**3.76**
SD	**0.28**	**0.27**	**0.32**	**0.32**	**0.21**	**0.26**	**0.41**

Table 56 Daily Secretion Rates (DSR) in all enamel regions of individuals 33, 38a and 39. Single measurements and means are displayed with standard deviation (SD).

region	33_LLM1	33_LLM2	33_LLM3	38a_URM1	38a_URM2	38a_URM3	39_LRP3	39_LRP4	39_ULM2
cuspal inner	3.56	3.21	3.72	3.96	4.42	3.66	3.53	3.90	4.33
	4.13	3.28	4.09	4.05	4.26	3.15	4.23	3.59	4.54
	4.26	3.01	3.86	3.59	3.93	3.47	3.75	3.10	3.35
	3.54	3.11	4.70	3.57	3.72	3.99	3.96	3.96	4.60
	4.37	3.01	4.34	3.52	3.55	3.46	3.98	3.67	3.60
mean	**3.97**	**3.13**	**4.14**	**3.74**	**3.97**	**3.55**	**3.89**	**3.65**	**4.08**
SD	**0.40**	**0.12**	**0.39**	**0.25**	**0.36**	**0.31**	**0.26**	**0.34**	**0.57**
cuspal mid	3.89	4.10	4.41	3.10	4.12	4.11	4.05	4.37	4.42
	3.48	4.30	4.43	4.21	4.27	3.89	3.77	3.85	3.82
	3.13	3.85	4.77	4.25	4.52	3.77	3.92	4.09	4.50
	3.25	4.21	4.57	4.63	3.95	3.73	4.30	3.95	4.43
	4.02	4.23	4.33	4.49	4.88	3.26	3.27	4.23	3.72
mean	**3.55**	**4.14**	**4.50**	**4.13**	**4.35**	**3.75**	**3.86**	**4.10**	**4.18**
SD	**0.39**	**0.18**	**0.17**	**0.60**	**0.36**	**0.31**	**0.38**	**0.21**	**0.38**
cuspal outer	3.24	4.63	4.88	3.55	5.10	4.10	3.86	4.67	4.13
	3.84	4.44	4.92	3.53	4.98	3.66	4.26	4.04	4.50
	3.76	4.14	4.52	3.47	4.88	4.26	3.82	4.92	4.92
	3.55	4.33	4.88	3.18	4.82	4.53	4.40	4.14	4.13
	4.35	4.60	4.85	3.02	4.52	4.06	3.82	4.18	4.46
mean	**3.75**	**4.43**	**4.81**	**3.35**	**4.86**	**4.12**	**4.03**	**4.39**	**4.43**
SD	**0.41**	**0.20**	**0.16**	**0.24**	**0.22**	**0.32**	**0.28**	**0.38**	**0.33**
lateral inner	3.31	3.31	3.72	4.48	4.17	3.83	3.44	4.11	4.06
	3.03	3.31	3.98	4.17	3.25	3.86	3.44	4.80	2.97
	3.52	3.38	3.23	3.99	4.02	3.77	4.26	3.98	3.32
	3.82	3.21	3.49	3.46	3.89	3.96	3.64	4.10	3.32
	3.55	3.35	3.28	3.70	3.57	3.94	3.34	3.99	4.20
mean	**3.45**	**3.31**	**3.54**	**3.96**	**3.78**	**3.87**	**3.63**	**4.20**	**3.58**
SD	**0.29**	**0.06**	**0.32**	**0.39**	**0.37**	**0.08**	**0.37**	**0.34**	**0.53**
lateral mid	4.47	3.95	3.66	4.18	4.52	3.95	4.35	4.60	3.94
	3.96	4.36	4.43	4.16	4.56	3.45	3.62	3.97	3.83
	3.91	4.26	3.70	4.52	4.28	3.30	3.57	3.60	4.65
	4.62	4.08	4.01	4.24	4.32	3.76	3.50	5.09	4.24
	4.55	4.22	3.57	4.92	4.08	4.45	3.89	4.58	4.38
mean	**4.30**	**4.18**	**3.87**	**4.40**	**4.35**	**3.78**	**3.79**	**4.37**	**4.21**
SD	**0.34**	**0.16**	**0.35**	**0.32**	**0.19**	**0.45**	**0.35**	**0.59**	**0.33**
lateral outer	4.90	4.06	4.33	4.02	4.17	4.06	4.52	4.18	3.84
	4.90	4.54	4.14	4.36	5.12	4.47	4.22	4.44	3.53
	4.70	4.44	3.98	4.21	4.96	4.03	4.86	4.96	4.75
	4.28	3.89	3.59	3.96	5.01	3.74	3.95	4.70	4.70
	4.79	4.24	3.35	4.60	4.52	3.84	4.45	4.70	4.33
mean	**4.71**	**4.23**	**3.88**	**4.23**	**4.76**	**4.03**	**4.40**	**4.60**	**4.23**
SD	**0.26**	**0.27**	**0.40**	**0.26**	**0.40**	**0.28**	**0.34**	**0.30**	**0.54**

Table 57 Daily Secretion Rates (DSR) in all enamel regions of individuals 43, 45 and 53. Single measurements and means are displayed with standard deviation (SD).

region	43_LLM1	43_LLM2	43_LLM3	45_LLM1	45_LLM2	45_LLM3	53_LLM2	53_LRM3
cuspal	4.33	3.50	3.59	3.62	3.77	3.39	3.25	3.62
inner	4.09	4.01	3.46	3.85	3.81	3.67	2.93	2.76
	3.79	3.58	3.60	3.60	3.11	3.20	4.08	3.93
	4.35	3.38	3.56	3.48	2.80	3.27	4.26	3.29
	3.91	3.56	3.14	3.87	2.93	3.15	3.93	4.54
mean	**4.09**	**3.60**	**3.47**	**3.68**	**3.28**	**3.33**	**3.69**	**3.63**
SD	**0.25**	**0.24**	**0.36**	**0.17**	**0.48**	**0.23**	**0.57**	**0.67**
	3.51	3.56	3.95	3.46	4.21	3.59	3.67	3.89
cuspal	4.28	4.09	3.31	3.89	3.76	3.61	3.96	3.87
mid	4.71	3.30	3.90	3.23	3.84	3.93	3.53	3.65
	4.29	4.26	3.53	3.68	3.38	4.13	3.86	4.13
	4.15	3.39	4.23	4.04	3.77	3.74	4.06	4.09
mean	**4.19**	**3.72**	**3.78**	**3.66**	**3.79**	**3.80**	**3.82**	**3.93**
SD	**0.43**	**0.43**	**0.36**	**0.32**	**0.30**	**0.23**	**0.22**	**0.19**
cuspal	5.05	4.43	4.45	3.67	3.24	4.45	3.55	3.54
outer	5.01	3.73	5.35	2.91	3.07	4.97	5.21	4.82
	4.13	3.55	4.20	4.96	2.92	4.61	3.87	3.66
	4.79	3.46	4.47	3.57	3.27	4.85	4.88	4.10
	5.13	4.18	4.53	4.40	2.68	4.70	5.38	3.92
mean	**4.82**	**3.87**	**4.60**	**3.90**	**3.04**	**4.72**	**4.58**	**4.01**
SD	**0.41**	**0.42**	**0.44**	**0.79**	**0.24**	**0.20**	**0.82**	**0.50**
lateral	3.00	3.84	3.27	4.01	2.37	4.49	3.02	2.98
inner	2.97	3.89	3.76	4.21	3.13	4.08	3.02	3.69
	3.39	3.39	3.83	4.02	3.79	3.39	3.38	3.02
	3.59	3.70	3.22	3.33	3.20	3.91	3.81	3.03
	3.79	3.95	3.20	4.20	3.70	3.82	3.13	3.17
mean	**3.35**	**3.75**	**3.46**	**3.95**	**3.24**	**3.94**	**3.27**	**3.18**
SD	**0.36**	**0.22**	**0.31**	**0.36**	**0.57**	**0.40**	**0.33**	**0.29**
lateral	3.76	4.21	3.65	4.54	4.24	3.53	3.69	4.24
mid	3.57	4.17	4.12	4.06	4.08	4.20	3.54	4.34
	3.41	3.33	4.45	4.88	3.10	3.60	3.40	3.96
	4.07	4.26	3.71	4.23	3.62	3.53	3.62	4.28
	3.32	3.73	3.96	4.03	3.79	3.66	3.73	3.90
mean	**3.62**	**3.94**	**3.98**	**4.35**	**3.76**	**3.71**	**3.60**	**4.14**
SD	**0.30**	**0.40**	**0.33**	**0.36**	**0.44**	**0.28**	**0.13**	**0.20**
lateral	3.35	3.21	4.02	4.45	4.52	3.81	4.20	4.28
outer	3.26	4.40	3.84	4.06	4.39	3.14	4.75	4.15
	4.64	4.30	4.77	4.19	4.46	3.92	4.34	4.23
	3.51	4.61	4.14	3.99	5.00	3.74	4.52	4.52
	4.34	3.82	4.65	3.89	4.90	3.96	4.55	4.18
mean	**3.82**	**4.07**	**4.28**	**4.12**	**4.65**	**3.71**	**4.47**	**4.27**
SD	**0.63**	**0.56**	**0.40**	**0.22**	**0.27**	**0.33**	**0.21**	**0.15**

Table 58 Daily Secretion Rates (DSR) in all enamel regions of individual 63a. Single measurements and means are displayed with standard deviation (SD).

region	63a_LLM1	63a_LLP4	63a_LLM2
cuspal	4.52	3.19	4.48
inner	4.26	3.84	4.04
	4.76	3.27	4.61
	3.50	3.05	4.27
	4.18	3.08	4.23
mean	**4.24**	**3.29**	**4.32**
SD	**0.47**	**0.32**	**0.43**
cuspal	3.03	3.71	3.56
mid	3.31	3.43	3.69
	3.29	3.62	4.43
	3.18	3.81	4.50
	3.01	3.31	4.05
mean	**3.16**	**3.58**	**4.05**
SD	**0.14**	**0.20**	**0.43**
cuspal	3.35	3.92	4.19
outer	3.06	3.62	4.55
	3.29	3.72	4.34
	3.10	3.57	3.79
	3.08	3.87	3.86
mean	**3.17**	**3.74**	**4.14**
SD	**0.14**	**0.15**	**0.32**
lateral	4.34	3.87	3.75
inner	3.47	3.23	4.06
	4.26	3.28	3.34
	3.90	3.77	3.58
	3.47	3.90	4.01
mean	**3.89**	**3.61**	**3.75**
SD	**0.42**	**0.33**	**0.30**
lateral	3.48	3.42	3.32
mid	3.01	3.54	3.52
	3.47	3.92	3.09
	3.51	3.11	4.30
	3.62	3.44	3.53
mean	**3.42**	**3.49**	**3.55**
SD	**0.24**	**0.29**	**0.46**
lateral	4.89	4.18	4.08
outer	4.38	4.10	3.71
	4.40	4.23	2.96
	4.68	3.90	3.79
	4.83	3.69	4.04
mean	**4.64**	**4.02**	**3.72**
SD	**0.24**	**0.22**	**0.45**

8.3 Fluoride content in human teeth measured by EDX

Table 59 Fluoride content of Hs01, Hs05-2 and Hs10-1 in weight percent before (b) and after treatment (a) with 250 ppm fluoride solution (pH 5.85) measured by EDX.

EDX-analysis no.	Hs01-b	Hs01-a	Hs05-2-b	Hs05-2-a	Hs10-1-b	Hs10-1-a
1	0.12	0.25	0.21	0.41	0	0.05
2	0.16	0.42	0	0.34	0	0
3	0.16	0.44	0.41	0.08	0	0
4	0.00	0.27	0.03	0.18	0.13	0
5	0.17	0.35	0.16	0.13	0	0
6	0.00	0.33	0.14	0.66	0.49	0.02
7	0.01	0.14	0.03	0.5	0	0.03
8	0.17	0.14	0	0.44	-	0.2
9	0.09	0.09	0.19	0.16	-	0.36
10	-	0.04	0.04	0	-	0
11	-	-	0.33	-	-	0.51
12	-	-	0.47	-	-	0
13	-	-	0.22	-	-	-

Table 60 Fluoride content of Hs04, Hs12-3 and Hs14-1 in weight percent before (b) and after treatment (a) with 250 ppm fluoride solution (pH 4.6) measured by EDX.

EDX-analysis no.	Hs04-b	Hs04-a	Hs12-3-b	Hs12-3-a	Hs14-1-b	Hs14-1-a
1	0.1	0.3	0.4	0.1	0.1	0.3
2	0.4	0.4	0	0	0.1	0.2
3	0.3	0.4	0.1	0	0	0.1
4	0.4	0.7	0	0	0.3	0
5	0.4	0.4	0	0.1	0.2	0.1
6	0.4	0.3	0	0	0.1	0.3
7	0.4	0.6	0.2	0	0.2	0
8	0.3	0.6	0.1	0.3	0.3	0.4
9	0.5	0.5	0	0	0	0.3
10	0.5	-	-	0	0.3	0.6
11	-	-	-	-	0	0.2
12	-	-	-	-	0.2	0.1
13	-	-	-	-	0.2	0.4

Table 61 Fluoride content of Hs05-1, Hs06 and Hs11-2 in weight percent before (b) and after treatment (a) with 18.998 ppm fluoride solution (pH 7.76) measured by EDX.

EDX-analysis no.	Hs05-1-b	Hs05-1-a	Hs06-b	Hs06-a	Hs11-2-b	Hs11-2-a
1	0.10	0.5	0.48	0.71	0.3	0.95
2	0.42	1.09	0	0.59	0.03	0.62
3	0.25	1.11	0	1.09	0.18	0.56
4	0.46	0.5	0.08	0.52	0.09	0.51
5	0.30	0.6	0	1.14	0.2	0.42
6	0.09	0.51	0.05	0.83	0.14	0.53
7	0.24	1.16	0.51	0.63	0	0.61
8	0.05	1.27	0	0.67	0	1.66
9	0.20	1.48	0	0.82	0	0.52
10	0.20	1.14	0	0.99	0.13	0.92
11	-	-	0	-	-	-

Table 62 Fluoride content of Hs03, Hs12-2 and Hs13 in weight percent before (b) and after treatment (a) with 18,998 ppm fluoride solution (pH 4.7) measured by EDX.

EDX-analysis no.	Hs03-b	Hs03-a	Hs12-2-b	Hs12-2-a	Hs13-b	Hs13-a
1	0.1	7.5	0.2	10.5	0.1	5.3
2	0	7.8	0.1	12.7	0.3	5
3	0.2	7.8	0	13	0	5.7
4	0.2	9.1	0	13.9	0	6.3
5	0	9	0.1	14.2	0	5.9
6	0.3	10.1	0.1	11.5	0	6.6
7	0	9.4	0.3	9.5	0.2	7.3
8	0.3	12.2	0.1	10.8	0.1	7.2
9	-	12.6	0	10.2	0	7.3
10	-	-	0.6	-	0.4	-
11	-	-	-	-	0.3	-
12	-	-	-	-	0.3	-
13	-	-	-	-	0.2	-

Table 63 Fluoride content of Hs12-1, Hs15-1 and Hs15-2 in weight percent before (b) and after treatment (a) with 250 ppm fluoride solution (pH 5.85) measured by EDX.

EDX-analysis no.	Hs12-1-b	Hs12-1-a	Hs15-1-b	Hs15-1-a	Hs15-2-b	Hs15-2-a
1	0	0	0.3	0.4	0	0
2	0	0	0.2	0	0.3	0
3	0.3	0	0.6	0	0.3	0.1
4	0.2	0	0.2	0	0	0.2
5	0	0	0.4	0	0.4	0
6	0.1	-	0.4	-	0.3	-
7	0	-	0.3	-	0.1	-
8	0	-	0.2	-	0.2	-
9	0	-	0.2	-	0.2	-
10	-	-	0.4	-	0.3	-
11	-	-	0.2	-	0	-
12	-	-	0.5	-	0.4	-

8.4 Descriptive statistics and statistical test for the Gevensleben sample

Descriptive statistics of the measured fluoride concentrations and the results of the Mann-Whitney tests for each tooth are summarised in **Table 64**.

Table 64 Descriptive statistics of fluoride concentrations before and after treatment, separated by teeth. SD, standard deviation; 25%P, 25% percentile; 75%P, 75% percentile; N = number of sites per tooth; two-sided p-values (exact Mann-Whitney test); medians are marked bold, when p<0.05; “before”, Baseline; “after”, after intervention

Intervention	Tooth	Measurement	Mean	SD	25%P	Median	75%P	Min	Max	N	p-value
250 ppm	Hs01	before	.10	.08	.01	**.12**	.16	.00	.17	9	**.03657**
		after	.25	.14	.14	**.26**	.35	.04	.44	10	
	Hs05-2	before	.17	.16	.03	.16	.22	.00	.47	13	n.s (> 0.1)
		after	.29	.21	.13	.26	.44	.00	.66	10	
	Hs10-1	before	.09	.18	.00	.00	.13	.00	.49	7	n.s (> 0.1)
		after	.10	.17	.00	.01	.13	.00	.51	12	
250 ppm pH 4.6	Hs04	before	.37	.12	.30	.40	.40	.10	.50	10	n.s (> 0.1)
		after	.47	.14	.40	.40	.60	.30	.70	9	
	Hs12-3	before	.09	.14	.00	.00	.10	.00	.40	9	n.s (> 0.1)
		after	.05	.10	.00	.00	.10	.00	.30	10	
	Hs14-1	before	.15	.11	.10	.20	.20	.00	.30	13	n.s (> 0.1)
		after	.23	.18	.10	.20	.30	.00	.60	13	
18,998 ppm	Hs05-1	before	.23	.14	.10	.22	**.30**	.05	.46	10	**0.00001**
		after	.94	.37	.51	1.10	**1.16**	.50	1.48	10	
	Hs06	before	.10	.20	.00	.00	**.08**	.00	.51	11	**0.00001**
		after	.80	.21	.63	.76	**.99**	.52	1.14	10	
	Hs11-2	before	.11	.10	.00	.11	**.18**	.00	.30	10	**0.00001**
		after	.73	.37	.52	.59	**.92**	.42	1.66	10	
18,998 ppm pH 4.7	Hs03	before	.14	.13	.00	.15	**.25**	.00	.30	8	**0.00008**
		after	9.50	1.85	7.80	9.10	**10.10**	7.50	12.60	9	
	Hs12-2	before	.15	.18	.00	.10	**.20**	.00	.60	10	**0.00002**
		after	11.81	1.70	10.50	11.50	**13.00**	9.50	14.20	9	
	Hs13	before	.15	.15	.00	.10	**.30**	.00	.40	13	**0.00001**
		after	6.29	.87	5.70	6.30	**7.20**	5.00	7.30	9	
pH 4.6	Hs12-1	before	.07	.11	.00	.00	.10	.00	.30	9	n.s (> 0.1)
		after	.00	.00	.00	.00	.00	.00	.00	5	
	Hs15-1	before	.33	.14	.20	.30	**.40**	.20	.60	12	0.01923
		after	.08	.18	.00	.00	**.00**	.00	.40	5	
	Hs15-2	before	.21	.15	.05	.25	.30	.00	.40	12	n.s (0.08177)
		after	.06	.09	.00	.00	.10	.00	.20	5	

8.5 Curriculum vitae

List of publications

Storsberg, J.; Loza, K.; Epple, M. Incorporation of Fluoride into Human Teeth after Immersion in Fluoride-Containing Solutions. Dent. J. 2022, 10, 153. DOI 10.3390/dj10080153

Storsberg, J.; Schmitt, M.; Hilken, G.; Dammann, P.; Begall, S.; Loza, K.; Caspar, K. R.; Epple, M. Auf den Zahn gefühlt: Einblick in die Zahnschmelzstruktur von Nagern und Insektenfressern. Biologie in Unserer Zeit 2022, 53(1), 58–66, DOI 10.11576/biuz-6104

Storsberg, J.; Loza, K.; Heske, I.; Epple, M. Life history reconstruction by dental enamel analysis of the medieval population (8th–10th Century AD) of Gevensleben (Lower Saxony, Germany). J. Archaeol. Sci. Rep. 2023, 52, DOI 10.1016/j.jasrep.2023.104251

List of scientific presentations

December 2021 Storsberg, J.
A look inside: enamel patterns, growth lines and co – What teeth reveal about an individual
School of Dentistry, Faculty of Health Sciences, Aristotle University of Thessaloniki, Thessaloniki, Greece, Online, **Oral presentation**

March 2022 Storsberg, J.; Schmitt, M.; Hilken, G.; Dammann, P.; Begall, S.; Loza, K.; Caspar, K.; Epple, M.
On the crystal arrangement in small mammal dental enamel,
30th Annual Meeting of the German Crystallographic Society (DGK), Online, **Oral presentation**

August 2022 Storsberg, J.; Heske, I.; Epple, M.
Weaning in the medieval population in Lower Saxony
18th International Symposium on Dental Morphology and 3rd Congress of the International Association of Paleodontology, Frankfurt, a.M., Germany, **Poster Presentation**

September 2022 Storsberg, J.; Loza, K.; Epple, M.
Incorporation of Fluoride into Human Teeth after Immersion in Fluoride-Containing Solutions
Annual Meeting of the German Society for Biomaterials (DGBM), Essen, Germany, **Poster Presentation**

March 2023 Storsberg, J.; Loza, K.; Heske, I.; Epple, M.
Life history reconstruction from tooth enamel of the medieval population in Lower Saxony
31st Annual Meeting of the German Crystallographic Society (DGK), Frankfurt a.M., Germany, **Oral presentation**

June 2023 Storsberg, J.
Methods for structural and chemical analyses of dental enamel
Graduate School of Dentistry, Division of Advanced Prosthetic Dentistry, Tohoku University, Sendai, Japan, **Oral presentation**

August 2023 Storsberg, J.; Loza, K.; Heske, I.; Epple, M.
Reconstructing the life history of a medieval population in Lower Saxony (Germany) with dental enamel
26th Congress and General Assembly of the International Union of Crystallography, Melbourne, Australia, **Oral Presentation**

8.7 Acknowledgments

I want to thank everyone who made this work possible:

Special thanks go to my supervisor, Professor Dr Matthias Epple, for allowing me to do this interesting interdisciplinary work in his working group and for the always valuable discussions and advice,

Professor Dr Ottmar Kullmer for the assessment of this dissertation,

Dr Immo Heske for his open-mindedness on this new cooperation and for kindly sharing a generous number of samples,

Dr Joachim Enax and Dr Frederic Meyer from Dr. Kurt Wolff GmbH & Co. KG for their helpful advice on oral care products,

Dr Kateryna Loza for SEM and EDS analyses and always helpful discussions,

Dr Oleg Prymak and Dietrich Tönnes for PXRD analyses,

Carola Fischer, Sabine Kiefer and Sabine Bollmann for their help in everyday organisational and technical matters,

All students and members of the working group: Aikaterini Karatzia, Natalie Wolff, David Mrosek, Jonas Sager, Benedikt Kruse, Nina Gumbiowski, Lisa-Sofie Wagner, Ivanna Kostina, Aileen Winter, Niklas Kost, Dr Kai Klein, Dr Kathrin Kostka, Dr Sebastian Kollenda, Dr Jonas Bals, Dr Nataniel Bialas, Dr Viktoriya Sokolova, Robin Meya, Tobias Bochmann, Ursula Giebel, Rui Guo, Jan Schießleder and Tamara Peters for the pleasant working environment and valuable discussions,

My friends, family and parents who always supported me.

8.8 Statutory declaration

I hereby declare that the presented thesis with the following title

“Morphology and Ultrastructure of Teeth: From the Middle Ages to Today”

is my work and is written independently. I further declare that I did not used other tools and references as listed. I also declare that the presented thesis has never been submitted in any other possible way to other faculties.

Hiermit versichere ich, dass die vorliegende Arbeit mit dem Titel

“Morphology and Ultrastructure of Teeth: From the Middle Ages to Today”

selbst verfasst habe und keine außer der angegebenen Hilfsmittel und Quellen verwendet habe. Außerdem versichere ich, dass die Arbeit in dieser oder ähnlicher Form noch an keiner anderen Universität eingereicht wurde.

Essen, 18.09.2023